Consolidation and drying of slurries

A Building with Nature study for the Marker Wadden

Barciela Rial, Maria

DOI
10.4233/uuid:ae11c3e7-86f2-4c6a-8d53-ee8781d56a72

Publication date
2019

Document Version
Final published version

Citation (APA)
Barciela Rial, M. (2019). *Consolidation and drying of slurries: A Building with Nature study for the Marker Wadden*. [Dissertation (TU Delft), Delft University of Technology]. https://doi.org/10.4233/uuid:ae11c3e7-86f2-4c6a-8d53-ee8781d56a72

Consolidation and drying of slurries

A Building with Nature study for the Marker Wadden

CONSOLIDATION AND DRYING OF SLURRIES

A BUILDING WITH NATURE STUDY FOR THE MARKER WADDEN

Proefschrift

ter verkrijging van de graad van doctor
aan de Technische Universiteit Delft,
op gezag van de Rector Magnificus Prof.dr.ir. T.H.J.J. van der Hagen,
voorzitter van het College voor Promoties,
in het openbaar te verdedigen op maandag 28 oktober 2019 om 15:00 uur

door

María BARCIELA RIAL

Master of Science in Water Engineering
Universidade da Coruña
geboren te Vigo, Spanje.

Dit proefschrift is goedgekeurd door de

promotor: prof. dr. ir. J.C. Winterwerp
promotor: prof. dr. J. Griffioen

Samenstelling promotiecommissie:

Rector Magnificus,	voorzitter
Prof. dr. ir. J.C. Winterwerp,	Technische Universiteit Delft
Prof. dr. J. Griffioen,	Universiteit Utrecht
Onafhankelijke leden:	
Prof. dr. ir. S.J.G. Aarninkhof,	Technische Universiteit Delft
Prof. dr. R.J. Schotting,	Universiteit Utrecht
Dr. P.J. Vardon,	Technische Universiteit Delft
Dr. C. Chassagne,	Technische Universiteit Delft
Prof. dr. ir. A.J.H.M. Reniers,	Technische Universiteit Delft, reservelid
Overige leden:	
Dr.ir. T. van Kessel,	Deltares

This research was funded by Netherlands Organization for Scientific Research (NWO), project no. 850.13.031 and the companies Royal Boskalis Westminster and Van Oord. The companies Deltares and Royal HaskoningDHV and the non-profit organisation Natuurmonumenten contributed in-kind.

Keywords: slurry, consolidation, drying, cohesive, clay, organic, vegetation, nature

Printed by: Gildeprint

Front & Back: Design by Maria Barciela Rial and picture by John Gundlach

ISBN 978-94-6384-073-6

An electronic version of this dissertation is available at
http://repository.tudelft.nl/.

To my father.

CONTENTS

SUMMARY

Fine cohesive sediment is starting to be used for nature building projects because traditionally used sandy sediment is becoming scarce. The Marker Wadden is one of the first projects using natural fine cohesive sediment for this purpose. The Marker Wadden aims to improve the ecosystem of Lake Markermeer (The Netherlands) by constructing a wetland with sediment from the lake. This is dredged from the bed and the resulting slurries are pumped into the project area. During this process, segregation and oxidation may occur. The native sediment composition and changes therein induced by the construction process affect the mechanical behavior of the wetland. Next to this, the initial stress state of the sediment is another variable determining the behavior. At a later stage, vegetation may colonize the wetland, influencing the mechanical properties of the sediment as well. These aspects are studied in this thesis.

First, the sediment composition of different natural sediment samples from Markermeer Lake was analyzed in detail: particle size, particle density, organic matter content and type, and bulk and clay mineralogy. Some of the samples were also sieved to study different degrees of segregation. Other samples were treated, including chemical oxidation and drying-rewetting, to mimic the ultimate effect of Markermeer sediment after being exposed, above water, to atmospheric conditions and oxidation. The composition of these sieved and treated samples was also analyzed. Samples had mass sand contents between 0 and 70% and total organic matter contents between 2.1 and 8.6 %. However, the reactivity or lability of this organic matter was found to vary between samples.

Multiple experiments were performed to test the consolidation, compressibility upon loading, undrained shear strength and drying behavior of samples with different compositions and initial stress states. First, consolidation experiments in settling columns at low initial concentrations below the gelling point (virgin consolidation) were performed and the material parameters were obtained. These parameters were different from the parameters obtained from the Seepage Induced Consolidation (SIC) test because of over-consolidated initial conditions induced by mixing. Numerical simulations were performed with a 1DV consolidation model to quantify the effect of over-consolidation and material parameters on the consolidation behavior. The computations show that remixing an equilibrium bed, formed by virgin consolidation, leads to further compaction resulting in larger bed densities. In contrast to this, when a consolidating bed was remixed during the first phase of consolidation, starting from a dilute suspension, there were no changes in the equilibrium profile.

Incremental Loading (IL) and Constant Rate of Strain (CRS) tests were performed to analyze the compressibility behavior, and Fall Cone tests were executed to determine the undrained shear strength. The results also show that the transition between cohesive and non-cohesive behavior occurs at a sand content > 40%. At a sand content of 70%, the sediment exhibited granular behavior. Furthermore, treating the samples increased the amount of fines necessary for cohesive behavior, which is attributed to the loss

of stabilizing organic matter. Samples exposed to atmospheric drying exhibited over-consolidated behavior.

The fractal theory was found to be a useful tool to normalize and identify the different behavior of samples for IL, CRS and Fall Cone tests, as well as for settling columns and SIC tests. Furthermore, the relation between the consolidation parameter of the fractal theory (Γ_c) and that from traditional soil mechanics theory was explained. A new equation for the compressibility parameter upon loading C_c as a function of fractal material parameters was also derived. From unloading tests performed with the CRS, the swelling coefficient C_{sw} was obtained. This C_{sw} was obtained by preventing the development of under pressures and, therefore, only quantifies the microscopic swelling of the clay particles and not the macroscopic rebound of the sample upon under pressure.

The drying behavior was analyzed with the Hyprop test, which was found to be a suitable device for slurries. The formation of an almost fully saturated crust was observed during these tests. The obtained Soil Water Retention Curves (SWRC) were fitted with a van Genuchten model. The model parameters obtained were found to be more influenced by the type of organic matter (OM) than by the total amount of OM.

Finally the effect of *Phragmites australis* (i.e. common reed) on the consolidation and drying was assessed with a newly designed column device. This set-up kept a constant boundary water level and measured the pore water pressure profiles. Columns were filled with slurries and the consolidation and drying behavior with and without reed was compared. The results show that reed induced suction and day-night cycles in the pore water pressure profile due to water uptake. Furthermore, the water loss of the consolidating sediment by evapotranspiration with the presence of reed was 6.5 larger than the loss by only evaporation. Thus, reed acted as an ecological engineer draining the sediment. However, no differences in the thickness of the sediment layer were found between the columns with and without reed, presumably because of armouring by roots.

The general conclusion is that over-consolidated initial conditions can be induced by different processes such as mixing and atmospheric drying. Furthermore, the composition of the sediment may change when exposed to segregation and oxidation. In particular, the type of organic matter affects the mechanical behavior of fine sediment at all stages (settling, consolidation, drying) and needs to be characterized. These aspects have traditionally been disregarded in engineering practice. However, the present research shows that they affect the mechanical behavior and need to be addressed in the design phase of a project using fine sediment as construction material. Herein, the material parameters need to be determined for the actual project conditions. Furthermore, in this design phase, a decision has to be made to allow or prevent the formation of a saturated crust, which affects the final strength and thickness of the bed. Preventing the formation of a crust allows to achieve the maximum bearing capacity. As a counterpart, the sediment surface is then less strong and more sensitive to erosion.

SAMENVATTING

Fijn, cohesief sediment wordt steeds meer gebruikt voor bouwen-met-natuur projecten omdat het traditioneel gebruikte, zandige sediment schaars wordt. De MarkerWadden is een van de eerste projecten waarbij fijn, cohesief sediment voor dit doel wordt gebruikt. De MarkerWadden heeft als doel het ecosysteem van het Markermeer te verbeteren door een moerasgebied te creëren met sediment uit het meer. Het sediment wordt van de bodem van het meer gebaggerd en de baggerspecie wordt naar het projectgebied gepompt. Tijdens dit proces kunnen segregatie en oxidatie optreden. De originele sedimentsamenstelling en de daarbinnen optredende veranderingen veroorzaakt door de aanlegmethoden hebben invloed op de mechanische eigenschappen van het sediment, dus de stabiliteit van het eiland. Daarnaast is de initiële spanningstoestand van invloed op het gedrag. In een later stadium zou vegetatie zich kunnen vestigen op het eiland en ook dit heeft invloed op de mechanische eigenschappen van het sediment. Deze aspecten zijn bestudeerd in dit proefschrift.

Als eerste is de samenstelling van verschillende natuurlijke sedimentmonsters uit het Markermeer uitgebreid geanalyseerd: korrelgrootte, korreldichtheid, de soort en gehalte van organische stof en bulk- en kleimineralogie. Sommige monsters zijn ook gezeefd om de mate van segregatie te bestuderen. Andere monsters zijn op verschillende manieren behandeld, onder andere door middel van chemische oxidatie of via een droog-herbevochtigingsproces, om het ultieme effect van het Markermeersediment na te bootsen nadat het sediment boven water is blootgesteld aan de atmosfeer en oxidatie. De samenstelling van de gezeefde en behandelde monsters is ook geanalyseerd. De monsters hadden zandgehaltes tussen de 0% en 70% van de totale droge massa, en een totaal organische-stofgehalte van 2.1% tot 8.6%. Daarbij moet worden opgemerkt dat de reactiviteit varieerde per monster.

Er zijn verschillende experimenten uitgevoerd om de zettingssnelheid bepalen en de samendrukbaarheid bij belasting, ongedraineerde schuifsterkte en het drooggedrag te bepalen van sedimentmonsters met verschillende samenstelling en initiële spanningstoestand. Als eerste zijn er consolidatie-experimenten uitgevoerd in bezinkkolommen met lage beginconcentraties onder het gellingpunt ("*virgin consolidation*") en hiermee zijn de materiaalparameters bepaald. Deze parameters verschillen van de parameters bepaald met de *Seepage Induced Consolidation (SIC) test*, vanwege de overgeconsolideerde omstandigheden veroorzaakt door menging. Met een 1DV-consolidatiemodel zijn numerieke simulaties uitgevoerd om het effect van overconsolidatie en materiaalparameters van het consolidatiegedrag te kwantificeren.De modelsimulaties laten zijn dat hermenging van de bodem in een normaal geconsolideerde evenwichtstoestand leidt tot verdere verdichting en dus hogere bodemdichtheid. Hiertegenover staat dat, wanneer een consoliderende bodem wordt gemengd tijdens de eerste fase van consolidatie, initieel vanuit een verdunde suspensie, er geen veranderingen zijn in het evenwichtsbodemprofiel.

Incremental Loading (IL) en *Constant Rate of Strain (CRS)* tests zijn uitgevoerd om

het samendrukbaarheidsgedrag te analyseren en *Fall Cone tests* zijn uitgevoerd om de ongedraineerde schuifsterkte te bepalen. De resultaten laten ook zien dat de overgang van cohesief naar niet-cohesief gedrag optreedt bij een zandgehalte dat groter is dan 40% van de totale droge massa. Bij een zandgehalte van 70% gaat het sediment korrelgedrag vertonen. Verder zorgde het behandelen van de monsters ervoor dat een grotere hoeveelheid fijn materiaal nodig was voordat er cohesief gedrag optrad, wat wordt toegeschreven aan de afname van stabiliserende organische stof. Monsters die aan de buitenlucht gedroogd zijn vertoonden overgeconsolideerd gedrag.

De fractaaltheorie was een handig hulpmiddel om de verschillende gedragingen van monsters bij *IL, CRS and Fall Cone tests* te normaliseren en identificeren, alsook voor bezinkkolommen en *SIC tests*. Verder is de relatie tussen de consolidatieparameter uit de fractaaltheorie (Γ_c) en die uit de traditionele grondmechanicatheorie verklaard. Ook is een nieuwe vergelijking afgeleid voor de samendrukkingsparameter bij belasting C_c als functie van de fractale materiaalparameters. Met ontlastproeven, uitgevoerd met de CRS, is de zwelcoëfficiënt C_{sw} bepaald. Deze C_{sw} is bepaald door de ontwikkeling van onderdrukken te voorkomen; daardoor wordt alleen de microscopische zwelling van kleideeltjes gekwantificeerd en niet de macroscopische terugvering van het monster door onderdruk.

Het drooggedrag is geanalyseerd met de Hydroptest, dit bleek een bruikbaar apparaat voor het analyseren van baggerspecie. Tijdens deze tests werd de vorming van een bijna volledig verzadigde korst geobserveerd. De ontstane *Soil Water Retention Curves (SWRC)* zijn gefit met een Genuchtenmodel. De gevonden modelparameters bleken meer beïnvloed door de soort organische stof dan door het totale organische-stofgehalte.

Als laatste is het effect van *Phragmites australis* (riet) op consolidatie en droging onderzocht in een nieuw-ontworpen kolom. In deze opstelling zijn profielen van de waterdruk in de poriën gemeten bij een constante waterstand aan de rand. De kolommen zijn gevuld met baggerspecie en het consolidatie- en drooggedrag met en zonder riet is vergeleken. De resultaten laten zien dat er zuigspanning en dag-en-nachtcycli in de poriewaterdrukken ontstaan door wateropname door het riet. Daarnaast is het waterverlies door evapotranspiratie door de aanwezigheid van riet 6,5 maal groter dan waterverlies door alleen maar verdamping. Riet gedroeg zich dus als ecologisch ingenieur door het sediment te draineren. Er zijn echter geen verschillen in de bodemdikte gevonden tussen de kolommen met en zonder riet, waarschijnlijk door versteviging door de wortels.

De algemene conclusie is dat initiële overgeconsolideerde condities veroorzaakt kunnen zijn door verschillende processen zoals menging en droging aan de atmosfeer. Daarnaast kan de samenstelling van het sediment veranderen wanneer het wordt blootgesteld aan segregatie en oxidatie. In het bijzonder zorgt het type organische stof voor beïnvloeding van de mechanische eigenschappen van fijn sediment in alle stadia (bezinken, consolidatie, droging) en dit moet worden gekarakteriseerd. Deze aspecten zijn in het verleden genegeerd in de ontwerppraktijk. Dit onderzoek laat zien dat deze aspecten invloed hebben op het mechanisch gedrag en dat er aandacht moet worden gegeven aan deze aspecten in de ontwerpfase van een project waarin fijn sediment wordt gebruikt als bouwmateriaal. De materiaalparameters moeten worden vastgesteld voor de werkelijke projectcondities. Daarnaast moet in de ontwerpfase worden beslist of het vormen van een verzadigde korst gewenst is. Deze heeft effect op de uiteindelijke sterkte en dikte

van de bodem. Het voorkomen van de vorming van een korst zorgt voor de maximale draagcapaciteit. Daar tegenover staat dat het sedimentoppervlak dan minder sterk is en meer gevoelig is voor erosie.

1

INTRODUCTION

Organic matter(s)!
E.J.W. Wattel-Koekkoek

1

1.1. MUD AND BUILDING WITH NATURE

SANDY sediments are traditionally preferred for reclamation projects to minimize deformation because fine grained sediments show significant settlement when consolidating and drying. Furthermore, the large consolidation time of fine sediment can be up to several decades. However, sandy sediment is becoming more scarce (*Vörösmarty et al.*, 2003). Therefore, fine sediments are progressively being used for nature building projects (e.g. *Haliburton et al.*, 1978; *Erwin et al.*, 2007). The *Marker Wadden* is one of the first projects in The Netherlands to use fresh unconsolidated mud for wetland construction.

The Marker Wadden is a Building with Nature project (BwN, e.g. *De Vriend et al.*, 2015). It aims to improve the ecosystem of Lake *Markermeer*, The Netherlands, by creating islands and marshes with slurries of sediment from the lake bed. The construction methodology of the Marker Wadden (Figure 1.1) strongly differs from traditional reclamation projects (e.g. Dutch polders, *Rijniersce* (1983)) or traditional island construction (e.g. Poplar island, Meriland; *Erwin et al.* (2007)). In the Marker Wadden, sediment is dredged from a borrow pit in the lake itself using a cutter-suction dredger. The dredged sediment is dumped and allowed to naturally settle and consolidate in calm areas protected by sand bars.

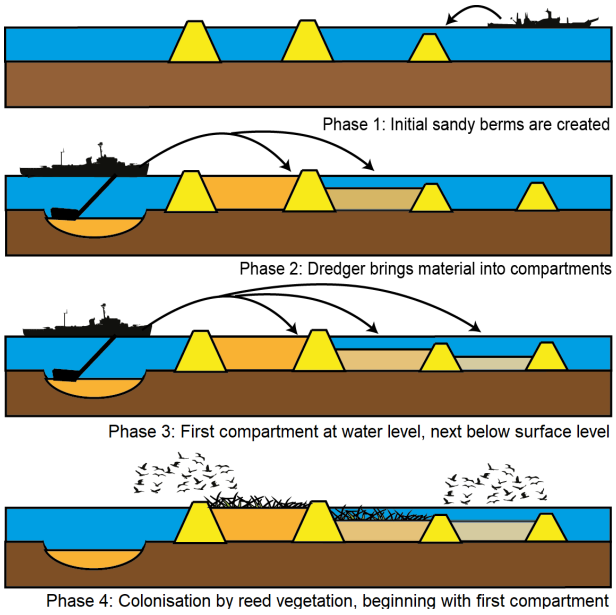

Figure 1.1: Method to build the artificial islands of the Marker Wadden wetland (adapted from *Gerretsen* (2014)). Sand dams create compartments of different heights, wherein the slurry is deposited. The new sediment, above and under water, will be used as habitat for flora and fauna.

The *Markermeer* is an artificial lake with an average water depth of 3.6 m and a surface area of 680 km^2 (*Rozari*, 2009). The uppermost layer of the lake bed consists of a thin (~10 cm) layer of soft silt, of which only the few upper mm's are oxic (*Van Duin*, 1992). A

thick layer of Holocene deposits (clay, peat or sand) is present underneath the soft silt (e.g. www.DINOloket.nl, *Rijkswaterstaat* (1995)).

The resuspension of the uppermost soft silt layer causes high turbidity levels in the lake. Consequently, lake Markermeer suffers from ecological problems (*Van Kessel and de Boer*, 2009; *Noordhuis et al.*, 2016). Herein, the aim of the Marker Wadden project is to locally reduce turbidiy to improve the light climate while creating a new wetland. In this way, the Marker Wadden aims to improve the ecosystem of lake Markermeer by creating more habitats for birds from sediment originating from the lake bed itself. Furthermore, it aims to scale up former building with mud pilot projects (*Dankers et al.*, 2015). Thus, a subsequent objective is to develop the fundamental knowledge and the engineering tools needed for a future broader use of mud as construction material in BwN projects. The research in this thesis is meant to contribute to this development.

Many uncertainties arise when mixing the sediment of the lake bed with water during the construction process:

- The sediment in the borrow area is a mixture of clay, peat, silt, sand and organic matter which exhibits cohesive behaviour.
- After mixing the sediment with water while dredging, the resulting slurry is quite diluted and not suitable for construction.
- Given the heterogeneity at the borrow area, it is difficult to assess the exact composition of the slurry at a given time.
- In the borrow pit, the native sediment is present at different degrees of consolidation and, therefore, different in-situ bulk densities.
- The longer the dredging pipe is, the larger the degree of dilution of the slurry required.
- During the dredging process, oxidation of organic matter and other reductants (i.e. compounds being oxidised in a redox reaction) may occur.
- When the material comes out of the pipe, the sand particles settle faster and closer to this dredging pipe. The fine sediments are transported longer and settle further away from the dumping point. Next to this radial segregation over a longer distance, vertical segregation also occurs. Consequently, differential settling and consolidation behaviour occurs within a single compartment.

The above mentioned uncertainties create the problem of having a non optimal construction material which is dilute and which composition varies largely. The composition varies locally in the borrow pit and also after deposition, because of segregation and oxidation during the dredging and dumping process. Therefore, solutions have to be found in order to build with these heterogeneous Markermeer slurries and to predict its mechanical behaviour. To build the wetland and achieve the desired sediment level and strength, it is first necessary to understand the cohesive behaviour of mud and the properties of each of the components of the sediment mixture. The next section describes sediment composition aspects that affect the physical behaviour during and after construction.

1

1.2. THE NATURE OF COHESIVE SEDIMENT

COHESIVE sediment, often called “mud”, is a heterogeneous particulate and porous material composed of solid, liquid and possible gas phases. The term ”cohesive” refers to the attractive forces between individual clay mineral particles and refers to the ductile behaviour that the sediment shows when being remoulded. Clay minerals have traditionally been defined as particles < 2µm, however some clay minerals can have a size up to 8µm as suggested by *Kontert and Vandenberghe* (1997) and *Buurman et al.* (2001). The solid phase of cohesive sediment is composed of a mixture of these clay minerals, other minerals (such as quartz) and organic matter of different nature and origin. Therefore, the inorganic solid phase is not only composed by cohesive clay minerals but also by non-cohesive silt and sand particles. The liquid phase is mainly water, which can be present in significant amounts: the mass of water can often exceed that of solids, particularly at the surface of unconsolidated sediment (*Grabowski et al.*, 2011). Gases may form primarily as a result of organic matter degradation or penetrate the soil because of the lowering of the water table (desaturation).

The behaviour of cohesive sediment is difficult to characterise, due to the interactions of clay particles with themselves and with other components. This is different from non-cohesive sand (particle size > 63µm) and silt (traditionally defined as particles with size between 2µm and 63µm). Sand particles are mostly composed of silicate minerals (mainly quartz) or rock fragments, while carbonates (shells) and oxides can also present. The mechanical properties of this non-cohesive sediment can be determined by its size distribution. Contrary, the mechanical properties of cohesive sediments depend on the type and content of clay minerals, the interactions between clay mineral surfaces and organic matter, pore water, saline or fresh water depositional environment and the stress history (*Wagner*, 2013). Consequently, hydraulic conductivity and the stress/strain properties of cohesive sediment strongly differ from those of sand. The clay content needed for a sediment to exhibit cohesive properties varies between 5-10% (*Mitchell*, 1976; *Van Ledden et al.*, 2004).

The colloidal size of the clay mineral particles present and their electrical charge lead them to adsorb water, hydrate and interact. Therefore the mechanical behaviour of cohesive sediment depends on its water content. Further, the behaviour of saturated cohesive sediment differs from that of unsaturated sediment. When mud starts to desaturate, a crust may be formed at the surface. However, the behaviour of unsaturated soil is out of the scope of this thesis.

1.2.1. TYPE OF CLAY MINERALS

The term "clay mineral" is defined by *Guggenheim and Martin* (1995) as "phyllosilicate minerals and minerals which impart plasticity to clay and which harden upon drying". In addition to clay minerals, the clay fraction of sediments (traditionally considered < 2µm) often contains non-phyllosilicate minerals, such as carbonates, feldspars, and quartz, together with the (hydr)oxides of iron and aluminium. Such minerals do not impart plasticity to clay and they are referred to as "associated minerals".

Clay minerals are divided in different types: kaolinites, smectites, illites, chlorites, vermiculites and others (e.g. *Holtz and Kovacs*, 1981; *Bergaya and Lagaly*, 2013). The kaolinite structure is formed by repeating layers of one tetrahedral (silica) sheet and one

octahedral (alumina) and is therefore referred to as a 1:1 clay mineral. Kaolinites are usually the largest clay minerals, with a thickness of 1 µm (*Holtz and Kovacs*, 1981). Smectites are 2:1 minerals consisting of two silica sheets and one alumina, where montmorillonite is a relevant member of this group. Montmorillonite minerals are the smallest clay minerals with a thickness of only a few nanometers. Illites also have a 2:1 structure but the interlayers are bonded by a potassium atom. Chlorite has a more complicated structure which could be considered as a 2:1:1 mineral, composed of repeating layers of silica sheet - alumina sheet - silica sheet - $(Mg^{2+}, Fe^{3+})(OH)_6$ sheet. This $(Mg^{2+}, Fe^{3+})(OH)_6$ interlayer sheet is often referred as brucite-like, due to the resemblance to the mineral brucite. As a particular type, vermiculite is a 2:1 mineral comparable to montmorillonite but with only two interlayers of water (e.g. *Murray*, 2006; *Brigatti et al.*, 2013).

The negatively charged surface of clay minerals attracts cations present in water. Furthermore, different clay minerals have different charge deficiencies which result into different tendencies to attract exchangeable cations. In this sense, vermiculite and montmorillonite are the minerals with the greater charge deficiency (and the subsequent greater ability to attract cations) while kaolinite has the smaller charge deficiency. Calcium (Ca^{++}) and magnesium (Mg^{++}) are the predominant exchangeable cations in terrestrial environments at neutral pH, followed by potassium (K^{+}) and sodium (Na^{+}). In acidic soils, aluminium (Al^{+++}) and hydrogen (H^{+}) are common (*Holtz and Kovacs*, 1981).

Different clay minerals exhibit different properties. For a given water moisture, the internal strength is different for every clay mineral. Kaolinite is the stronger mineral, followed by illite and finally smectite (*Wagner*, 2013; *Murray*, 2006). At the same water content, the hydraulic conductivity is lower for smectite than for illite and kaolinite (*Wagner*, 2013; *Murray*, 2006). The compressibility of saturated specimens of clay minerals increases in inverse order: kaolinite < illite < smectite (*Wagner*, 2013). Regarding the swelling/ shrinkage potential, the more plastic the minerals, the higher the potential for swelling and shrinkage (*Wagner*, 2013). In this sense, smectite is the most swelling mineral (*Barshad*, 1955; *Taylor and Smith*, 1986; *Pająk-Komorowska*, 2003; *Barshad*, 1955) while vermiculite does not usually exhibit volume changes to the same extent as smectites (*Taylor and Smith*, 1986). These minerals are followed by smectite/illite interstratified layers, illite and kaolinite. Primary chlorite does not swell much but when it weathers its swelling potential increases (*Kohut and Warren*, 2002).

1.2.2. CLAY FABRIC

The arrangement of clay minerals and their adsorbed water layer constitute the physical basis for the structure of a soil originating from cohesive sediment. Clay particles can flocculate or be repelled (dispersed, separated). In this sense, the presence of ions, organic matter and other environmental conditions such as pH affect the flocculation process and, consequently, the final soil structure.

The presence of salts can reduce the double layer thickness of clay particles, in the same way as exchangeable cations such as K^{+}, and therefore increase cohesion. For high salinity values, clay particles aggregate very fast resulting in an open floc structure. However for lower salinity values, such as the ones present in freshwater systems, the resulting flocs are more compact (e.g *Mietta*, 2010).

The pH also affects flocculation. Contrary to most ions, H^{+} and OH^{-} ions can interact

chemically with the clay's surface and change its surface charge. Sometimes, the surface charge of the clay particles can even be of different sign on the edges and on the faces, causing strong attractions between the positive edge of one particle and the negative face of another. These changes in surface charge occur at low pH (acidic conditions), e.g. *Mietta et al.* (2009).

The salinity in lake Markermeer is low (i.e. freshwater) and the pH is neutral to slightly alkaline (depending on the temperature) (*Van Duin*, 1992). Furthermore they are stable over the whole lake and are not expected to strongly influence the mechanical behaviour of the sediment. Therefore salinity and pH are not addressed in this research. However, organic matter is present at various amounts and quantities at lake Markermeer (*Van Duin*, 1992) and therefore studied. The next subsection explains the nature of organic matter and its interaction with clay.

1.2.3. SOURCES OF ORGANIC MATTER AND INTERACTION WITH CLAY

Organic matter (OM) in the aquatic system originates from anthropogenic, autochthonous and allochthonous natural sources and can exhibit different degrees of degradation (*Hart*, 1986). It can be found in dissolved, particulate or colloidal form. Particulate organic matter (POM) has a size > 0.45 µm while dissolved organic matter (DOM) is operationally defined as < 0.45 µm [1]. Colloidal organic matter is the fraction between 1 nm and 1 µm (e.g. *Mostofa et al.*, 2013). According to the type/composition, OM can be divided in non-humic substances (NHS), humic substances (HS) and black carbon. NHS and HS can be found at any fraction (POM, DOM or colloidal). Black carbon is the strongest light-adsorbing component of POM which originates from combustion processes.

NHS are labile compounds formed by a complex mixture of elements by covalent bonds. They can be classified according to similarities of their functional groups and metabolic functions in organisms (*Libes*, 2009). The most important classes are carbohydrates (e.g. monosaccharide, polysaccharides), amino acids and proteins, lipids and lignins. Lignin is an important carbon source which constitutes approximately 25–30% of the dry weight of carbon in the biosphere (*Artifon et al.*, 2019).

Jones (1998) defined the HS as structurally complex macromolecules with a yellow to black appearance, acidic and generally heterogeneous. Another definition was provided by *Breemen and Buurman* (2002), who defined them as "decomposed plant material that has been transformed to dark-coloured partly aromatic, acidic, hydrophilic, molecularly flexible polyelectrolyte materials". HS consist of carbon, oxygen, hydrogen and sometimes small amounts of nitrogen and occasionally phosphorous and sulphur. In general, the structures can be described as assemblies of covalently linked aromatic and aliphatic residues carrying carboxyl, phenolic and alkoxy groups. However, sulphate esters, alanine, semiquinone, phosphate ester and hydroquinone groups have been found to exist in some humic isolates (*Jones*, 1998). HS are classified in humic acids (HAc), fulvic acids (FAc) and humins according to polyelectrolitic properties and consequent solubility in alkaline and acidic media (*Piccolo et al.*, 1996). FAc are soluble for all pH conditions, HAc only for pH>2 and humins are insoluble for every pH condition. HAcs and FAcs constitute a significant fraction of DOM (40 to 80%) in the aquatic environment (*Artifon et al.*, 2019).

[1] Note this is not a chemical definition but an operational one

Fulvic and humic acids (HAs) are formed from plant and animal residues by microbial decay caused by humification occurring in soils, sediments and natural waters. The presence of HS plays an important role inside the ecosystem dynamics, being a main agent in many physical and chemical processes. FAcs and HAcs are polar organic acids which present hydrophobic and hydrophilic portions within their molecules. They form coatings on clays and minerals that strongly affect the nutrient and contaminant migration in soil and water (*Ghabbour et al.*, 2004). Further, they also interact with organic solute sorption, biomineralisation and metal binding. In this sense, authors as *Abate and Masini* (2003) highlighted that HS, notably the hydrophilic fractions, adsorb on particles of clay minerals and hydroxides of Fe(III), Mn(IV), Al(III) and Si(IV). This adsorption affects their aggregation and colloidal properties in soils and aquatic environments. Herein, functional groups (i.e. groups of atoms) of more labile OM are responsible for most metal binding (*Carrie et al.*, 2012) while the hydrophobic portions of HS, adsorb to black carbon.

In consolidated sediments, OM has undergone significant alteration with a much greater abundance of refractory OM than was initially present during deposition. During diagenesis, most of the functional groups are removed. The potential of subsoils as long-term sinks for organic matter is larger than that of topsoils (*Kaiser and Guggenberger*, 2003) due to the increasing organic matter input to subsoil horizons or layers (e.g. dissolved organic C).

1.2.4. BULK DENSITY, WATER CONTENT AND PLASTICITY

Bulk density (kg/m^3) is dependent on specific particle density, the density and amount of water, and the presence of gas. The definition of water content (w%) varies depending on the field. In soil mechanics, w% is defined as M_w/M_s while in fluid mechanics it is defined as M_w/M_t, where M_w, M_s and M_t are the mass of water, solids and the total mass, respectively. In this thesis the first definition is mainly used.

The water content has an important influence on the behaviour of a cohesive sediment. For instance, it affects its plasticity [2] or propensity to undergo permanent deformation when kneaded. The Atterberg limits describe these transitions: the plastic (PL) and liquid limits (LL) define the minimum and maximum water content needed for plastic response, respectively. A high LL indicates a high compressibility and a high shrinkage/swelling potential. In this sense, many published regression equations for the prediction of the coefficient of compressibility (C_c) are based on the LL (*Terzaghi and Peck*, 1967; *Skempton and Jones*, 1944). The difference between plastic and liquid limit is called the plasticity index PI. The PI has been used to normalise the behaviour of cohesive soils (*Winterwerp and van Kesteren*, 2004; *Jacobs*, 2011). In the plasticity chart (Figure 1.2), the PI is plotted as a function of the LL. This plot can be used not only to classify the sediment between inorganic (above B line) or organic (below A line), but also to estimate the type of minerals present in the sediment sample (*Mitchell*, 1976).

Further, the liquidity index (LI) is a measure of the actual water content (w) in relation to the Atterberg limits, defined as:

$$\mathrm{LI} = \frac{w\% - \mathrm{PL}}{\mathrm{LL} - \mathrm{PL}} \tag{1.1}$$

[2] The plasticity behaviour depends not only on the water content but also on the mineral composition and particle size fractions, eg: *ISO* (2017)

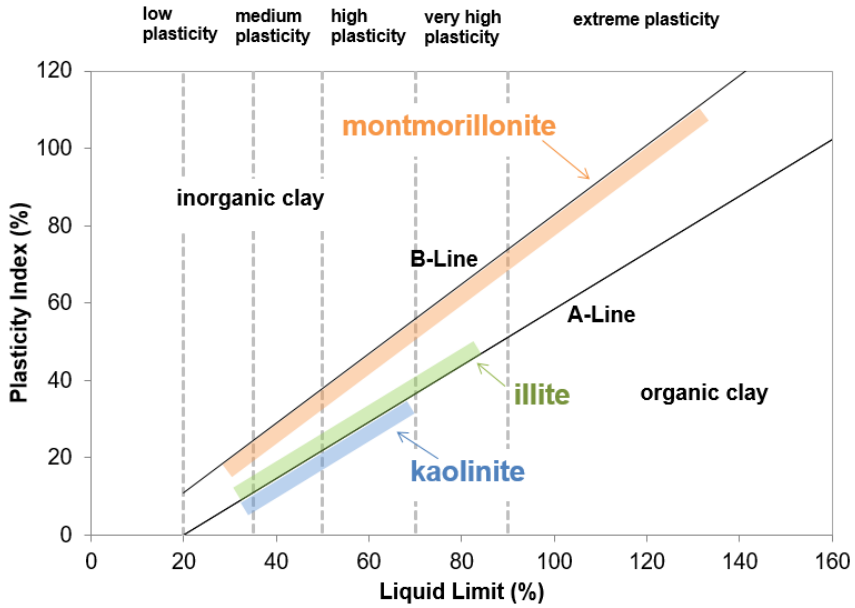

Figure 1.2: Plasticity chart including location if most common clay minerals. Redrawn from *Holtz and Kovacs* (1981).

The LI can be used to approximately correlate different samples with diverse clay contents and minerals. This is relevant because two mud samples from different locations and different dominant clay minerals may have identical densities, while the undrained shear strength, the permeability and the erodibility may differ considerably (*Winterwerp and van Kesteren*, 2004). Consequently, density alone cannot be used to correlate mechanical properties.

1.3. PROBLEM DESCRIPTION

IN building with mud projects, the material properties affect the consolidation time, thickness, strength and structure of newly formed beds. Therefore, to ensure a certain surface of sediment above water and a certain soil strength, attention needs to be paid to the sediment composition. This allows to estimate the behaviour and also the volume of the dredged materials, which determines the costs.

The sediment composition also affects the drying behaviour of the newly formed areas and eventually their fertility and suitability for vegetation colonisation. This vegetation may play an important role during the drying process while contributing to sediment stability. However, by extracting water from deeper sediment layers, plants may affect the level of sediment. Therefore, to comply with a required surface of wetland above water, the drainage effect of plants needs to be known in advance.

Furthermore, consolidation models are important tools for the design of building with mud projects because they allow to scale-up experimental results and predict the engineering behaviour of thicker layers. In this thesis, a 1DV (1 Dimension Vertical) model

was used for this purpose.

All the above mentioned aspects are relevant for the construction of a wetland system, The Marker Wadden, addressed in this thesis. Furthermore, this knowledge is also useful for any other project using cohesive sediment as construction material such as reinforcement of dikes or traditional land reclamation projects or the construction of (Dutch) polders.

1.4. OBJECTIVE & RESEARCH QUESTIONS

THE main objective of this thesis is the understanding and quantification of the consolidation and drying characteristics of a saturated muddy bed partly above water. The research is carried out within the framework of the Marker Wadden restoration project. Therefore, the sediment studied comes from the bed of Lake Markermeer.

Figure 1.3 shows a scheme of all the processes acting during consolidation and drying of the Marker Wadden islands. The initial conditions are driven by self-weight consolidation of a slurry (i.e., a highly concentrated sediment suspension with initial concentration above the gelling point) in a sheltered basin. Contrary to self-weight consolidation of a suspension below the gelling point, slurry self-weight consolidation has not been studied much (*Barciela-Rial et al.*, 2017). After the first layer of sediment has consolidated enough, a new layer of slurry is deposited above. This process is repeated until the desired sediment level above water is achieved. Herein, the bottom layers experience the load of the upper layers of sediment while continue consolidating. The upper interface of the newly formed soil is in contact with air and therefore may start to (partially) desaturate. This sediment-water mixture continues consolidating, expelling pore water. The pore water flow is driven not only by self-weight consolidation but also by capillarity triggered by atmospheric suction (drying by evaporation). At this point, geochemical processes (mostly oxidation) accelerate. Moreover, horizontal drainage towards the water body may occur because of the water head difference (with respect to the lake) and the denser crust. Note that a crust, because it is denser, can be considered as a load over the saturated soft sediment underneath. Thus a crust has a strong effect on the consolidation of this sediment. Furthermore, a crust is less permeable and therefore acts as a lid above the very permeable saturated underlying sediment. After heavy rainfall, surface run-off may occur if the infiltration capacity of the newly formed soil is not sufficient. The process of surface run-off and the formation of an unsaturated crust are beyond the scope of this thesis.

At a final stage, the new soil is colonised with plants, which (*Saaltink*, 2018):

- accelerate desaturation by evapotranspiration
- accelerate aeration and oxidation of the sediment via the roots
- change soil structure.

The cohesive nature of the sediment used and the geochemical changes induced by all acting physical processes during construction and consolidation induce several uncertainties on the mechanical behaviour. The present thesis aims to address some of these uncertainties to gain understanding on the consolidating and drying behaviour of cohesive sediment depending on the solid fraction composition. Herein, the composition of the solid fraction (e.g. particle size, OM amount and type, minerals) and the effect of drainage are also studied. In particular, the research questions of the present study are:

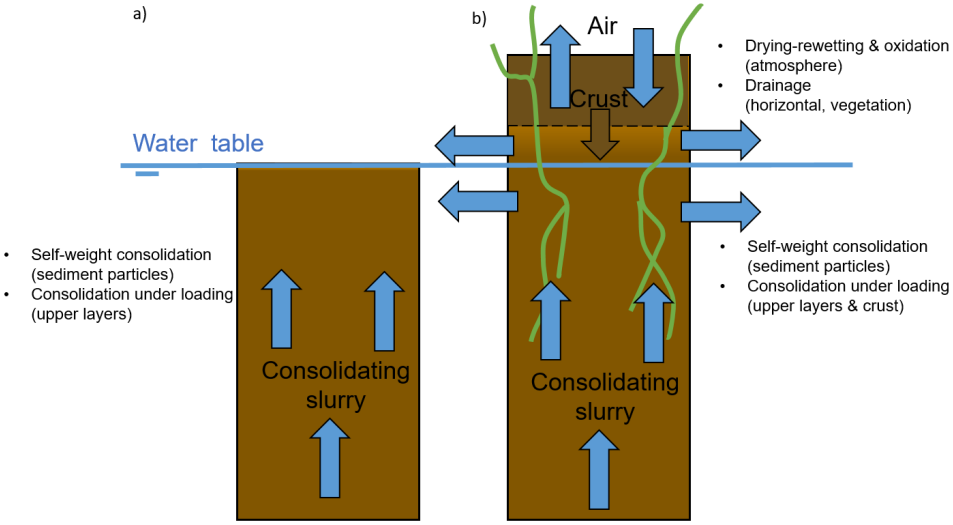

Figure 1.3: Processes acting during the consolidation of Marker Wadden sediment: a) before the sediment emerges over the water table and b) after the sediment has emerged. Self-weight consolidation induces vertical flow of water while the upper layers induce a load over the underlying sediment. When the sediment emerges above the water level of the lake, drying starts and oxidation accelerates. Horizontal drainage occurs if the ground water table of the sediment is above the surface of the lake. As a consequence of the drying of the top layer, a crust may be formed. A crust represents an extra load. Finally vegetation colonises the sediment, draining water, oxidising the sediment and changing the future soil structure. The blue arrows represent water flow.

- How does the initial slurry density, sand content and organic matter affect the consolidation, drying, plasticity and undrained shear strength of Markermeer slurries?
  - Is the effect of natural organic matter dependent only on the amount or also on the type?
  - How does organic matter oxidation affect this behaviour?
  - What are the implications of the mineral composition on this behaviour?
- *Merckelbach and Kranenburg* (2004a) proposed a theoretical model based on a fractal description (*Kranenburg*, 1994) of the behaviour of very soft sediments at low stresses. Is this fractal approach also applicable at the range of stresses of traditional soil mechanics?
  - Which are the most suitable experimental devices to determine the material parameters of slurries and its behaviour under loading?
  - Are the material parameters obtained stress dependent?
  - How do the traditional soil mechanics parameters and the fractal approach correlate?
  - How does initial under/ over consolidation affect the results and its interpretation?
- How does *Phragmites australis* (common reed) and its drainage affect the consolidation of Markermeer slurries?

The approach used to determine the mechanical behaviour was multidisciplinary and experimental. The tests performed were:

- The self-weight consolidation of sediments at concentrations below and above the gelling point was studied with settling column tests.
- The material parameters of the slurries were determined with the settling columns and the Seepage Induced Consolidation test.
- The behaviour under loading was analysed with Incremental Loading (IL) and Constant Rate of Strain (CRS) tests.
- The Hyprop device was used to study the drying of slurries.
- A new column experimental set-up was designed to analyse the effect of drainage and plants on the consolidation of slurries.

The material parameters obtained from the experimental work were used as input in a 1DV point model (*Winterwerp*, 1999), which allowed to scale-up the results.

1.5. THESIS STRUCTURE

IN Chapter 2 the sediment composition is characterised for samples with varying particle size and organic matter types and content. This sediment characterisation is done following standard and non-standard techniques. In Chapter 3, the compressibility behaviour and the undrained shear strength are analysed. Herein, traditional soil mechanics theory is compared with the fractal theory often used from a fluid mechanics approach. Chapter 4 experimentally studies the consolidation of slurries under water, determining the material parameters from settling columns and Seepage Induced Consolidation tests. Furthermore in this Chapter 4, the adaptation of the 1DV model for the study of the consolidation of slurries (initial concentration above the gelling point) is presented and used to up-scale the experimental results. Chapter 5 describes the drying behaviour of the samples and the differences on the water retention depending on composition. Chapter 6 describes the new developed experimental set-up and influence of vegetation and drainage on consolidation and drainage of cohesive sediment. Finally, in Chapter 7, the general discussion, conclusions and recommendations are presented.

2

SEDIMENT CHARACTERISATION

2.1. INTRODUCTION

In this Chapter, the different sediment samples are characterised with standard and non standard procedures. It is shown how some simple but non standard tests, such as the Rock Eval, can provide relevant information to understand differences between samples.

The drying behaviour of the samples detailed in the current chapter is presented in Chapter 5.

2.2. SAMPLE COLLECTION AND PREPARATION

THE sediments characterised originate from Lake Markermeer, The Netherlands. Sediment samples from the uppermost soft silt layer and the underlying Holocene sediment were sampled. The sediment samples were collected from the bed of the lake with a Van Veen grab at two different locations: the Southwest (SW) and the Northeast (NE) site, in the vicinity of the cities of Amsterdam and Lelystad, respectively (see Figure 2.1). The Holocene sediment from the SW site is referred to as clay and the one from the NE site as sandy clay. The uppermost material is referred as soft silt. The sediment was stored after sampling in dark conditions in a climate chamber at 4 °C.

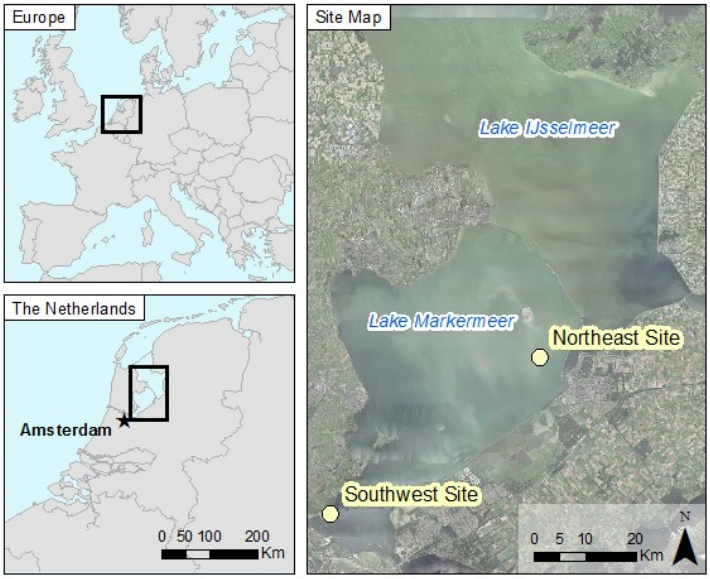

Figure 2.1: Location of the Markermeer (left) and study area with sampling sites (right). Source image: PDOK 2016

Some samples were sieved and separated into fine and coarse fractions before testing to understand the effect of different sand contents that may occur naturally or be caused by segregation during dredging, dumping and deposition. In this sense, not only the characteristics of the bulk samples collected but also of their fine (<63 µm) and coarse fractions (>63 µm) was analysed.

Furthermore, some samples from both sites were pre-treated, prior to the start of the drying (Chapter 5) and compressibility (Chapter 3) tests, to mimic the final natural remoulded behaviour of Markermeer sediment after drying-rewetting cycles and atmospheric oxidation of the OM. Since natural oxidation is slow, the oxidation process was accelerated in the laboratory. Samples were chemically oxidised with hydrogen peroxide (H_2O_2) with a concentration of 6%, following an adapted procedure from the *BS* (1990a). This procedure included two drying-rewetting cycles. First, the samples were dried in an oven at a constant temperature of 50°C, for circa 1 week, until there was no more mass loss with accuracy 0.01 g. Then, subsamples of 100 grams were rewetted by addition of demineralised water and oxidised according to *BS* (1990a). When the oxidation process was finished, the oxidant (6% H_2O_2) was removed by centrifugation, also according to *BS* (1990a). Afterwards, the material was dried again at 50°C and finally rewetted with filtered Markermeer water. The filter had a size of 8-10 µm to remove plankton and other organics and floating woody debris. The pH was measured before and after oxidation by immersing a pH electrode in the samples.

2.3. SAMPLE CHARACTERISATION PROCEDURES

The basic characterisation included particle size distribution, total organic matter (TOM), total organic carbon (TOC), particle density and Atterberg limits (see Table 2.1). The particle density was measured with a gas pycnometer (ISO, 2014a). The following subsections give details on the protocols for sample characterisation. Next, mineralogy was studied for the bulk and clay fractions.

Table 2.1: Description of the samples studied.*Indicates assumed value, not measured.

Site	Depth [m]	Type	ID	Sand [%mass]	Silt [%mass]	Clay [%mass]	D50 [µm]	TOM [%]	TOC [%]	ρ_s [kg/m^3]	LL [%]	PL [%]	PI [%]
Southwest	*0.1-0.5*	*Bulk clay*	*SW1B*	8	63	29	10	8.6	3.3	2530	104	46	58
		Fines fraction	*SW1F*	0	69	31	8	8.7	3.1	2570	129	59	70
		Bulk treated	*SW1T*	8*	63*	29*	10*	6.7	2	2620	60	31	29
	0-0.1	*Bulk soft silt*	*SW2B*	28	54	18	32	6.4	3	2560	103	46	57
Northeast	*0 -0.1*	*Bulk soft silt*	*NE1B*	42	49	9	69	3.4	1.2	2590	72	40	32
		Fines fraction	*NE1F*	0	86	14	26	4.8	2	2540	83	49	34
		Bulk treated	*NE1T*	42*	49*	9*	69*	2.1	0.5	2700	33	23	10
	0.1-0.5	*Bulk sandy clay*	*NE2B*	69	21	10	87	2.1	0.7	2640	41	25	16
		Sand fraction	*NE2S*	100	0	0	108	0.3	0.1	2710	-	-	-

2.3.1. PARTICLE SIZE

The particle size distribution was determined for all dispersed natural samples by hydrometer and dry sieving according to *BS* (1990b). The particle size distribution of primary particles of the treated samples is assumed to be the same as of the original natural sample. The natural clay samples from the Southwest site are less sandy than those from the Northeast site. The sand can be classified as fine for all samples (i.e. 0.063 - 0.15 mm). The coarser particles all consisted of fragments of shells and large OM particles, see Figure 2.2). The upper part of the bed (i.e the soft silt layer) was bioturbated and showed the presence of more shells (carbonates) with respect to deeper sediments. At the Southwest of the Lake, the upper soft silt layer (SW2B) is sandier that the underlying clay layer (SW1B)

whereas the pattern is the opposite in the Northeast (comparison NE1B with NE2B).

To check if the treatment causes particle aggregation, the particle size distributions of treated and untreated samples were compared with the Malvern particle sizer. All the samples were previously deflocculated with 5 minutes ultrasonic bath. The use of the Malvern instead of hydrometer was necessary because of the limited amount of material. The measurement showed that some aggregation occurred (see Figure 2.3). These results are used only qualitatively.

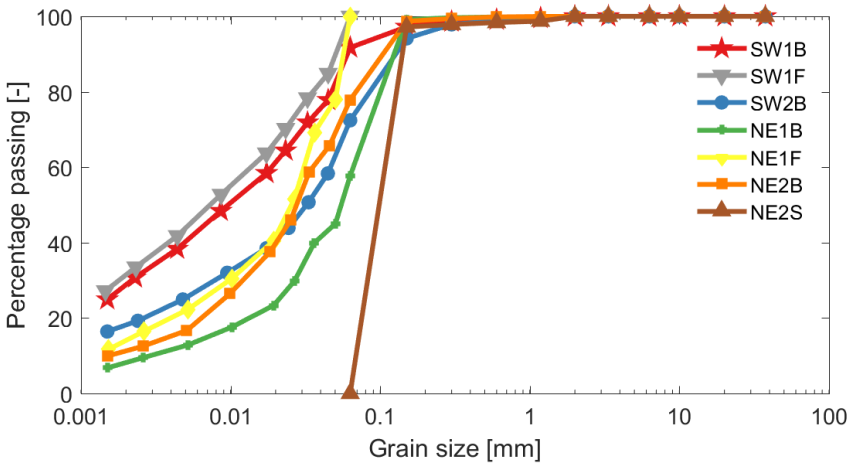

Figure 2.2: Particle size distribution of the various samples, determined by hydrometer and sieving

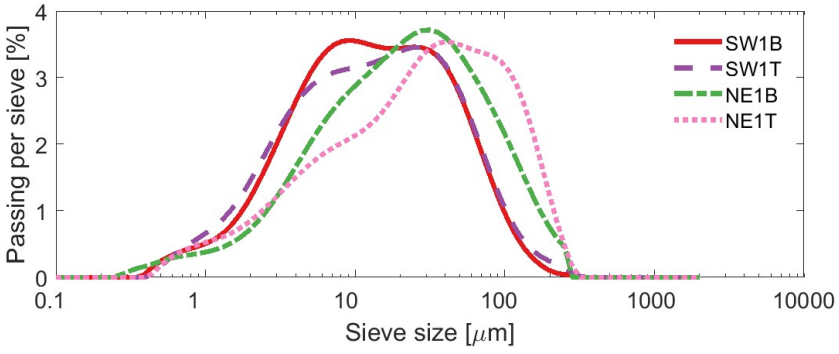

Figure 2.3: Particle size distribution measured with the Malvern2000 for samples SW1 and NE1 before (SW1B, NE1B) and after (SW1T, NE1T) treatment.

2.3.2. TOTAL ORGANIC MATTER (TOM)

The TOM content was determined by loss on ignition (LOI) according to *RAW124* (2005) and European *Standard* (2012), through which identical mass losses were obtained. The

treatment, including chemical oxidation, decreased the LOI from 8.6 to 6.7% for the natural clay from the Southwest site and from 3.4 to 2.1% for the natural clay from the Northeast. The main reason why it was not possible to oxidize all OM may be that sorption to minerals reduces the susceptibility of OM to oxidation, as explained by *Kaiser and Guggenberger* (2003).

In general for Markermeer sediment, the sandier the natural clay is, the lower its TOM. The specific particle density also increases for natural samples when more sand is present (see Table 2.1). For the SW clay, the LOI after sieving decreased and the particle density increased. This may be due to the presence in the mother sample of big organic elements, e.g. fibrous plant remains, which were removed by sieving. For the NE clay, the particle density increased when the particle density was measured after LOI and for the treated samples. This is due to the reduction of TOM present in the sample (see Table 2.1).

2.3.3. ROCK EVAL AND TOTAL ORGANIC CARBON (TOC)

The Rock Eval test (*Behar et al.*, 2001) was used to determine the type of organic matter according to its kerogen (solid OM) type and lability (reactivity). The Rock Eval consists of a two-step process, which involves pyrolysis in an inert atmosphere and subsequent combustion in an oxic atmosphere. However, not all the kerogen in the sediment can be converted to hydrocarbons and there is always some inert carbon left at the end of a Rock Eval test. The amount of pyrolysable carbon (PC) and the proportion of residual carbon (RC) were determined. The sum of the PC and the RC is the TOC. The residual carbon (total weight %) refers to strongly resistant and refractory compounds (*Carrie et al.*, 2012).

The PC corresponds with the labile OM and comprises three major fractions: S1, S2, and S3. S1 and S2 are measured by flame ionisation detection (FID). The S1 fraction (mg hydrocarbons (HC)/g sample) is composed of small volatile molecules. Figure 2.4 shows that there is a larger amount of these volatile molecules (S1 fraction) present in the uppermost material. Furthermore, the curves are steeper, which also suggests that the OM of the upper layers reacts fiercer. The S2 fraction (mg HC/g) comprises larger, thermally cracking molecules of hydrocarbons originating from kerogen (e.g. algal cell wall detritus). Figure 2.4 shows that the S2 fraction also reacts at lower temperature for the uppermost bioturbated material of both sites. This suggests that the OM of the top layer of the bed is more labile (i.e. reactive) at both sites. From the S2 fraction, the hydrogen index (HI) was determined, which represents the relative importance of hydrogen-rich aliphatic compounds (*Carrie et al.*, 2012). The HI was calculated as S2 fraction of the carbon divided by all the carbon in the kerogen (i.e. the TOC). The HI decreases with the degree of degradation of the OM (*Disnar et al.*, 2003). By relating the temperature T_{max} at which the highest amount of organic material reacts (see peak in S2 curve on 2.4) against the HI, the organic matter can be characterised as a function of its kerogen type (*Lafargue et al.* (1998); *Carrie et al.* (2012)). All Markermeer samples were characterised as Type III, according to their kerogen type. This type represents gas prone, low hydrogen content, mostly terrestrial origin organic matter. Thus, despite of the different lability, the fact that T_{max} is the same for all materials indicates that their composition is still similar.

The S3 fraction is measured in mg CO_2/ g dry sediment and comprises oxygen-containing organic molecules. The S3 fraction was used to calculate the Oxygen Index OI. Contrary to the HI, the OI increases as the OM undergoes greater degradation/oxidation

(*Disnar et al.*, 2003; *Carrie et al.*, 2012). Thus, the ratio OI/HI (Table 2.2) can be used as an estimate of the degree of degradation of the organic matter: the higher this ratio, the higher degree of degradation. The results show that this ratio is larger for the sandier samples than for the finer ones. Furthermore, Table 2.2 also shows that the treatment increased the OI/HI value.

The RC obtained for the samples SW1B and SW2B was 2.5% TOC and 0.9% TOC, respectively. The fact that the TOC values of the treated samples (Table 2.1) are larger than the RC value of the original samples suggests that not all the non-residual carbon present of the original sediment is oxidizable with H_2O_2.

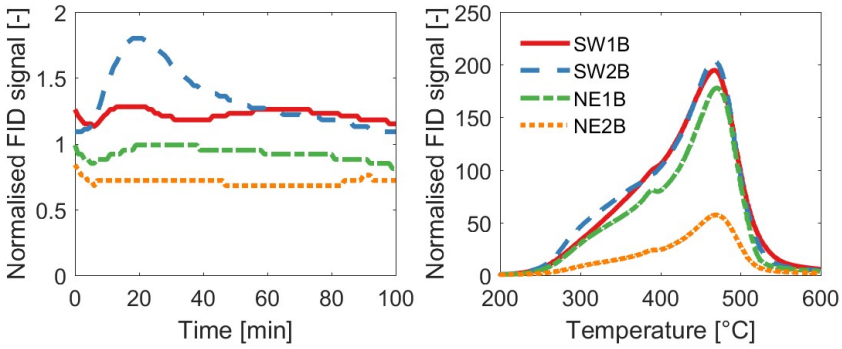

Figure 2.4: Rock Eval results for uppermost soft silt and deeper samples of both sites showing the S1 curve (volatile compounds; left) and the S2 curve (right). Vertical axis: flame ionisation detection (FID signal).

Table 2.2: Values of the HI, OI and OI/HI ratio obtained from the Rock Eval test.

ID	*SW1B*	*SW1F*	*SW1T*	*SW2B*	*NE1B*	*NE1F*	*NE1T*	*NE2B*	*NE2S*
HI [-]	157	154	157	201	201	230	206	185	83
OI [-]	204	216	289	223	275	230	387	303	458
OI/HI [-]	1.30	1.40	1.84	1.11	1.37	1.0	1.88	1.64	5.5

TOC and TOM are related depending on the type and state of decomposition and can be converted (e.g. *Schumacher* (2002)). Traditionally, a conversion factor of 1.724 (*Nelson and Sommers* (1996)) has been used (i.e., g OM /l.724 = g TOC). However, there is no universal conversion factor as it depends on OM composition. Different conversion values were observed for the different Markermeer samples.

2.3.4. ORGANIC FUNCTIONAL GROUPS

Identification of the functional groups (carboxylic acid, alcohols, etc.) was performed with Nuclear Magnetic Resonance (NMR) to get more insight on the type of OM present in Markermeer sediment.

Nuclear magnetic resonance (NMR) is a physical process in which a nuclei absorbs and re-emits electromagnetic radiation while exposed to a magnetic field (*Barton and Schnitzer*, 1963; *Wershaw*, 1989). When the hydrogen-1 nuclei is used, the test is referred

to as proton NMR or 1H NMR. In the same way, carbon-13 NMR (also known as 13C NMR or carbon NMR) is the carbon analogous to proton NMR (1H NMR). 13C NMR identifies carbon atoms in an organic molecule like proton NMR identifies hydrogen atoms. *Baldock et al.* (1992) divided the carbon NMR spectra into four regions according to their chemical shift (ppm). These four main spectral regions correspond to: 1) alkyl carbon for 10–45 ppm, 2) O-alkyl carbon for 45–110 ppm, 3) aromatic and phenolic carbons for 110–160 ppm and 4) carboxyl and carbonyl carbons for 160–200 ppm. These regions were further detailed by e.g. *Mao et al.* (2000).

A NMR test can be done on a solid state or liquid (solution) state of the material (*Wershaw*, 1989). The latter has been proven to provide more detailed structural information due to increased resolution as compared to solid-state NMR methods (*Simpson et al.*, 2008; *Clemente et al.*, 2011). Consequently, various authors tried to combine and correlate the traditional solid carbon NMR with 1H liquid state NMR (*Clemente et al.*, 2012).

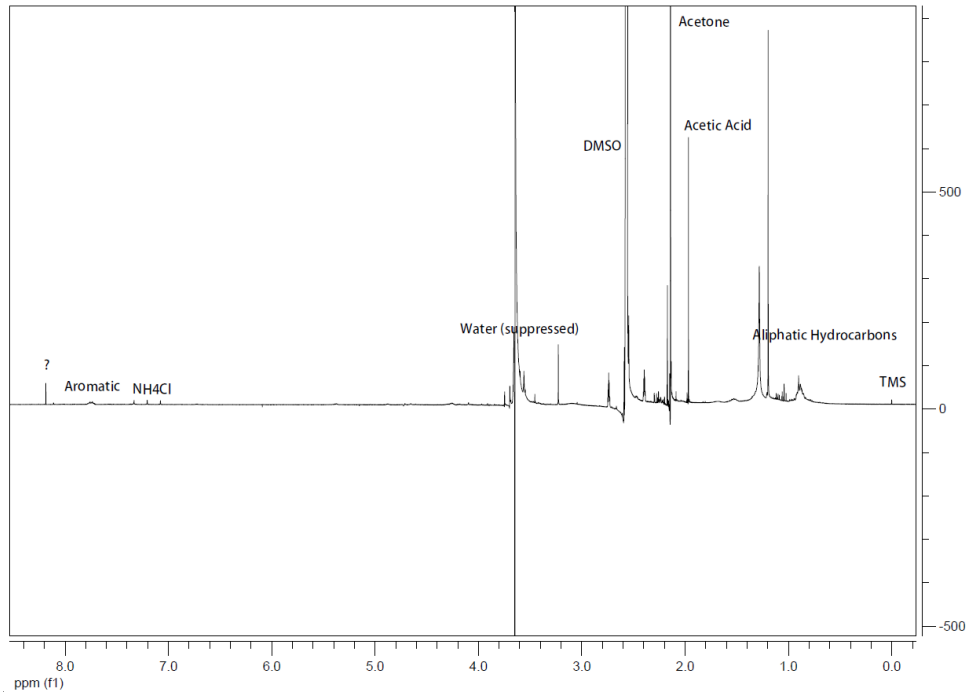

Figure 2.5: Preliminary solution state 1H NMR prior to desiccation- acetone extract. The y-axis represents the intensity of the signal. The x-axis represents the chemical shift in parts per million (ppm).

The procedure used in the present research consisted of acetone Soxhlet extraction of the OM (*Luque de Castro and Priego-Capote*, 2010) and subsequent analysis with liquid state 1H NMR. The original objective was to identify the functional groups present and link the behaviour of the sediment to a particular type of OM. However, given the large variability of compounds present, this was not possible. As a result, only sample SW1B (TOC 3.5%) was analysed. A preliminary proton NMR was performed directly on this extracted organic matter. The results of this preliminary test are shown in Figure 2.5:

ammonium chloride (or some other salt of ammonia), some kind of aromatic hydrocarbon (a derivative of benzene) and long chain organic molecules (kerosene) were identified. Next to these compounds, a peak was observed at 2.5 ppm, corresponding with the solvant used (DMSO). Furthermore, the result of this first proton NMR showed that there was still acetone and moisture water present. Therefore, the extracted OM was placed in a desiccator (with vacuum) for 20 days until only dry organic matter stuck to the walls of the container. The dried extracted OM was analysed again with liquid state 1H NMR, but also with liquid 13C NMR to see if more clear results could be observed. All the NMR tests were performed at a constant temperature of 25 degrees Celsius. The solvent used during all NMR tests was DMSO (Dimethyl sulfoxide).

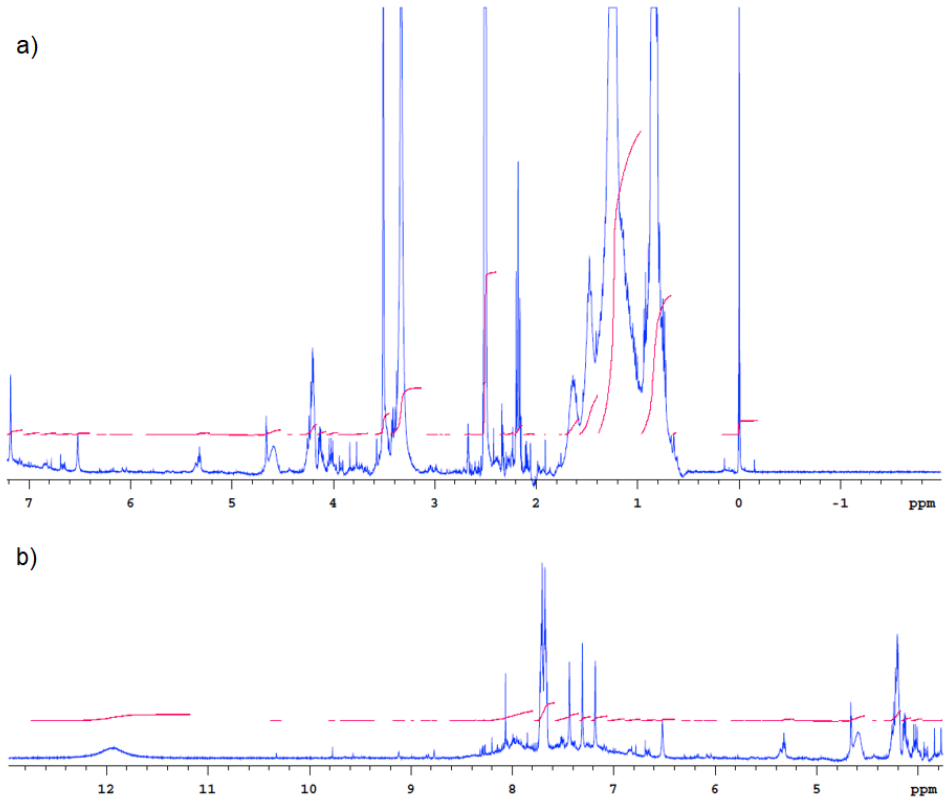

Figure 2.6: Solution state 1H NMR after desiccation- acetone extract. The y-axis represents the intensity of the signal. The x-axis represents the chemical shift in parts per million (ppm): a) range between 7 and -1 ppm; b) range between 12 and 5 ppm.

Figure 2.6 shows the results of the solution 1H NMR after drying of the extracted OM, where the presence of the compounds already identified in the preliminary test can be more clearly observed: ammonium chloride, aromatic hydrocarbon and long chain organic molecules. However, the results from the 13C NMR were inconclusive because peaks of compounds could not be identified separately because of noise over the whole

spectra.

2.3.5. MINERALOGICAL COMPOSITION

X-ray diffraction (XRD) (e.g. *Moore*, 1989)) was used to determine the mineralogical composition of the samples and mineralogical changes due to chemical oxidation. Both the bulk and the clay fraction were analysed by XRD. The analysis was performed at the laboratory of Q-mineral, Belgium. For the bulk sample, 2.7 g of each mother sample was subsampled. To each subsample, 0.3 g of Zincite (ZnO) was added. The mixtures were mixed and ground in a McCrone micronizing mill in ethanol. After drying, the samples were analysed with the XRD using CuKα radiation. For the clay fraction, the < 2 µm fraction of a representative part of about 5 g of each mother sample was separated. The size separation was performed by centrifugation after thorough chemical treatment to remove cementing agents (carbonates, OM, iron and manganese oxides/hydroxides). In the < 2 µm subfraction, all minerals were exchanged to their Ca-form, i.e., removing all exchangeable cations of the mixed layers in the clay and replacing them by Ca (Calcium). Clay minerals were reoriented (i.e., reorganised) by sedimentation in porous ceramic plates (*Shaw*, 1972). This reorientation aims to increase the basal reflections to be measured. Basal reflections give the thickness of the silicate layers. For most layer silicates, basal reflections are of the Miller index type 00L, being L an integer. The oriented minerals were analysed by XRD measuring their 00L reflection (*Zeelmaekers*, 2011). The systematic absence (and variations) in the reflection intensity indicate the positions of atoms in the unit cell. The XRD patterns were refined with the Rietveld method (*Rietveld*, 1969). The XRD analysis on the bulk mineralogical composition of the samples (Table 2.3) showed that all sediment types have a similar mineralogy, and that they mainly consist of quartz (36.5-47.7%) and feldspar minerals (8.5–14.3%). The samples have considerable calcite contents (7-9%), which is the dominant carbonate. The calcite amounts present in the Markeermeer sediment are large enough to buffer pH. This was proved by chemical oxidation of the samples, which lowered the pH of the sediment samples by only 0.4 units (from 7.9 to 7.5). From the oxides group, hematite is identified at low concentrations (<1%). Pyrite is the dominant sulphide identified (which indicates in-situ anoxic conditions), albeit in low concentrations (<1%).

Regarding the clay minerals, the 2:1 AL phyllosicates are the most abundant (13.0-35.6 %). This differs from the assumption of chlorite being the dominant phyllosilicate at Markermeer made by *De Lucas Pardo* (2015). This author used Environmental Scanning Electron Microscope (ESEM) to estimate the mineralogical composition. However, XRD is a more reliable, direct method to characterise clay mineralogy. The results of the mineralogical analysis of the clay fraction (Table 2.4) reveal that three types of 2:1 phyllosilicates were present: illite, smectite and mixed layers illite/smectite. All samples have a comparable composition in their clay fraction. This suggests that the applied treatment did not change the general soil mineralogy. However, the present analysis of the clay fraction showed a gentle increase in the ratio smectite/illlite minerals after treatment (Table 2.4). This spread in the value may be due to sample heterogeneity. Further research is needed to determine whether this increase is significant.

Soukup et al. (2008) pointed out that the effective use of H_2O_2 for OM removal requires acidic conditions. However, the pH for Markermeer samples stayed alkaline after the

Table 2.3: Quantitative bulk mineralogical compositions (in weight percentages) of the crystalline fraction of the various samples

ID	SW1B	SW1F	SW1T	SW2B	NE1B	*NE1F*	*NE1T*	*NE2B*	NE2S
Non-phyllosilicates									
Silicates									
Quartz	36.5	n.a.	42.2	47.7	45.8	46	46.5	59.8	n.a.
Plagioclase	6.6	n.a.	6	7.5	8.2	6.5	6.8	8.7	n.a.
Alkali feldspar	1.9	n.a.	7.1	3.5	3.7	6.3	7.5	4.6	n.a.
Carbonates									
Calcite	9.1	n.a.	6.9	8.6	11.9	11.7	11.4	7.3	n.a.
Dolomite	1.3	n.a.	1.3	1	2.8	2.1	1	2.1	n.a.
Ankerite (Fe0.2)	0.1	n.a.	-	0.3	-	-	-	-	n.a.
Ankerite (Fe0.54)	0.2	n.a.	-	0.2	-	-	-	-	n.a.
Ankerite (Fe0.68)	0.2	n.a.	-	0.1	-	-	-	-	n.a.
Oxydes/Hydroxides									
Hematite	0.3	n.a.	-	-		-	-	-	n.a.
Rutile	0.2	n.a.	-	0.1	0.1	-	-	0.2	n.a.
Anatase	0.3	n.a.	0.1	-	0.3	0.4	0.2	0.1	n.a.
Sulphides/Sulphates									
Pyrite	0.6	n.a.	0.7	0.6	1	1.2	0.7	0.4	n.a.
Gypsum	-	n.a.	0.4	-	-	1.2	0.2	-	n.a.
Total Non-phyllosilicates	57.3	n.a.	64.7	69.7	73.7	75.4	74.3	83.2	n.a.
Phyllosilicates									
2:1 Al phyllosilicates	35.6	n.a.	32	26.6	22.1	22.9	22.4	13	n.a.
Kaolinite	2.2	n.a.	1.9	1.2	1.9	0.8	1.7	2.5	n.a.
Chlorite	4.9	n.a.	1.4	2.4	2.3	0.9	1.6	1.6	n.a.
Total Phyllosilicates	42.7	n.a.	35.3	30.3	26.3	24.6	25.7	16.8	n.a.

Table 2.4: Quantitative clay mineralogy of the < 2µm fraction of various samples (in weight percentage)

ID	SW1B[1]	SW1F	SW1T[3]	SW2B[1]	NE1B[2]	NE1F[3]	NE1T[2]	NE2B[2]	NE2S
Illite/Smectite mixed layer	31	n.a.	42	33	46	43	40	47	n.a.
Illite (I)	29	n.a.	12	28	18	13	13	18	n.a.
Kaolinite	10	n.a.	10	11	5	10	10	5	n.a.
Smectite (S)	24	n.a.	33	22	27	30	34	26	n.a.
Chlorite	6	n.a.	3	6	4	4	3	4	n.a.

[1]Abundances of 65 % I and 35 % S in the I/S mixed layer
[2]Abundances of 73 % I and 27 % S in the I/S mixed layer
[3]Abundances of 72 % I and 28 % S in the I/S mixed layer

treatment. This is caused by the presence of carbonates, which were not removed prior to chemical oxidation. Carbonates were left to avoid large changes in pH and protect the clay minerals, mimicking natural oxidation conditions. Because the mineralogy before and after chemical oxidation was observed to be very similar, we show that most of the known drawbacks of hydrogen peroxide as reactant (*Mikutta et al.*, 2005) can be avoided when adapting the procedure according to the sediment composition. Yet, the treatment dissolved carbonates and changed soil texture and consistency. Mineralogy also influences the effect of drying-rewetting on aggregation -e.g. *Burroughs et al.* (1992); *Mermut et al.* (1997). Soils dominated by swelling clays show low aggregate stability, while oxides and kaolin clays are responsible for highly stable aggregation (*Six et al.*, 2004). Smectite is the most swelling mineral (*Barshad*, 1955; *Taylor and Smith*, 1986; *Pająk-Komorowska*, 2003; *Barshad*, 1955), followed by smectite/illite interstratified layers, illite and kaolinite. Primary chlorite does not swell much but when it weathers it shows increasing swelling potential because of the breakup of the interstratified hydroxyl layer (*Kohut and Warren*, 2002). Conversely, smectites swell less after weathering. Consequently, the changes on the clay fraction before and after treatment may be an indication of changes on the sensitivity to swelling of the samples caused by the treatment, provided that they are not caused by sample heterogeneity.

The presence of ankerite in the Markermeer sediments was unexpected as this mineral is usually formed under hydrothermal condition or in deeper sediments and usually involves warm conditions (*Deer et al.*, 1992). *Jorstad, K., Salbu, B., and Roaldser* (1982) reported ankerite being formed in the bed sediments of a Norwegian lake (50-60 cm depth) with pyrite underneath. Some analogue may exist with our study site but it is beyond the scope of this thesis to further study this.

2.3.6. SOIL CONSISTENCY

The consistency or Atterberg limits were determined for remoulded samples according to the international standard (ISO, 2012). For the liquid limit (LL), fall cone tests were performed using an 80 grams cone with tip angle of 30°. The plastic limit (PL) was determined by the rolling thread test. The results are shown in Table 2.1. Most non treated samples showed a plasticity index (PI) higher than 30 (Figure 2.7) and can therefore, be classified as highly plastic (*Sowers*, 1979). The plasticity chart can also be used to link mineralogy to plasticity (*Dumbleton et al.*, 1966; *Bain*, 1971). For the sediment studied, this plasticity chart suggests the dominance of illite over smectite present, which is consistent with the XRD results.

The Markermeer sediments vary in lithology and OM content. A lower content of fine sand mostly implies a higher content of OM (Table 2.1) and an increase of the value of the consistency limits for Markermeer sediment. This increase in Atterberg limits is due to the higher contents of organics and clay minerals that are available to trap and hold water. Consequently, the materials from the Southwest site showed higher Atterberg limits (Table 2.1).

The more labile upper bioturbated samples (Figure 2.7) also seem to bind more water (Table 2.1). For instance, for the Southwest sampling site, the bioturbated mud has almost identical consistency indices than the deeper clay deposit despite the higher sand and lower OM content of the bioturbated sediment. This may be caused by the higher lability

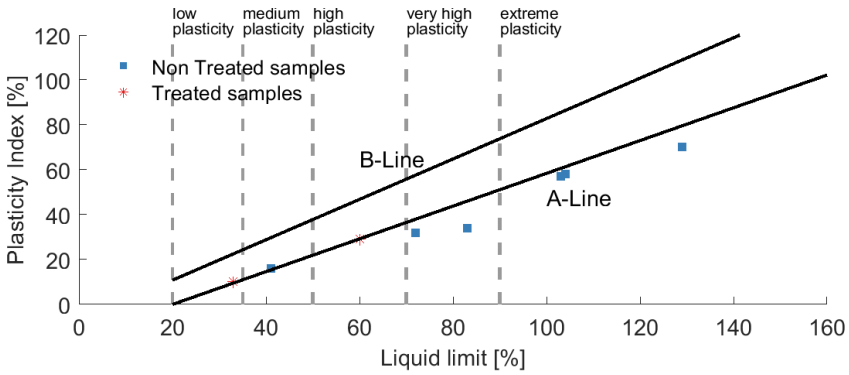

Figure 2.7: Plasticity chart for the samples studied.

of the organics (Figure 2.4), which suggests the necessity of a more detailed composition characterisation than in traditional engineering practice. The Atterberg limits show a decrease with increasing sand fraction and an increase with increasing TOC (Figures 2.8 and 2.9, as expected.

The H_2O_2 treatment decreased the LL from 104% to 60% for the Southwest sediment SW1B and from 72 to 33% for the Northeast sediment NE1B. The PL went from 46 to 31% for the Southwest SW1B and from 40 to 23% for the Northeast NE1B. Consequently, the sediment was less able to hold water. SW1T has a PI below 30% and is classified as a medium plastic clay, while NE1T is just slightly plastic with a PI of 10%. These treated samples are plotted as outliers in Figure 2.8 and Figure 2.9. The few treated samples follow a correlation with the same slope as the non-treated samples but lower because of smaller ability to bind water. Here, these treated samples combine the effect of changes in OM composition by oxidation with drying. The effect of natural OM on Atterberg limits has been shown before by diverse authors (e.g. *Zuur*, 1958; *Terzaghi et al.*, 1996).

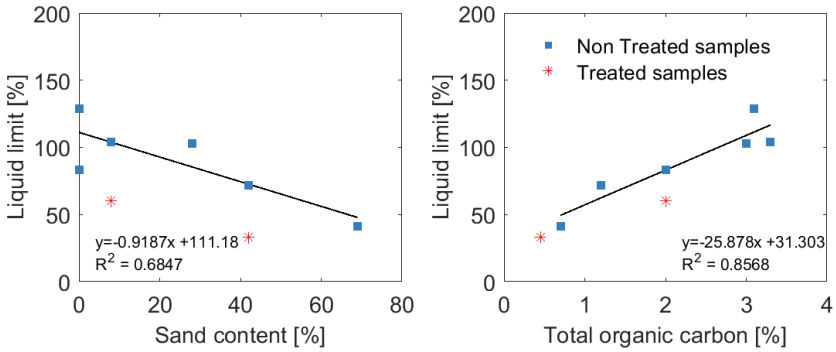

Figure 2.8: Liquid limit as a function of the sand (left panel) and TOC (right panel) contents.

A correlation of organic matter content with the consistency limits was found, in the same way as *Keller and Dexter* (2012). Further, a linear relationship was found between

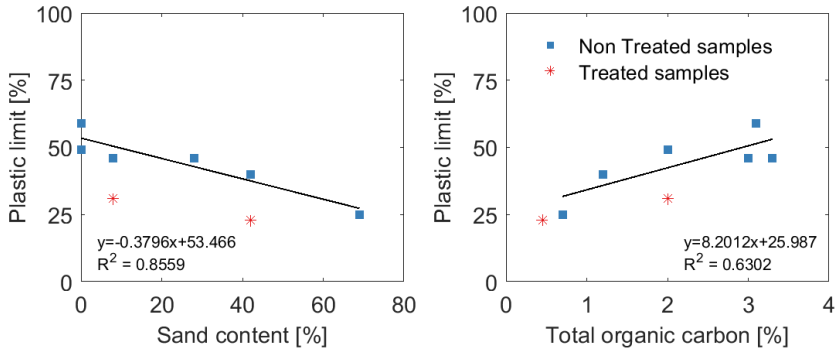

Figure 2.9: Plastic limit as a function of the sand (left panel) and TOC (right panel) contents.

the Atterberg limits and sand content, which agrees with literature as well (e.g. *Kumar and Wood*, 1999; *Al-Shayea*, 2001; *Mitchell and Soga*, 2005).

3

THE EFFECT OF SLURRY COMPOSITION ON ITS COMPRESSION AND SHEAR BEHAVIOUR

Parts of this chapter have been submitted to Canadian Geotechnical Journal.

3.1. INTRODUCTION

SANDY sediment is becoming scarce. Therefore there is an increasing need to use cohesive fine sediments for land reclamation and nature building. These sediments exhibit larger deformations and consolidation time than sandy sediment, and are therefore more challenging building materials to use.

In Lake Markermeer, The Netherlands, a pilot wetland is being constructed with the cohesive fine sediment from the bed of the lake itself. This wetland is referred to as the Marker Wadden. The behaviour of such cohesive sediment varies greatly with small variations of sediment composition (e.g. *Barciela-Rial et al.*, under review). Subsequently, determining the local material properties prior to construction becomes important.

The construction procedure to build the Marker Wadden consists on building sand bars which create protected areas where slurries are deposited and allowed to settle and consolidate (see Figure 1.1). The material parameters of the slurries, and the subsequent mechanical behaviour, depend on the sediment composition. During the construction of the Marker Wadden, segregation and oxidation of the sediments may occur (e.g. *Ganesalingam et al.*, 2013; *Van Olphen*, 2016). Subsequently, the behaviour of Markermeer sediment may change. The effect of sand content on the mechanical properties of clayey sediments has been substantially studied over the last decades. For example, *Cabalar and Mustafa* (2015) showed the decrease of the liquid limit and undrained shear strength with an increasing percentage of sand in a clay matrix. *Al-Shayea* (2001) found a large decrease on permeability with decreasing sand content from 100 % to 60% sand, below which the reduction was less significant. In the same line, other authors (e.g. *Thevanayagam et al.*, 2002; *Winterwerp and van Kesteren*, 2004; *Monkul and Ozden*, 2007; *Peters and Iv*, 2010; *Jacobs*, 2011) studied the effect of sand content on the behaviour of clay-sand mixtures and determined a Transition Fines Content (TFC) threshold. Sand-dominated sediment with granular behaviour changes to fines-dominated sediment with cohesive behaviour when the fines content is beyond the TFC. *Simpson and Evans* (2016) found that this TFC depends on the mechanical property studied. The effect of organic matter (OM) has also been studied, e.g. *Santagata et al.* (2008) related an increase of 8-10% of OM with a three- to fivefold increase in permeability of a normally consolidated soil. *Zentar et al.* (2009) found an increase of the consistency limits with increasing OM content.

Furthermore, over the last years, there is an ongoing discussion about the influence of slurry density on the resulting in situ density (*Reid and Fourie*, 2015). In this sense, *Martins et al.* (2001) and *Nocilla et al.* (2006), identified sediments for which the compression curves were a function of the initial void ratio and non-convergent and therefore without an unique Normal Consolidation Line. Later, *Shipton and Coop* (2012) found that, while for some of the soils they investigated convergent or non-convergent behaviour could be identified at small stresses, other soils needed to be tested at high stresses (>1000 kPa) to confirm if convergence occurs.

The incremental loading (IL) test or oedometer test (e.g. *ISO/TS*, 2004a) has traditionally been used for the determination of the consolidation parameters of clayey sediments. More recently, the CRS (Constant Rate of Strain) consolidation test has gained acceptance as a more suitable test for the determination of consolidation properties of fine grained soils instead of IL tests (e.g. *Fox et al.*, 2014), because of the continuous monitoring of the pore water pressures. The behaviour of cohesive soils is strain rate dependent and

hence the results of a CRS test are sensitive to the imposed rate of strain (e.g. *Crawford*, 1988; *Holm*, 2016). However, by imposing limits on the strain rate, CRS tests provide comparable results to IL test. Furthermore, a CRS test provides continuous effective stress data rather than only at the end of each loading interval. In the present paper, the compressibility behaviour of Markermeer sediment is studied with both IL and CRS tests.

To analyze CRS results, *Smith and Wahls* (1969) suggested a theory assuming a constant coefficient of volume compressibility m_v, i.e. the relationship between strain and effective stress is linear. Later, *Wissa et al.* (1971) developed a non-linear theory, assuming a constant coefficient of compression C_c. *Sheahan and Watters* (1997) suggested modified non-linear equations. In 2006, the American Society for Testing and Materials (ASTM) standardised the CRS tests with a norm describing a procedure not suitable for very soft sediment. This standard was updated (*ASTM*, 2014) including the modifications suggested by *Fox et al.* (2014). From the 80's, work has been done on the application of CRS for very soft clayey soils undergoing self-weight consolidation. *Umehara and Zen* (1980) developed a new interpretation of the test results accounting for large strain and based on finite difference solutions of the basic equation of consolidation.

Merckelbach and Kranenburg (2004a) proposed a theoretical model, based on the clay and sand volume fractions, for clay dominated soil . This model is referred as the fractal model because it is based on a fractal description (*Kranenburg*, 1994) of the sediment and its mechanical properties. The self-similarity on all scales, on which this fractal model is based, implies an unique relationship between aggregate size and number of primary particles that form the aggregate (*Kranenburg*, 1994). The fractal model has proved to work well with slurries (*Winterwerp and van Kesteren*, 2004) yielding power relationships between the water content and the hydraulic conductivity and effective stress. Therefore, *Winterwerp and van Kesteren* (2004) promoted the use of power low relationships for soft sediments (e.g. *Liu and Znidarčić*, 1991) instead of widely used exponential relationships (e.g. *Wichman*, 1999; *Bartholomeeusen et al.*, 2002; *Van Kessel and de Boer*, 2009).

In this chapter, the consistency, undrained shear strength and compressibility of natural as well as sieved and treated (dried-rewetted and oxidised) Markermeer slurries with varying sand, organic matter and initial water content were analysed. The differences on undrained shear strength and compressibility upon IL and CRS were quantified using the fractal theory. Finally, swelling behaviour was quantified using the CRS test.

3.2. THEORETICAL BACKGROUND

The fractal model for clays (*Merckelbach and Kranenburg*, 2004a; *Winterwerp and van Kesteren*, 2004) is based on the volumetric concentration of sediment ϕ_s:

$$\phi_s = \frac{V_s}{V_t} \tag{3.1}$$

where V_s is the volume of solids and V_t is the total volume. When only fines (i.e. particles <63 µm) are present, $\phi_s = \phi_s^f$, where ϕ_s^f is the volumetric concentration of fines. However, if the sediment also contains some passive sand (i.e. there is not a sand skeleton), the ϕ_s can be corrected (ϕ_{corr}, *Winterwerp and van Kesteren* (2004)) for the amount of sand

present according to Equation 3.2.

$$\phi_{\text{corr}} = \left(\frac{\phi_s^f}{1 - \phi_s^{sa}} \right) \tag{3.2}$$

ϕ_s^{sa} is the volumetric concentration of sand. When sand is present, ϕ_{corr} should be used instead of ϕ_s in the equations presented in this section.

The undrained strength c_u can be approximated by the yield strength τ_y (e.g. *Winterwerp and van Kesteren*, 2004). Then, the empirical intrinsic parameter K_y [Pa], representing the effect of the sediment particles on the strength of the sediment and the fractal dimension n_f [−], representing the fractal structure of the sediment flocs (*Kranenburg*, 1994), can be obtained with (*Winterwerp and van Kesteren*, 2004):

$$c_u \approx \tau_y = K_y \phi_{\text{s}}^{\frac{2}{3-nf}} \tag{3.3}$$

To quantify the compressibility behaviour during a loading test, the compression index C_c can be calculated. This coefficient is defined as:

$$C_c = -\frac{\text{d}e}{\text{d}\log(\sigma_{\text{t}})} \approx -\frac{\Delta e}{\Delta \log(\sigma_t)} \tag{3.4}$$

where Δe is the change in void ratio along a linear section of the compression curve and $\Delta \log \sigma_t$ the change in logarithm of applied stress along that linear section of the compression curve (*ISO/TS*, 2004a). Next to this traditional coefficient of compressibility, the corrected $C_{\text{c,corr}}$ is defined with the corrected void ratio e_{corr}, as:

$$e_{\text{corr}} = \frac{e_s^f}{1 - e_s^{sa}}, \tag{3.5}$$

where e_s^f is the void ratio of the fine fraction and e_s^{sa} the void ratio of the sand fraction.

Furthermore, a new definition of the C_c coefficient as a function of the volumetric concentration of solids can be derived for the fractal theory, starting from rewriting Equation 3.4:

$$C_c = -\frac{\text{d}e}{\text{d}\phi_{\text{s}}} \frac{\text{d}\phi_{\text{s}}}{\text{d}(\log \sigma_{\text{t}})} \tag{3.6}$$

where e and ϕ_s are connected as $1 + e = 1/\phi_s$, and

$$\frac{\text{d}\phi_{\text{s}}}{\text{d}\log \sigma_{\text{t}}} = \ln(10)\sigma_t \frac{\text{d}\phi_{\text{s}}}{\text{d}\sigma_{\text{t}}} \tag{3.7}$$

Substituting Equation 3.7 in Equation 3.6 leads to:

$$C_c = -\frac{\text{d}e}{\text{d}\phi_{\text{s}}} \ln(10)\sigma_t \frac{\text{d}\phi_{\text{s}}}{\text{d}\sigma_{\text{t}}} = \frac{1}{{\phi_s}^2} \ln(10)\sigma_t \frac{\text{d}\phi_{\text{s}}}{\text{d}\sigma_{\text{t}}} \tag{3.8}$$

where, given the relation between e and ϕ_s, $\text{d}e/\text{d}\phi_{\text{s}} = -1/\phi_{\text{s}}^2$.

At the end of each loading step of an IL test, the vertical effective stress σ_{eff} is equal to the total stress σ_t (*ISO/TS*, 2004a). The fractal description for σ_{eff} (*Merckelbach and Kranenburg*, 2004a) reads:

$$\sigma_{\text{eff}} = K_\sigma \left(\frac{\phi_s^f}{1-\phi_s^{sa}} \right)^{\frac{2}{3-n_f}} \tag{3.9}$$

where the coefficient K_σ is material specific.

The fractal equation for C_c, obtained after substitution of Equation 3.9 in Equation 3.8 and derivation, indicates that C_c is inversely proportional to ϕ_s:

$$C_c = \frac{3-n_f}{2} \frac{\ln(10)}{\phi_s} \tag{3.10}$$

The results obtained from this Equation 3.10 can be compared with the C_c values obtained from the traditional soil mechanics definition (Equation 3.4).

The coefficient of consolidation c_v was obtained according to *ISO/TS* (2004a) with the logarithmic time curve-fitting method. The value of the hydraulic conductivity k was estimated with Equation 3.11, following *Terzaghi and Peck* (1967) and *Terzaghi et al.* (1996):

$$k = \gamma_w m_v c_v \tag{3.11}$$

where m_v is the coefficient of volumetric compressibility and γ_w is the specific weight of water ($\gamma_w = \rho_w g$, where ρ_w is the density of water and g de acceleration of gravity). The calculated hydraulic conductivity values were fitted with the Equation 3.12 (*Merckelbach and Kranenburg*, 2004a) describing a fractal behaviour:

$$k = K_k \left(\frac{\phi_s^f}{1-\phi_s^{sa}} \right)^{-\frac{2}{3-nf}} \tag{3.12}$$

where K_k is an empirical material parameter.

The famous Terzaghi small strain consolidation equation (*Terzaghi and Peck*, 1967) reads:

$$\frac{\partial \sigma_{\text{eff}}}{\partial t} - c_v \frac{\partial^2 p_e}{\partial z^2} = 0 \tag{3.13}$$

where p_e is the excess pore water pressure and it relates the total stress σ_{t} as follows:

$$\Delta\sigma_{\text{eff}} = \Delta\sigma_t - p_e \tag{3.14}$$

where $\Delta\sigma_{\text{eff}}$ is the portion of the consolidation stress increment which, at a given time, is transmitted through the structure of soil and p_e is the corresponding excess pore water pressure (*Terzaghi and Peck*, 1967). In the final phase of consolidation, compaction rates are very small and $\frac{\partial \sigma_{\text{t}}}{\partial t} \approx 0$. For the case of constant total loading over time Equation 3.13 can be rewritten as a function of σ_{eff} to:

$$\frac{\partial \sigma_{\text{eff}}}{\partial t} - c_v \frac{\partial^2 \sigma_{\text{eff}}}{\partial z^2} = 0 \tag{3.15}$$

For the case of only fines present, i.e. $\phi_s^f = \phi_s$, this Equation 3.15 can be written as a function of ϕ_s (see Appendix 3A):

$$\frac{\partial \phi_s}{\partial t} - c_v \frac{\partial^2 \phi_s}{\partial z^2} = 0 \tag{3.16}$$

In the same way, the large strain consolidation theory of *Gibson et al.* (1967) can be simplified, for the case of small deformations and written as function of ϕ_s as (see Appendix 3A):

$$\frac{\partial \phi_s}{\partial t} - \Gamma_c \frac{\partial^2 \phi_s}{\partial z^2} = 0 \tag{3.17}$$

where Γ_c is a consolidation parameter defined as

$$\Gamma_c = \frac{2}{3 - n_f} \frac{K_k K_\sigma}{g \rho_w} \tag{3.18}$$

Equations 3.16 and 3.17 show that, for the case of small deformations:

$$c_v \approx \Gamma_c \tag{3.19}$$

Therefore, the c_v values obtained according to *ISO/TS* (2004a) from an Incremental Loading test can be compared with the values obtained from the fractal parameters according to Equation 3.18, which follow from settling column tests.

3.3. EXPERIMENTAL METHODS

3.3.1. SEDIMENT COLLECTION AND PREPARATION

The sediments tested originate from Lake Markermeer, The Netherlands. Different samples were collected with a Van Veen grab sampler at two locations: the Southwest (SW) and the Northeast (NE) site (see Figure 2.1). The upper layer of the lake bed consists of a thin (~ 0.1 m) layer of soft silt (*De Lucas Pardo*, 2015), of which only the few upper mm's are oxic (*Van Duin*, 1992). The sediment composition of this soft silt layer is detailed in Table 3.1. Underneath the soft silt layer, a thick layer of Holocene deposits (clay, peat or sand) is present (*Rijkswaterstaat*, 1995). Material from this layer is referred to as clay for the Southwest of the lake and sandy clay for the Northeast, according to its lithological composition (Table 3.1). Markermeer sediment mineralogy is dominated by illite and smectite at all sampling sites, while kaolinite (<11%) and chlorite (<6%) are present in small amounts (i.e *Barciela-Rial et al.*, under review), see Chaper 2. The sediment collected was stored in dark conditions in a climate chamber at 4 °C.

For the IL tests, one "mother" sample from the Northeast (NE) site of the lake (see Figure 2.1) was used. This is sample NE2B. From this material NE2B (Chapter 2), subsamples were prepared in the lab with 0, 10, 20 and 40% sand content with respect to the total dry mass, i.e. $M_{\text{sand}} / M_{\text{dry,total}}$. The value of these % sand contents in mass is almost identical to their correspondent % sand in volume, because of the similar particle densities measured for sand and fines. These subsamples were obtained by separating the fines and sand content by sieving and recombining afterwards. The desired % mass of dried Markermeer sand (also obtained by sieving) was added to the sieved fine fraction.

In this way, the water content with respect to the fine fraction was kept constant for all the samples. For the CRS test, natural samples with varying sand and organic matter content were analyzed. These samples were collected at different locations and sampling depths. Notably, sample NE3B was collected by dredging after previous removal of the 2 upper meters of the Lake bed. In addition to these natural samples, the behaviour of the fine fractions and a control sample of commercial Speswhite Kaolinite were also studied, as well as the behaviour after oxidation of one of the samples.

Furthermore, a subsample from the 40% sand sample from the NE, tested with IL test, and sample SW1B, tested with the CRS test, were oxidized to mimic the behaviour of Markermeer sediment after being in contact with atmospheric conditions for a long time. As natural oxidation is slow, the oxidation process was accelerated in the laboratory. Samples were chemically oxidised with hydrogen peroxide (H_2O_2), following an adapted procedure from the British Standards (*BS*, 1990a) including two drying-rewetting cycles. First, the samples were dried in an oven at a constant temperature of 50 °C until there was no further mass loss. Then, subsamples of 100 grams were rewetted by adding demineralised water and oxidised according to the standard. After centrifuging to remove the oxidant, the material was dried again at 50 °C and finally rewetted with filtered Markermeer water. The pH was measured before and after oxidation by immersing a pH electrode in the samples. The origin and composition of all the samples for the IL and CRS tests are described in Table 3.1.

3.3.2. SAMPLE CHARACTERIZATION

The consistency or Atterberg limits and undrained shear strength were determined according to international standards: *ISO/TS* (2004b) and *ISO* (2016), respectively. For the determination of the liquid limit (LL), 80 grams/30° tip angle fall cone tests were performed. The plastic limit (PL) was obtained by the rolling thread test. The Total Organic Matter (TOM) content was determined by loss on ignition (LOI), carried out according to the European Standard (*EN*, 2012) and the amount of Total Organic Carbon (TOC) and its reactivity were determined with Rock Eval (*Behar et al.*, 2001). The particle density was measured with a gas pycnometer (*ISO/TS*, 2004c). The results are compiled in Table 3.1.

Table 3.1: Sediment properties of all samples studied.* Not measured, estimated from correlations presented in Chapter 2. Last row indicates if the sample was tested with IL or CRS tests.

Site	*Southwest*				*Northeast*									*n.a.*
Depth [m]	*0.1-0.5*			*0-0.1*	*0 -0.1*				*0 -0.1*				2-4.5	
Type	*Bulk clay*	*Fines*	*Bulk treated*	*Upper silt*	*Fines upper silt*	*Bulk sandy clay*	*Lab*				*Treated*		Deep clay	*Kao*
ID	SW1B	SW1F	SW1T	SW2B	NE1F	NE2B-70%	NE2B-0%	NE2B-10%	NE2B-20%	NE2B-40%	NE2B-40%-T	NE3B	Kao	
Sand [%]	8	0	8*	28	0	69	0	10	20	40	42	32	0	
Silt [%]	63	69	63*	54	86	21	68	61	54	41	49	49	2	
Clay [%]	29	31	29*	18	14	10	32	29	26	19	9	19	80	
D50 [µm]	10	8	10*	32	26	87	17	13	25	51	69	44	4	
TOM [%]	8.6	8.7	6.7	6.4	4.8	2.1	5.7	4.8	3.8	3.4	2.1	7	0	
TOC [%]	3.3	3.1	2	3	2	0.7	2.2	1.9	1.5	1.2	0.5	n.a.	0	
ρ_s [kg/m^3]	2530	2570	2620	2560	2540	2640	2540	2550	2570	2600	2700	2580	2600	
LL [%]	104	129	60	103	83	41	89	80	69	52	33	73	70	
PL [%]	46	59	31	46	40	25	34	30	27	23	23	28	38	
PI [%]	58	70	29	57	43	16	55	50	42	29	10	46	32	
test	CRS	CRS	CRS	CRS	CRS	IL	IL	IL	IL	IL	IL	CRS	CRS	

3.3.3. UNDRAINED SHEAR STRENGTH

The fall cone test was used to determine the undrained shear strength according to *ISO/TS* (2004b). The undrained shear strength c_u results were fitted with the fractal model, i.e., Equation 3.3.

3.3.4. INCREMENTAL LOADING TEST

IL (oedometer) tests were performed according to *ISO/TS* (2004a) to characterize the compression and consolidation properties of the samples with 0, 10, 20, 40 and 70 % sand. These IL tests are referred as I-NE2B-0% sand, I-NE2B-10% sand, I-NE2B-20% sand, I-NE2B-40% (where I indicates that the initial water content of the fine fraction was the same for all theses tests) and III-NE2B-70% sand (started at a different initial fines water content); see Table 3.1. Additionally, two extra IL tests were performed to gain insight in the compression behaviour depending on the initial water content of treated samples with 40% sand content. One test started at a water content of 1.6 LL (Liquid Limit) (test II-40%-T), and another one at 1.2 LL (test III-40%-T). This corresponds with a water content (w%) of the fines fraction of 0.9 and 0.7 [$M_w/M_{s,fines}$], where $M_{s,fines}$ refers only to the dry mass of the fraction <63 µm (Table 3.2). The 1.6 LL water content was selected as it was the maximum water content of the sample below which no self-weight consolidation occurred (*Van den Bosch*, 2016). Reduction of water content below this 1.6 LL for samples II-NE2B-40%-T and III-NE2B-40%-T was done by atmospheric drying. For the second additional test (III-NE2B-40%-T) and for the 70% sand content test (III-NE2B-70% sand), a different loading program with higher initial stresses was applied. This was necessary because of the higher stiffness of these samples. The three different loading plans (I, II and III) are described in Table 3.3.

Table 3.2: Initial and final water contents of the IL tests, including water content of the fine fraction and ratios between initial and final water contents and the Liquid Limit.

Test ID	I-NE2B-0%	I-NE2B-10%	I-NE2B-20%	I-NE2B-40%	III-NE2B-70%	II-NE2B-40%-T	III-NE2B-40%-T
Fines content	1	0.9	0.8	0.6	0.3	0.6	0.6
				INITIAL			
w [-][Mw/Ms]	1.38	1.23	1.05	0.8	0.42	0.53	0.4
w/LL [-]	1.55	1.54	1.53	1.53	1.02	1.62	1.2
w fines [-][Mw/Ms,fines]	1.38	1.36	1.31	1.33	1.39	0.89	0.66
				FINAL			
w [-][Mw/Ms]	0.62	0.58	0.52	0.38	0.28	0.30	0.23
w/LL [-]	0.70	0.73	0.75	0.74	0.68	0.90	0.71
w fines [-][Mw/Ms,fines]	0.62	0.65	0.65	0.64	0.93	0.5	0.39

To determine the bulk and dry density, the specimen is weighted before the test and after drying for 24 hours in the oven at 105 °C. The laboratory in which the IL experiment was performed had a constant room temperature of 10 °C.

3.3.5. CONSTANT RATE OF STRAIN TEST

The CRS tests were performed according to *ASTM* (2014). The set-up consists of a triaxial cell with a sample enclosed by a stainless steel ring. Vertical strain was applied by a computer controlled servo system and the sample was axially compressed. Drainage was provided at the top plate and the pore pressure was measured at the bottom sealed plate.

Table 3.3: Loading plan for the IL tests in kPa.

	Series I	Series II	Series III
Loading step 1	0.6	0.6	3.1
Loading step 2	1.3	1.3	6.3
Loading step 3	4.3	4.3	12.6
Loading step 4	10.2	10.2	25.1
Loading step 5	25.0	25.0	50.3
Loading step 6	-	57.9	100.5
Loading step 7	-	119.1	-
Loading step 8	-	241.3	-

The force was measured with an internal load cell. Vertical strain was measured on the plunger axis by a LVDT (Linear Variable Differential Transformer). Volume change was measured by weighting of the transferred water. Overall control of strain and pressures was done using Deltares software programmed in HP-Basic. Testing was done on 3 cm high, 63 mm diameter samples.

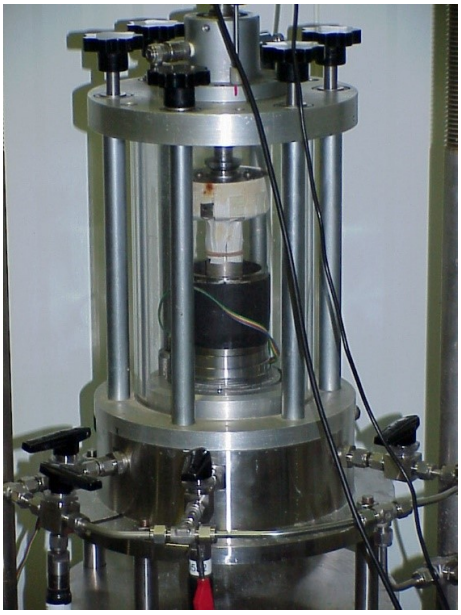

Figure 3.1: CRS set-up.

The assumptions for the interpretation of the CRS tests are: 1) saturated and homogeneous soil, 2) negligible compressibility of soil particles, 3) water flow is only vertical and follows Darcy's law, 4) constant ratio between soil hydraulic conductivity and compressibility during the time interval between two reading sets and 5) the compressibility of the base excess pressure measurement system is negligible in comparison to the one of the soil.

The initial water content of the samples was selected such that self-weight consoli-

dation was not taking place. *Van den Bosch* (2016) and *Barciela-Rial et al.* (submitted) performed settling experiments with the same sediment used in here. From these data, *Barciela-Rial et al.* (submitted) calculated the void ratio at the end of self-weight consolidation. The minimum gravimetric ratio between the water content (w_0) and the Liquid Limit (LL) at the end of self-weight consolidation was for all cases above 1.4. Therefore, all samples were tested at an initial water content of 1.4 times the LL. Preparation of the samples at this initial w_0 was done by atmospheric drying with frequent gentle spoon mixing to avoid the formation of a dry crust at the surface. For sample NE1F, two extra tests were performed. One at initial water content of 1.8 LL and another at 0.9 LL. For both cases, self-weight consolidation had already finished for this specific material. The initial gravimetric water contents of the samples are shown in Table 3.4.

Table 3.4: Initial water content w_0, ratio w_0/LL, bulk density $\rho_{b,0}$, void ratio e, rate of strain, device used and loading plan applied for the performed CRS tests.

ID	SW1B	SW1F	SW1T	SW2B	NE1F-I	NE1F-II	NE1F-III	NE3B	Kao
w_0 [-] [M_w/M_s]	1.4	1.8	0.8	1.4	1.8	1.2	0.7	1.0	1.0
w_0/ LL [-]	1.4	1.4	1.4	1.4	2.2	1.4	0.8	1.4	1.4
w_0 [-] fines	1.5	1.8	0.9	1.9	1.8	1.2	0.7	1.5	1.0
$\rho_{b,0}[kg/m^3]$	1417	1254	1427	1305	1223	1346	1621	1662	1386
e_0	3.3	4.8	2.2	4.1	4.9	3.2	1.5	2.2	2.7
Rate [mm/min]	0.002	0.0012	0.002	0.0012	0.0012	0.0012	0.0012	0.002	0.0012
ID device used	CRS1	CRS1	CRS2	CRS2	CRS2	CRS2	CRS2	CRS2	CRS2
ID loading plan	L1	L2	L2	L2	L2	L2	L2	L2	L2

The loading plans are shown in Table 3.5. They indicate the values of total stress induced by the prescribed constant strain rate at which the loading, unloading and relaxation steps start and finish. This means that a strain was applied to a sample until a certain total stress was reached, which indicates the end of that step. During an unloading step, the rate of strain has the same absolute value but an opposite direction than during a loading step and the development of negative pore pressures was prevented. For each test, a relaxation step was prescribed when the measured total stress reached 130 kPa. During a relaxation step, the rate of strain is equal to zero. For the sample SW1B, the first unloading phase at 50 kPa was not performed. In order to compare the different behaviour of the different samples, the rate of strain was kept constant as much as possible. For most of the samples, a rate of 0.0012 mm/min was applied. However, for the treated sample SW1T and the sandier sample NE3B, a slightly larger rate of 0.002 mm/min was applied to ensure enough pore pressure development. Both strain rates are of the same order of magnitude and the results are therefore comparable. The strain rates were selected to keep the pore pressure: total stress ratio (referred as pressure ratio) within the limits recommended in the *ASTM* (2014) (i.e., between 3 and 15%). However, ratios above 15% were observed for the softer sediment samples and below 3% for the sandier. Values above 15% were observed, in particular, during the initial moments of the test. For the sandy sample NE3B, values below 3% were observed at the end of a test (see Figure 3.13). The effective stress and the hydraulic conductivity were calculated according to the non-linear method of *ASTM* (2014) because all the samples showed non-linear behaviour (see 3.10).

The CRS effective stress and hydraulic conductivity results were plotted as a function

Table 3.5: Loading plans L1 and L2 for the CRS tests

L1: Preliminary test (sample SW1B)		L2: All other samples	
Stress loading step	-	Stress loading step	50 [kPa]
Stress unloading step	-	Stress unloading step	25 [kPa]
Stress reloading step	100 [kPa]	Stress reloading step	100 [kPa]
Stress unloading step	50 [kPa]	Stress unloading step	50 [kPa]
Stress reloading step	130 [kPa]	Stress reloading step	130 [kPa]
Stress relaxation step	130 [kPa]	Stress relaxation step	130 [kPa]
Maximum stress	170[kPa]	Maximum stress	170 [kPa]
Unload to 20 kPa -end of test		Unload to 20kPa -end of test	

of ϕ_{corr}. The traditional soil mechanics material parameters C_c and C_{sw} were calculated to compare the ratio between compressibility and unloading (swelling) coefficients of the present samples with literature. The coefficient of compressibility C_c [-] was calculated for each loading step according to *ISO/TS* (2004a) with Equation 3.20, i.e. from the slope (CR) of the logarithmic of the effective stress (σ_{eff}) and strain (ε_v) and the initial void ratio e_0:

$$C_c = CR(1+e_0) = \frac{\Delta\varepsilon_v}{\log\left(\frac{\sigma_{\text{eff}}+\Delta\sigma_{\text{eff}}}{\sigma_{\text{eff}}}\right)}(1+e_0) \tag{3.20}$$

In the same way, the swelling coefficient C_{sw} [-] was calculated for each unloading step according to *ISO/TS* (2004a) with Equation 3.21, using the slope SR of the unloading curve:

$$C_{sw} = SR(1+e_0) = \frac{\Delta\varepsilon_v}{\log\left(\frac{\sigma_{\text{eff}}+\Delta\sigma_{\text{eff}}}{\sigma_{\text{eff}}}\right)}(1+e_0) \tag{3.21}$$

3.4. RESULTS

3.4.1. PLASTICITY AND ACTIVITY CHARTS

The plasticity chart (Figure 3.2) shows the relation between the LL and the PI for all the samples of the IL and CRS tests. All Markermeer samples are around the A-line, which represents the transition between inorganic (non-humical) and organic clays (clay-humic complexes). This is consistent with the determined composition of the solid fraction, which shows the presence of organic matter (see Table 3.1). The samples move closer to the A-line after the treatment, i.e., they moved from the organic towards the inorganic part of the chart while their PI and LL decreased drastically. Thus, the treatment largely decreased the plasticity.

The left panel of Figure 3.3 shows the traditional activity plot. Herein, the activity is determined as the slope obtained by plotting the PI as a function of the clay content (*Skempton*, 1969; *Winterwerp and van Kesteren*, 2004). The activity is determined by analysing only the IL samples, because they all originate from the same mother sample and, therefore, the composition of the OM present is the same. This ensures that the changes on PI are only related to a difference on the composition of the sediment and not

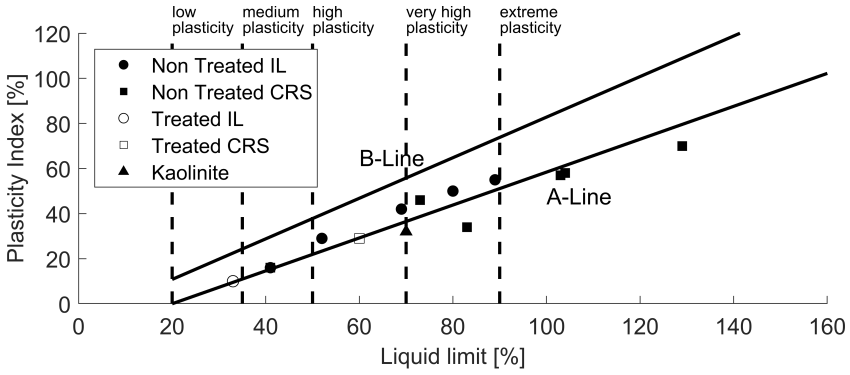

Figure 3.2: Plasticity chart samples IL and CRS

the OM. For Markermeer sediment, the activity (A) value was 1.8. Note that a correction for the minimum clay content to have a PI of 7% (i.e. the PI thereshold to not behave like sand) was applied following *Winterwerp and van Kesteren* (2004). This value of $A = 1.8$ suggests the dominance of illites and smectites (*Skempton*, 1969; *Winterwerp and van Kesteren*, 2004). The large value of activity indicates that Markermeer sediment can be classified as active (*Skempton*, 1953). Active sediments undergo considerable changes of volume when wetted (swelling) or dried (shrinkage), (*Mitchell and Soga*, 2005). The minerals present estimated from the activity values agree with the quantitative mineralogical composition of the clay fraction (Chapter 2 and *Barciela-Rial et al.* (under review)) for Markermeer sediment, quantifying ranges of 22-33% smectite (S), 12-29% of illite (I) and 31-47% I/S mixed layers. Smectite is the mineral that induces larger volume changes, followed by smectite/illite interstratified layers, illite and kaolinite (*Barshad*, 1955; *Taylor and Smith*, 1986; *Pająk-Komorowska*, 2003).

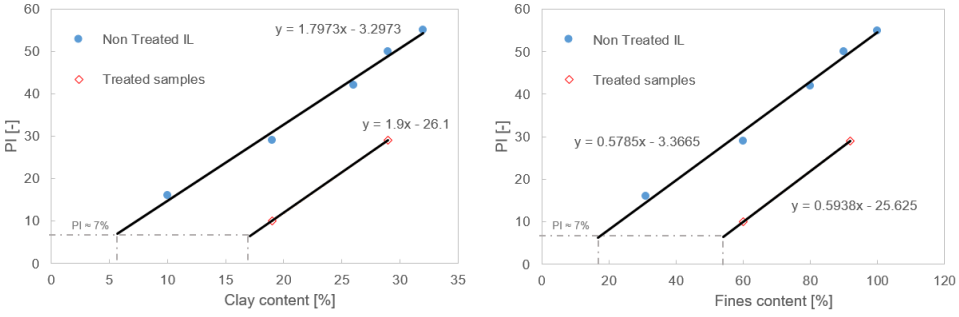

Figure 3.3: Activity plot for the natural samples of the IL test and for the treated samples

In Figure 3.3, right panel, the determination of the activity related to the fines (clay and silt) fraction is shown. This alternative method can be attractive because the determination of the sand content by sieving is straightforward while the values obtained for the clay fraction depend on the device used (*Ibanez Sanz*, 2018; *Winterwerp and van*

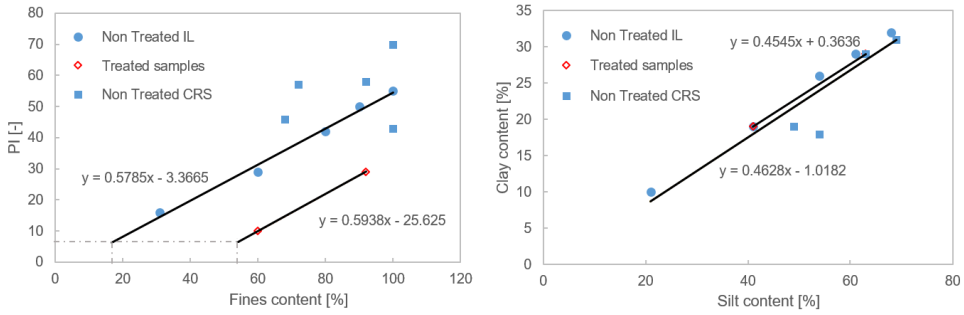

Figure 3.4: Activity plot for all non-treated samples of the IL tests and for all the treated samples (left) and clay:silt ratio (right).

Kesteren, 2004). This alternative method is possible because the clay:silt ratio is more or less constant at one particular (e.g. *Flemming*, 2000). Plotting the clay: silt ratios for Markermeer samples (Figure 3.4), the clay:silt ratio obtained is 1:2. Hence, the activity can be calculated from the fines content - PI plot (Figure 3.3) by multiplying the slope by 3, obtaining an $A = 1.7$.

Figure 3.4 shows that the inclusion of the CRS samples for the calculation of the activity leads to a large scatter. This is because samples with the same % fines have a different PI. These differences in PI suggest that differences in OM composition influence the values of the PI. For this reason, the authors used samples with different sand content coming from the same mother sample for the determination of the activity. In this way the sand content is the only variable changing, i.e. the organic matter present in the sample has the same composition.

3.4.2. UNDRAINED SHEAR STRENGTH

The results of the undrained shear strength (c_u) tests are shown in Figure 3.5. Herein c_u is plotted against the non-corrected ϕ_s (i.e $\phi_s^f + \phi_s^{sa}$) and ϕ_{corr}. The results show, for each sample, a decrease in undrained shear strength with larger water content (lower ϕ_s or ϕ_{corr}). Plotting against ϕ_s does not allow to identify the point at which the TFC is reached nor to determine patters of similar behaviour. However, the normalised results (c_u against ϕ_{corr}) shows that the samples containing 0%, 10% , 20% and 40% sand overlap. However, sample SW1B shows lower ϕ_{corr} than these samples because of its larger amount of OM and subsequent larger ability to bind water. Sample 70% is not in the same range as the other natural samples with the same fines composition, indicating that the fines content is below the TFC. Therefore the correction used in Equation 3.2 is not valid and the fractal approach not applicable because sand particles start to create a network. Other authors found the same values for the TFC. For example, *Thevanayagam* (1998) showed how clay matrix governed the undrained shear strength behaviour below 70% (mass) sand content while *Kumar and Wood* (1999) found a TFC between 30 and 40% (mass) fines content. On the other hand, treated samples moved to the right because of the drastic decrease of the PI and their loss of ability to bind water. In the same way, the natural sample from the Southwest sampling site SW1B was located left to the NE samples in Figure 3.5, because

of the larger OM content of this sample and associated larger ability to bind water.

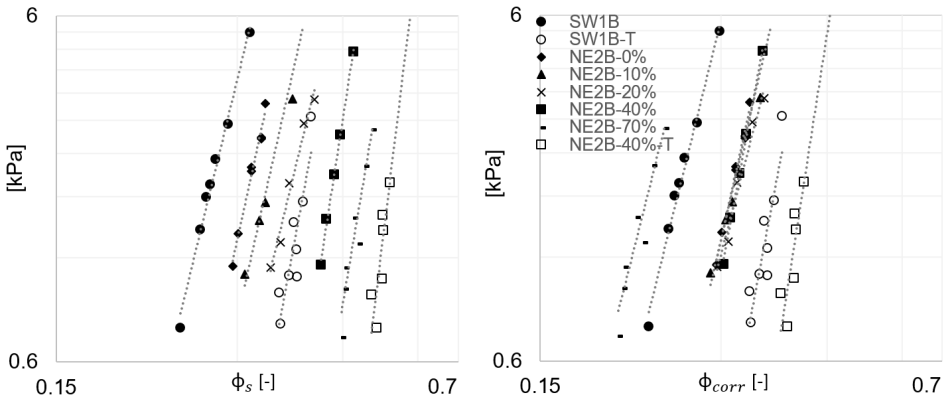

Figure 3.5: Undrained shear strength as a function of ϕ_s (left) and ϕ_{corr} (right).

Table 3.6: Empirical material parameters obtained by fitting the c_u results

ID	K_y [kPa]	n_f [-]	ID	K_y [kPa]	n_f [-]
SW1B	2.7E+04	2.72	NE2B-20%	4.86E+03	2.71
SW1B-T	5.9E+04	2.78	NE2B-40%	5.58E+04	2.78
NE2B-0%	3.3E+04	2.75	NE2B-40%-T	2.10E+04	2.81
NE2B-10%	1.1E+04	2.73	NE2B-70%	7.12E+04	2.75

Table 3.6 shows the empirical parameters obtained from fitting the data. The small differences of the parameters of different samples originate from differences in sediment composition and accuracy. The n_f values obtained are slightly larger than previously found for Markermeer sediment from settling column tests (*Barciela-Rial et al.*, submitted). Previously, *De Lucas Pardo* (2015) found (for different Markermeer samples) n_f values ranging 2.67-2.68, while *Merckelbach* (2000) had found values between 2.72-2.75 for other Dutch sediments.

3.4.3. INCREMENTAL LOADING TEST

The effective stress against the corrected volumetric concentration ϕ_{corr} obtained for the IL tests is presented in Figure 3.6. All the non treated samples below the TFC (i.e. tests I-NE2B-0%, I-NE2B-10%, I-NE2B-20% and I-NE2B-40% sand) show a power law relation with lines following the same slope in a log-log plot. The treated samples (tests II-NE2B-40%-T, III-NE2B-40%-T) still follow a power law relationship, even though the floc structure has been destroyed by the treatment and primary particles touch each other. These treated samples have a steeper slope, implying a larger increase of effective stress for an increase of ϕ_{corr} with respect to the non-treated samples. Furthermore, treated samples also have larger values of ϕ_{corr} (i.e. less ability to bind water). The sample of test III-NE2B-70% sand is above the TFC and, therefore, out of the range where the correction of the ϕ value is applicable because of the existence of a granular skeleton. However, it

is remarkable that it stills follows a power law while, for instance, *Schultze and Moussa* (1961) presented exponential relationships for sand compressibility. Furthermore, it is remarkable that the slope is the same as for treated samples.

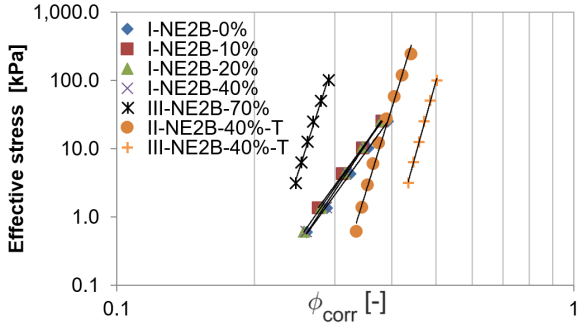

Figure 3.6: Effective stress as a function of ϕ_{corr}

After fitting Equation 3.9 to the ϕ_{corr}- effective stress data, the empirical parameters in Table 3.7 were obtained . Samples with 0 to 40% sand content have similar material parameters. By treating the NE2B-40% sample, the floc structure was destroyed so it deviates from the fractal approach. Notably, treated samples show a larger n_f values suggesting a more densely packing due to the low OM and water content. For the sample with 70% sand, the fractal theory is not applicable because the sand content is large enough to form a sand skeleton.

Table 3.7: Material parameters calculated from the effective stress data as obtained from IL tests.

ID	K_σ [kPa]	n_f [-]	K_k [m/s]	n_f [-]
I-NE2B-0%	1.5E+05	2.78	1E-12	2.74
I-NE2B-10%	1.6E+05	2.78	8E-13	2.74
I-NE2B-20%	2.9E+05	2.79	3E-12	2.69
I-NE2B-40%	4.2E+05	2.80	2E-12	2.72
III-NE2B-70%	2.0E+13	2.90	2E-15	2.82
II-NE2B-40%-T	2.0E+10	2.91	2E-15	2.88
III-NE2B-40%-T	2.0E+09	2.92	4E-16	2.90

The coefficient of compressibility C_c (Equation 3.4) and the corrected coefficient of compressibility (Equation 3.5) are presented in Figure 3.7. The results are presented as a function of the effective stress and ϕ_{corr}. C_c is nearly constant for the last phase of the test. No changes on C_c were observed between sand contents of 0% and 10% because the sand particles are too diluted in the fines matrix to affect the compression, i.e. they are passive. For sand contents of 20% or more, the C_c coefficient calculated without correcting for the sand content (i.e. using e and not e_{corr}) decreased (see Figure 3.7). This decrease in compression is caused by the fact that sand particles are incompressible. This decrease in C_c with an increase in sand content has frequently been observed in literature (e.g. *Watabe et al.*, 2011; *Monkul and Ozden*, 2007; *Simpson and Evans*, 2016). *Simpson and Evans* (2016) observed a constant compression for sand contents between 0% and 10%,

as found in this study case of Markermeer sediment. However, when correcting for the amount of sand (C_c corrected), samples with 0 to 40% sand overlap because the TFC has not been reached (see Figure 3.7). The treated sample has a smaller C_c values given the smaller ability to bind water (*Barciela-Rial et al.*, under review), which implies a lower amount of water to be expelled upon loading. The C_c - stress plot (Figure 3.7) also shows that, when not correcting, the compressibility behaviour of the treated sample with 40% sand (40%-T) and the natural sample with 70% sand content is the same for the same loading scheme with higher initial stress.

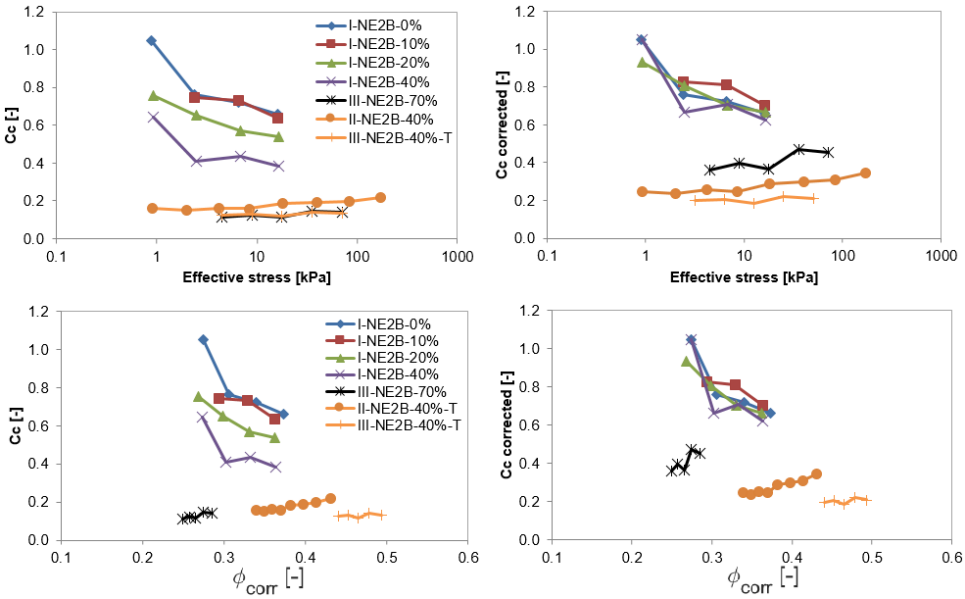

Figure 3.7: Compressibility coefficient C_c without correcting for the presence of sand (left) and after correcting for sand (right). The top panels present C_c as function of the stress and the bottom panels as function of ϕ_{corr} (Equation 3.2).

Figure 3.8 shows the values of the corrected C_c obtained from the fractal Equation 3.10. The C_c of samples from 0 to 40% sand overlap, having the same values of C_c that the corrected values presented on Figure 3.7.

Figure 3.9 shows the values of the coefficient of consolidation c_v as calculated with Equation 3.19 and with the logarithmic time curve-fitting method (*ISO/TS*, 2004a) directly from the IL data. The results from both methods are in the same order of magnitude with the exception of the 70% sand sample. The coefficient of consolidation c_v is in the same range for a sand content between 0 and 20%. However, the values were slightly larger for 40% sand and clearly larger for 70% sand, as well as for the treated samples. The results suggest that, when large enough, the content of sand can influence the coefficient of consolidation speeding up the consolidation process. Literature *Simpson and Evans* (2016) describe a positive link between sand and c_v for a sand content between 40 and 70%. The results of the current experiment agree with these findings. For the fractal approach data, the difference of the values of the c_v between the 0, 10% sand samples

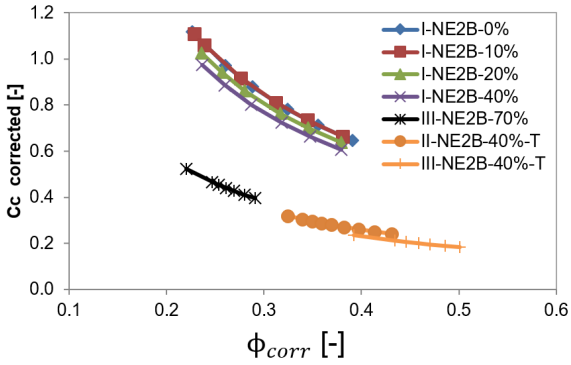

Figure 3.8: C_c as calculated directly from material parameters with the Equation 3.10 and plotted as function of ϕ_{corr}

and the 20% sand sample is an indication of the accuracy of the values obtained with this approach (Figure 3.9).

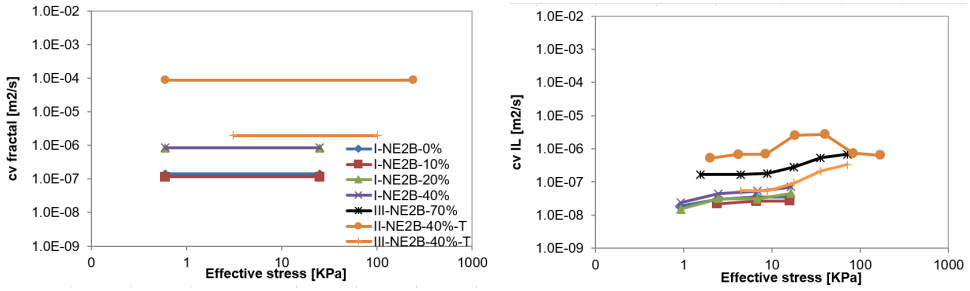

Figure 3.9: Coefficient of consolidation c_v as calculated from the fractal parameters (left) and according to *ISO/TS* (2004a) (right). Note that calculating from the fractal approach (Equation 3.19) leads to a straight line given the constant values of Γ_c and n_f and that for 70% sand the values obtained are outside of the range showed.

The hydraulic conductivity cannot be measured with the oedometer set-up used. Therefore, it was calculated with Equation 3.11. The results are presented in Figure 3.10. The data point at the lowest stress of sample 40%-T and the first two data points for the 10% sample were not plotted because strain could not be measured. This occurred because the ring containing the sample hindered the movement of the porous stone at the beginning of the test. The log stress-k plot indicates that the hydraulic conductivity k is not affected by the sand ratio for sand contents up to 40%. For a sand content of 70%, a small increase in hydraulic conductivity at the same stress was observed. According to literature, when large enough, the presence of sand creates flow paths increasing the hydraulic conductivity (e.g. *Al-Shayea*, 2001; *Watabe et al.*, 2011; *Simpson and Evans*, 2016). For example, *Al-Shayea* (2001) reported an increase in hydraulic conductivity for sand contents above 60%. The results show that, for Markermeer sediment this threshold occurs between 40% and 70% sand. Below this sand content, the hydraulic conductivity

of Markermeer sediment is governed by the fines matrix and sand is too diluted to form skeleton structures.

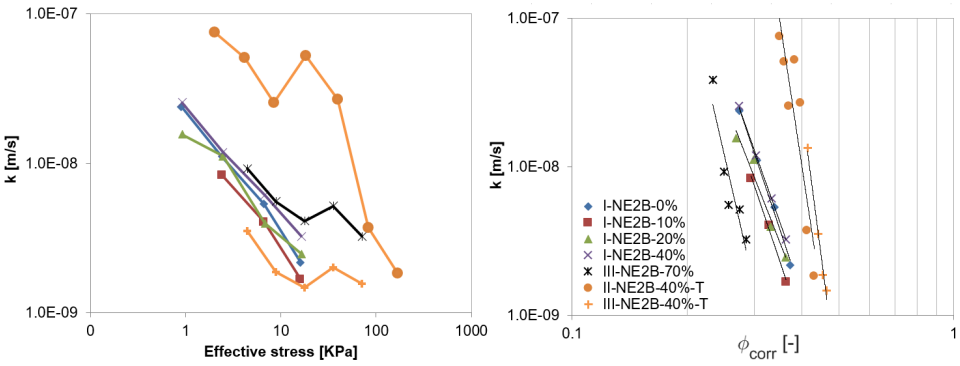

Figure 3.10: Hydraulic conductivity as a function of stress (left) and ϕ_{corr} (right). Note log-log scale.

Correcting for passive (non-structural) sand (ϕ_{corr}) shows that k decreases with the increase of the solids fraction; Figure 3.10, according to theory (e.g. *Huang and Bowers*, 1986). The slope of the treated samples and the 70% sand sample is steeper, i.e. faster decrease of hydraulic conductivity upon loading than the 0%-40% sand samples. These low sand content samples overlap. Regarding the empirical material parameters obtained from k (i.e. K_k and n_f in Table 3.7), the values of the fractal dimension are lower with respect to the values obtained from fitting the effective stress. These differences of the n_f values are explained by the lower accuracy of the results of the k, caused by the fact that k was back-calculated from Equation 3.11 and not measured. The K_k values of the natural samples are in upper range of the values found in literature. For instance, *De Lucas Pardo* (2015) found values of K_k between 1.77×10^{-13} and 9.03×10^{-14} m/s, *Van den Bosch* (2016) between 1.23×10^{-13} and 2.18×10^{-13} m/s and *Merckelbach* (2000) between 4.5×10^{-13} and 1.2×10^{-15} m/s.

3.4.4. CONSTANT RATE OF STRAIN TEST

In this section the compressibility behaviour as studied with CRS testing is presented for the different materials. Figure 3.11 shows the effective stress development as a function of ϕ_{corr}. The fact that, after each unloading and reloading, the lines continue with the same slope, suggests elastic behaviour during unloading and that, therefore, the samples retain their structure. Samples SW1F, NE1F-I, NE1F-II, NE1F-III have only fines and a water content above the LL. These samples have a similar slope on the ϕ_{corr}-effective stress relationship for $\phi_{corr} > 0.22$ and the range of stresses studied, albeit decreasing with a higher initial ϕ_{corr}. The Kaolinite sample has a steeper slope. With respect to the effect of the different initial water contents or slurry density (samples NE1F-I, NE1F-II and NE1F-III), the results suggest convergence at larger stresses (Figure 3.11). However, this convergence did not occur at the modest stresses tested (<170 kPa). Testing at large stresses (> 1000 kPa) would be necessary to prove convergence (e.g *Shipton and Coop*, 2012). For the range of stresses tested in the current experiment, the compression curves

of the NE1F samples seem dependent on the initial ϕ_{corr}.

Figure 3.11 shows that when sand is present, the lines are less steep. Figure 3.12 shows the hydraulic conductivity as a function of ϕ_{corr}. Like the effective stress, Markermeer samples with only fines (SW1F, NEIF-I and NEIF-II) exhibit similar behaviour and differ from the Kaolinite sample. Sandy samples (SW1B, SW2B, NE3B) show steeper slopes. The treated sample SW1T, has a slope (fractal dimension n_f) between both groups of samples. Furthermore, large vertical oscillation of the hydraulic conductivity values occurred during unloading steps. This is caused by a large drop in pore water pressures when unloading and the rapid increase of pore water pressure at the first moments of re-loading thereafter (see Appendix 3B). The development of negative pore pressures was prevented when unloading. Large scatter of the pore pressure measurements occurred for the first samples tested SW1B and SW1T, which resulted in the large scatter of the hydraulic conductivity for this samples. For this reason, all the other samples were tested with another CRS apparatus (Table 3.4).

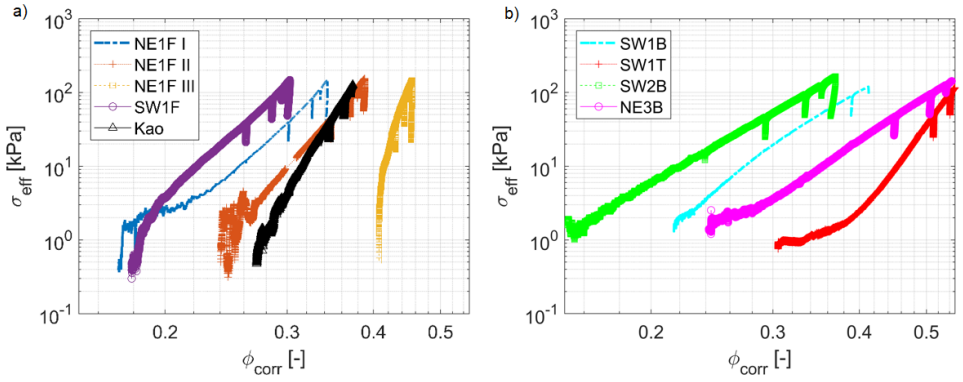

Figure 3.11: Relationship between the effective stress and ϕ_{corr}. a) Samples without sand, where: samples NE1F I,II and III are the same material with different initial water contents, sample SW1F is from a different sampling site and Kao is industrial kaolinite. b) samples including sand, where: SW1T is the result of treating sample SW1B, sample SW2B comes from the uppermost layer of the lake bed and has more reactive OM than sample SW1B and sample NE3B is from a different sampling site.

The same order of magnitude of rate of strain was used for all the samples so that the results were comparable. However, the ratio pore pressure:total stress should be constrained to avoid the development of large pressure gradients during the test. *Wissa et al.* (1971) recommended strain rates that result in maximum pore pressure ratios between 20 and 50%, while *Armour and Drnevich* (1986) defended allowing a maximum value of 40 or 50% as long as non-linear theory is used to calculate c_v. The standard *ASTM* (2014) constrains the pressure ratio between 3 and 15 %. Figure 3.13 shows the pressure ratio development of the two extreme samples that exceed the upper 15% limit (sample NE1F, only fines and large water content) or lower 3% limit (sample NE3B, very sandy). This figure shows that the pressure ratios are constrained within acceptable pressure ranges with the exception of the beginning of the tests, when significant gradients developed for very fine samples. This explains the large scatter at the initial stage observed in Figures 3.11 and 3.12.

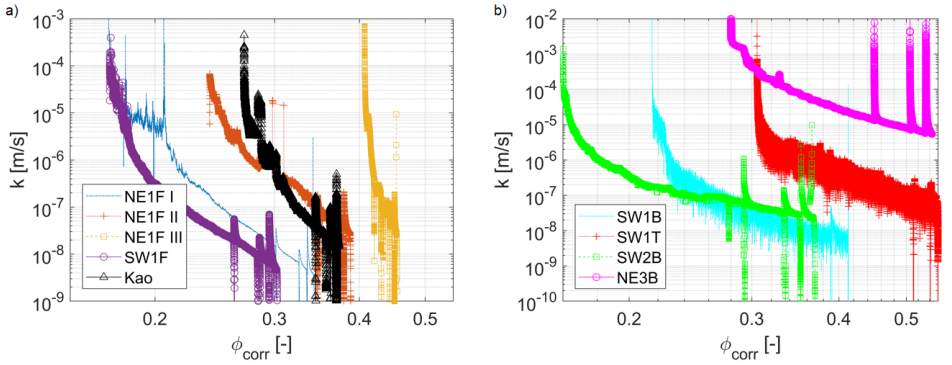

Figure 3.12: Relationship between the hydraulic conductivity and ϕ_{corr}. a) Samples without sand, where: samples NE1F I,II and III are the same material with different initial water contents, sample SW1F is from a different sampling site and Kao is industrial kaolinite. b) samples including sand, where: SW1T is the result of treating sample SW1B, sample SW2B comes from the uppermost layer of the lake bed and has more reactive OM than sample SW1B and sample NE3B is from a different sampling site.

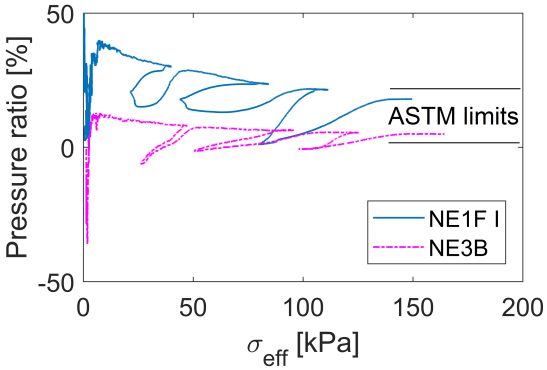

Figure 3.13: Pressure ratio for samples NE1F-I and NE3B.

The evolution of C_c as a function of ϕ_{corr} is shown in Figure 3.14. Herein, the C_c of the softer samples (SW1F, Ne1F-I, NE1F-II and SW2B) is larger at the initial state of the tests and decreases afterwards, while for the rest of the samples the values stay more constant. Regarding the water content (i.e. comparison NE1F samples), the larger the initial w%, the larger the compressibility: i.e. larger strain for an increase or decrease on stress (Figure 3.11 and Appendix 3D). However, C_c is fairly constant at larger ϕ_{corr} as well as for less soft materials (i.e. samples NE1F-III, NE3B, SW2B and KAO).

Calculating the C_{sw} of a slurry is less straightforward because the slope of the unloading $\log\sigma_{eff}$- strain ϵ plot varies largely during an unloading step. Figure 3.15 illustrates this. It shows that, determining the slope from the beginning of the unloading step for sample SW1F would result into smaller values than when determining it from the end of the unloading step.

To assess the range for the determination of a representative C_{sw}, let us assume that

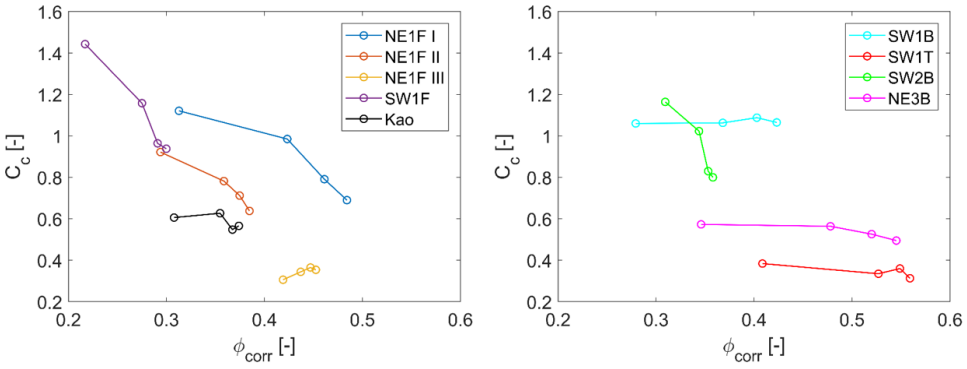

Figure 3.14: Coefficient of compressibility $C_c \pm 0.008$ as a function of ϕ_{corr} for the samples with only fines (left) and the ones also containing sand (right).

relaxation of σ_{eff} upon unloading follows an exponential function. Then, an estimation of the time scale for swelling (T_{sw}) can be done with (*Winterwerp and van Kesteren*, 2004):

$$\sigma_{eff} = \sigma_{eff,0} e^{-\frac{t}{T_{sw}}} \tag{3.22}$$

where $\sigma_{eff,0}$ is a reference effective stress. From the slopes of the swelling curve with time (t), T_{sw} can be determined. The results are compared with the actual swelling time t_{sw} in Table 3.8. All unloading times t_{sw} were of the same order of magnitude as T_{sw} . This implies that the tangents drawn in Figure 3.15 are representative for C_{sw}. For sample NE1F-III, $t_{sw} > T_{sw}$ and all the data points of the actual unloading curve were used for the calculation of the C_{sw} values (Figure 3.15). For all the other samples, the values of C_{sw} were obtained by fitting the data points at the end of the unloading step (see sample SW1F on Figure 3.15).

Table 3.8: Duration of the unloading step t_{sw} and calculated time for swelling T_{sw} for unloading step between 100 and 50 kPa.

ID	t_{sw} (h)	T_{sw} (h)	ID	t_{sw} (h)	T_{sw} (h)
NE1F-I	1.10	1.69	SW1B	1.62	2.60
NE1F-II	1.21	1.81	SW1T	0.86	1.25
NE1F-III	0.86	0.79	SW2B	1.43	2.03
SW1F	1.28	2.15	NE3B	1.32	1.61
Kao	1.15	1.85			

Figure 3.16 shows the calculated C_{sw} values. The treatment decreased the ability of the material to swell (compare SW1B and SW1T), as well as its compressibility. This agrees with the IL results. The large difference of behaviour between the natural and the oxidased samples upon (un)loading can be explained not only by the different amount of OM present but mainly because of the difference in composition and structure of OM. *Nguyen et al.* (2010) found a more open structure of the oxidised carbon. According to their

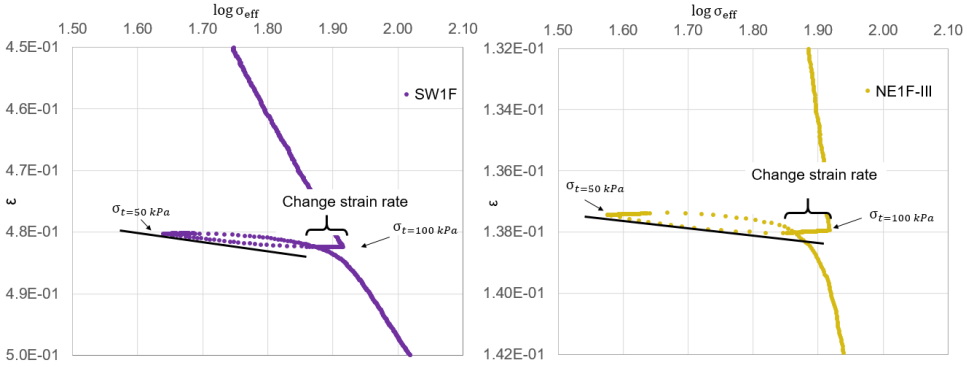

Figure 3.15: Example of the large variation of the slope of the logσ_{eff}- strain ϵ relationship for the sample SW1F (left) and NE1F-III (right) during the unloading step from 100 to 50 kPa total stress.

findings, nutrient contents may also affect the process of black carbon mineralization and not only the carbon structure itself. Further, black carbon oxidation may not only lead to carbon loss, but also to an increase in negative surface charge (likely through formation of carboxylic groups by oxidation); e.g. *Nguyen et al.* (2010). This increase in negative surface charges of the organic matter may explain the bigger repulsion (e.g. *Oades*, 1984) of the clay particles observed in the oxidised samples. This repulsion of clay particles may explain why an oxidised fine dominated sample behaves similar to a sand dominated sediment (e.g. samples III- 40%-T and III-70% sand for the IL test or, to a lesser extent, samples SW1T and NE3B for the CRS test). The fact that the samples group by sampling sites (i.e. SW samples C_c, C_{sw}), suggests that the composition of organic matter influences the behaviour (because the composition of the sand and clay fractions is the same at both sampling sites). In this sense, sample SW2B behaves like samples with no or very low (8%) sand content because of the compensating action of the labile organic matter present. Notably, Figure 3.16 shows that the higher organic matter (and more labile) content (samples SW2B, SW1F, SW1B), the larger the swelling. This agrees with literature (e.g. *Kassiff and Shalom*, 1971).

Table 3.9: Ratio between the swelling and the compressibility coefficient at different stress levels.

ID	SW1B	SW1F	SW1T	SW2B	NE1F-I	NE1F-II	NE1F-III	NE3B	Kao
duration test [h]	165.7	214.8	135.8	248.6	277.8	264.5	103.1	151.4	203.2
C_{sw}/C_c at 50-100 kPa	0.03	0.05	0.05	0.06	0.02	0.004	0.01	0.04	0.06
C_{sw}/C_c at 130-170 kPa	0.02	0.04	0.01	0.05	0.01	0.01	0.004	0.03	0.06

The ratio C_{sw}/C_c obtained from CRS for two 50 kPa unloading steps are shown in Table 3.9. From unloading steps with the oedomer, elastic rebound often occurs, which has traditionally been referred to as swelling. However, in the present research, the development of negative pressures was prevented during unloading. Consequently, only the swelling of clay particles was measured and no elastic occurred because there were no under pressures to be compensated with inflow of water. For this reason, the ratios C_{sw}/C_c found in this research are up to 2 orders of magnitude smaller than traditionally

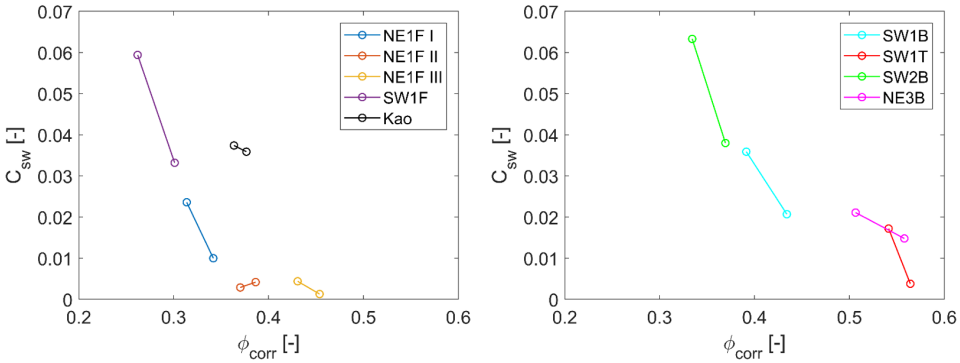

Figure 3.16: Coefficient of swelling C_{sw} as a function of ϕ_{corr} for the samples with only fines (left) and the ones also containing sand (right).

found in literature. Herein, (e.g *Lambe and Whitman*, 1969) reported this ratio to be around 0.4.

3.5. DISCUSSION

Below, a conceptual model describing the behaviour of the sediment studied in this presented. Furthermore, the effects of sample preparation and the scientific and engineering impact of the present Chapter are discussed.

3.5.1. CONCEPTUAL MODEL

Figure 3.17 proposes a conceptual model for the mechanical behaviour of cohesive sediment. Herein, the collapse of the flocs upon loading is not addressed. In this soil model, the different behaviour found for Markermeer samples are presented 1.1) fines dominated and OM (no sand), 1.2) fines dominated and OM (passive sand particles), 2) fines dominated oxidised OM (passive sand particles), 3) sand dominated and OM (passive clay) and 4) sand dominated oxidised OM (passive fine particles). The TFC determines the change from case 1.2 to case 3 and case 4.

For sand contents below 70% the behaviour of Markermeer sediment was dominated by the fine fraction. However, for the sediment sample with 70% sand, the sand particles form a skeleton and dominate the behaviour of the sediment. The same sand dominated behaviour was observed for the treated samples. Therefore, the fractal approach was not applicable for samples 70% sand and 40%-T because the sand was passive. However, it is remarkable that these samples still followed a power σ_{eff}-ϕ_{corr} relationship (Figure 3.11).

The fact that the oxidation of the OM changed the behaviour of a sample with 40% sand from fine dominated to sand dominated suggests that the physical particle interactions are also affected by the presence of OM and for the type of organic matter present. Chapter 2 of the present thesis already showed the importance of the reactivity of the OM. The implications of the type of OM will be discussed further in Chapter 5.

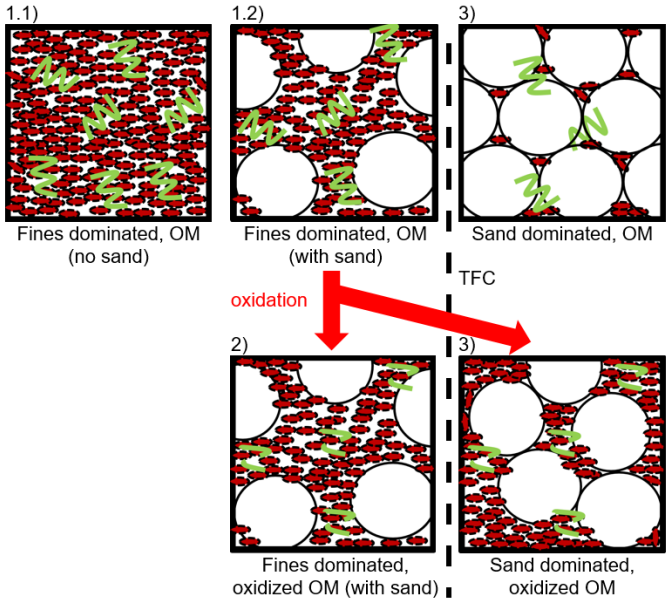

Figure 3.17: Conceptual model of the composition and behaviour of the studied sediment. Legend: curly lines represent OM, dashed curly lines represent oxidized OM, small oval particles represent fines, big round particles represent sand.TFC= Transitional Fines Content.

3.5.2. SAMPLE PREPARATION AND STRESS HISTORY

The fact that, for the IL test, all the ϕ_{corr} - effective stress relationships of the non treated samples above the TFC overlapped is an indication of a normal (virgin) consolidation process. The sample preparation consisted of removing the supernatant water of the fines fraction after sieving and adding the desired mass of dry sand to these fines. This represents a difference with respect to the CRS samples which were exposed to atmospheric drying to achieve the desired initial water content. The high suctions (*Laloui et al.*, 2010) needed to remove the water from the small pores of the fine fraction makes the sediment behave as over-consolidated. This can be observed in Figure 3.11 from comparing samples NE1F-I, NE1F-II and NE1F-III. The ϕ_{corr}- σ_{eff} relationships of these samples did not overlap because the samples were exposed to different degrees of drying. Herein, sample NE1F-III was exposed to the most drying to lower its w_0 below the LL and exhibited the most marked over-consolidated behaviour. The over-consolidation behaviour caused by desiccation had previously been observed by other authors (e.g. *Burland*, 1990). This highlights the importance of sample preparation and history. Finally, it is remarkable that all samples, independently of the initial over-consolidation conditions, still follow a power law ϕ_{corr}-σ_{eff} relationship. This indicates that the sediment structure is still self-similar.

3.5.3. SCIENTIFIC IMPACT OF THE RESULTS

The fractal approach frequently used in fluid mechanics (e.g *Merckelbach and Kranenburg*, 2004a) has been proved to work well at lower initial water contents than previously studied

by other authors (e.g *De Lucas Pardo*, 2015). Furthermore the present research proved that the fractal approach works well for the analysis of traditional soil mechanics experimental results such as undrained shear strength and compression test. For the IL test, normalising the volumetric concentration of sediment as ϕ_{corr} showed that the behaviour of all the natural samples with fines content above the TFC overlapped on the log-log ϕ_{corr}-σ_{eff} graph (Figure 3.6). However, the behaviour of the treated samples II-40%-T and III-40%-T did not overlap with the natural samples and exhibited steeper behaviour. This is also related to the increase of the critical clay content after treatment, as already observed from the Activity plot. The amount of clay present in the treated sediment (see Table 3.1) is below the minimum amount needed for the sediment to behave cohesive, i.e. was below the critical clay content. However, the c_u did not show the same marked increase of the slope of the ϕ_{corr}-c_u relationships for the treated samples SW10-T and 40%-T, suggesting that the fine content of these samples may be just at the TFC limit for the undrained shear strength behaviour. This less marked behaviour observed with the c_u results agrees with *Simpson and Evans* (2016). They found a lower amount of fines needed for fines dominated behaviour for their Fall Cone results than for their IL results. This may also explain why the increase of slope of the ϕ_{corr}-c_u relationship was also very small for the 70% sand sample.

Furthermore, in the present chapter, the swelling of clay particles of slurries has been quantified. Herein the results showed that the C_{sw} obtained when preventing negative pressures during unloading is up to two orders of magnitude smaller than the values traditionally presented in soil mechanics literature. This is because, without under pressures, only microscopic swelling of clay minerals is measured.

Finally, the effect that the treatment including oxidation had on the mechanical behaviour of the samples suggests the importance of characterising the type of OM present prior to studying the mechanical behaviour of fine sediments. This has traditionally been ignored in literature. Furthermore, the treated sample behaved as sand dominated for a lower sand content than the non- treated samples. This suggested that the type of organic matter (oxidised or labile) may impact the TFC.

3.5.4. ENGINEERING RECOMMENDATIONS

The findings suggest that the composition of the OM oxidises in contact with the air should be accounted for the estimation of the future behaviour of the sediment. This represents a difference with traditional engineering practice were mostly particle size, water content, plasticity and TOM are determined previous to construction. Furthermore, currently and unlike sand, the organic matter effect and the differences on lability are not accounted in the fractal model and further work implementing this would be recommended.

Furthermore, samples exposed to drying prior to testing showed over-consolidated behaviour upon loading. This indicates that the uppermost layer of the newly formed Marker Wadden islands while behave as over-consolidated after being exposed to atmospheric drying.

3.6. CONCLUSION

In classical soil mechanics, sediments are tested at quite high stresses and low initial water contents. The slurry samples studied in this Chapter had a much larger w_0. The mechanical behaviour of these slurries could be described well with power laws. Furthermore, the fractal theory works well for the analysis of the results from IL, CRS and Fall Cone tests. It has shown to be an adequate tool to normalise the behaviour for these tests. The slopes of the functions (n_f) describing the behaviour of Markermeer sediment depended on the composition of the solid fraction.

Quantitatively small changes in the amount or type of organic matter, by e.g. oxidation, had a big impact on the compressibility and undrained shear strength of the material. The results predict a large decrease on the ability to bind water of Markermeer sediment, after long-term exposure to atmospheric conditions. The undrained shear strength after oxidation decreased for the samples from both sampling sites. In particular, oxidised material with 40% sand (sample I-40% sand) was able to bind the same amount of water as natural virgin sediment with 70 % sand, having the same ϕ_{corr}-k relationship. For the material with 8% sand (SW1B), an even more pronounced change of behaviour was observed upon oxidation, given the higher initial amount of OM present. Furthermore, the changes in behaviour of Markermeer sediment caused by the natural variability and segregation-induced changes on the sand content were studied. The behaviour of Markermeer sediment was mostly dominated by the fine fraction. However, the threshold of transitional fine content TFC was passed at 70% sand content. In the same way, the treatment by including oxidation reduced the amount of fines at which the transitional behaviour to sand dominated occurred. It is remarkable that samples with a sand dominated granular behaviour also follows a power law. Furthermore, for 70% sand content, the hydraulic conductivity (k) slightly increased for the same water content of the fines fraction. The coefficient of consolidation (c_v) also increased and the compressibility (C_c) decreased. Equations according to fractal theory were presented for the calculation of c_v and C_c. The first is directly proportional to ϕ_{corr} while the latter is inversely proportional. The results obtained from these new fractal equations were satisfactory compared with the results obtained with standard procedures of geotechnical norms.

The slurries tested at different initial densities did not reach a unique compression line for the stress levels tested. However, further testing at larger stresses would be needed to conclude if the behaviour shows convergence at larger stresses.

The CRS test showed the advantage, with respect to the IL test, of continuous monitoring of the pore water pressures. This allowed to prevent the development of negative pressures and to check that large hydraulic gradients were not occurring during the test. Furthermore, unloading cycles were performed with the CRS test and the swelling coefficient was determined. These C_{sw} values and the ratio C_{sw}/C_c were very small given the prevention of negative pressures during unloading. Finally, the effect of overconsolidation induced by prior desiccation of the CRS samples was shown.

3.7. APPENDIX 3A: COMPARISON OF TERZAGHI AND GIBSON CONSOLIDATION THEORIES

Terzaghi's consolidation theory (*Terzaghi*, 1923) is based in the following assumptions:

- Saturated and uniform "soil".
- Soil particles and pore water are incompressible.
- Loading is 1DV (and the settlement and the flow of water are also vertical): lateral stresses are small.
- Flow of water follows Darcy Law.
- Compressibility and hydraulic conductivity are constant. Therefore, c_v is also constant.
- Deformations are small, which implies that strains can be computed from undeformed geometry. I.e.: the change in the volume of soil due to consolidation is negligible compared to the initial volume of soil. Therefore, this is a small strain theory.
- Secondary compression does not occur. Compression takes place only due to expulsion of pore water.

Because of all the assumptions included in Terzaghi's consolidation equation, direct substitution of fractal definitions herein may not be the most suitable way to link small strain Terzaghi consolidation theory with large strain consolidation theory (*Gibson et al.*, 1967). Thus, starting from the more general Gibson equation is the approach taken in the present work.

The Gibson equation in Eulerian coordinates (as obtained from the combination of the continuity equation, Darcy equation and definition of excess pore water pressure) in its general form reads:

$$\frac{\partial \phi_s}{\partial t} - \frac{\partial}{\partial z}\left(\frac{\rho_s - \rho_w}{\rho_w} k {\phi_s}^2\right) - \frac{\partial}{\partial z}\left(\frac{k}{g\rho_w}\frac{\partial \sigma_{eff}}{\partial z}\phi_s\right) = 0 \tag{3.23}$$

Gibson et al. (1967) suggested that for the case of thin layers, the influence of self-weight consolidation is negligible compared with that due to the applied total stress upon loading. Furthermore, they suggested that this approximation could be done by setting ρ_s=ρ_w. With this approximation, the Gibson equation can be simplified to:

$$\frac{\partial \phi_s}{\partial t} - \frac{\partial}{\partial z}\left(\frac{k}{g\rho_w}\frac{\partial \sigma_{eff}}{\partial z}\phi_s\right) = 0 \tag{3.24}$$

This Equation 3.24 can be rewritten by multiplying and dividing by $\partial\phi_s$, obtaining:

$$\frac{\partial \phi_s}{\partial t} - \frac{\partial}{\partial z}\left(\frac{k}{g\rho_w}\frac{\partial \sigma_{eff}}{\partial \phi_s}\frac{\partial \phi_s}{\partial z}\phi_s\right) = 0 \tag{3.25}$$

The consolidation coefficient of Terzaghi's consolidation theory is defined as:

$$c_v = \frac{k}{g\rho_w m_v} \tag{3.26}$$

where m_v is the coefficient of volumetric compressibility defined as

$$m_v = \frac{\partial \phi_s}{\phi_s \partial \sigma_{eff}} \tag{3.27}$$

and therefore

$$c_v = \frac{k}{g\rho_w} \phi_s \frac{\partial \sigma_{eff}}{\partial \phi_s} \tag{3.28}$$

Substituting 3.28 in 3.25 yields

$$\frac{\partial \phi_s}{\partial t} - c_v \frac{\partial^2 \phi_s}{\partial z^2} = 0 \tag{3.29}$$

On the other hand, substitution of the fractal description for effective stress and the consolidation parameter γ_c in Equation 3.24 leads to Equation 3.30.

$$\frac{\partial \phi_s}{\partial t} - \Gamma_c \frac{\partial^2 \phi_s}{\partial z^2} = 0 \tag{3.30}$$

3.8. APPENDIX 3B: EXCESS PORE WATER PRESSURE EVOLUTION DURING CRS TEST

The excess pore water pressures were continuously measured at the (undrained) bottom of the samples. At the beginning of the tests, before straining the samples, these pore pressures were equal to zero. The pore pressures exhibited fluctuations at the beginning of the straining but increased gradually thereafter during loading (Figure 3.18). When each sample was unloaded, a large drop on pore water pressures occurred. However, this reduction in pore pressures was lower than the total stress reduction in unloading because consolidation happens during the test. At the first moments of each re-loading, the excess pore pressure increased rapidly.

The excess pore pressures did not become negative for most of the samples because the strain rate and unloading time were controlled (Tables 3.5 and 3.4) to prevent it. The strain in unloading is actually very small (in Figure 3.18 it is almost imperceivable). This Figure 3.18 shows the pressure development for the soft clay NE1F-I sample (left) and the sandier sample NE3B (right). It is noted that in the case of the sandier sample NE3B, the (excess) pore pressures become negative during unloading, being the only sample developing (very limited) negative excess pore pressures.

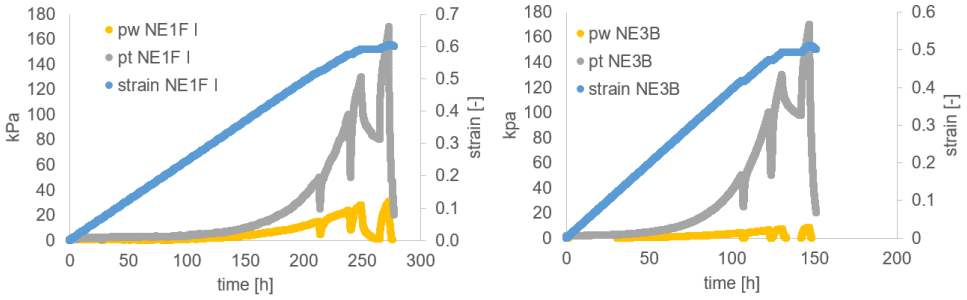

Figure 3.18: Pore water pressure pw, total stress pt and strain for samples NE1F I (0% sand, initial water content 1.8LL) and NE3B (70% sand and initial water content 1.4LL). Rate of strain for both tests:0.0012mm/min. Note that sample NE3B is the only one for which negative pressures were observed.

3.9. APPENDIX 3C: COMPARISON IL AND CRS RESULTS

In the experiments performed in this chapter, neither the total load nor the strain rates were identical for the IL and CRS tests. Furthermore, no identical samples were tested for the two experimental devices. Therefore, the performance of further experiments to gather enough data to compare the two set-ups is necessary. Namely, the performance of experiments with the CRS on the same samples tested with the IL applying all the (non constant) strain rates of the IL tests. However, some first comparisons can already be done.

Figure 3.19 shows the variation of strain rates during the first step of loading of the IL test I-0% sand. The average strain rate during this step is 0.003 mm/min. However, during the initial minutes of the test, the strain rate was 0.033 mm/min, i.e. more than 10 times larger.

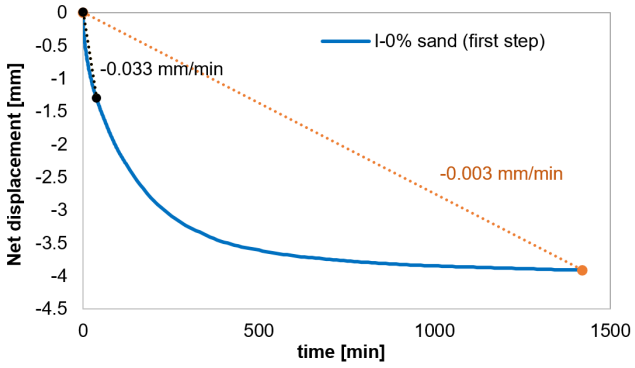

Figure 3.19: The strain rate is not constant during an IL test. Example of the variation of the strain rate during the first loading step of the Il test with 0% sand.

An approximate comparison of the IL and CRS results was performed by plotting the effective stress-ϕ_{corr} relationships for similar samples (0% sand and NE1F II) with only fines from the same sampling site. For the CRS sample NE1F II, the applied constant rate

was 0.0012 mm/min. Figure 3.20 shows that the relationships between effective stress and ϕ_{corr} have the same slope for both tests. The same occurs with the hydraulic conductivity. The smaller effective stressed obtained with the IL tests are more likely caused by the lower ranges of total stresses tested with the IL tests (comparison Table 3.3 and Table 3.5).

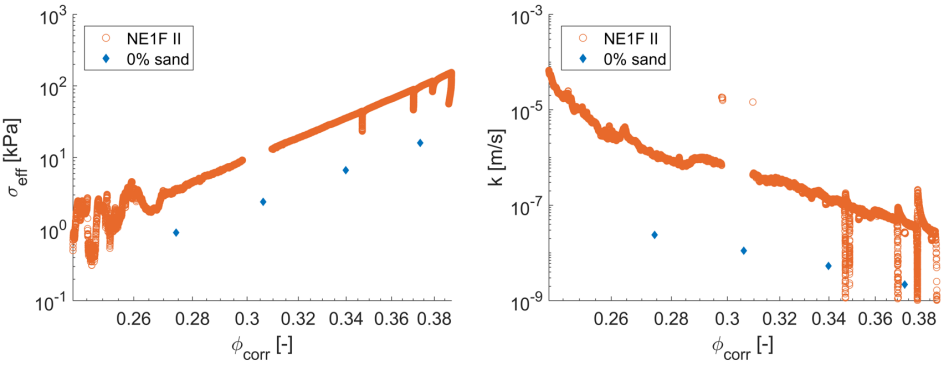

Figure 3.20: Comparison between the results of the CRS (sample NE1F-II) and IL test (sample 0% sand) for a sample with only fines: effective stress (left) and hydraulic conductivity (right).

3.10. APPENDIX 3D: CRS NON-LINEAR EFFECTIVE STRESS-STRAIN BEHAVIOUR

Figure 3.21 shows the effective stress-strain relationship for the soft sediment NE1F when the test was started at different initial water contents. The larger the initial water content, the steeper the stress-strain curves. Further, it can be seen that the higher the initial water content, the less constant the slope is of these curves on a linear scale, notably for the samples with larger initial water content NE1F I and NE1F II. This non-linear effective stress-strain relationship implies that the coefficient of volumetric compressibility m_v is not constant. However, by plotting on the semi-logarithmic scale, it can be seen that the slope of the log-effective stress- strain is close to constant for the major part of the test, notably for $\sigma_{eff} > 100$ kPa. This implies that, like the IL test, the C_c is almost constant during that part of the test, which corroborates that the behaviour of the samples is non-linear (*ASTM*, 2014).

All the other fine and sandy samples also exhibited the same non-linear behaviour.

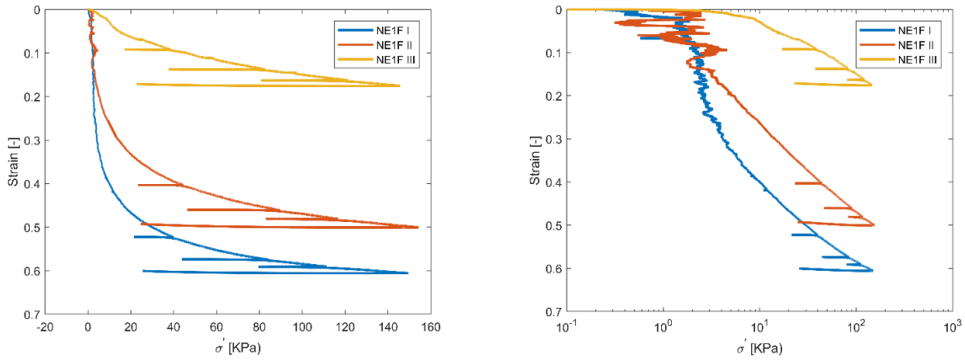

Figure 3.21: Effective stress-strain for samples of sediment NE1F, at different initial water content (1.8, 1.2 and 0.7, respectively). Linear (left) and logarithmic (right) x axis

4

CONSOLIDATION OF SLURRIES UNDER WATER

Parts of this chapter have been submitted to Canadian Geotechnical Journal.

4.1. INTRODUCTION

A cohesive sediment-water mixture can behave like a dense fluid, when the pore pressure is equal to the total stress, or like a soft soil, when the pore pressure is lower than the total stress and therefore effective stress exists (*Terzaghi*, 1923; *Terzaghi and Peck*, 1967). The density at which effective stress develops is referred as structural density (*Sills*, 1998) or gelling point (*Winterwerp*, 1999; *Dankers*, 2006). At the structural density, flocs are space-filling and a network structure starts to build-up. The concentration of solids at this point is referred as c_{gel}.

Slurries at concentrations above the gelling point are used for reclamation and Building with Nature (BwN) projects. The Marker Wadden project in The Netherlands is an example of a BwN project using slurries, originating from the sediment deposited in Lake Markermeer, to create a new wetland in the lake. In order to use the sediment of the lake bed, the sediment has to be diluted with water so that it can be pumped. These slurries are then pumped and deposited in calm areas where they are allowed to settle and consolidate. In this chapter the effect of the initial concentration on the final density profile and bed height was studied.

The settling and consolidation behaviour of mud at initial concentrations below this gelling point has been thoroughly studied by various authors (e.g. *Gibson et al.*, 1967; *Been and Sills*, 1981; *Toorman*, 1999; *Merckelbach*, 2000; *Dankers*, 2006; *De Lucas Pardo*, 2015). These authors showed that the material parameters can be determined from simple settling columns experiments (*Merckelbach and Kranenburg*, 2004b). Such material parameters can be used to calculate the hydraulic conductivity and the effective stress from equations based on the volumetric concentration of solids (*Merckelbach and Kranenburg*, 2004a). However, the consolidation behaviour of mixtures above the gelling point has been studied less and the determination of the material characteristics requires more sophisticated experimental devices. *Imai* (1979) proposed a seepage induced consolidation (SIC) test in which a downward seepage force is imposed by creating a constant head difference. Herein, the pore water pressures are continuously measured and the void ratio is obtained at the end by slicing the sample. This method was later improved by *Znidarčić and Liu* (1989). In this improved configuration, a constant flow rate is imposed across the sample instead of a constant head. This enables testing under small gradients leading to more reliable results at the low effective stress ranges of soft cohesive soils. The SIC test allows to obtain void ratio- hydraulic conductivity and void ratio-effective stress relations (*Huerta et al.*, 1988; *Liu and Znidarčić*, 1991).

The initial concentration of solids c_0 at which a settling test is performed may influence the settling and consolidation behaviour of the sediment. When starting a hypothetical settling experiment by remixing the final density (equilibrium) profile over the final bed height h_∞ obtained from a suspension ($c_0 < c_{\text{gel}}$), the initial concentration c_0 of the newly prepared slurry is significantly larger than c_{gel}. In a similar way, when remixing at an earlier phase of consolidation of a suspension, c_0 may still be above c_{gel}. In both mixing situations shown in Figure 4.1, there is a mismatch between the in-situ stresses and the at-rest virgin consolidation behaviour. The top part of such a mixed slurry is over-consolidated while the bottom part is *under-consolidated*. The upper over-consolidated part has a lower water content w% and hydraulic conductivity than the original suspension equilibrium profile. This upper part has a larger density and is less

permeable, thus acts as a "crust" over the under-consolidated part. The water of this bottom part can therefore not escape in the vertical direction as easy as in the case of a low concentrated suspension.

In classical soil mechanics unloading, negative pore pressures would result in elastic rebound of the material, often defined as swelling (e.g. *Lambe and Whitman*, 1969). During the Constant Rate of Strain tests presented in Chapter 3, this elastic rebound was not induced because negative pore pressures were prevented. Therefore, only the microscopic swelling of clay particles was measured. The coefficients of swelling determined in Chapter 3 are thus applicable to the consolidation slurries studied in the present chapter.

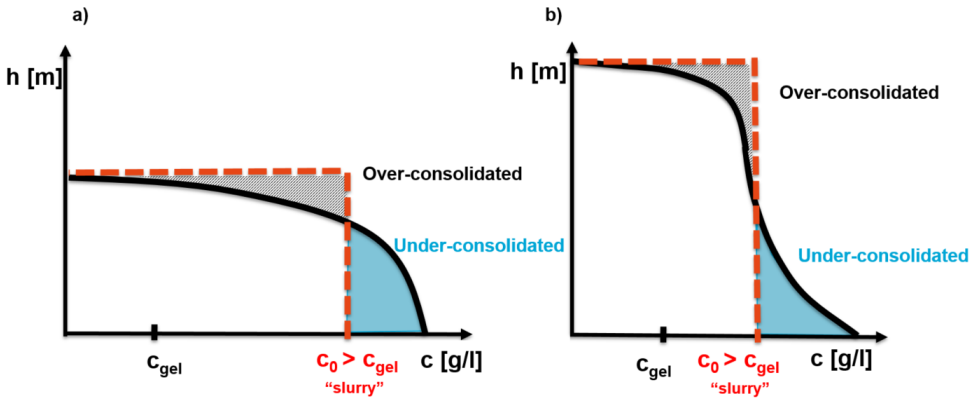

Figure 4.1: a) Initial concentration(c_0) profile for a slurry after remixing the final equilibrium concentration profile obtained from a suspension by virgin consolidation. b) Initial concentration profile for a slurry after remixing the concentration profile during the first stages of consolidation. The initial sediment concentration c_0 is now smaller than in the previous case. However, $c_0 > c_{gel}$ for both cases. X-axis represents the concentration. Y- axis represents the height.

In the present chapter, the influence of the initial concentration c_0 on the consolidation behaviour of mud was studied for mud mixtures with an initial concentration above the gelling point. Herein, the effect of the degree of dilution of the sediment was analysed with a 1DV consolidation model. For that, the material parameters were calculated for $c_0 > c_{gel}$ with the Seepage Induced Consolidation test (*Liu and Znidarčić*, 1991) and compared with the results obtained from settling columns for $c_0 < c_{gel}$.

4.2. METHODS

4.2.1. SEDIMENT USED

THE Markermeeer sediment used in this chapter was NE1F, which detailed composition is presented in Chapter 2. Sample NE1F represents the fine fraction of a natural sample of the upper layer of sediment from the Northeast of Lake Markermeer. NE1F has 0% sand, 4.5% Total Organic Matter and a particle density ρ_s of 2540 kg/m^3.

Various authors have determined the gelling concentration for different Markermeer sediment samples. The lowest value was obtained by *De Lucas Pardo* (2015), who found a c_{gel} of 70 g/l, while *Hendriks* (2016) obtained the highest value, with 85 g/l.

4.2.2. EXPERIMENTAL METHODS

The material parameters of Markermeer mud were obtained with two different experimental methods: settling columns (for $c_0 < c_{gel}$) and Seepage Induced Consolidation (SIC) tests (for $c_0 > c_{gel}$).

The settling column tests were performed at concentrations below c_{gel} (40, 50 and 60 g/l) and above (100, 200, 300 and 400 g/l). Additionally, two duplicate settling column tests were performed for 200 and 400 g/l to test reproducibility of the results (see Figure 4.2). At the end of the settling column tests, the density profiles of all columns were measured with an Ultrasonic High Concentration Meter (UHCM).

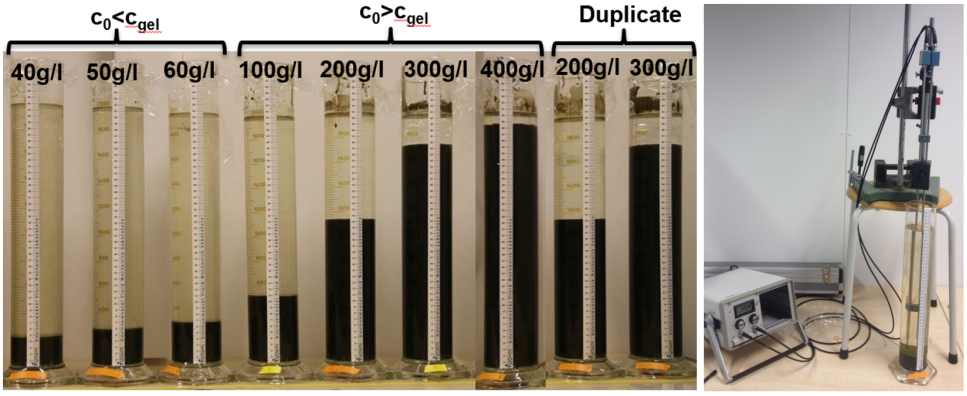

Figure 4.2: Settling column experiments performed and concentrations (left) and UHCM final density profile measurement (right).

MATERIAL PARAMETERS BELOW GELLING POINT

The material parameters for initial concentrations c_0 below the expected gelling point (*De Lucas Pardo*, 2015; *Hendriks*, 2016) were determined with settling column experiments. From these tests, the effective velocity w_s of the settling interface can be obtained directly as the slope of the settling curve. *Dankers and Winterwerp* (2007) established a relationship between w_s and the volumetric concentration of flocs ϕ_f:

$$w_s = w_{s,0} \frac{(1-\phi_f)^m (1-\phi_s)}{1+2.5\phi_f} \tag{4.1}$$

where $w_{s,0}$ is the settling velocity of one individual particle and $\phi_s = c/\rho_s$ is the volumetric concentration of solids (primary particles), in which c is the mass concentration and ρ_s the particle density. The volumetric concentration of flocs ϕ_f is equal to c/c_{gel} because $\phi_f = \phi_s/\phi_{gel}$ by definition. The empirical parameter m that accounts for non-linearity was set to 2, according to *Dankers and Winterwerp* (2007). From two settling curves started at two different concentrations, the unknown variables $w_{s,0}$ and c_{gel} were calculated.

Assuming that the cohesive sediment flocs and bed behave as self-similar fractal structures (*Kranenburg*, 1994), the material parameters were obtained from the settling columns experiments. The calculation was done according to *Merckelbach and Kranenburg* (2004b). First, the sediment- water interface during the first phase of consolidation,

when the effective stresses are still small, was plotted and the following equation was fitted:

$$h(t) - \zeta_s^{sa} = \left(\frac{2-n}{1-n}\zeta_s^f\right)^{\frac{1-n}{2-n}} (n-2)\, K_k \left(\frac{\rho_s - \rho_w}{\rho_w}\right)^{\frac{1}{2-n}} t^{\frac{1}{2-n}} \tag{4.2}$$

where ρ_w is the density of water, ζ_s^{sa} is the Gibson height accounting for sand (particles > 63µm) and ζ_s^f is the Gibson height of the fines fraction (particles < 63µm). ζ_s^f is equal to $\phi_s^f H_0$, where ϕ_s^f is the initial volumetric concentration of fines and H_0 the initial thickness of the slurry layer (here corresponding to the height of the settling column). Because the sediment studied did not contain sand, the volumetric concentration of sand ϕ_s^{sa}=0 and ζ_s^{sa}=0 . Further, $h(t)$ [m] is the height of the mud-water interface, t [s] is the time and K_k [m/s] is the permeability material parameter. The scalar n is related to the fractal dimension n_f as $n = 2/(3-n_f)$. Next, the effective stress parameter K_σ was calculated, from equilibrium conditions, with Equation 4.3:

$$h_\infty - \zeta_s^{sa} = \frac{n}{n-1}\frac{K_\sigma}{g\left(\rho_s - \rho_w\right)}\left(\frac{g\left(\rho_s - \rho_w\right)}{K_\sigma}\zeta_s^f\right)^{\frac{n-1}{n}} \tag{4.3}$$

where h_∞ is the final consolidation height and K_σ [Pa] is the effective stress material parameter.

The permeability and effective stress material parameters, K_k and K_σ, are used to calculate the hydraulic conductivity k and effective stress σ_{eff} of the sediment according to Equations 4.4 and 4.5 (*Merckelbach and Kranenburg*, 2004a):

$$k = K_k \left(\frac{\phi_s^f}{1-\phi_s^{sa}}\right)^{-\frac{2}{3-nf}} \tag{4.4}$$

$$\sigma_{\text{eff}} = K_\sigma \left(\frac{\phi_s^f}{1-\phi_s^{sa}}\right)^{\frac{2}{3-nf}} \tag{4.5}$$

MATERIAL PARAMETERS ABOVE GELLING POINT

The material parameters for initial concentrations c_0 above the gelling point were determined with the SIC test device available at Deltares, Delft. The device used is based on *Znidarčić and Liu* (1989) and *Abu-Hejleh et al.* (1996). The set-up consists of a frame, a triaxial cell, a volume displacement pump, water supply cells, pressure, force and displacement transducers and a data acquisition system (see Figure 4.3).

The samples tested in the SIC tests originated from the settling column experiments. After equilibrium was attained in each settling column, the supernatant water was removed and the sediment from the newly formed bed was transferred to a container in which it was gently mixed to homogenize the sample, avoiding air entrapment. The water content was then determined by drying a subsample in an oven at 105 °C to derive the initial void ratio e_0. Then, the sediment was put into the sample holder ring of the triaxial cell and allowed to rest for three days. The triaxial cell was filled with water to extrude air and the test was started. Three SIC tests were performed. They are referred as SIC200,

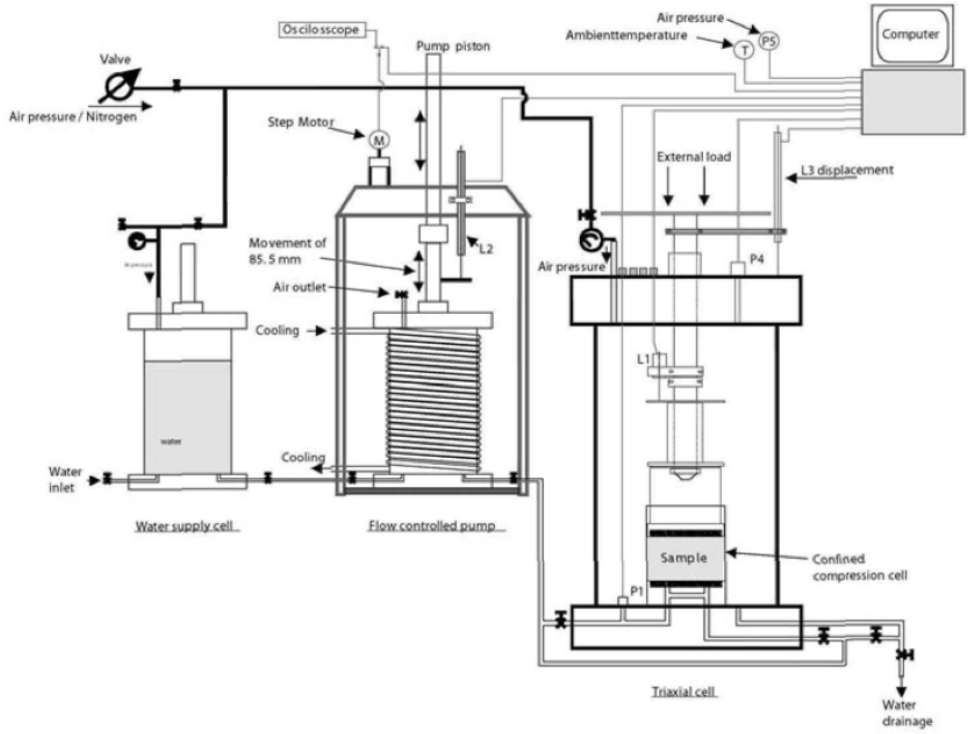

Figure 4.3: Diagram of the Seepage Induced Consolidation set-up.

SIC300 and SIC400 because the sediment originated from the settling columns with initial concentration 200, 300 and 400 g/l, respectively. There was not enough sediment in the column with c_0=100 g/l to fill in the SIC sampling ring.

To obtain compressibility and hydraulic conductivity data, each SIC test was run for seven loading steps followed by permeability steps. These loading and permeability steps are listed in Table 4.1. The loading steps were undrained at the bottom of the sample to allow measurement of the excess pore water pressure in time. After equilibrium was reached and the pressure stabilized (i.e, excess pore water was close to zero), a permeability step was applied by imposing a small downward water flux across the sample. The downward flow of water consolidates the sample, increasing the pressure difference across the sample with time. The same flow rate was maintained until steady state conditions were reached, no further consolidation occurred and the pressure difference across the sample became constant.

The void ratio was calculated continuously from the sample height during the tests and the initial void ratio e_0. At the end of the test, the final void ratio e_∞ was determined by oven-drying of a sub-sample at 105 °C. The data was fitted to power law functions to obtain the hydraulic conductivity and effective stress. Here, two sets of power law functions were used. The first set was dependent on the volumetric concentration ϕ_s and consisted of the equation with the fractal descriptions used for the settling columns, i.e.,

Table 4.1: Seepage Induced Consolidation test plan including all the loading and permeability steps performed to each sample. *For the SIC400, a load of 30 kPa was applied instead of 10 kPa.

Step	Load [N]	Stress [Pa]	Discharge [mm^3/s]
Loading (filter stone)	1.8	98.5	
Loading	2.0	111.7	
Permeability (seepage)			0.5
Permeability (seepage)			1.0
Loading	5.0	279.2	
Permeability (seepage)			2.0
Permeability (seepage)			1.0
Loading	10.0*	558.4	
Permeability (seepage)			1.0
Permeability (seepage)			1.5
Loading	50.0	2792.1	1.0
Permeability (seepage)			1.5
Permeability (seepage)			
Loading	100.0	5584.0	
Permeability (seepage)			1.0
Permeability (seepage)			1.5
Loading	500.0	27920.7	
Permeability (seepage)			1.5
Permeability (seepage)			1.0
Permeability (seepage)			0.2
Permeability (seepage)			0.3
Loading	900.0	50257.3	
Permeability (seepage)			0.3
Permeability (seepage)			0.2
Permeability (seepage)			0.2
Permeability (seepage)			0.1

Equations 4.4 and 4.5. The second set was a function of the void ratio e and consisted of the following equations (*Liu and Znidarčić*, 1991):

$$k = C_k e^{D_k} \tag{4.6}$$

$$\sigma_{\text{eff}} = \left(\frac{e}{A_\sigma}\right)^{-\frac{1}{B_\sigma}} \tag{4.7}$$

where A_σ, B_σ, C_k and D_k are empirical parameters obtained from fitting. The void ratio e and the volumetric concentration of sediment ϕ_s (in this case $\phi_s = \phi_s^f$) are related as $1 + e = 1/\phi_s$. For convenience, Equation 4.7 is also presented as:

$$e = A_\sigma {\sigma_{\text{eff}}}^{-B_\sigma} \tag{4.8}$$

4.2.3. THE 1DV-SLURRY MODEL

To compare the behaviour of suspensions ($c_0 < c_{\text{gel}}$) with the one of slurries ($c_0 > c_{\text{gel}}$), the two sets of parameters obtained from the settling columns and from the SIC tests were used as input for a the 1DV-slurry model to compute density profiles. This 1DV-slurry

model is a version of the 1DV model (*Winterwerp*, 1999) adapted for highly concentrated mixtures (i.e., slurries). The numerical experiment included remixing of suspensions ($c_0 < c_{gel}$) up to the bed-water interface. As a result, the new settling material had a new initial concentration profile ($c_0 > c_{gel}$) and a smaller initial height than the previous suspension. The maximum time step in the computations was limited by the settling velocity and the size of the computational layers.

THEORETICAL BACKGROUND

The introduction of the fractal approach (equations 4.4 and 4.5) leads to the consolidation equation 4.9, which for the case of only fines present ($\phi_s^f = \phi_s$), reads:

$$\frac{\partial \phi_s}{\partial t} - \frac{\partial}{\partial z}\left(\frac{\rho_s - \rho_w}{\rho_w} k {\phi_s}^2\right) - \Gamma_c \frac{\partial^2 \phi_s}{\partial z^2} = 0 \tag{4.9}$$

where Γ_c is a consolidation coefficient defined as

$$\Gamma_c = \frac{2}{3 - n_f} \frac{K_k K_\sigma}{g \rho_w} \tag{4.10}$$

The unloading or swelling behaviour of Markermeer sediment was experimentally quantified in Chapter 3, where the coefficient c_{sw} was obtained from unloading cycles during Constant Rate of Strain tests. For the material studied in the present chapter, a value of c_{sw}=0.015 was found. This small value implies that only little (elastic) rebound occurs.

To account for over-consolidated initial conditions, the effect of elastic swelling was implemented in the 1DV-model referred to as the 1DV-slurry model. Herein, the consolidation coefficient Γ_c obtained from the settling columns was reduced a factor of hundred for (partially) over-consolidated initial conditions. This reduction of Γ_c accounts thus for the small rebound effect. For the case of normal consolidation, the measured Γ_c was used.

MODELLING APPROACH

The density profiles computed with the 1DV-slurry model were then compared with the profiles measured with the Ultrasonic High Concentration Meter (UHCM) at the end of all the settling experiments. This allowed to validate the model.

The sensitivity of the model results was evaluated by also using the material properties obtained from the different experimental set-ups (SIC and settling).

Prognostic simulations were performed to test the influence of the over-consolidation effect induced by the initial density profile. They consisted of remixing the density profile at equilibrium and during the second phase of consolidation. This enabled to test the influence of the degree dilution upon dredging on the newly formed (reclaimed) wetland.

4.3. RESULTS

4.3.1. MATERIAL PARAMETERS BELOW GELLING POINT

Figure 4.4 shows the settling curves for the tests below the gelling point. The slopes during the hindered settling phase (i.e. first minutes of the test) correspond with an effective velocity w_s of 3.95×10^{-6}, 2.19×10^{-6} and 1.50×10^{-6} m/s for c_0 = 40, 50 and 60 g/l respectively.

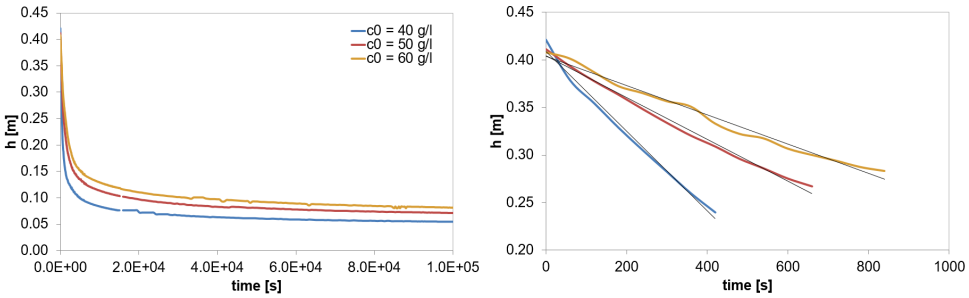

Figure 4.4: Settling curves for the experiments at $c_0 < c_{gel}$ (left) and zoom in during the settling phase (right).

The pairs $w_{s,0}$ - c_{gel} obtained with Equation 4.1 are shown in Table 4.2. From these results, the intermediate gelling concentration value of 92.2 g/l was used for the subsequent calculations. The material parameters obtained with the fractal approach are shown in Table 4.3.

Table 4.2: Gelling concentrations and sediment particle velocity of the sediment studied for $c_0 < c_{gel}$ settling experiments.

c_{gel} [g/l]	$w_{s,0}$ [m/s]
95.1	2.30E-03
92.2	2.61E-03
88.5	2.84E-03

Table 4.3: Material parameter for the sediment studied as determined from settling experiments at $c_0 < c_{gel}$.

c_0 [g/l]	n_f [-]	K_k [m/s]	h_∞ [m]	K_σ [Pa]
40	2.70	1.23E-13	4.3E-02	1.12E+07
50	2.69	2.18E-13	5.3E-02	8.10E+06
60	2.70	1.74E-13	6.2E-02	1.26E+07

The density profiles measured at the end of the settling column tests for the columns with $c_0 < c_{gel}$ are shown in Figure 4.5. The overshoots observed on these data are common when using an aquatic device to measure. Herein, it can be seen that the settling column experiments with c_0 of 40, 50 and 60 g/l were stopped before reaching equilibrium (e.g. *Sills*, 1998).

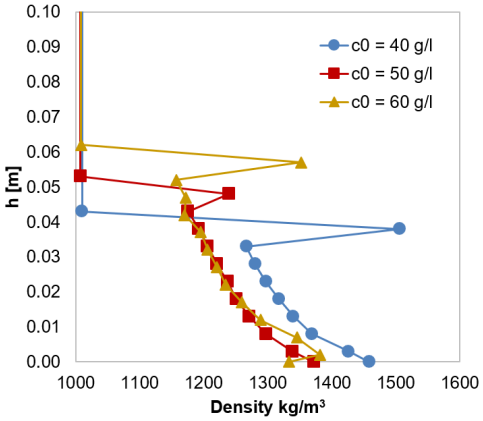

Figure 4.5: Measured density profile at the end of the settling column tests for $c_0 < c_{gel}$.

4.3.2. MATERIAL PARAMETERS ABOVE GELLING POINT

Figure 4.6 shows the consolidation curves for the tests above the gelling point and the density profiles which were measured with the UHCM device at the end of the tests. The consolidation curves for $c_0 > c_{gel}$ showed an initial linear phase caused by a higher density than at equilibrium in the upper part of the mud layer (over-consolidated). This excess density caused the upper layer to be heavier and less permeable and therefore act like a crust.

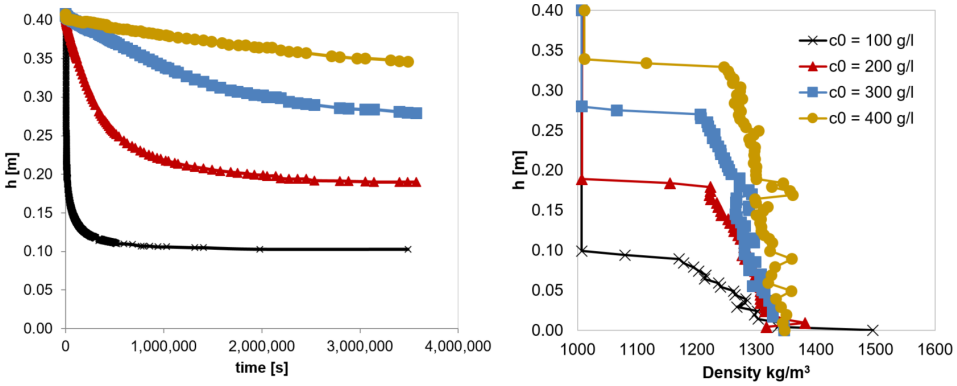

Figure 4.6: Measured settling curves (left) and density profiles at the end of the test(right). $c_0 < c_{gel}$.

For the columns with 200, 300 and 400 g/l, the material parameters were determined with the SIC tests after the settling column tests were finished. The results from the SIC tests as a function of ϕ_s are shown in Figure 4.7. From fitting the fractal Equations 4.4 and 4.5, the material parameters presented in Table 4.4 were obtained. The fact that these material parameters are not identical to the ones determined previously with the settling column tests suggests an influence of the stress history and plastic deformation upon remixing of the settled bed, which may induce over-consolidated behaviour during the

SIC tests.

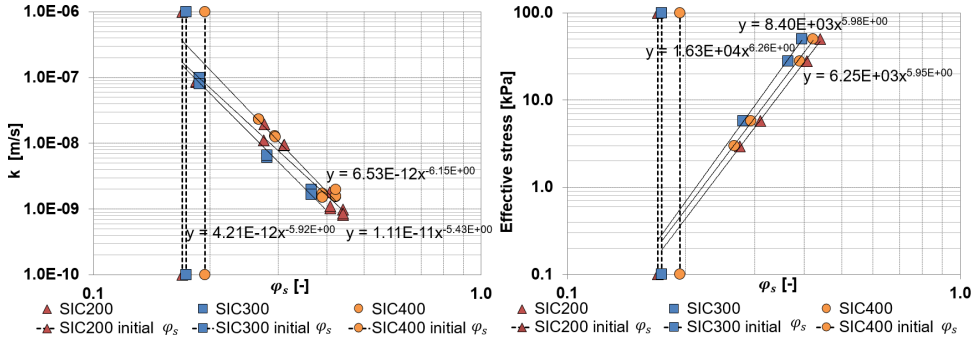

Figure 4.7: Hydraulic conductivity k and effective stress obtained from the Seepage Induced Consolidation tests. Results plotted as function of ϕ_s to obtain the fractal parameters.

Table 4.4: Fractal and *Liu and Znidarčić* (1991) material parameters as obtained from the Seepage Induced Consolidation tests.

	From k data		From σ data		From k data		From σ data	
ID	n_f [-]	K_k [m/s]	n_f [-]	K_σ [Pa]	C_k [m/s]	D_k [-]	A_σ [1/Pa$^{B_\sigma}$]	B_σ [-]
SIC200	2.63	1.11×10^{-11}	2.66	6.25×10^{6}	3.53×10^{-10}	3.78	3.83	0.29
SIC300	2.66	4.21×10^{-12}	2.68	1.63×10^{7}	1.47×10^{-10}	4.30	3.89	0.24
SIC400	2.68	6.53×10^{-12}	2.67	8.40×10^{6}	3.64×10^{-10}	4.03	3.68	0.25

The material parameters calculated according to *Liu and Znidarčić* (1991) are shown in Table 4.4. They were obtained from fitting Equations 4.6 and 4.8 to the results as a function of the void ratio (see Figure 4.8). Note that the comparison of the set of Equations 4.4 and 4.5 with Equations 4.6 and 4.7 yields to the following approximate equation to calculate D_k:

$$D_k = \frac{n_f}{B_\sigma} \tag{4.11}$$

which gives values of D_k of the same order of magnitude that presented in Table 4.4.

4.3.3. THE 1DV-SLURRY MODEL

VALIDATION OF THE MODEL

The density profiles computed with the 1DV-slurry model were compared with the profiles measured with the Ultrasonic High Concentration Meter (UHCM) at the end of the settling experiments after 67 days. This was done for initial concentrations of 200 and 300 g/l. Figure 4.9 shows that there is a good agreement between the measured and computed density profiles where the latter were calculated using the SIC parameters. However, the agreement between the profile computed with the settling column parameters from c_0 = 40 g/l showed offset with respect to the measured profile for the case of c_0 = 300 g/l. In particular, the computed profile with these parameters did not indicate equilibrium at

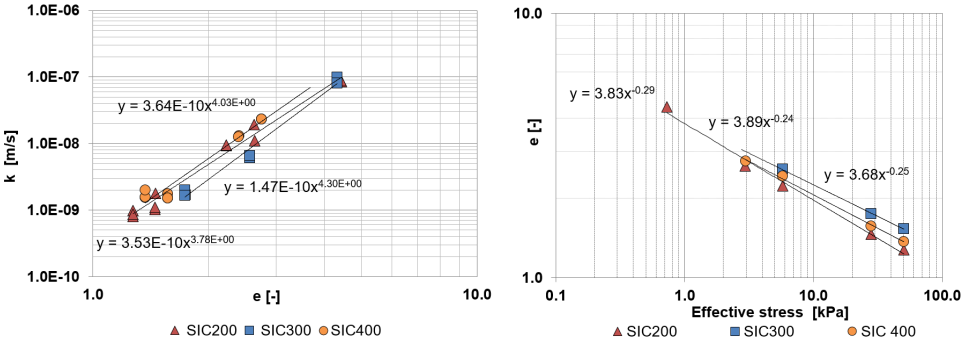

Figure 4.8: Hydraulic conductivity k (left) and effective stress (right) obtained from the Seepage Induced Consolidation tests. Results plotted as function of void ratio to obtain the material parameters according to *Liu and Znidarčić* (1991). For convenience, the effective stress is presented on the x- axis (see Equation 4.8).

4

t = 67 days. This suggests that the offset may be caused by the permeability coefficient K_k from the settling columns, which was one order of magnitude smaller than the correspondent SIC parameter. Thus, even if final bed heights may be predicted correctly when using the different sets of material parameters, the consolidation time may vary considerably due to differences of the K_k values.

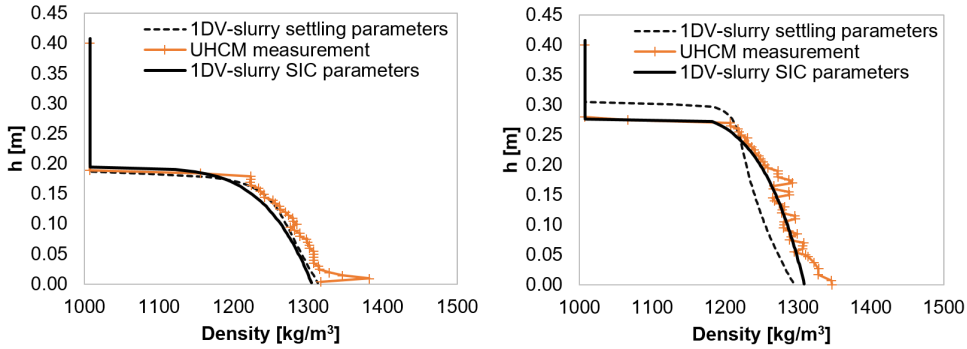

Figure 4.9: Validation of the 1DV-slurry model used for c_0=200 g/l (left) and c_0=300 g/l (right): measured and computed profiles with SIC and settling column material parameters at t=67 days.

The results show that the determination of the material parameters with the SIC tests provide more accurate results of the settling and consolidation of slurries from $c_0 > c_{gel}$ than the determination from settling column tests. Material parameters from settling columns may be used to get a first estimate.

SENSITIVITY ANALYSIS

The sensitivity of the 1DV-slurry model results was evaluated by interchanging the coefficients of the material properties obtained from the different experimental set-ups (SIC and settling). Thus, a computation with c_0=200 g/l and the SIC 300 parameters and

another one with c_0=300 g/l and the SIC 200 parameters were performed. Figure 4.10 presents these results which show that the model is stable.

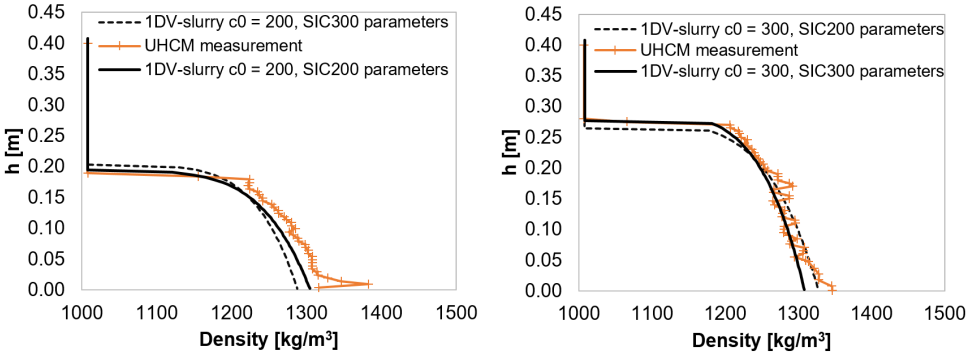

Figure 4.10: Sensitivity analysis. Comparison between the measured density profile and the computed profiles from SIC results 200 and 300 after interchanging parameters.

PROGNOSTIC SIMULATIONS

The evolution of density and effective stress profiles for a 5 m high consolidating layer with an initial concentration of 60 g/l are shown in Figure 4.11. The material parameters used come from Table 4.3, as determined with the small-scale settling column experiments.

Figure 4.12 shows the evolution of density profiles from the prognostic simulations starting at concentrations of 175.6 and 558.1 g/l. They correspond with the concentrations after redistribution of the total consolidating sediment mass across the entire thickness of the layer (remixing) at t = 36 h (first phase of consolidation) and t = 1200 days (equilibrium). The results show that further settling occurred after remixing the equilibrium profile of the virgin consolidated suspension. Furthermore, the results show that after remixing at t = 36 h the same final bed height than for the virgin suspension (Figure 4.11) was obtained (but after a larger consolidation time).

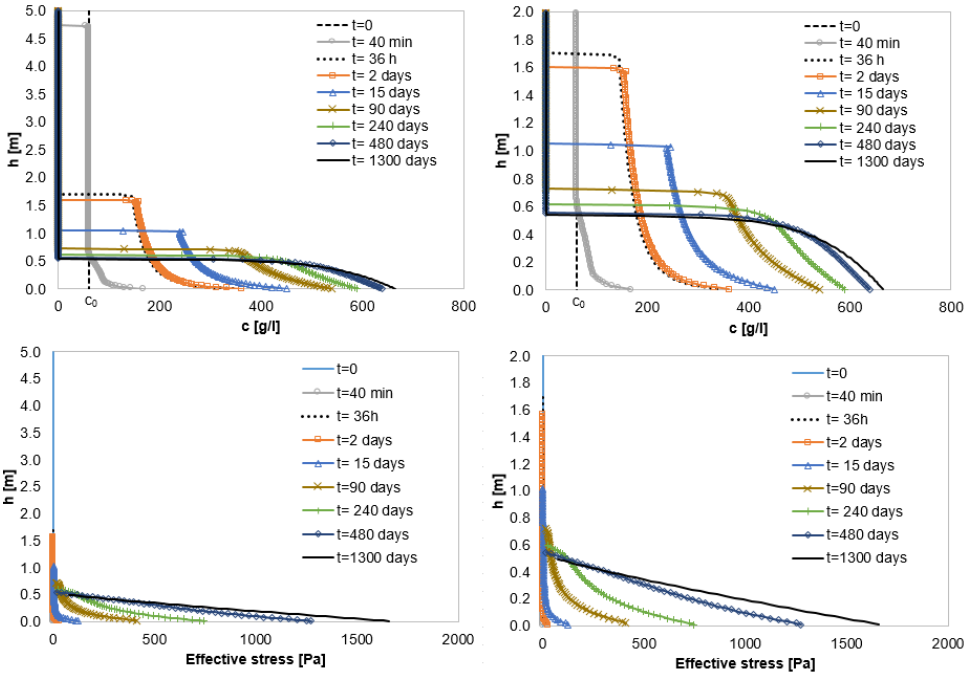

Figure 4.11: Top panel: Density profiles during virgin consolidation of a 5 m height column of a suspension with c_0 = 60 g/l. Bottom panel: effective stress development herein.

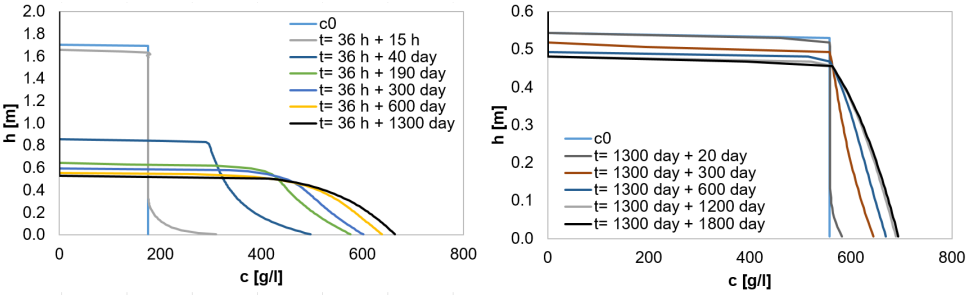

Figure 4.12: Density profiles starting with an initial concentration of 175.6 g/l after remixing the density profile during the first phase of consolidation (at t=36 h of Figure 4.11) of a suspension (left) and a concentration of 558.1 g/l after remixing the equilibrium profile (t= 1300 days of Figure 4.11) (right).

4.4. DISCUSSION

In this section, the effect of mixing on the material parameters is discussed. Furthermore, the imbalance of stresses after mixing and the impact of the initial conditions on the final bed density and height are also addressed. Finally, the scientific impact and the engineering recommendations that can be derived from the results of the present Chapter are also discussed.

4.4.1. MATERIAL PARAMETERS, MIXING AND STRESS HISTORY

Figure 4.13 shows the fractal material parameters determined as a function of the initial volumetric concentration of solids $\phi_{s,0}$ for the present research. Herein, the results are also compared to results from *Hendriks* (2016) and *De Lucas Pardo* (2015), who both have used similar sediment from lake Markermeer. This figure shows the sensitivity of the K_k parameters to $\phi_{s,0}$, which varies various order of magnitude for different samples. This is different with respect to the K_σ parameter, which values are quite stable. The *Liu and Znidarčić* (1991) material parameters determined from the SIC test were in the order of magnitude as the ones found previously for Markermeer sediment *Van Olphen* (2016). They found A_σ=2.55-3.19 [1/Pa$^{B_\sigma}$], B_σ= 0.11-0.15 [-], C_k=1 × 10^{-10} –1 × 10^{-11} [m/s] and D_k=6.04-7.00 [-].

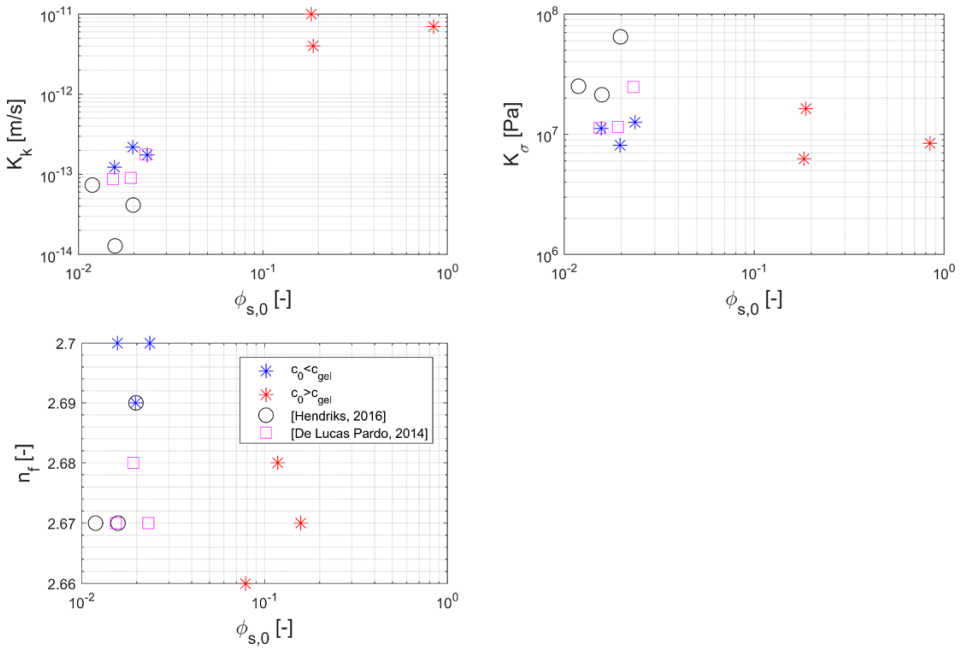

Figure 4.13: Comparison of the fractal material parameters obtained with respect to the initial volumetric concentration, including the results of *De Lucas Pardo* (2015) and *Hendriks* (2016).

In Figure 4.14, the k and effective stress calculated (Equations 4.4 and 4.5) with the material parameters obtained from settling tests (Table 4.3) were extrapolated to ranges

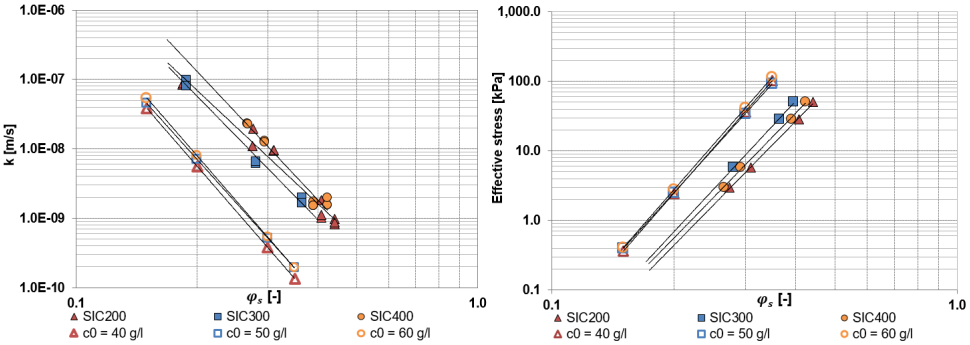

Figure 4.14: Obtained hydraulic conductivity (left) and effective stress (right) from the settling column and SIC tests. The figure includes extrapolated data (to ranges of ϕ_s occurring during the SIC tests) of the k and effective stress obtained from settling column tests.

of ϕ_s tested with the SIC. This was done to investigate the influence of the $\phi_{s,0}$, mixing and stress history at which the material parameters were determined. The results show that, compared to the extrapolated settling data, the SIC hydraulic conductivity was larger while the effective stress was smaller (Figure 4.14). The SIC tests were performed after mixing the sediment of the settling columns. Thus, the results suggest an effect of the mixing and stress history on the parameters determined. In particular, Equations 4.4 and 4.5 are applied to an averaged ϕ_s for the case of the SIC. Therefore, the results must differ from the outcome of applying these equations to the settling columns, where the ϕ_s is not averaged over the vertical. Given the negative power of Equation 4.4, the SIC hydraulic conductivity obtained from the averaged ϕ_s is larger. In the same way, the positive power of Equation 4.5 explains the smaller effective stress of the SIC test.

4.4.2. IMBALANCE OF STRESSES AFTER MIXING

Figure 4.15 shows the computed effective stress profiles just before and just after mixing the consolidating layer after 36h of consolidation time and at equilibrium for a virgin consolidating layer of a suspension. The presence of the over- and under- consolidated parts of the layer is indicated by the model results. This represent the stress situation before and after mixing Markermeer sediment with water to dredge and pump the sediment. Figure 4.15 shows that the degree of over- consolidation is different depnding on the mixing time.

4.4.3. IMPACT OF INITIAL CONDITIONS ON FINAL DENSITY PROFILE AND SEDIMENT HEIGHT

Figure 4.16 shows the settling curves and final density profiles for all the prognostic simulations observed. The results show that the final bed height h_∞ for a 5 m column suspension with c_0= 60 g/l was 0.519 m. Remixing the 60 g/l suspension at t=36 h, produced a slurry with c_0= 175.6 g/l that reached the same final height (h_∞ = 0.506).The small difference of these two height values is caused by numerical accuracy (i.e. the interface is detected at one grid cell or at the imminent next one). Finally, remixing the final pro-

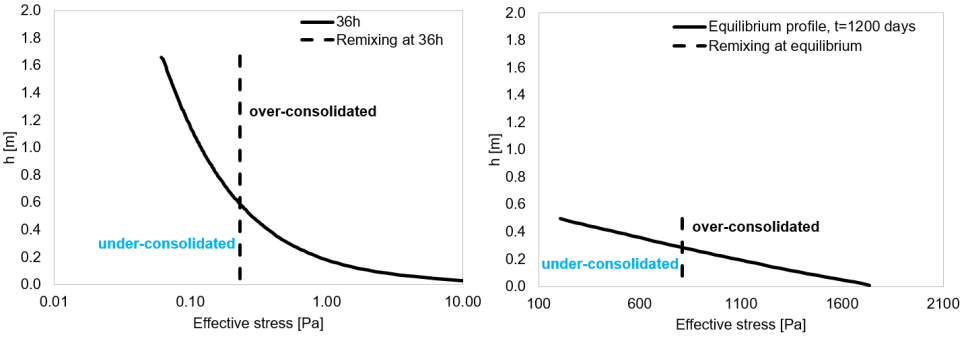

Figure 4.15: Imbalance of stresses occurring when mixing the sediment with water when dredging. Left panel shows this effect when mixing a virgin consolidating bed at t=36 h (first phase of consolidation). Right panel shows the effect when remixing a virgin bed at equilibrium. Note the different scale of the x-axis.

file of the virgin consolidated bed formed from the 5 m 60 g/l suspension, resulted in a slurry with c_0= 558.1 g/l and h_∞ =0.469. Thus, contrary to remixing at 36 h, remixing at equilibrium did allow further consolidation (multiple grid cells).

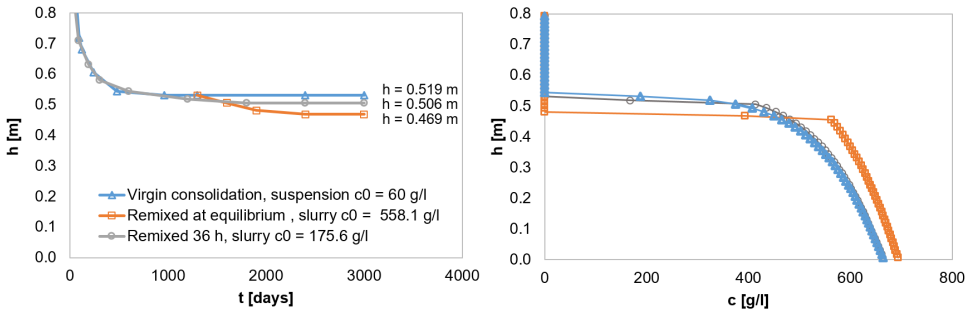

Figure 4.16: Computed settling curves (left) and final concentration profiles (right) for the prognostic simulations.

4.4.4. SCIENTIFIC IMPACT OF THE RESULTS

The present study gives insight in the consolidation behaviour of slurries with $c_0 > c_{gel}$, which have been little not studied. *Torfs et al.* (1996) had found that a c_0 larger c_{gel} prevents segregation of sand when present. The current research contributed to understand the importance of the initial (unbalanced) stress state caused by the mixing and the initial concentration. Furthermore, it was shown that determining the material parameters for this slurries from settling columns of suspensions with $c_0 < c_{gel}$ leads to parameters that overestimate the values of k and underestimates the values of effective stress for a given ϕ_s. As shown in the results, this is caused by the over-consolidated initial conditions of the SIC test which strongly differ with the virgin consolidation conditions of a settling column test.

4.4.5. ENGINEERING RECOMMENDATIONS

Figure 4.16 showed that different c_0 provided different final conditions of the settled bed. These aspects are particularly important for land reclamation and wetland construction, where decisions have to be made with respect to the degree of dilution according to the targeted final state desired. If a larger thickness of the final layer is desired, initial concentrations close to the gelling point (92.2 g/l in the present study) are recommended. This is the situation attained with c_0 = 175.6 g/l for in the present study. However, a very large c_0 (e.g. c_0=558.1 g/l in this research) can provide a much denser (thus stronger) but less thick bed.

A final factor to take into account for construction proposes is the consolidation time, which varies according to the initial concentration, the remixing or not of sediments and mainly the thickness of the slurry layer.

4.5. CONCLUSION

The aim of the present Chapter was to study the influence of the initial concentration c_0 on the consolidation behaviour of slurries for the case of $c_0 > c_{gel}$. Furthermore the research presents two different experimental procedures, the settling columns and the SIC tests, which showed consistent results when determining material parameters for hydraulic conductivity and effective stress. Here, the material parameters of the two different set-ups were not identical, suggesting an influence of the stress history and plastic deformation during mixing (when preparing the SIC test sample) on the values obtained. Consequently, the values of k obtained from the SIC tests were larger than the one determined with the settling columns while the pattern with the effective stress was opposite. Furthermore, the results indicate that these differences on material parameters affect in particular the value of K_k and, therefore, the consolidation time.

The initial concentration profile of sediment is also found to play an important role in the consolidation behaviour. By diluting Markermeer sediment with water by dredging, an imbalance in the stresses is created with respect to the situation prior to dredging. This creates over-consolidated initial conditions which affect the consolidation behaviour and final properties of the sediment. In particular, the degree of dilution affects the final density profile and the final bed height attained because of different degrees of over-consolidated initial conditions. Herein, a c_0 of 558.1 g/l when remixing an equilibrium profile provided larger final densities. However, the sediment-water interface was lower (i.e. a less thick bed layer was obtained). A concentration of 175.6 g/l provided the same layer thickness and density profile than for virgin consolidation but after a larger consolidation time.

4.6. APPENDIX 4A: SETTLEMENT UNDER LOADING FOR SIC TEST

Figure 4.17 shows the settlements for the given loads measured during the SIC tests performed. It shows that until a certain load the porous stone was jammed into the ring and prevented settlement of the sample. The value of this load was 50 N, 100 N or 30 N for tests SIC200, SIC300 and SIC400 respectively. As a consequence, the first measured values of void ratio or volumetric concentration are not representative and were not presented in this thesis.

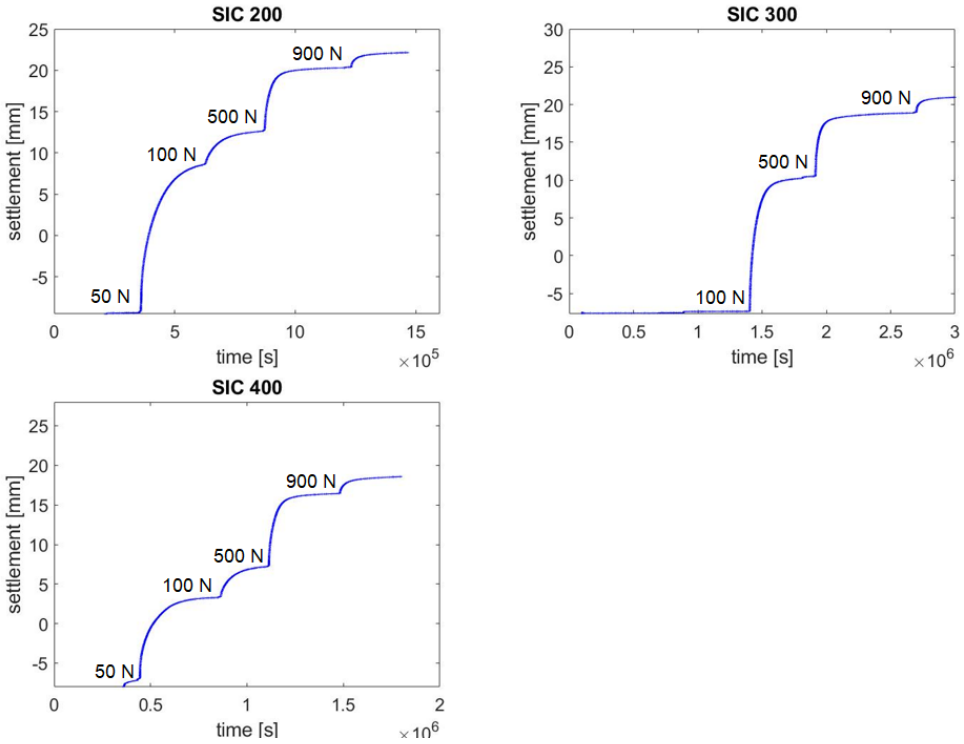

Figure 4.17: Settlement in time under loading for the Seepage Induced Consolidation tests.The labels indicate the loading step which induces each settlement.

5

THE EFFECT OF SOLIDS PHASE COMPOSITION ON DRYING BEHAVIOUR OF SLURRIES

This chapter is under review at Vadose Zone Journal for publication

5.1. INTRODUCTION

SANDY sediments are traditionally preferred for reclamation projects to minimize deformation after construction as muddy sediments show significant settlement when consolidating and drying. However, sandy sediment is becoming more scarce (*Vörösmarty et al.*, 2003). Therefore, fine sediments are progressively being used for nature building projects (e.g. *Haliburton et al.*, 1978; *Erwin et al.*, 2007)). The Marker Wadden is one of the first projects in The Netherlands to use fresh unconsolidated cohesive sediment for wetland construction. The Marker Wadden is a Building with Nature (BwN, e.g. *De Vriend et al.* (2015)) project aiming to improve the ecosystem of Lake Markermeer, The Netherlands, by creating a new wetland with slurries originating from the sediment of the lake bed (Figure 1.1, Chapter 1). These slurries are deposited within compartments made of sand.

The Markermeer is a lake with an average water depth of 3.6 m and a surface area of 680 km^2 (*Rozari*, 2009). The uppermost layer of the lake bed consists of a thin ($\sim 10^{-1}$ m) layer of soft silt (*Van Duin*, 1992). Underneath the soft silt layer, a thick layer of Holocene deposits (clay, peat or sand) is present (*Rijkswaterstaat*, 1995).

5

During dredging of the slurry and filling of the compartments, segregation and oxidation of the sediments may occur (e.g. *Ganesalingam et al.*, 2013; *Van Olphen*, 2016). After deposition, the sediment settles while losing water through self-weight consolidation. Once the fill material emerges above the water table, the slurry will dry because of evaporation and may ultimately desaturate. Furthermore, oxidation of organic matter (OM) and inorganic minerals will happen when the sediment becomes exposed to air (*Saaltink et al.*, 2016). Due to the heterogeneous composition of the dredged Markermeer material and its spatial variability, these processes may be highly variable depending on initial composition, degree of oxidation and environmental conditions.

The water balance of a drying soil is characterised by its soil water retention curve (SWRC) , suction profile and the hydraulic conductivity curve (HCC). Various measuring techniques and empirically fitted models to determine the SWRC have been developed over the last decades (e.g. *Lu and Likos*, 2004; *Fredlund et al.*, 2012). However, a measuring device that allows determination of the SWRC over the entire soil moisture range is not yet available (*Schelle et al.*, 2013). Therefore, it is common to construct composite curves using multiple techniques (e.g. *ASTM*, 2016). Once the pairs of water content- suction are experimentally obtained, they may be analysed with specific analytical functions such as those by *Brooks and Corey* (1964) and *Van Genuchten* (1980).

Considering that the major part of deformation in dewatering slurries takes place in the low ranges of suction, using high precision tensiometers seems an appropriate way to measure the pore water pressure. Using tensiometers, *Wind* (1966) developed an evaporation method, standardised by *ISO* (2004). *Schindler and Müller* (2006) modified and simplified this evaporation method by taking only measurements of mass and tension at two depths in a soil sample. Furthermore, this last method allowed the simultaneous determination of the HCC. An increasingly popular and semi-automated version of this method is the Hyprop® measurement system, commercialized by METER Group (Munich, Germany). This is the instrument used in the present paper because it replicates at small scale the drying conditions at the Marker Wadden and allows to obtain the SWRC and the HCC. The SWRC, soil suction and HCC depend on the composition of the sediment.

Notably organic matter OM, particle size distribution and soil texture strongly influence these curves. For instance, *Rawls et al.* (2003) found that the effect of OM on the water retention differs at high and low organic carbon contents and depends on the soil texture. *Santagata et al.* (2008) related an increase of 8-10% in OM with a three- to fivefold increase in hydraulic conductivity of a normally consolidated soil. *Tisdall and Oades* (1982) and *Chenu* (1993) found that the water-stability of soil micro-aggregates depends on the characteristic clay-organic matter binding. However, most of the effort on linking OM to SWRC has been done focusing on the amount of OM and not on the type or reactivity of OM.

In a similar line, other authors studied the effect of sand content on the behaviour of clay-sand mixtures and the pattern shift after reaching a transition threshold in fines content (e.g. *Thevanayagam et al.*, 2002; *Winterwerp and van Kesteren*, 2004; *Monkul and Ozden*, 2007; *Peters and Iv*, 2010). Furthermore, some authors (e.g. *Catana*, 2006; *Marinho*, 2006) tried to find correlations between the rheological properties of the soils such as Atterberg Limits and the SWRC.

Although there is sufficient evidence for the impact of sand content and OM on hydrologic and rheological soil properties, the effect of the type of OM has not yet been studied. Further, the Hyprop approach has not been tested for clayey slurries.

The objective of this paper is to investigate the drying behaviour of slurries with different solid composition with the Hyprop device. From the Hyprop, suction profile, SWRC and HCC were obtained and *Van Genuchten* (1980) functions were fitted to the SWRC data. The sediment studied consisted of slurry samples from Lake Markermeer with varying sand and OM content. Furthermore, the effect of OM type and degree of maturity was also studied. To isolate the effect of different sediment fractions, several samples were manipulated prior to testing. For some samples, fines (< 63 µm) were separated from coarse (> 63 µm) grains. Other samples were dried, rewetted and chemically oxidised. The goal of drying-rewetting and chemically oxidising the samples is to compare this mimicked final behaviour with the behaviour of the original sediment of the bed. The study of hysteresis is beyond the scope of this study. The composition of the solid fraction of all samples was determined using various standard and non-standard procedures to prior to the Hyprop drying experiments.

5.2. MATERIALS

THE sediments tested originated from Lake Markermeer, The Netherlands. Sediment samples were taken from the uppermost soft silt layer and the underlying Holocene sediment (for details about sample collection, see Chapter 2). Table 5.1 summarizes the properties of all the samples studied. The properties of the sediment and the chemical treatment of some samples have extensively been described in Chapter 2. Herein, it was shown that the samples of soft silt contain a more reactive type of OM. This reactivity was quantified in Chapter 2 with the ratio between the Oxygen Index and the Hydrogen Index OI/HI. This ratio increased with the degree of degradation of the OM present in the samples and thus exhibited the larger values for the treated samples. Chapter 2 also showed that the presence of carbonates buffered the pH during the treatment and that this treatment, including chemical oxidation with H_2O_2, did not change the general sediment mineralogy.

Table 5.1: Sample description: sampling sites, contents of different grain fractions, D50, Total Organic Matter content (TOM), Total Organic Carbon content (TOC), degradation ratio OI/HI, particle density (ρ_s) , Liquid Limit (LL), Plastic Limit (PL) and Plastic Index (PI) Treated refers to chemically oxidised dried rewetted samples. * Indicates assumed value, not measured for the sample.

Site	Depth [m]	Type	ID	Sand [%mass]	Silt [%mass]	Clay [%mass]	D50 [µm]	TOM [%]	TOC [%]	OI/HI [-]	ρ_s [kg/m^3]	LL [%]	PL [%]	PI [%]
Southwest	*0.1-0.5*	*Bulk clay*	*SW1B*	8	63	29	10	8.6	3.3	1.3	2530	104	46	58
		Fines fraction	*SW1F*	0	69	31	8	8.7	3.1	1.4	2570	129	59	70
		Bulk treated	*SW1T*	8*	63*	29*	10*	6.7	2	1.8	2620	60	31	29
	0-0.1	*Bulk soft silt*	*SW2B*	28	54	18	32	6.4	3	1.2	2560	103	46	57
Northeast	*0 -0.1*	*Bulk soft silt*	*NE1B*	42	49	9	69	3.4	1.2	1.4	2590	72	40	32
		Fines fraction	*NE1F*	0	86	14	26	4.8	2	1	2540	83	49	34
		Bulk treated	*NE1T*	42*	49*	9*	69*	2.1	0.5	1.9	2700	33	23	10
	0.1-0.5	*Bulk sandy clay*	*NE2B*	69	21	10	87	2.1	0.7	1.6	2640	41	25	16
		Sand fraction	*NE2S*	100	0	0	108	0.3	0.1	5.5	2710	-	-	-

5.3. EVAPORATION EXPERIMENTS

5.3.1. METHODS

THE Hyprop device (Figure 5.1) was used for the determination of the suction profile of the soil, the HCC and the SWRC for the slurries listed in Table 5.2. The slurries of the untreated samples were prepared at a water content lower than sampled in the field. The different samples were allowed to settle in the storage containers to achieve the desired initial gravimetric water contents w_0 [M_w/M_s]. The w_0 of all samples, listed in Table 5.2, was determined according to *ISO/TS* (2014) by oven drying. Table 5.2 also shows the initial bulk densities ($\rho_{b,0}$) and water ratios ($WR_0 = V_w/V_s$). To analyse the drying behaviour at different initial water contents, replicates (I and II) were prepared at different w_0 for some samples. The treated samples were prepared at a water content of 1.5 times the LL. This water content was selected as being representative of the consistency at the end of self-weight consolidation for this sediment. After addition of water to attain the 1.5 LL water content, the samples were allowed to equilibrate for 48 hours prior to testing. The 100% sand samples were prepared by first adding filtered Markermeer water to the container and then pouring in the sand. For each sediment sample, two evaporation experiments were performed (I and II), with the exception of the oxidised samples and the soft silt sample from the northeast (NE1B), because of limited sediment availability.

Table 5.2: Initial parameter values for the Hyprop evaporation experiments: initial water content w_0, ratio w_0/ LL [%], initial bulk density $\rho_{b,0}$ and initial water ratio WR_0, at start of experiment.

ID	SW1B		SW1F		SW1T	SW2B		NE1B	NE1F		NE1T	NE2B		NE2S	
Test	I	II	I	II	-	I	II	-	I	II	-	I	II	I	II
w_0 [-] [M_w/M_s]	1.4	2.1	5.1	2.6	0.9	1.8	1.9	0.9	3.8	2.0	0.5	0.7	0.7	0.3	0.3
w_0/ LL [%]	1.4	2.0	4.0	2.0	1.5	1.8	1.8	1.3	4.6	2.4	1.5	1.8	1.8	-	-
$\rho_{b,0}$ [kg/m3]	1318	1226	1106	1170	1492	1271	1260	1294	1150	1222	1683	1537	1527	1977	1949
WR_0 [V_w/V_s]	3.5	5.3	13.1	6.7	2.3	4.7	4.9	2.3	9.7	5.0	1.4	1.9	1.9	0.7	0.7

The Hyprop device is based on the simplified evaporation method (*Schindler and Müller*, 2006). Hyprop consists of a metallic cylindrical container with inner diameter of 8 cm and height 5 cm enclosing a volume of 250 cm^3 of sediment sample. Balances with an accuracy of 0.01 g monitored continuously the mass loss of each sample during the evaporation experiments in a locked climate room at constant temperature of 24 °C (± 1 °C) and

relative humidity of 34% (± 6%) where vibrations were prevented. The reproducibility of the results was tested by the performance of replicate experiments with identical samples at identical initial water contents. Two vertical ceramic tip tensiometers, with a diameter of 5 mm, measure the suction pressure at 12.5 mm and 37.5 mm from the bottom of the sample, allowing to determine the suction profile of the sample. The tensiometers were previously filled with de-aired de-mineralised water to improve accuracy, delay cavitation and avoid retarded tensiometric measurements, as suggested by *Durner and Or* (2005).

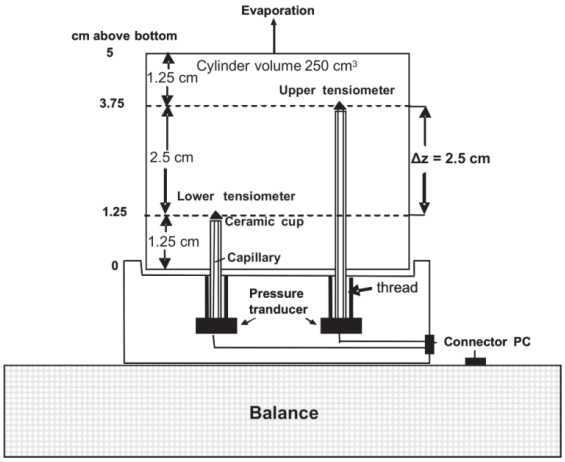

Figure 5.1: Schematic of the experimental Hyprop® set-up (after *Schindler et al.*, 2010).

For all the clay and silt samples, once the set-up was installed (i.e. the tensiometers and the ring were in place), the metallic container was gently filled with the slurry, avoiding air entrapment. A spoon was used to avoid trapping air in the sample when filling the Hyprop ring. The Evaporation tests were continued until both tensiometers cavitated. Afterwards the samples were removed from the container and dried in the oven at 105 °C to determine the residual moisture content and mass of solids. To check that the sample filling method results in homogenous samples, one CT-scan was performed.

SUCTION PROFILE

We define suction as a positive pore water pressure. Therefore, the hydrostatic pressure, i.e., the water pressure above atmospheric pressure, is indicated as negative. The measured pore water pressure is the result of multiple factors, such as the actual suction pressure, the hydrostatic pressure, the over-/under pressure generated by sample preparation, potential self-weight consolidation, and an off-set of the equipment (*Tollenaar*, 2017).

The tensiometers ceramic's air-entry value of 8800 hPa was used as an additional measure for the slurry matric suction, following the extrapolation method of *Schindler et al.* (2010) and *UMS* (2015) for extending the measurement range. This additional value was used under the assumption that the contact between the tensiometer and the soil is guaranteed until the air entry value is reached because of the tendency of clayey soils to

shrink. However, even if detached, the tensiometer would still be in hydraulic contact with the soil through the saturated vapour in between. Therefore, the 8800 hPa point gives a measure of the water content corresponding to high suctions.

HYDRAULIC CONDUCTIVITY CURVES

According to *Schindler et al.* (2010), the Hyprop set up can be used to determine the hydraulic conductivity curve (HCC). The unsaturated hydraulic conductivity k has traditionally been calculated according to the Darcy-Buckingham's law, assuming quasi-steady state (constant flux and hydraulic gradient) and a linearly decreasing water content across the sample height over the measuring interval (*Schindler and Müller*, 2006):

$$k(\overline{h}) = \frac{\Delta V}{2A \cdot \Delta t \cdot i_m} \tag{5.1}$$

where $\overline{h}$ is the mean hydraulic head, ΔV is the evaporated volume during the interval, A is the cross sectional area, the time interval and i_m is the hydraulic gradient. The hydraulic gradient is calculated according to:

$$i_m = \frac{1}{2}\left(\frac{p_{\mathrm{t1,upper}} - p_{\mathrm{t1,lower}}}{\Delta z} + \frac{p_{\mathrm{t2,upper}} - p_{\mathrm{t2,lower}}}{\Delta z}\right) - 1 \tag{5.2}$$

where h refers to hydraulic head, $t1$ and $t2$ to two consecutive time steps, upper and lower to upper and lower tensiometer measurements, and Δz is the 2.5 cm vertical distance between the two tensiometers. This equation gives the vertical gradient in hydraulic head, corrected for the gradient in hydrostatic pressure. The -1 originates from this correction ($\Delta z/\Delta z$). Because some samples showed vertical shrinkage (for details see Appendix 5C), it was tested whether the above assumptions and equations were still valid for the slurries studied. When the assumptions were valid, the two tensiometers measurements were used to calculate the hydraulic conductivity.

SOIL WATER RETENTION CURVES

The SWRC of the sediment were presented as a function of water ratio WR (V_w/V_s), as defined by *Tollenaar et al.* (2018), instead of traditional volumetric water content(V_w/V_t). The WR is preferred because of the large water content of the studied slurries. If a sample is fully saturated, the WR is equal to the void ratio (e) and the volumetric water content is equal to the porosity.

Only the measured pressure of the lower tensiometer was used for the calculation of the SWRC, because the upper tensiometer emerged above the surface of the slurry in most tests, particularly those on the clay samples because of the high initial water content. Further measurements with the upper tensiometer were then meaningless. The consistency between the two Hyprop tensiometers was investigated by *Breitmeyer and Fissel* (2017), who concluded that the Hyprop results obtained with either one (top or bottom) or two tensiometers were not statistically different. We hence used only the bottom tensiometer in our study.

5.3.2. RESULTS AND DISCUSSION

SUCTION PROFILE

The evaporation experiments with Hyprop provide tensiometer and mass loss data as output parameters. Figure 5.2 shows a typical example of the measured raw data. The suction pressure rised until cavitation started. The effect of self-weight consolidation on measured suction pressure was very small (for details see Appendix 5A) and was neglected.

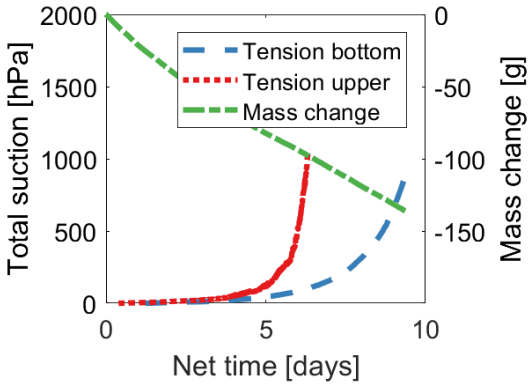

Figure 5.2: Raw upper and bottom tensiometer and weight change measurements for the bulk clay SW1B-II.

HYDRAULIC CONDUCTIVITY CURVES

For some samples with large initial water contents (samples SW1F, NE1F), the difference in suction between the upper and lower tensiometers remained constant during the first few days (Figure 5.3). The same was observed for samples with large sand content and for the treated sample with significant sand content NE1T (see Figure 5.3). A constant pressure difference indicates that the hydraulic conductivity does not limit dewatering. Based on these observations, the assumptions of quasi-steady state and linear gradient in the water content are not met anymore. These assumptions are necessary to calculate the hydraulic conductivity. Hence, these observations suggest that this method cannot be used to determine the hydraulic conductivity with the Hyprop for these samples

Figure 5.3 also shows the suction difference (as an indication for the gradient) for the samples SW1B, SW1T, SW2B and NE1B for which the assumptions of quasi steady-state and linear pressure gradient are considered to be valid. Figure 5.4 shows the results of the hydraulic conductivity as a function WR for these samples water. To determine the hydraulic conductivity, Equation 5.1 was used. As expected, the hydraulic conductivity decreases with decreasing water ratio (increasing matric suction). The results also shown that the samples with lower clay content and larger OI/HI ratio (Table 5.1) have a larger hydraulic conductivity. Herein, the dominance of the OI/HI ratio over the grain size to characterise the behaviour of the most reactive sample SW2B highlights the importance of the type of OM determining the material properties of the sediment.

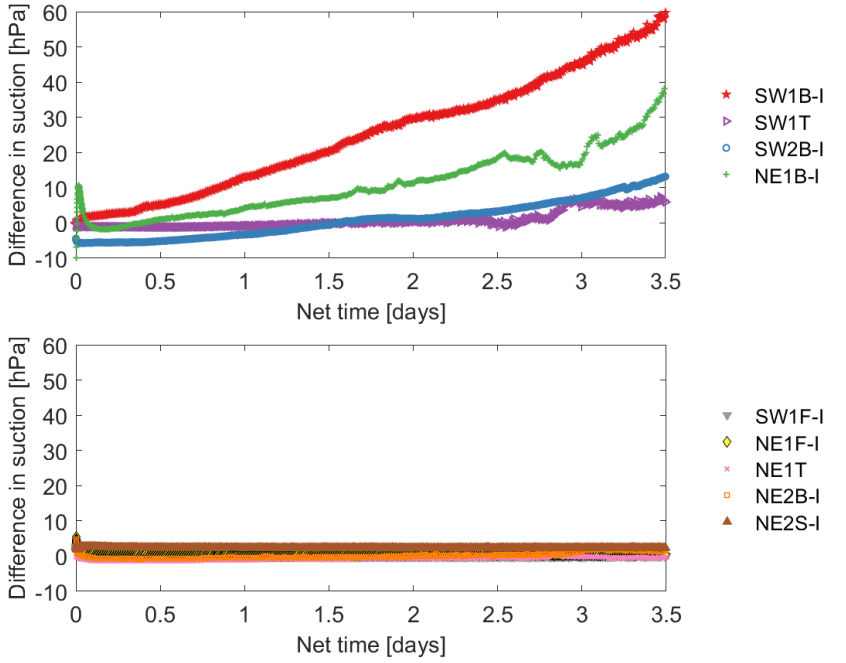

Figure 5.3: Suction pressure difference between the upper and lower tensiometer for the samples showing linear increase (top) and no increase (bottom) on difference between suction at the upper and the lower tensiometer.

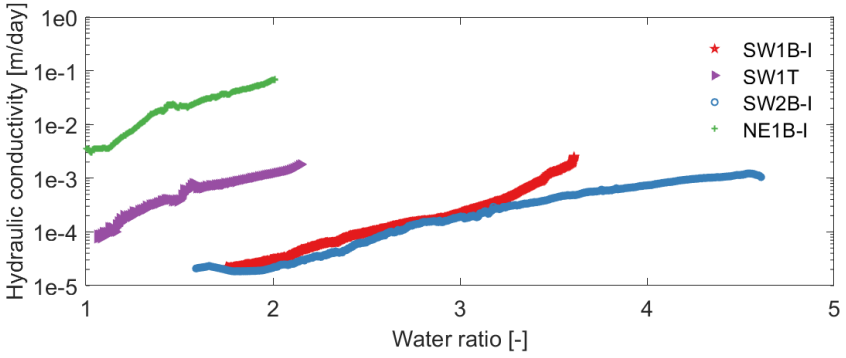

Figure 5.4: Hydraulic conductivity as a function of the water ratio of the samples meeting the requirements for the application of Darcy-Buckingham's law.

SOIL WATER RETENTION

SWRCs were estimated for all samples from the measured suction pressures and mass. The SWRCs presented include an additional extrapolated point computed as from the ceramic's air entry value. Figure 5.5 shows that the results presented in the current section are reproducible: two tests identical samples show perfect overlap. Table 5.3 shows the gravimetric water content and WR at the end of the Hyprop experiments.

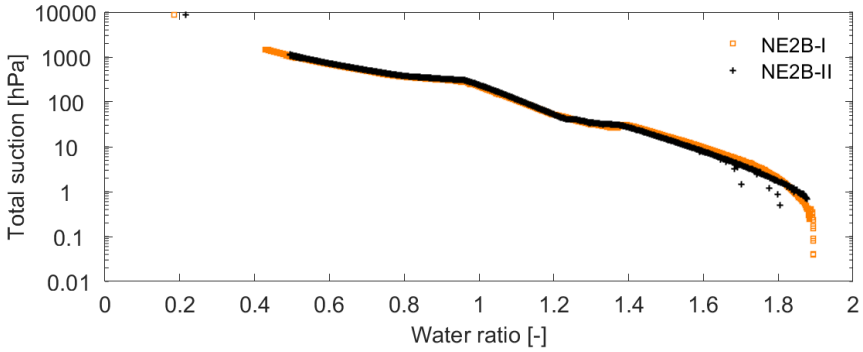

Figure 5.5: Water retention curves for replicates started at same initial water content for the NE2B sediment sample, i.e., sandy clay with 69% sand.

Table 5.3: Final gravimeteric water contents w_f and water ratios WR_f at the end of the hyprop tests.

ID	SW1B		SW1F		SW1T	SW2B		NE1B	NE1F		NE1T	NE2B		NE2S	
Test	I	II	I	II	-	I	II	-	I	II	-	I	II	I	II
w_f [-] [Mw/Ms]	0.36	0.43	4.47	0.4	0.23	0.3	0.73	0.13	0.27	0.47	0.07	0.07	0.08	0.01	0.01
WR_f [-] [Vw/Vs]	0.91	1.08	1.21	1.02	0.6	0.78	1.86	0.77	0.69	1.2	0.18	0.19	0.22	0.02	0.02

Figure 5.6 illustrates that the samples show different behaviour, with the more coarse-textured samples showing lower initial WR and steeper SWRCs. This agrees with the data presented in the literature (e.g *Lu and Likos*, 2004; *Fredlund et al.*, 2012). Thus, the influence of grain size distribution on the drying behaviour of Markermeer sediment is large, notably the effects of sand content (see Table 5.1).

The SWRC of the bulk soft silt and the bulk clay samples differed only at during the low suction stage (compare sample SW2B with SW1B and NE1B with NE2B in Figure 5.6). Differences were expected at low suctions because of the different particle size distribution of the samples, according to literature (e.g. *Hillel*, 1998). However, the fact that coarser soft silt samples (i.e. SW2B-1 and NE1B-I) showed higher initial water ratios than finer-textured samples (SW1B , NE2B) suggests an influence of the more labile OM present in the upper soft silt layer (see Figure 2.4, Chapter 2) is able to bind more water. Thus, the labile and binding OM of the upper soft silt seems to produce a less steep SWRC at low pressure suctions. The smaller difference between the Northeast samples may be explained by a coarser particle size distribution of NE2B sediment. The results agree with *Rawls et al.* (2003), who concluded that water retention of soils with coarser textures was substantially more sensitive to the presence of organic matter than fine-textured soils.

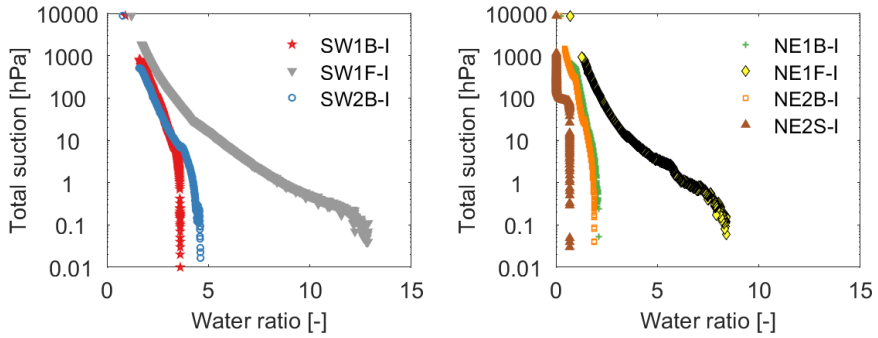

Figure 5.6: Water retention curves for studied samples having a different sand content. Left panel, SW samples. Right panel, NE samples. Sand contents are 0% (SW1F-I and NE1F-I), 8% (SW1B-I), 28% (SW2B-I), 42% (NE1B-I), 69% (NE2B-I) and 100% (NE2S-I).

5

The samples from both sites showed steeper SWRCs after treatment (Figure 5.7). This behaviour corresponds with results from the Atterberg tests, which showed a decrease in LL with decreasing OM (see also *Zentar et al.* (2009)). The result agrees with previous literature, such as *Skempton* (1969) and *Burland* (1990) who showed that the slope of the compression curves, defining the compression index, experienced a similar dependency on sediment composition as observed in the current research. *Santagata et al.* (2008) also found a decrease in compressibility with a decrease in OM. The effect of OM on water retention properties has also been studied in other disciplines. *Pons and Zonneveld* (1965) described soils as a mixture of colloidal (fine OM and clay) and non-colloidal materials (silt, sand and coarse OM). They interpreted ripening (as they defined the soil pedogenical processes) as a process involving a change in the micro-structure of the clay minerals and the fine colloidal OM, together with a loss of water. *Rawls et al.* (2003) found that a decrease in carbon content (at low carbon contents) leads to a decrease in water retention of coarse-textured soils but to an increase in fine textured soil. *Haynes* (2005) pointed out that labile OM can be an indicator of soil quality that influences soil function. For the case of the Marker Wadden, the presence (and type) of OM may also play an ecological role on the development of the ecosystem at later stages.

Figure 5.8 shows that the initial water ratio only affected the water retention curve at low suction levels. At high suction levels all SWRCs of the same material converge, similar to observations reported by *Tollenaar* (2017).

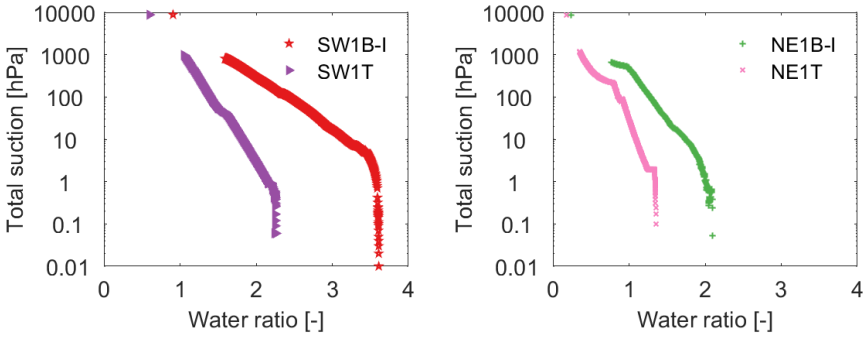

Figure 5.7: Water retention curves for natural and treated bulk clay samples SW (left) and NE (right).

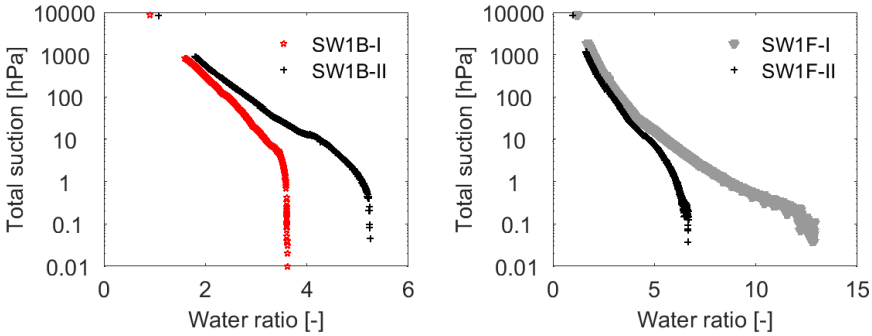

Figure 5.8: Water retention curves for replicates starting at different initial water content. Left panel, SW bulk clay. Right panel, SW fine fraction. Note the different horizontal scale.

5.4. MODELLING THE SWRC

THE SWRCs were fitted with a Van Genuchten model (*Van Genuchten*, 1980) following Equation 5.3:

$$WR = e_0\left(1 + (\alpha h)^n\right)^{-m} \tag{5.3}$$

where α [1/cm], n [-] and m [-] are free fitting parameters, h [cm] is the suction head, e_0 is the initial void ratio and WR is the water ratio, which equals to the void ratio in case of full saturation. The fitting parameters α, n and m are shown in Table 5.4. These parameters were plotted against different composition factors to obtain correlations between the solid composition and the shape showed by the SWRC.

Table 5.4: Fitting parameters obtained from the Van Genuchten model.

ID	SW1B		SW1F		SW1T	SW2B		NE1B	NE1F		NE1T	NE2B		NE2S	
Test	I	II	I	II	-	I	II	-	I	II	-	I	II	I	II
α	0.7	-	1.3	-	0.5	0.18	-	0.15	1.5	-	1.3	0.25	-	0.12	-
n	1.15	-	1.0	-	1.18	1.15	-	1.0	0.9	-	1.2	1.1	-	30.0	-
m	0.18	-	0.24	-	0.11	0.2	-	0.17	0.22	-	0.08	0.14	-	0.2	-

5

Figure 5.9 shows the parameter m as a function of the OI/HI ratio, the TOC %, the PI % and the % of clay. A clear trend with the OI/HI ratio was found. This relationship is more clear than the relation between the parameter m and the total amount of OM. This result emphasizes the importance of the type of organic matter. Furthermore, the scatter observed in Figure 5.9 is more likely to be due to the fact that the van Genuchten model was fitted over the entire range of suctions. Therefore, the value of m presented is an averaged value of high and low ranges of suction. SWRCs at low suction pressures is dominated by capillarity and is therefore strongly dependent on soil structure (e.g. *Hillel*, 1998). At high suction pressures, SWRCs are dominated by adsoption and therefore influenced by organic matter (e.g. *Lu and Khorshidi*, 2015).

Figure 5.10 shows the parameter n as a function of the OI/HI ratio. The samples are analysed separately for both sampling sites. This was done because the parameter n determines the shape at the intermediate range of suctions and the different particle size distributions found at the different sites (Figure 2.2 in Chapter 2) may influence the results. The results show a clear relation of this parameter n with the type of organic matter.

Despite of being affected by the type of material, the parameter α was not studied because it mostly depends on the initial void ratio.

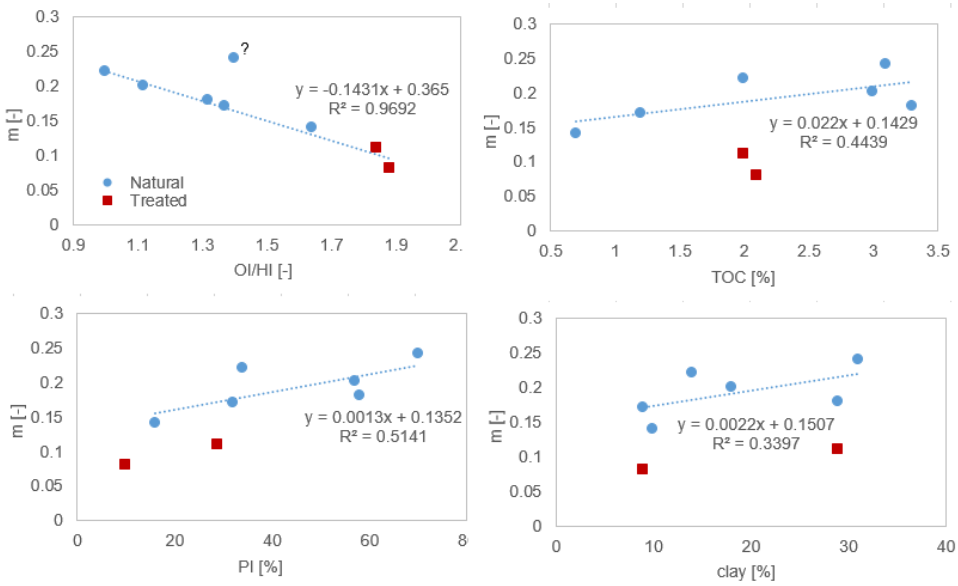

Figure 5.9: Correlation between the van Genuchten parameter m and different solid composition parameters.

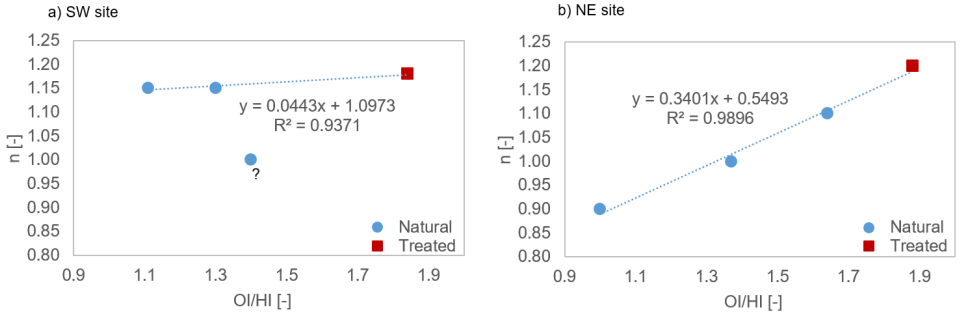

Figure 5.10: Correlation between the van Genuchten parameter *n* and the OI/HI ratio for the SW (left) and NE (right) samples.

5.5. CONCLUSIONS

The effects of the type of organic matter and its oxidation as well as changes in sand content on the hydrological properties of Markermeer sediment were evaluated. Samples were characterised and the soil water retention behaviour was studied with the evaporation method using the Hyprop set-up. This device proved to be a rapid and efficient method to evaluate the SWRC behaviour of slurries. Because of the large initial water content of the slurries, the SWRCs were presented as a function of the water ratio (V_w/V_s) instead of the more traditional volumetric water content (V_w/V_t).

The natural sand variability in sediment composition did not have a large effect on the water retention behaviour. However, the SWRCs changed substantially when segregation occurred. The SWRC of sandy samples were steeper and fine-textured sediments showed large water ratios. This suggests that deformations or residual settlement after deposition of the sediment layer may be strongly affected if segregation occurs during the construction of the Marker Wadden. This may lead to large differences in the final sediment volumes. The water retention behaviour of the upper soft silt layer differed from the sediment layer underneath, particularly under conditions of low matric suction. A part of this behaviour is attributed to the difference in lability of the OM, as identified using Rock Eval analysis.

The results show the importance of organic geochemical controls in the bulk physical properties of a clayey slurry. Herein, the present research showed the important physical implications of the lability of OM. Treating samples, mimicking the exposure to oxidation and to drying and rewetting, showed a significant effect on water retention and a large reduction of the Atterberg Limits. The water retention capacity and compressibility decreased, while the hydraulic conductivity increased after treatment. Therefore, the effect of oxidation and drying-rewetting should be taken into account when building new land with slurries, because the properties of the sediment may change significantly. However, future research on the effect of pre-treatment may still be necessary, since the effects of drying and oxidation should be studied separately to gain further understanding.

5.6. APPENDIX 5A: SELF-WEIGHT CONSOLIDATION DURING EVAPORATION TESTS

Haliburton et al. (1978) identified a water content of 1.8 times the LL, which they defined as the 'decant point', at which a thin drying skin would form on freshly dredged material. After this point, changes in water content at shallow depth were only the result of a deficit between evaporation and the capillary resupply potential of the slurry. Therefore, *Haliburton et al.* (1978) identified 1.8 LL water content as the transition between consolidation and evaporation predominance. *Van den Bosch* (2016) and the present research (Chapter 4) carried out settling experiments with the NE1F sample studied in this paper. After reaching equilibrium from self-weight consolidation, they found a final average bulk density of ρ_b = 1300 kg/m^3, slightly varying with initial concentration. This corresponds to a void ratio of e = 4.1, which for this sediment type represent a water content of 1.9 LL.

Based on the observations of *Van den Bosch* (2016), Chapter 4 and *Haliburton et al.* (1978), some consolidation may have occurred during the first stage of the experiments for some of the samples (see Table 5.2 and Table 5.5). However, the maximum excess pore water pressures during consolidation are expected to be a small fraction of the maximum effective stress. Given the height of the sample, the maximum effective stress at the base of the sample is 1.5 hPa for a density of 1300 kg/m^3. During self-weight consolidation, this effective stress gradually builds up.

Table 5.5: Possibility of occurrence of self-weight consolidation given the initial water content of the tests.

ID	SW1B		SW1F		SW1T	SW2B		NE1B	NE1F		NE1T	NE2B		NE2S	
Test	I	II	I	II	-	I	II	-	I	II	-	I	II	I	II
Self weght consolidation	No	Yes	Yes	Yes	No	Yes	Yes	No	Yes	Yes	No	No	No	No	No

In the tensiometer measurements, there is always an initial offset caused by the pressure induced by the sediment above the sensor. Figure 5.11 shows the tensiometric measurement for the experiment SW1F-I, which was performed at the largest initial water content with $\rho_{b,0}$= 1106 kg/m^3. Thus for the upper tensiometer (at 1.25 cm from the top of the sample), this offset should be 1.4 hPa (i.e. the pressure caused by the mass of slurry above the tensiometer). However, Figure 5.11 shows a larger negative offset, in the order of 0.7 hPa larger than the calculated 1.4 hPa, which suggests that this sample is experiencing self-weight consolidation. The same pattern was observed with the bottom tensiometer, being the extra negative suction of the same order of magnitude. This was the experiment with larger initial WR, which implies that this was the test exhibiting the larger effect of self-weight consolidation. However, this maximum effect was still 200 orders of magnitude smaller than the values stresses by suction when drying. Therefore, the effects of self-weight consolidation were neglected in the present study.

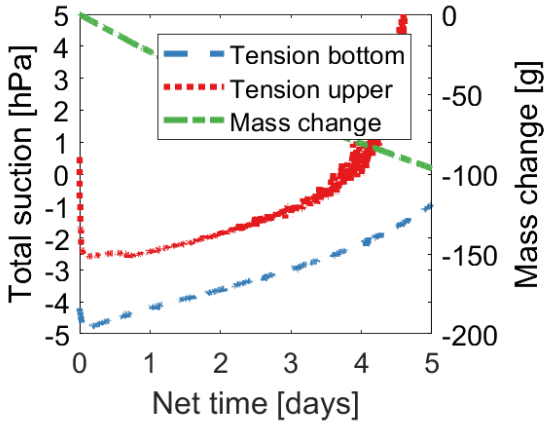

Figure 5.11: Initial suction measurements for experiment SW1F-I.

5.7. APPENDIX 5B: CORRECTION OF THE TENSION MEASUREMENTS

The suction data presented in the present chapter include two corrections. These corrections were applied to the suction measurements to improve the interpretation of the water retention characteristic curve at suction values below 3 kPa, which are relevant in case of drying and shrinking slurries. First, the minimum value of suction (i.e., maximum negative pore water pressure) was subtracted from the measured values to correct for the initial off-set caused from the sediment weight above the tensiomenters. This offset corresponds to the pressure caused by the mass of sediment above each tensiometer (and by self-weight consolidation, if occurring).

Finally, a correction for the loss of hydrostatic pressure caused by the evaporated mass of water was also applied. This pressure loss was determined by dividing the measured mass loss at each time step by the cross sectional area of the sample ring.

5.8. APPENDIX 5C: SWRC AND SHRINKAGE

The theory of water retention curves (e.g. *Brooks and Corey*, 1964; *Van Genuchten*, 1980; *Leong and Rahardjo*, 1997) was developed for materials showing no to limited shrinkage. For many years, the effect of volume change caused by shrinkage was neglected. However, it is nowadays known that a part of the tension measured upon drying is caused by shrinkage. Therefore, to separate the effects of both processes, soil shrinkage curves (SSC) have to be measured.

The effect of the shrinkage and the subsequent change in density was studied by *Schindler et al.* (2015) without finding significant effects on density. However, the soils tested by these authors experienced much less shrinkage than the slurries tested in this study. Therefore, it is expected that the SWRC of the present study show the combined effect of drying and shrinkage.

Starting from a slurry, the Markermeer sediment samples with high initial void ratio underwent significant volume change during drying. During the initial stage of drying, they only showed vertical shrinkage. At a certain moment a crack appeared at the boundary of the sample between the ring and the slurry, after which the sample separated from the ring and lateral shrinkage commenced. In some cases, this release from the ring was accompanied by a drop in suction. Similar observations were made by *Tollenaar* (2017) and *Van Paassen et al.* (2018). They attributed this drop in suction to redistribution of suction pressures within the sample. At the end of the Hyprop tests, small superficial cracks were observed for some of the samples.

To estimate the effect of shrinkage in the SWRC, the method suggested by *Fredlund et al.* (2012) was used. In this method, the Soil Shrinkage Curve (SSC) is described as:

$$e(w) = e_{\min}\left(\frac{w^{c_{sh}}}{{b_{sh}}^{c_{sh}}} + 1\right)^{\left(\frac{1}{c_{sh}}\right)} \tag{5.4}$$

where $e(w)$ is the void ratio as a function of the gravimetric water content w, e_{min} is the minimum void ratio (i.e., the void ratio at shrinkage limit), b_{sh} is the slope of the tangent and c_{sh} the curvature of the SSC. *Fredlund et al.* (2012) suggested that b_{sh} and c_{sh} can be estimated once the shrinkage limit and specific gravity of the sample are measured. Therefore, we measured the dimensions of the samples after oven drying to determine the shrinkage limit. With these dimensions, we determined the void ratio after drying, e_{min}.

For the samples with a high initial void ratio, the final volumetric water ratio (WR_f) was still significantly higher than the void ratio at the shrinkage limit (e_{min}), see Table 5.6. Assuming a bilinear shrinkage curve (high c_{sh} value), the sample will first shrink before it starts to desaturate. This means that when the water ratio is higher than the void ratio at the shrinkage limit, the sample is assumed to be fully saturated and the change in water volume is equal to the change in total volume.

Table 5.6: Dry height and diameter(h_s, $\varnothing$), minimun void ratio e_{min} and final water ratio WR_f.

ID	SW1B		SW1F		SW1T	SW2B		NE1B	NE1F		NE1T	NE2B		NE2S	
Test	I	II	I	II	-	I	II	-	I	II	-	I	II	I	II
h_s [cm]	3.4	2.7	1.6	2.1	3.6	2.9	2.9	3.9	1.5	2.6	3.9	3.8	3.8	5	5
$\varnothing$ [cm]	6.3	6.2	5.3	5.7	7	6	6	7.3	5.9	6.3	7.4	7.2	7.2	8	8
e_{min} [V_v/V_s]	0.96	1.06	0.93	0.68	0.8	0.86	0.91	1.13	0.7	0.93	0.56	0.77	0.78	0.72	0.76
WR_f [-] [V_w/V_s]	0.91	1.08	1.21	1.02	0.6	0.78	1.86	0.77	0.69	1.2	0.18	0.19	0.22	0.02	0.02

Figure 5.12 confirms that assuming a bilinear shrinkage curve is appropriate, particularly for slurries with high initial void ratio. Determination of the shrinkage behaviour at the dry end of the shrinkage curve may involve significant uncertainty, which is related to crack formation within the sample and the estimation of the minimum void ratio. Inclusion or exclusion of cracks will affect the value depending on the scale of observation. Similar observations were reported by *Smoor* (2015), who indicated that the shrinkage curve was significantly affected by test conditions and volume definition.

For further analysis, measuring the SWCC and shrinkage together or testing with a pressure plate or Fredlund set-up (that can measure volumetric deformation and volu-

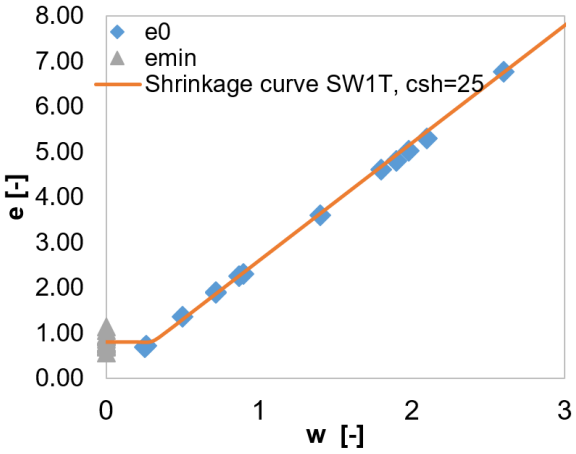

Figure 5.12: Example of an average calculated curve for the sample SW1T. Range of e0 and emin for all sediment samples.

metric water content changes) may be beneficial, because of the significant shrinkage of the fine samples.

5.9. APPENDIX 5D: SATURATED CRUST

The water contents stayed close to fully saturation at the end of most experiments. This prevented the formation of a desaturated crust. Instead, a highly saturated pseudo-crust was formed while the grain skeleton collapsed. (Figure 5.13). This pseudo-crust formed on the top and also at the sides of the clay and sandy clay samples. The lack of formation of an unsaturated crust can also be explained because the range of suction pressures needed to remove water from the smallest capillary pores of the fine-textured soils was not reached during the evaporation experiments (e.g., 750 kPa for the silty clay soil).

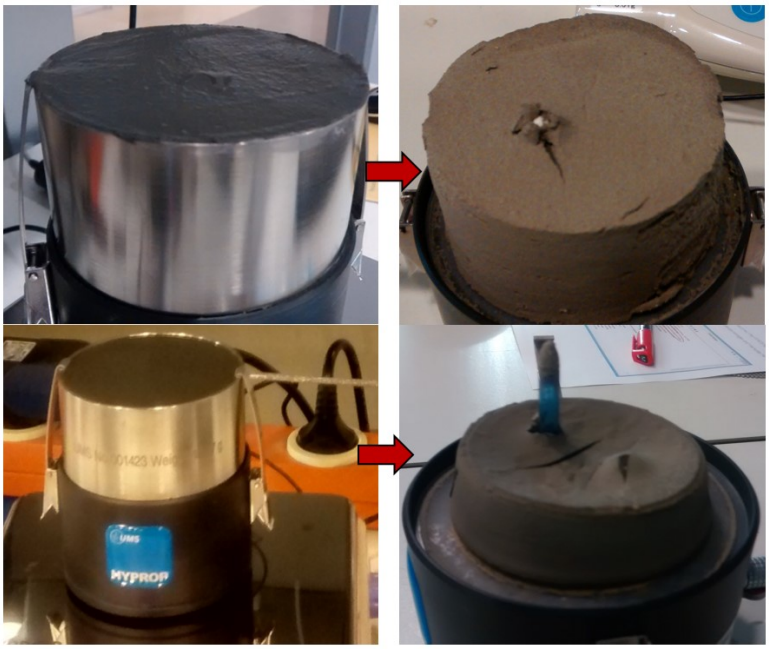

Figure 5.13: The formation of saturated pseudo-crusts was observed at the top and the sides of the samples: sample NE1B (top) and sample NE1F-I (bottom).

The hydraulic conductivity of this saturated crust decreased while gaining strength. Consequently, the more impermeable crust may decrease the consolidation rate of the mud layers underneath for the case of the Marker Wadden. As an implication for wetland building, the consolidation rate of soft mud under water is likely higher than above water, because of the presence of a saturated skin crust that prevents further desaturation of the sediment underneath.

6

DRAINAGE EFFECT OF VEGETATION ON CONSOLIDATION AND DRYING OF SLURRIES

Que din os rumorosos
na costa verdecente,
ó raio transparente
do prácido luar?
(What do the murmurers say
On the verdant coast
Under the transparent beam
Of the calm moonlight?)

Eduardo Pondal

Parts of this chapter have been published in HESS-Discussions.
This Chapter is the result of a joint experiment. The ecological part of the present chapter has been conducted by Rémon Saaltink.

6.1. INTRODUCTION

COHESIVE sediment is progressively being used for land reclamation (e.g., Poplar Island in the Chesapeake Bay, USA; *Derrick et al.* (2007)). The construction of wetlands with soft sediment has become increasingly important worldwide (e.g. *Mitsch et al.*, 2012; *Saaltink et al.*, 2018; *Barciela-Rial et al.*, under review). Conventional drainage is often used to speed up the consolidation process when building with soft cohesive sediments (*Humphrey and Holtz*, 1986). The most common methods to drain these sediments include the instalment of prefabricated vertical strip drains, horizontal vacuum drains or sand drains (*Holtz*, 1987; *Cognon et al.*, 1994; *Li and Rowe*, 2001). Cohesive sediment deposits consolidate primarily via self-weight consolidation (e.g. *Gibson et al.*, 1967; *Been and Sills*, 1981; *Winterwerp and van Kesteren*, 2004). This consolidation process can be sped up by artificially draining the sediment, thereby increasing the erosion threshold, vane strength, and overall stability soon after construction (*Fagherazzi and Furbish*, 2001; *Chen et al.*, 2012). However, conventional drainage techniques are relatively expensive, are invasive and may degrade the natural value of the ecosystem (e.g., via disturbance). Our current research focusses on exploring an alternative approach which uses natural processes, rather than a technological solution, to speed up drainage of soft cohesive sediment. We refer to the concept of ecological engineering, which aims to fit environmental technology with ecosystem services (*Odum and Odum*, 2003). This approach foresees the use of ecological engineers that speed up processes like sediment stability, soil formation, consolidation, and soil drainage (*Jones et al.*, 1994).

Plants are excellent examples of ecological engineers as they directly interact with the physical and chemical components in the sediment (*Angers and Caron*, 1998; *Ehrenfeld et al.*, 2005). Furthermore, plants also affect the hydrodynamic stresses (e.g *Nepf*, 2012). Within the soil, plants are known to 1) increase the erosion threshold via roots (mechanical armouring) and thereby stabilize the sediment (*Waldron and Dakessian*, 1982; *Friend et al.*, 2003; *Reubens et al.*, 2007), 2) promote soil formation by oxidizing the sediment and by altering and initiating biogeochemical processes (*Visser et al.*, 2000; *Saaltink et al.*, 2016), 3) compact clay particles in the vicinity of roots, which promotes consolidation (*Dorioz et al.*, 1993), 4) change the soil hydraulic properties and soil moisture content by modifying the soil pore configuration (*Angers and Caron*, 1998; *Kodešová et al.*, 2006; *Gerke and Kuchenbuch*, 2007) and 5) induce an overburden by their mass. Therefore, plant roots can be considered as a cost-effective alternative to conventional vertical drainage to speed up sediment consolidation and stability.

During vegetative development, the increase in transpirational water loss is compensated by an increase in water uptake by roots, which is mainly done by increasing the root surface area (*Suku et al.*, 2014). As roots elongate, the zone in soils where water is most actively being taken up, changes as roots are more porous near their tips (*Sanderson*, 1983; *Zwieniecki et al.*, 2002). Hence, the part of the sediment that is drained by plant roots is expected to change both horizontally and vertically over time (*Gerke and Kuchenbuch*, 2007). Many field studies have found that suction induced by vegetation alters pore water pressure and soil water retention (e.g. *Lim et al.*, 1996; *Smethurst et al.*, 2006; *Leung et al.*, 2015).

Although in principle the hydraulic function of a plant root resembles that of a porous pipe (*Zwieniecki et al.*, 2002), little is known about the potential effect of living plant roots

on the consolidation process in soft cohesive sediments, especially due to the nonlinear behavior of water distribution during vegetative development. A better understanding of how and to what extent plant roots drain cohesive sediments is essential to successfully deploy plants as eco-engineers when soft cohesive sediment is used for constructing wetlands.

In the Netherlands, a project started where soft cohesive sediment is used to construct a large wetland in Lake Markermeer. This is a dynamic and biodiverse wetland system, while the concept of ecological engineering is used to speed up ecosystem development. To combat soil erosion and speed up ecosystem development, *Phragmites australis* (common reed) has been used as the ecological engineer to enhance the consolidation process and to improve sediment stability.

In controlled column experiments, we studied in a mechanistic way how and to what extent *P. australis* can increase drainage in soft cohesive sediment, thereby potentially promoting consolidation. Vegetated columns were deployed as well as a control column without vegetation. This study isolates the effects of plant roots thereby enhancing the understanding of the important plant-soil interactions in terms of consolidation by means of vertical drainage. The suitability of this species as an ecological engineer to speed up the consolidation process on newly constructed wetland can be assessed accordingly and be applied to wetland construction with soft material worldwide.

6.2. MATERIAL AND METHODS

6.2.1. EXPERIMENTAL SET-UP

CONSOLIDATION experiments were conducted in perspex (methyl methacrylate) columns (inner diameter 10 cm, height 120 cm) in the fluid mechanics laboratory of Delft University of Technology in the period November 2016 – August 2017. To allow the control of boundary conditions, a hollow stainless-steel pipe (outer diameter 2 cm, inner diameter 1 cm) was fixed in the middle of each perspex column - see also *Barciela-Rial et al.* (2015). This stainless-steel pipe contained Vyon 3.2D filters in its wall allowing the water resupply of the sediment columns. These filters control the water table and prevent sediment leaking into the pipe. We refer to this pipe as a drainage pipe. To induce the constant water table at the desired level in the perspex columns, the drainage pipe was connected to another column which contained Markermeer water at a fixed level of 77 cm from the bottom of the column. Water flowing from this water column to the drainage pipe (i.e., because of water loss via plant transpiration and/or evaporation) was replenished from a Mariotte bottle containing Markermeer water. Figure 6.1 presents a sketch of this setup.

In total, six perspex columns were used in two experimental series (Table 6.1). Four columns with plants were harvested in experiment 1 to determine root and shoot variables, while two columns were left intact and used for pore pressure measurements. One of the two columns for pore pressure measurements was left unplanted (control column), the other column was planted with reed (vegetated column). Experiment 1 was conducted in the laboratory hall from November 2016 till February 2017 (= 118 days), with temperatures fluctuating between 15 °C and 20 °C, averaging at 17.3 °C. The average relative humidity was 72%, fluctuating between 50% and 80%. Because the pressure

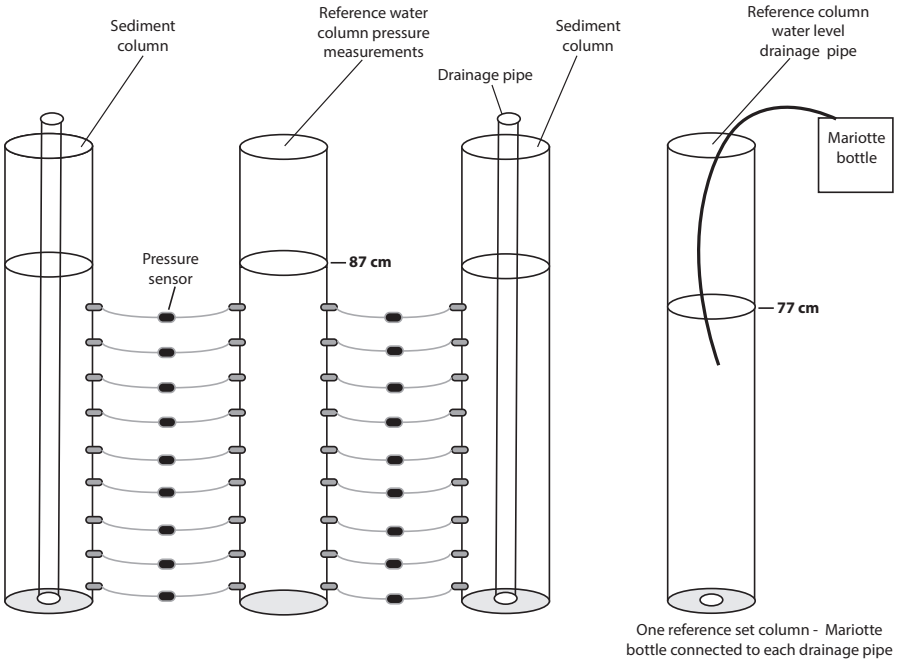

Figure 6.1: Experimental set-up of the columns and location of the sensors

sensors are very sensitive to small changes in temperature, and because marginal changes in the water table were recorded, it was decided to redo the experiment in a climate room. Experiment 2 took place from March 2017 till August 2017 (t = 129 days). The environmental conditions in the climate room were kept constant at the average conditions measured in the laboratory hall. A grow light in both experimental runs was installed at the same height. Because the variation in temperature and humidity in the laboratory hall was small (± 5 °C), we could link the morphological root and shoot traits measured in the first experimental run to the changes in pore pressure of the sediment in the second experimental run. Hence, the vegetation development data used in this paper was obtained from experiment 1, and the pressure sensor data was obtained from experiment 2.

Table 6.1: Description of the two experimental series that are part of this study

Experimental series		
Experiment 1	November 2016 – February 2017	
Condition	Set-up: Laboratory hall; Average temperature: 17.3 °C; Relative humidity: 50-80%; Photon flux density (light): 300 µmol s m-²; Water level: fluctuating around 77 cm from the base of the column.	
Column	**Variables**	**Used in this study**
1. Harvest column		Yes
2. Harvest column	Shoot:leaf surface area, biomass	Yes
3. Harvest column	Root: surface area, length, biomass, rooting depth	Yes
4. Harvest column		Yes
5. Vegetated column	Pore pressure, evapotranspiration (Mariotte bottle), transpiration (Li-Cor)	No
6. Control column	Pore pressure, evaporation (Mariotte bottle).	No
Experiment 2	March – August 2017	
Condition	Set-up: Climate room; Fixed temperature: 17.3° C; Relative humidity: 50-80%; Photon flux density (light): 300 µmol s m-²; Water level: stabilized at 77 cm from the base of the column.	
Column	**Variables**	**Used in this study**
1. Vegetated column	Pore pressure, evapotranspiration (Mariotte bottle), transpiration (Li-Cor)	Yes
2. Control column	Pore pressure, evaporation (Mariotte bottle).	Yes

The columns used for pore pressure measurements were installed with 0.5 Pa Honeywell differential pressure sensors at 0.4, 10.4, 20.4, 30.4, 40.4, 50.4, 60.4, 70.4, and 80.4 cm from the base of the column. All the sensors were provided with a degassing system to avoid inaccuracy induced by air. Furthermore, a filter was installed at each connection point of the sensor to measure pore water pressure, instead of total pressure. To increase the accuracy by measuring differential pressures, all the pressure sensors were connected to a reference column filled with a constant water level, thus measuring relative overpressures (e.g., Figure 6.1). The calibration procedure of the pressure sensors is presented in the Appendix 6A.

The perspex columns were filled with mud from Lake Markermeer, collected by dredg-

ing (coordinates 52.54622°N; 5.38783°E). The sediment was thoroughly mixed before adding to the columns. The bulk density of the suspension was about 1260 kg/m^3, the gravimetric water content was 66.7% (water mass / total mass) and the initial concentration of solids was 425 g/L. The specific solids density was 2580 kg/m^3. The sediment was placed in the columns and remixed. After remixing, the suspension height was 118 cm in all columns.

The sediment could settle and consolidate for 14 days, during which the sediment surface lowered to 92.5 cm in the control column and to 92.3 cm in the vegetated column (but still without vegetation). Because this 2 mm difference between the columns is likely the result of irregularities of the bed surface at the measurement location, the consolidation rates in the two columns were considered the same, thus showing reproducibility of the consolidation experiments. Before the start of the experiment, the pore water squeezed out during self-weight consolidation was removed from above the sediment without disturbing the consolidating sediment. The removal of water from above the sediment marks the start of the experiment (time = 0 days). The mean bulk density of the sediment at t = 0 was 1332 kg/m^3 for both columns.

It is to be noted that the vertical dry density and pore water pressure distributions in the initial phase of an experiment are largely affected by the experimental setup and the addition of the slurry. The drainage pipe in the middle of the column was meant to control the water table during the experiments. However, part of the slurry will dewater immediately when pouring in through the porous drainage pipe, in particular lower in the pipe, while higher in the pipe vertical drainage prevails. Furthermore, as the very upper part of the drainage pipe was not porous, complex pore water circulations within the soil and the drainage pipe may have been introduced, as suggested by irregular pore water distributions. This is explained further in Appendix 6C.

At t = 0 days, three shoots (size 2 cm) of *Phragmites australis* (common reed) were transplanted into the vegetated column and the harvest columns (Table 6.1). A grow light (Spectrabox Gold) with a photon flux density of 300 µmol s m-² was installed at a height of 123 cm above the sediment surface. The climate room was surrounded by a white cover to maximize irradiance from the grow light. A ventilator blew constantly within the climate room to ensure air circulation.

6.2.2. DATA COLLECTION

Pore pressure data from the sensors were transferred to a PC by using an analogue-digital converter and stored every second using DasyLab. Unfortunately, some data gaps occurred due to connection problems of the sensors to the computer. From the 129 experimental days, pore pressure data were recorded for 69 days. Data gaps are evenly distributed, as shown in supplementary Figure 6.12 of the Appendix 6B. The quality and the resolution of the data were sufficient to capture temporal changes in pore pressure due to plant transpiration.

From the pore pressure data and the water losses, the hydraulic conductivity (k) in both columns can be calculated. As the horizontal spatial scales are much smaller than the vertical scales, drainage takes place preliminary in the horizontal plane (i.e., via the drainage pipe in the centre of the column). Thus, the continuity equation on cylindrical coordinates was solved accounting for radial pore water flow towards the drainage pipe

(see Appendix 6F).

$$k = \frac{\rho g Q_{sink} R^2}{2\pi \Delta P (R^2 - {r_0}^2) H} \left(\ln\left(\frac{R}{r_0}\right) - \frac{1}{2} + \frac{{r_0}^2}{2R^2} \right) \tag{6.1}$$

Here, k is the hydraulic conductivity in m/s, ρ is the density of water [kg/m^3], g [m/s^2] is the acceleration of gravity , ΔP [Pa] is the pressure difference between the measured pressure at the column wall ($r = R$) and the pressure in the porous pipe ($r = r_0$), Q_{sink} is the measured flow in m^3/s, R is the radial coordinate, r_0 is the radius of the drainage pipe, and H is the drainage length.

At experimental time t = 40, 71, 88, and 102 days, one column was harvested in experimental run 1 to measure root and shoot parameters. Above-ground biomass was cut off, after which the photosynthetic area was measured immediately. Plant tissue was air-dried at 70 °C for 48 h to determine its dry weight. The leaf per mass area (LMA) could then be calculated. Samples of 5 cm sediment were serrated from the column, after which the roots were sieved from the sediment. The root surface area and the root length in each sample were determined with SmartRoot in ImageJ (*Lobet et al.*, 2011). The dry weight mass of the roots was determined per sample after drying, following the same procedure as the aboveground biomass.

Plant transpiration and photosynthetic activity were measured on three leaves per plant per column using the Li-Cor portable photosynthesis system (LiCor 6400) at experimental time t = 41, 61, 81, and 97 days. Conditions within the Li-Cor chamber were kept constant: the ambient CO_2 concentration was kept at 450 ppm, the temperature in the chamber was set to 17.3°C, the relative humidity was maintained at 60% and the light intensity in the chamber was set to 1500 PAR.

Photosynthetic parameters of *P. australis* were determined with the statistical package R (*Duursma*, 2015) to check whether plants remained healthy and were adapted to the low-light conditions in the climate room. The results in Table 6.2 shows that the photosynthesis rates are realistic, with a maximum rate of the Rubisco carboxylase activity (Vcmax) varying between 115 and 39.8 µmol 1/m^2 1/s and a maximum rate of the photosynthetic electron transport (Jmax) varying between 161 and 72.9 µmol 1/m^2 1/s. Both variables decrease in time, which indicates a decrease in leaf effectiveness when the leaves of *P. australis* mature (i.e., photosynthesis and transpiration decreases per unit leaf area). More detailed information on photosynthetic parameters is presented in supplementary Figure 6.14, which shows net CO_2 assimilation rates versus light intensity.

Table 6.2: Photosynthetic parameters of *P. australis* at 61, 81 and 97 days. The maximum rate of Rubisco carboxylase activity (Vcmax), the maximum rate of photosynthetic electron transport (Jmax) and the respiration rate (Rd) are presented (±S.E.) as well as the light compensation point (Γ*). All values are in µmol m-2 s-1

	Day 61		Day 81		Day 97	
V_{cmax}	115.00	*±8.72*	59.21	*±3.50*	39.80	±1.20
J_{max}	161.00	*±6.17*	108.00	*±4.84*	72.90	±1.89
R_d	1.67	*±0.68*	3.99	*±0.55*	0.46	±0.18
Γ*	28.79	-	28.84	-	28.63	-

6.3. RESULTS

6.3.1. PLANT DEVELOPMENT AND WATER LOSS

Table 6.3 shows that leaf area and leaf biomass increased in the first months to 406 cm^2 and 1.48 g at day 88, after which leaves started to wilt and leaf area and leaf biomass decreased to 263 cm^2 and 1.00 g at the end of the experiment. The plant roots proliferated throughout the column and reached the bottom of the column at the end of the experiment (84 cm, day 129). The length, the area and the biomass of the roots increased with time. Because the plants in the harvest columns did not grow at the same speed, we corrected the root area per depth interval for leaf area as measured right before harvest. The corrected root area as calculated from the four harvests is presented in Figure 6.2 a, showing that the root area relative to the leaf area at each depth interval increased with time. A peak is observed from the first harvest (40 days) in the top 5 cm (1.65 cm^2 per unit leaf area). This is because plants invest more in their root system than in aboveground biomass after transplantation. At 40 days, root biomass increased to 0.9 mg/cm^3, while leaf biomass increased to only 0.17 g (Table 6.3).

Table 6.3: Plant characteristics at 40, 71, 88 and 102 days as measured from harvested columns. Root length, root area, root biomass, and root volume are expressed per cm-3 column volume

Property	unit	40 days	71 days	88 days	102 days
Leaf area	cm^2	48.8	189	406	263
Leaf biomass	gr	0.17	0.67	1.48	1
Leaf mass per area (LMA)	g m^2	342	354	365	382
Stem biomass	gr	0.43	1.46	2.13	2.42
Max. rooting depth	cm	18	48	68	80
Root length	cm/cm^3	0.26	0.36	0.6	0.59
Root area	cm^2/cm^3	0.07	0.18	0.33	0.29
Root biomass	mg cm^3	0.9	0.8	1.3	1.07
Root volume	mm^3/cm^3	0.42	5.5	16	15
Shoot:Root ratio		0.49	0.74	0.54	0.53
Sediment volume	cm^3	6469	6432	6424	6414

Evaporation led to water loss in the control column, while both evaporation and plant transpiration led to water loss in the vegetated column. Figure 6.3 presents evaporation rates during the experiment for the control column only. All evaporation rates fall in-between 0.3 and 0.7 mm/day, averaging at 0.6 mm/day. For the vegetated column, it was difficult to separate these two mechanisms of water loss from the sediment. Although we are aware that plants alter evaporation to a minor extent via transpiration, we used the average evaporation of 0.6 mm/day from the control column to calculate evapotranspiration in the vegetated column (i.e., when measuring leaf transpiration, we added 0.6 mm to determine evapotranspiration). The evapotranspiration data are presented in Figure 6.2 b. This figure shows that increasing the leaf area led to a non-linear increase in water loss via evapotranspiration. The lowest measured value of 1.4 mm/day corresponds to a total leaf area of 31 cm^2. At a leaf area of 276 cm^2, the highest evaporation rate was found (7.7 mm/day). Evapotranspiration rates do not scale linearly with leaf area, as leaves become less effective in terms of photosynthetic capacity when maturing (Table 6.3). The average evapotranspiration rate of 3.9 mm/day found in this study closely agrees with the average

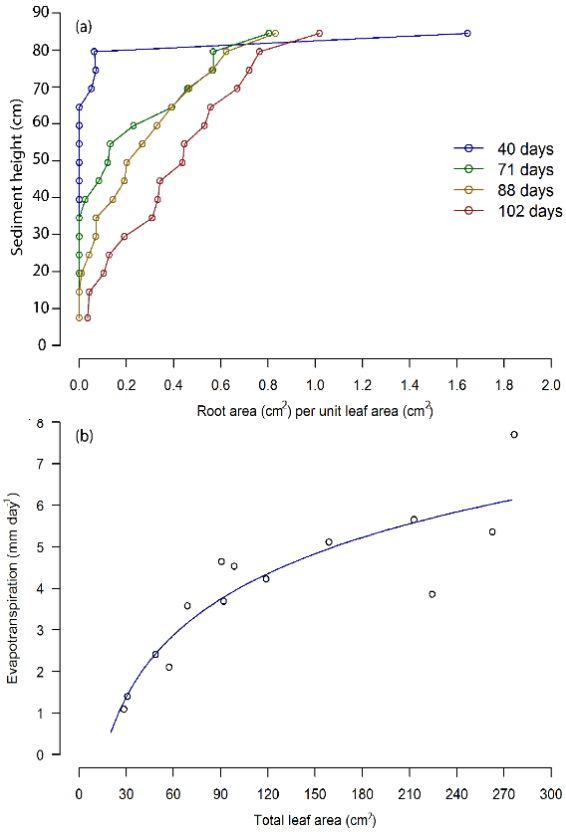

Figure 6.2: Root surface area per unit leaf area (cm^2) across sediment height at four different time steps (a) and evapotranspiration (mm/day) as a function of total leaf area (cm^2) in the vegetated column (b). Evapotranspiration rates measured in experimental run 1 and 2 are combined.

evapotranspiration value of 3.7 mm/day measured in reedbeds in the Teesmouth Estuary in England during the growing season *Fermor et al.* (2001). Similar rates were measured in the Biebrza wetlands in Poland, averaging between 3.0 and 3.5 in the summer months (*Siedlecki et al.*, 2016).

6.3.2. TOTAL PORE PRESSURE GRADIENTS

We selected three phases based on the successive stages of consolidation and drainage in the experiment as well as on the sediment height presented in Figure 6.8. For the first phase, we selected data of the time steps $t = 0$ and $t = 1$ days, during which fast initial consolidation occurred. We used data of the period $t = 12$-40 days for the second phase as we lack pore pressure data from $t = 2$ until $t = 11$ days (Figure 6.12). During this phase, slow consolidation occurred with little influence of plant transpiration (i.e., plant roots started to grow but did not have a big impact on pore pressure). After 40 days, the effects of plant transpiration on total pore pressure increased. Therefore, total pore pressure

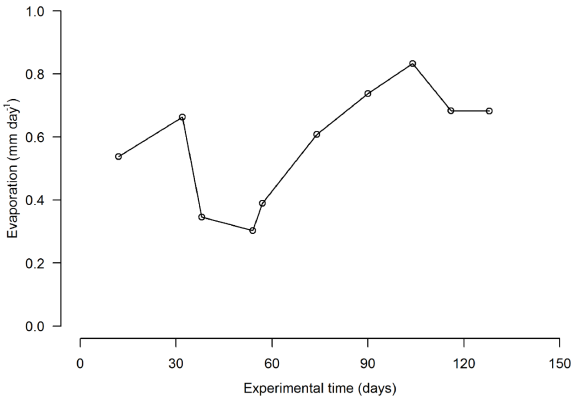

Figure 6.3: Temporal change in evaporation rate for the control column (mm/day).

data of the period t = 41-129 is used for the third phase.

Figure 6.4 shows the measured total pore water pressure for all three phases for the control column and vegetated column. The pore water pressures are rather identical for the two columns for stages 1 and 2. However, the pore pressure at the top (i.e., 2.5 cm above the water table) decreased from 1.1 kPa in phase 1 to -1.0 kPa in phase 3 in the vegetated column, while the pore pressure at the top in the control column decreased from 2.3 kPa to 0.3 kPa. The positive pore pressures above the water table in the control column are induced by the experimental set-up, as explained above. In phase 3 of the vegetated column (Figure 6.4 c), the pore pressure decreases remarkably from 1.2 kPa at 70 cm to -0.9 kPa at 50 cm, peaking at -1.7 kPa at t = 74 days. This reduction in pore pressure is likely caused by water uptake by plant roots as a result of an increase in total root area increased through time (Table 6.3), thereby increasing water uptake from the sediment.

These results show that plants altered total pore pressure especially between 40 and 60 cm from the bottom of the column by water extraction via roots. The negative pore pressures at these depths suggest that suction of water is an important process during consolidation in presence of plants. The pore water pressure profile is clearly led by evapotranspiration and not by self-weight consolidation since the excess pore pressure decreased at the height of the active root part indicating water transport to the roots.

6.3.3. DAILY CYCLES IN PORE PRESSURE

Water is taken up by plant roots to compensate for water loss via leaf transpiration. Plants transpire especially during photosynthesis, when stomata are open for gas exchange. Hence, it is expected that pore pressures within the sediment follow a daily cycle in the presence of plant roots. Figure 6.5 shows pore pressures during a 6-day period. In the control column, no difference in pore pressure is observed between day and night (Figure 6.5 a). However, large variation is observed in the vegetated column, especially between 40 and 50 cm height from the bottom of the column (Figure 6.5 b). These results suggest that during the day plants effectively lower pore water pressure at the point where the

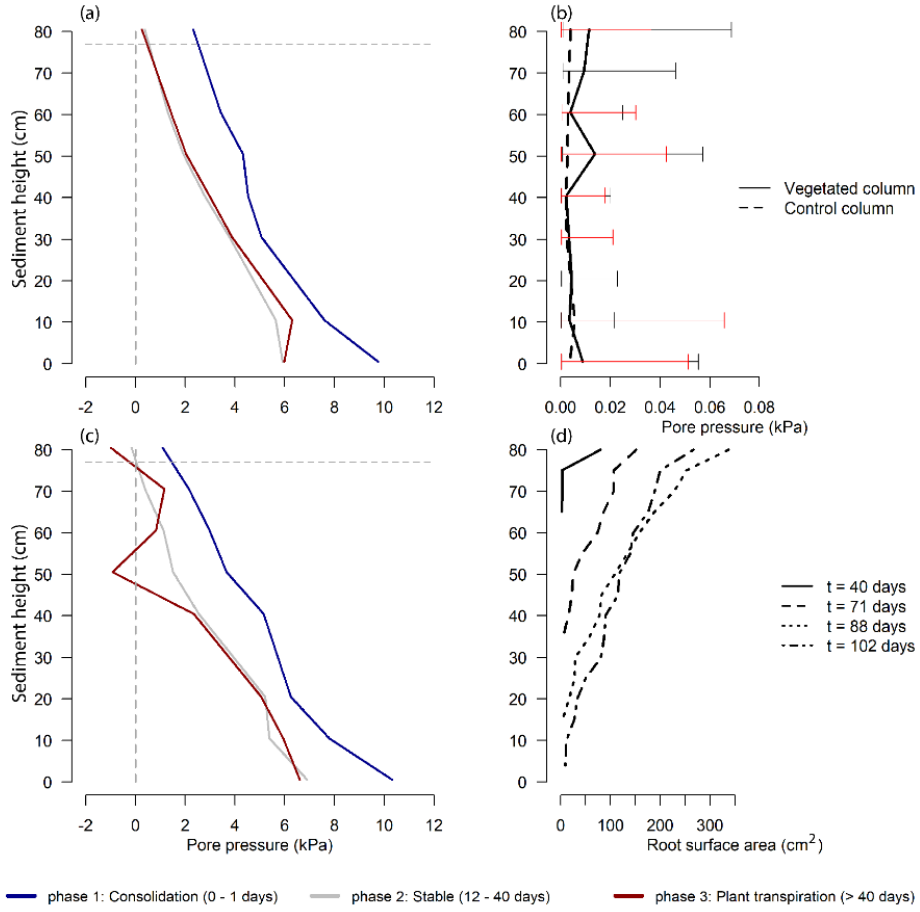

Figure 6.4: Pore pressure (kPa) relative to the water column in the control column (a) and vegetated column (c). Average daily errors (kPa) for each pressure sensor are shown (± the band of measured values found during the experiment, as indicated by the bars; red is for the control column and black is for the vegetated column) (b). The average daily errors indicate the accuracy of the sensors (6.9 10-3 kPa) and are based on the hourly data points. Root surface area is presented from experiment 1 (d). Note that these root surface areas are from four individual plants (n = 1).

roots are extracting most of the water (50 cm from the bottom of the column). During the night, the pore water pressures increased relative to day-time. This suggests that the dominant flow of water at night occurs from the drainage pipe into the sediment to compensate for the water losses during the day. A reverse cycle is visible in the vegetated column at 70 cm, indicating that during the night, water flow from the drainage pipe decreased pressure values, likely because of a lowered water table due to plant drainage during the day. It is likely that water flow was insufficient to maintain the water table at a fixed level at short time scales because of a low hydraulic conductivity.

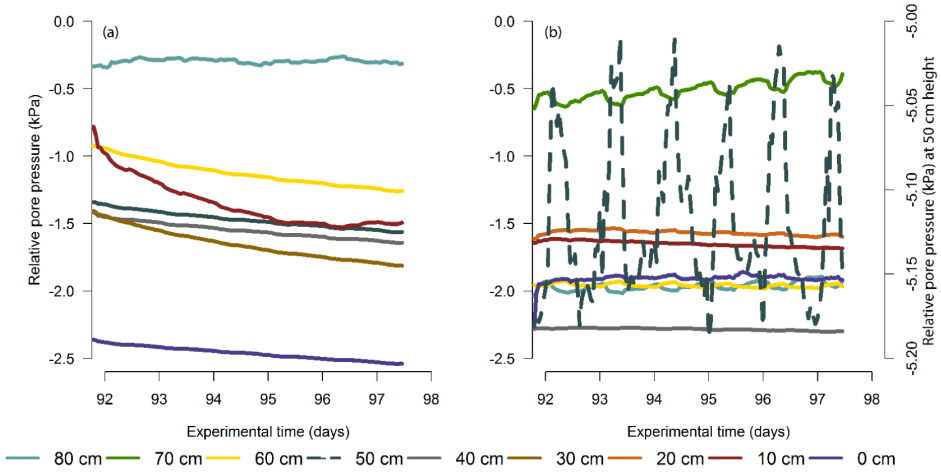

Figure 6.5: Hourly time series (t = 92-98 days, to be compared with day >40 of Fig 4) of pore water pressure relative to the reference column (see Figure 1) for the control column (a) and vegetated column (b). Note that the sensor at 50 cm depth has a different y-axis in graph (b).

6.3.4. HYDRAULIC CONDUCTIVITY

The measured water fluxes for the experimental columns are presented in Figure 6.6 and were used for calculating the hydraulic conductivity using Equation 6.1. The theoretical evaporation rate of 0.6 mm/day is defined as the daily-average of the evaporation rates presented in Figure 6.3. The vegetated column reached that evaporation rate after 30 days, after which the water flux increased up to 6.2 mm/day via plant transpiration. The flow in the vegetated column decreased at the end of the experiment due to maturing of the leaves of *P. australis* (Table 6.2).

Figure 6.7 shows the calculated hydraulic conductivity profiles ($k(z)$ from Equation 6.1) of the vegetated column and the control column. The water loss via leaves (transpiration) is included in the hydraulic conductivity calculations because the sum of water losses is used in Equation 6.1 (i.e., evaporation and transpiration). Thus, the hydraulic conductivity of the vegetated column is based on water transport in-between the soil particles plus water transport through the plant roots. In supplementary Figure 6.13, the depth-averaged hydraulic conductivity of the control column and vegetated column for the duration of the experiment are presented. In the first two days of the experiment

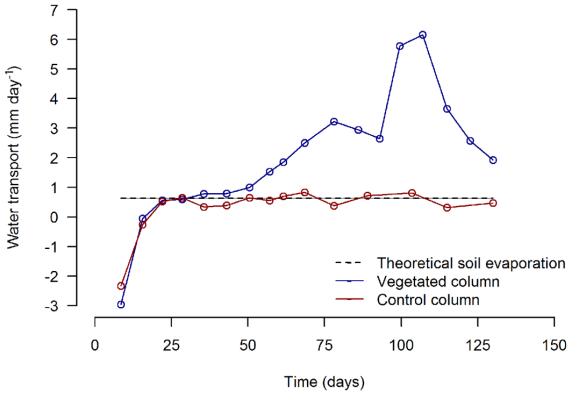

Figure 6.6: Water transport measured during the experiment for the control column (consolidation or evaporation) and the vegetated column (consolidation or evaporation and plant transpiration) compared to the theoretical soil evaporation rate. Negative values indicate consolidation (dewatering via the drainage pipe) and positive values indicate evaporation (and transpiration as well).

(phase 1), the hydraulic conductivity started relatively high on average (8.8×10^{-9} m/s for the vegetated column and 5.3×10^{-9} m/s for the control column). The hydraulic conductivity rapidly decreased due to self-weight consolidation in phase 2 to 1.3×10^{-11} m/s on average in the control column and to 1.1×10^{-10} m/s on average in the vegetated column. This is in line with Figure 6.8, which shows that the sediment height in both columns lowered rapidly in the first 15 days. The difference in the initial hydraulic conductivities between the control column and the vegetated column might be caused by small disturbances induced when transplanting the reed seedlings at $t = 0$ days. The hydraulic conductivities in both columns stabilized on average to 3.2×10^{-10} m/s in the control column and 1.3×10^{-9} m/s in the vegetated column. In phase 3, the hydraulic conductivity in the vegetated column averaged at 1.9×10^{-10} m/s, while the hydraulic conductivity in the control column averaged at 1.3×10^{-10} m/s. Thus, the hydraulic conductivity increased with a factor 1.4 compared to the control column due to enhanced drainage via transpiration in the phase when plants became active. Note that at $t = 0$, the hydraulic conductivity computed in the vegetated and non-vegetated columns differ considerably. These differences can be explained from Equation 6.1. While we measure ΔP , we have no information on $Q(z)$, thus using its depth-average value. However, a larger or smaller ΔP would affect Q locally. Together with the inherent inhomogeneities in the soil, this leads to errors in $k(z)$. These errors reduce over time, as flow rates, and thus their absolute errors, decrease over time.

6.3.5. SEDIMENT HEIGHT

Figure 6.8 presents the sediment height over time. Both sediment columns had almost identical sediment heights during the experiment, ranging from 92.5 cm at the beginning of the experiment down to 85.1 cm at the end. Thus, the sediment height is the same despite a maximum root volume increase of 16 mm^3/cm^3 sediment volume in the vegetated column (Table 6.3). The sediment height (Figure 6.8) and the increase in hydraulic

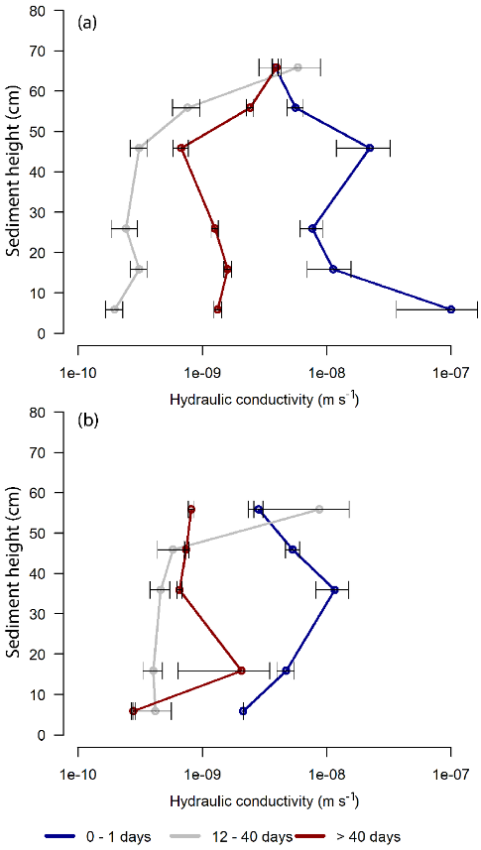

Figure 6.7: Conductivity profiles (m s-1) for the vegetated column (a) and the control column (b) with standard errors. Profiles are averaged for three different time phases: 1) fast consolidation phase (0-1 days), 2) stable phase (12-40 days), and 3) plant transpiration phase (> 40 days).

conductivity in the vegetated column (Figure 6.7), suggest that the volume once occupied by water is being replaced by roots. Because of continuous water supply from the drainage pipe, drainage by roots did not influence the sediment height.

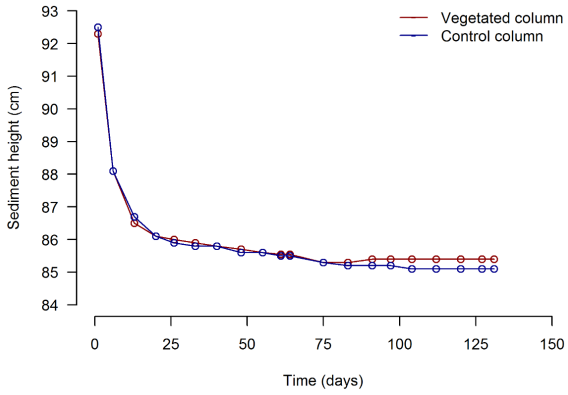

Figure 6.8: Sediment height (cm) during the experiment for the vegetated column (red) and for the control column (blue).

6.4. DISCUSSION

6.4.1. ALTERED PORE PRESSURE GRADIENTS

The results of this study showed that *P. australis* effectively alters the pore pressure gradient in soft cohesive sediments. The shape of all pressure depth profiles (Figure 6.4) is comparable with typical profiles of bare silty soils (e.g *Blight*, 2003). For the vegetated column, there is a sharp drop in pore pressure between 40 and 60 cm from the base of the column. In the soil layer where plant roots extracted water, we found pressures up to four times higher than in the control column because of vegetation induced suction. Similar impacts of plants have been found by *Leung et al.* (2015); *Leung* (2016). They showed that the air entry value (i.e., the pressure point after which air recedes into the soil pores) increased four times in presence of Ivy trees (*Schefflera heptaphylla*) compared to bare soil, presumably because of the reduction of the size of the pores (e.g *Nimmo*, 2004). The part in the column where roots extract water did not change during the experiment: pore pressure was reduced remarkably between 40 and 60 cm from the bottom of the column. This was unexpected as roots of *P. australis* penetrated deeper in the sediment in time (Figure 6.4 d) and water uptake is supposed to be largely restricted to the part near the root tip (*Kramer and Boyer*, 1995). The fact that pore pressure below 40 cm height was relatively unaffected even though root area increased in deeper sediment layers (Figure 6.2 a), suggests that the changing sediment physical properties were limiting water extraction to a sediment height of 40-60 cm from the bottom of the column. The deep rooting depth of *P. australis* is a common trait of this species and gives it an advantage over most graminoid plants sharing wetland habitats (*Moore et al.*, 2012). According to *Zhuang et al.* (2001), root hydraulic characteristics co-determine where water is taken up and this depends on the pattern by which the different parts of the root contribute to the overall

water transport. These root characteristics were not measured in this experiment and it is, therefore, hard to explain why the part where water was extracted did not shift downwards in the column through time. Because of the daily cycles present at a sediment height of 50 cm, we are confident to link the observed reduction in pore pressure at this depth to water loss by root extraction (Figure 6.5 b). Moreover, we measured an average water loss via evapotranspiration of 3.9 mm/day in the vegetated column, whereas water loss via evaporation amounted on average to 0.6 mm/day in the control column. Although pore pressure restored during the night, the reduction in pore pressure during the day was larger than the increase during the night. This – together with the fact that root area kept on increasing in the zone of water extraction – might explain why pore pressures decreased with time. During the night, the effect of recovery of the water table is observed at a sediment height of 70 cm in the vegetated column (Figure 6.5 b). At this height, water flow from the drainage pipe decreased suction values during the night because of a decreased water table due to plant drainage during the day.

Though Figure 6.7 is not conclusive, it is to be expected that deeper into the soil, where density increases, hydraulic conductivity decreases. While roots grow and penetrate the soil, they open drainage channels, facilitating pore water flow along their wall (*Orozco-López et al.*, 2018). Thus, we argue that below 60 cm this effective conductivity exceeds the soils own hydraulic conductivity. Water uptake at a depth greater than 60 cm would then originate from above.

Last, as discussed in the Introduction, plants are expected to enhance drainage, favourably affecting consolidation. The current experiments did not show any enhanced settling rates, though. This may be due to the experimental setup chosen. However, there are a number of other arguments that need to be considered, though we have no data to quantify:

1. Plants can only root when the soil has gained a minimum strength. Consolidation rates are relatively large in the initial phase of consolidation, i.e. when plants cannot yet root.
2. The consolidation rate of soils is a function of its initial thickness and its material properties. Thus, the consolidation rate likely has other time scales than root formation, which is a biological process. Thus, consolidation time scales and root formation time scales have to be compared in assessing the effectiveness of vegetation-induced consolidation and drainage,
3. The roots themselves strengthen the soil, thus also its resistance to consolidation. Hence, this armouring counteracts the additional drainage by the roots. Which of these two processes wins may be site-specific, depending on vegetation type and soil properties and its initial conditions prior to consolidation.

6.4.2. EFFECTS ON HYDRAULIC CONDUCTIVITY

The results of this study showed that *P. australis* increased the average hydraulic conductivity of the sediment by 40% compared to bare soil. But this induces merely circulation/ventilation, as consolidation has stopped. As discussed above, the overall hydraulic conductivity of a soil-plant complex likely consists of three parts: 1) the inherent hydraulic conductivity of the soil itself, which is a function of the soil composition and its state of consolidation, 2) the drainage by the roots, enhancing pore water flows through

the soil-plant complex, and 3) drainage channels along the roots or elsewhere in the soil in the form of root-induced cracks. Thus, the hydraulic properties of the soil and roots are closely coupled (*Lobet et al.*, 2014). A mechanism by which plants increase the permeability in sediments involves the development of drainage channels of which the main driver is root growth (*Ghestem et al.*, 2011; *Orozco-López et al.*, 2018). In our case, these macropores represent pores made by living or decaying roots of *P. australis* (i.e., root channels). Especially in cohesive sediments, these root channels are the dominant flow paths of water (*Perillo et al.*, 1999) and can contribute to 70-100% of total macropore space in the top 8 cm of a sediment (*Noguchi et al.*, 1997; *Newman et al.*, 2004). However, a low fraction of macropores of total porosity already increases water flow of saturated soil (*Beven and Germann*, 1982). This is especially relevant in artificial wetlands where fast initial consolidation is important. In our experiment, we found that the hydraulic conductivity increased only to a limited extent compared to bare soil, despite the increasing root area. Similar observations were reported by *Vergani and Graf* (2015), who observed stagnation in the increase of sediment permeability due to root proliferation when root length densities approached 0.1 cm cm-3. This can be explained by two opposing processes taking place when roots proliferate in the sediment: 1) the contact area of water increases with increasing root density; at low root densities this accelerates water flow through the soil, and 2) the film thickness of mobile water inside the root-induced cracks decreases with increasing root densities, deaccelerating water flow (*Lange et al.*, 2009). Hence, a stagnant point is reached when the film thickness of the water becomes too thin to promote water flow. Another reason might be that photosynthesis and transpiration decrease per unit leaf area as leaves mature as was observed for leaves of *P. australis* in our experiment (Table 6.2). The observed stagnation of the increase in hydraulic conductivity is, therefore, likely caused by a combination of a reduced photosynthetic capacity of the leaves and a reduction in film thickness.

6.4.3. COMPARISON WITH FIELD CONDITIONS

The photosynthetic parameters measured during the experiment showed that *P. australis* behaved as expected from field conditions; the leaves were optimized to the low-light conditions in the experimental facility. Hence, the set-up of the experiment did not affect stomatal gas exchange and data from this experiment can thus be translated to field conditions. The average evapotranspiration rate of 3.9 mm/day indeed closely coincides with average evapotranspiration rates found in wetlands (e.g *Fermor et al.*, 2001; *Siedlecki et al.*, 2016). Therefore, the data acquired from this experiment can be used to model the speed of drainage and consolidation in constructed wetlands build with soft, clay-rich material. Such a model would help to estimate the difference between mudflats transplanted with and without *P. australis*. However, some complex variables were not taken into account in our experiment that will influence drainage and consolidation behavior in the field, such as variations in the topography and the depth of the water table. Moreover, if vegetation develops in patches this will also result in spatially non-uniform plant-soil interactions. Furthermore, the higher the actual evapotranspiration of the plant species, the faster the suction recovery after a rainfall event for the same root biomass (*Garg et al.*, 2015). Apart from the drainage effect, vegetation also induces biogeochemical processes (*Saaltink et al.*, 2016), which induce pedogenic processes that

accelerate the maturation or ripening of the soil (e.g. *Pons and Zonneveld*, 1965; *Barciela-Rial et al.*, under review). Despite these complexities, upscaling the presented results in a predictive plant-soil model will provide useful insights for the implementation of ecological-engineers, such as *P. australis*, to speed up soil forming processes.

6.5. CONCLUSIONS

The results presented in this study identified how ecological engineers interfere with the physical processes involved in sediment drainage and consolidation. Phragmites australis effectively altered the pore pressure gradient in the soft, clay-rich sediment. In our experimental set-up, this is the case for the top 40 cm of the sediment. In this zone, daily cycles in pore pressures were observed which could directly be linked to the diurnal cycle of stomatal gas exchange. On average, water loss via evaporation and transpiration of leaves of *P. australis* amounted to 3.9 mm/day, whereas evaporation of bare soil amounted on average to 0.6 mm/. Moreover, the depth-averaged hydraulic conductivity increased on average by 40% in presence of *P. australis*. These findings highlight the feature of this plant to act as an eco-engineer to fasten drainage in soft cohesive sediment. This might lead to enhanced consolidation rates. However, the experiments were not fully conclusive on a number of important interactions, and further dedicated experiments and measurements are required to resolve the following questions:

1. Roots enhance the effective drainage and hydraulic conductivity of a soil-plant complex. The inherent hydraulic conductivity of the soil itself is enhanced by root-growth induced cracks, forming macropores and drainage channels, On the other hand, root-growth disturbs the soil structure locally, which may result in densification of the soil. Further, we have indications that the roots themselves enhance drainage within the soil by promoting pore water flow along their wall.
2. Though drainage increases, this does not necessarily imply enhanced consolidation rates. The roots also strengthen the soil by armouring, as in reinforced concrete. If the latter effect wins, consolidation rates may even be retarded, as suggested by the current experiments.

6.6. APPENDIX 6A: CALIBRATION PROCEDURE

Before the start of the experiment, all pore pressure sensors were thoroughly calibrated. The reference column and the two sediment columns were filled with water up to 88 cm prior to calibration (Figure 6.9). At this point, the relative pressure difference between each sediment column and the reference water column is zero and the output of all pore pressure sensors was set to 0.000 mV. Then, the water level in the reference column was increased/decreased with increments of 2 cm, while the water level in both sediment columns stayed at 88 cm. The output in mV was recorded at five relative water levels: -2 cm, 2 cm, 4 cm, 6 cm, and 8 cm (Figure 6.9). Calibration curves were determined for each pore pressure sensor. Figure 6.10 and 6.11 present these calibration curves for the control column and the vegetated column respectively.

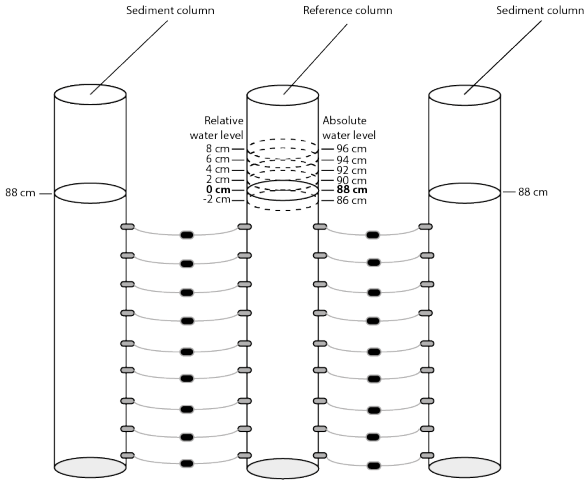

Figure 6.9: Schematic overview of the calibration set-up. All pore pressure sensors are calibrated using six different water heights relative to the water height in the sediment columns: -2, 0, 2, 4, 6, and 8 cm.

When converting the output of the pore pressure sensors in mV to kPa, we assumed a water density of 998.774 kg/m^3, corresponding to the constant lab temperature of 17.4 °C. Furthermore, we worked with a gravity acceleration of 9.8125 m/s^2, corresponding to the latitude of the location of the laboratory (i.e., 52° N). This means that 0.01 m of water results in a pressure increase of 0.01 m x 998.774 kg/m^3 x 9.8125 m/s^2 = 0.098004 kPa.

Using the equations of the calibration lines in Figures 6.10 and 6.11, we calculated the relative difference in pressure between the reference column and the sediment column for each pore pressure sensor: pressure (kPa) = 0.098004 (a mV + b – 87 cm). Because the water level in the reference column was fixed at 87 cm during the experiment, changes in kPa are directly related to changes in pore pressure in the sediment columns.

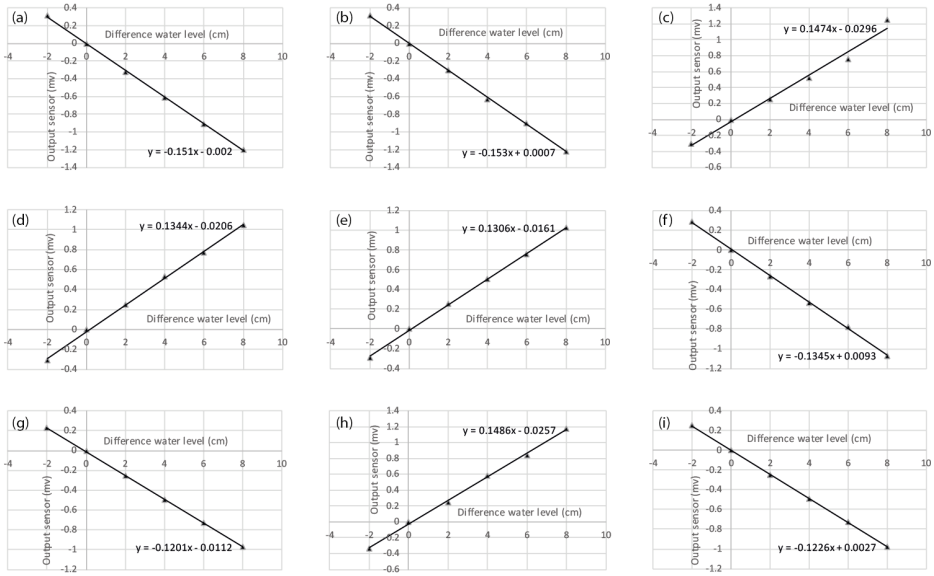

Figure 6.10: Calibration lines of all pore pressure sensors attached between the reference column and the control column: 4 cm depth (a), 14 cm depth (b), 24 cm depth (c), 34 cm depth (d), 44 cm depth (e), 54 cm depth (f), 64 cm depth (g), 74 cm depth (h), and 84 cm depth (i).

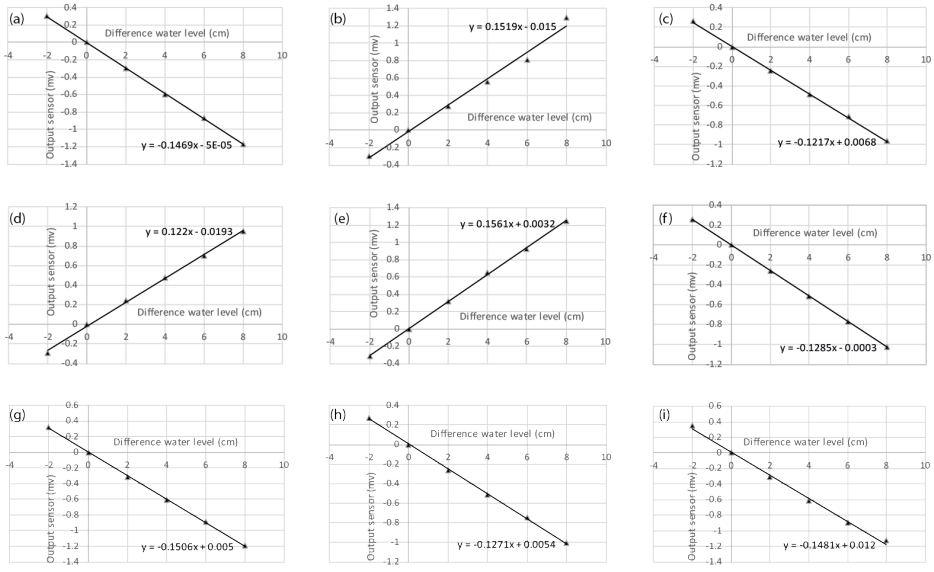

Figure 6.11: Calibration lines of all pore pressure sensors attached between the reference column and the vegetated column: 4 cm depth (a), 14 cm depth (b), 24 cm depth (c), 34 cm depth (d), 44 cm depth (e), 54 cm depth (f), 64 cm depth (g), 74 cm depth (h), and 84 cm depth (i).

6.7. APPENDIX 6B: SUPPLEMENTARY FIGURES

This appendix includes three Figures with supplementary information of the experiments presented in this chapter. Figure 6.12 shows the evolution of the measured pore pressures. These pore pressure values were used to obtain the evolution of the depth-averaged hydraulic conductivity shown in Figure 6.13. Finally, Figure 6.14 shows the Net CO_2 assimilation rates of the studied *P. australis* as a function of light intensity (for details about this figure, see *Saaltink* (2018)).

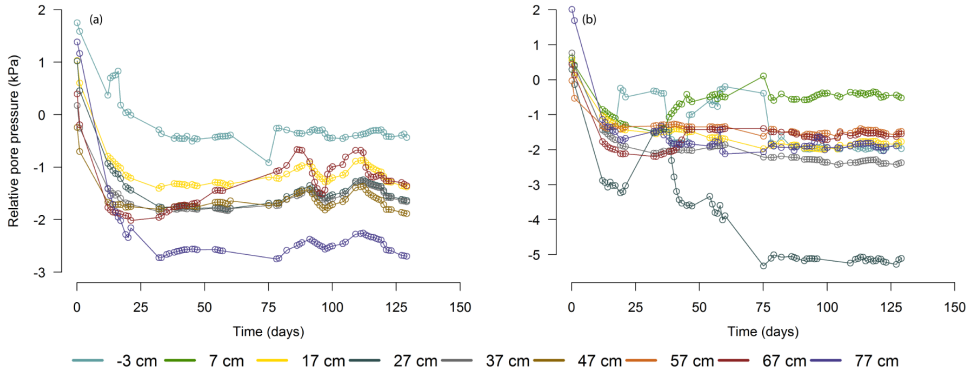

Figure 6.12: Relative pore pressure (kPa) relative to the reference water column at all depths of the control column (a) and the vegetated column (b) for the duration of the experiment. Each pore pressure sensor is connected at the same height at the sediment column and at the reference water column. This reference column has a constant height of water of 87 cm.

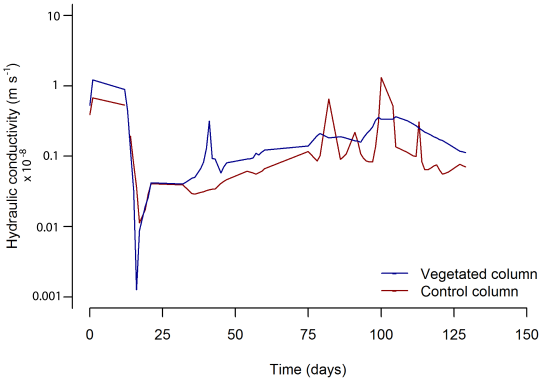

Figure 6.13: Depth-averaged conductivity (m s-1) for the control column and the vegetated column.

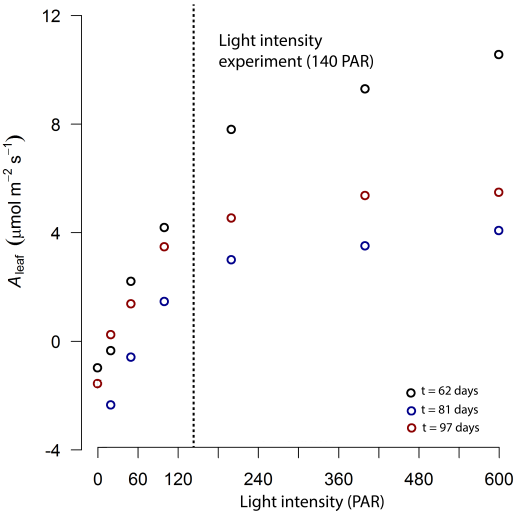

Figure 6.14: Net CO_2 assimilation rates (µmol m-2 s-1) versus light intensity (PAR) at 61, 81 and 97 days after the start of the experiment. The vertical grey dotted line represents the light condition during the experiment (140 PAR).

6.8. APPENDIX 6C: ANALYSIS OF THE EVOLUTION OF THE PRESSURE PROFILES

In the present chapter, pore water pressures were measured to study the effect of vegetation on the pore pressure profile of slurries experiencing consolidation and drying. However, the analysis of the results was not trivial because of effects induced by the experimental set-up on the pressure measurements. The objective of the present appendix is to study and understand the pressure distributions at relevant time steps: beginning and end of experiment and moments when the set-up could have affected the results.For that, the measured pore pressure profiles were plotted together with the slurry total and hydrostatic pressures for these steps. The hydrostatic pressure inside the drainage pipe was also plotted. To calculate the hydrostatic pressure in the drainage pipe, the level of water herein needs to be known. After the connection of this pipe with the reference water column, this level is constant an equal to 77 cm. However, prior to this connection the level is expected to vary. This water level was not measured but can be calculated from a pseudo- force balance described in Figure 6.15. The word pseudo refers here to the fact that the pipe is not permeable above 72 cm from the bottom and consequently the forces in the drainage pipe and the slurry are not directly connected above 72 cm. Thus, to calculate the total pressure at each side of the pipe wall, the following integration was done:

$$\int_{z_0}^{z_b} (p_0 + \rho g z) dz = p_0 L + \frac{1}{2} \rho g L^2 \tag{6.2}$$

where z is the vertical axis positive upwards, z_b is the bottom of the column ($z = 0$) and z_0 is the position at which the drainage pipe stops to be permeable (z = 72 cm, Figure 6.15). L corresponds to the length of 72 cm that the pipe is permeable and p_0 represents the pressure above the drainage level of z_0, i.e above z = 72 cm. The p_0 in the water of the drainage pipe is referred as $p_{w,0}$ while the p_0 over the slurry is referred as $p_{sl,0}$. This yields to the following pseudo force balance between both sides of the drainage pipe:

$$p_{w,0}L + \frac{1}{2}\rho_w g L^2 = p_{sl,0}L + \frac{1}{2}\rho_{sl} g L^2 \tag{6.3}$$

which is valid assuming unconsolidated sediment. The water level can be calculated from $p_{w,0}$ because

$$p_{w,0} = \rho_w g h_{w,0} \tag{6.4}$$

where $h_{w,0}$ is the height of water in the drainage pipe above the 72 cm.

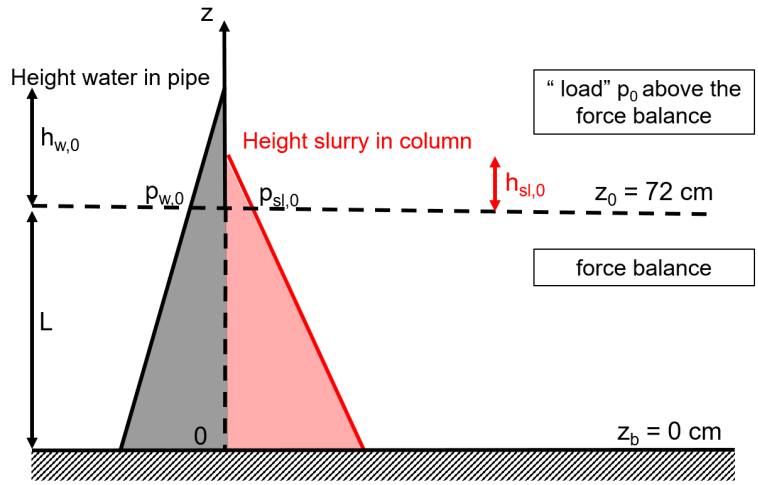

Figure 6.15: Schema of the pseudo force balance between the forces acting over the wall of the drainage pipe. Legend: $h_{w,0}$ is the height of water above z_0 = 72 cm which yields an hydrostatic pressure $p_{w,0}$ at z_0; $h_{sl,0}$ is the height of slurry above z_0 which yields herein an hydrostatic pressure $p_{sl,0}$. L is the length over which the drainage pipe is porous.

In the next subsections, these pressure profiles are presented for different time steps. First, the profiles for the control column are presented and, afterwards, the profiles for the column with vegetation.

6.8.1. CONTROL COLUMN

Figure 6.16 shows the pressure distribution at t =-14 days, i.e. the moment at which the slurry was poured in the column. It had a bulk density of 1263 kg/m^3 and the column was filled up to the height of 118 cm, which yielded a total pressure ($\sigma_{t,slurry}$) of 144.5 hPa at the bottom of the column. Immediately after pouring in the slurry, water flows inside the porous pipe. This accelerates consolidation by drainage at the bottom of the column.

Furthermore, the height of the water inside the drainage pipe needs to be higher than in the column, because of the lower density of water with respect to the slurry. This water height was calculated to be equal to 139.6 cm. This leaded to a maximum hydrostatic pressure in the pipe of 136.9 hPa which implies an hydrostatic pressure and the bottom of this pipe of 136.9. Two weeks after the filling of the column, a layer of water expelled by self-weight consolidation was present above the sediment. At this moment (Figure 6.17), the following steps were done:

- At $t = 0^-$: removal of the supernatant water. After this, the computation of the unknown water level in drainage pipe was done with Equation 6.3. This Equation assumes non consolidated material and the results can thus only be approximate at this stage. The calculated value of this water level was 111.3 cm. This water height yielded a maximum hydrostatic pressure ($p_{h,dr}$) of 109.1 hPa at the bottom of the drainage pipe. This $p_{h,dr}$ at $t = 0^-$ is lower than the measured pore water pressure in the slurry (Figure 6.17), which implies that the water flows from the drainage pipe to the slurry.
- At $t = 0$: the valve of Figure 6.23 was open. This means that the drainage pipe was connected to the reference water level of 77 cm. The sediment height at $t = 0$ was measured to be 92.5 cm. This lower sediment interface with respect to t = -14 days is due to self-weight consolidation and evaporation. Thus, at this moment, the averaged sediment concentration c was 542 g/L, which represents a bulk density of 1332 kg/m^3. The hydrostatic water pressure of the slurry ($p_{h,slurry}$) at this moment was 90.7 hPa at the bottom of the column.
- At $t = 0^+$: The water level of the drainage pipe was equal to the reference water table of 77 cm and the measurement of the pore water pressures of the slurry started. At this moment, $p_{h,dr}$= 75.5 hPa at the bottom of the pipe. Thus, at $t = 0^+$, the pore water pressure at the slurry ($p_{w,slurry}$) > $p_{h,dr}$ (Figure 6.17) and water flows from the slurry towards the pipe.

At t = 32 days, c = 584.5 g/l, ρ_{slurry} = 1358 kg/m^3. Therefore, $\sigma_{t,slurry}$ = 114.30 hPa at the bottom of the column. The measured pore water pressure ($p_{w,slurry}$) < $p_{h,dr}$ up to about 70 cm from the bottom of the column (Figure 6.18). This implies that, to compensate for evaporation, water flows from the drainage pipe towards the slurry. However, above 70 cm, $p_{w,slurry} > p_{h,dr}$, suggesting that the water flows from the slurry towards the pipe. However, the drainage pipe is not porous above 72 cm and water only can flow upwards. Furthermore, extrapolation of the pore water measurements yields a value of $p_{w,slurry}$=0 at the surface, which suggests that the water table is at the surface. If the water table would be at the surface, instead that at the prescribed 77 cm, $p_{h,slurry}$ = 84.2 hPa at the bottom of the column instead of 75.54 hPa.

At the end of the experiment, t_∞= 129 days : c = 589.3 g/l, ρ_{slurry}= 1361 kg/m^3, $\sigma_{t,slurry}$= 113.62 hPa. Figure 6.19 shows that, at this time step, the measured pore pressure is below the hydrostatic pressure of the drainage pipe below the drainage level (72 cm). This induces a water flow from the drainage pipe towards the slurry for this layer of sediment. However, above the level of drainage, the pore pressure is above the hydrostatic pressure of the drainage pipe. This implies that the water would tend to flow towards the drainage pipe, but this is not possible and therefore water has to flow up towards the sediment

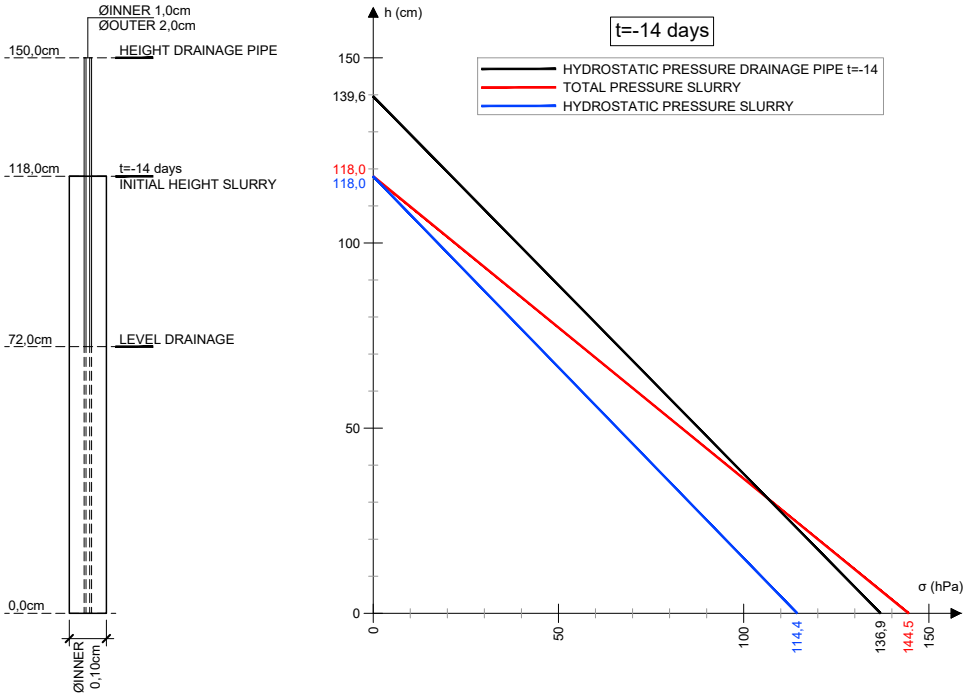

Figure 6.16: Pressure profiles at t = -14 days (i.e. the moment at which the slurry was poured in) for the control column during the performance of the consolidation and drying experiment.

surface. When the measured pore water pressure is extrapolated, the value of zero pore water pressure is achieved at around the sediment surface, which suggests that the water table is at the surface and not at the "prescribed" 77 cm. Therefore, this would imply that $p_{\mathrm{h,slurry}}$= 83.5 hPa at the bottom of the column.

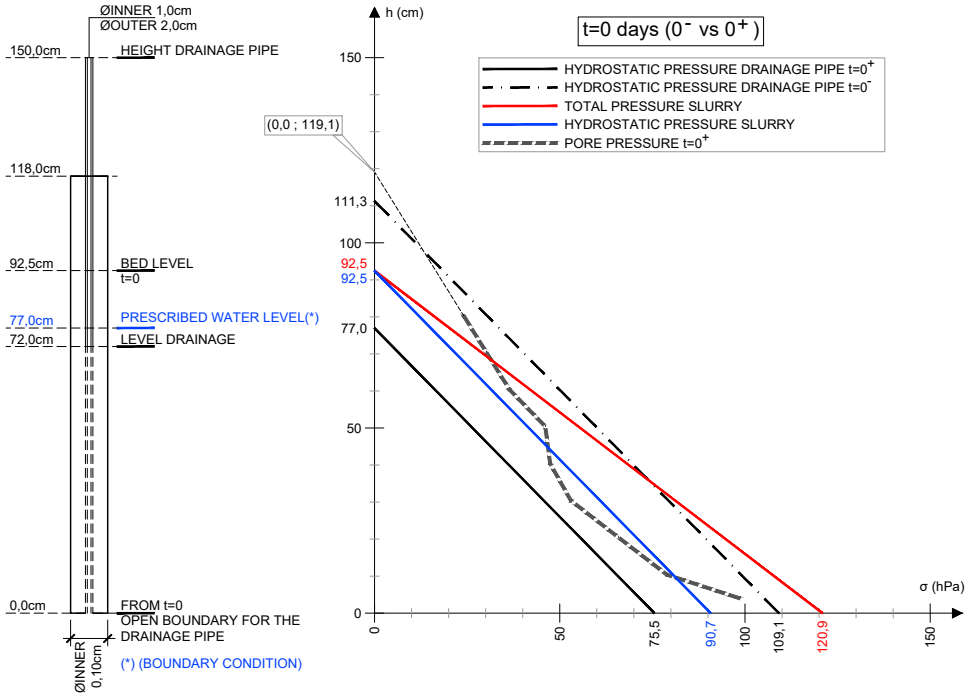

Figure 6.17: Pressure profiles at $t = 0$ days for the control column during the performance of the consolidation and drying experiment. This figure includes the hydrostatic pressure in the drainage pipe at $t = 0^-$ (before connecting the pipe to the reference water table) and at $t = 0^+$ (after this connection by opening of the valve, see Figure 6.23).

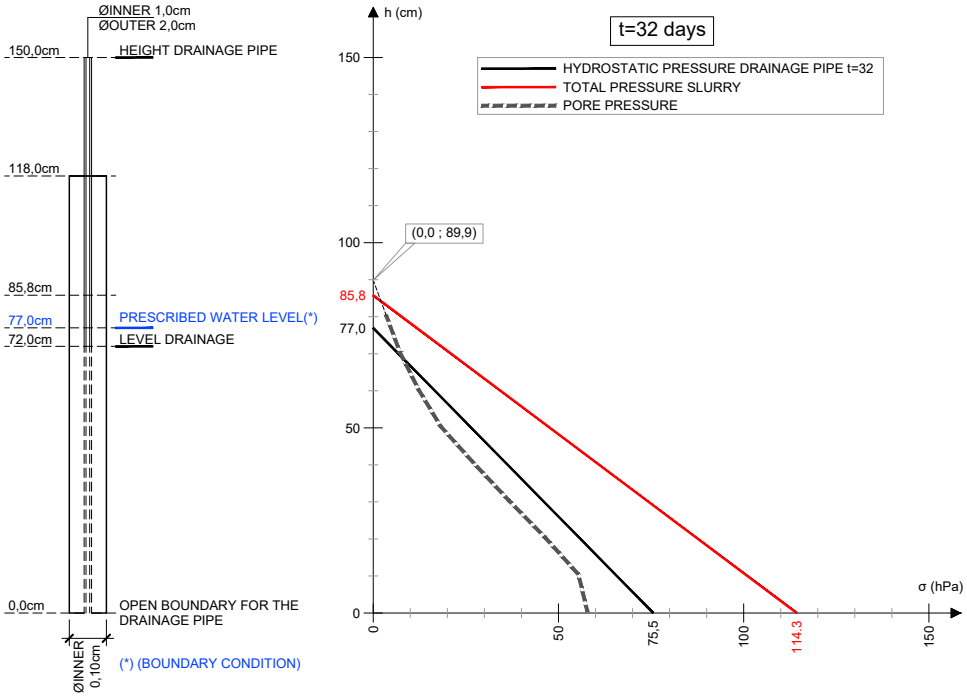

Figure 6.18: Pressure profiles at $t = 32$ days for the control column during the performance of the consolidation and drying experiment.

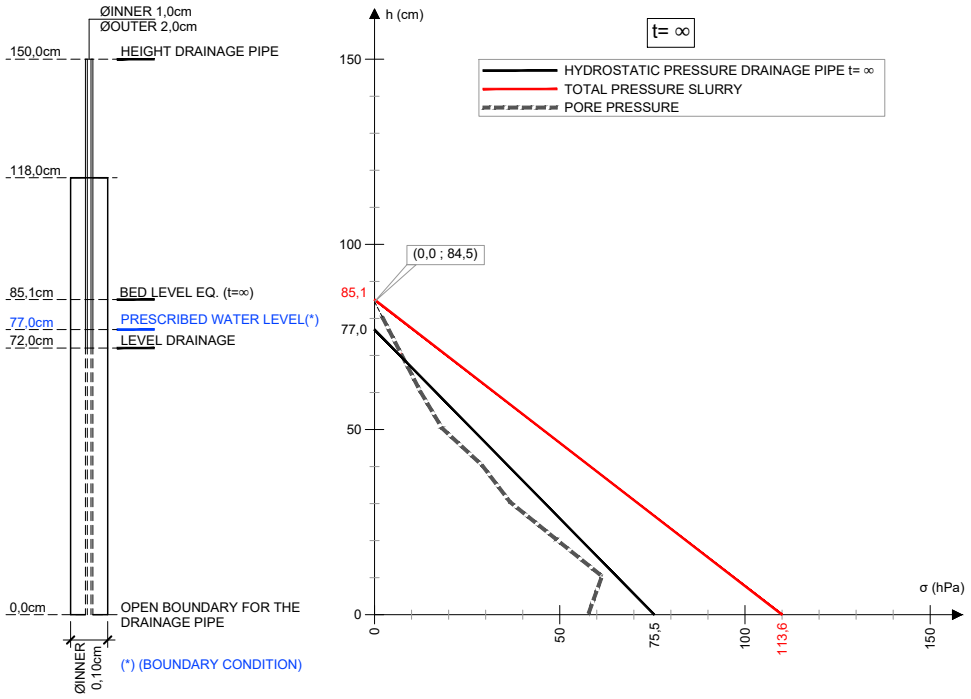

Figure 6.19: Pressure profiles at $t = \infty$ days for the control column during the performance of the consolidation and drying experiment.

6.8.2. VEGETATED COLUMN

At t = -14 days vegetation was not yet planted and therefore pressure profiles were the same in all columns. At t = 0, further to the connection of the drainage pipe to the reference level, three 2 cm shoots of *P. australis* were planted into the slurry. Presumably, plantation of the vegetation caused some dissipation of excess pore water pressure. This would explain why $p_{w,slurry}$ almost overlaps $p_{h,slurry}$ and has smaller values than for the case of the control column (compare Figure 6.20 with Figure 6.17). With respect to the direction of the water flow, the behaviour is the same as in the control column: at $t = 0^-$ water flows from the drainage pipe to the slurry and at $t = 0^+$ this direction is inverted.

At t = 32 days (Figure 6.21), $\sigma_{t,slurry}$ and $p_{h,dr}$ are identical to the case without vegetation. The measured pore water pressure profile is also similar. However, it exhibits more irregularities caused by the vegetation. At this time, water flows from the drainage pipe to the slurry over almost the whole column hight, because $p_{w,slurry} < p_{h,dr}$. However, this pattern is opposite at the upper cm's of the column, because of evaporation and plant transpiration.

At t_∞ =129 days, the vegetation has fully developed, inducing suction that can be observed in the measured pore water pressure profile (Figure 6.22). Vegetation induced larger suction at around 50 cm from the bottom of the column and at the sediment surface.

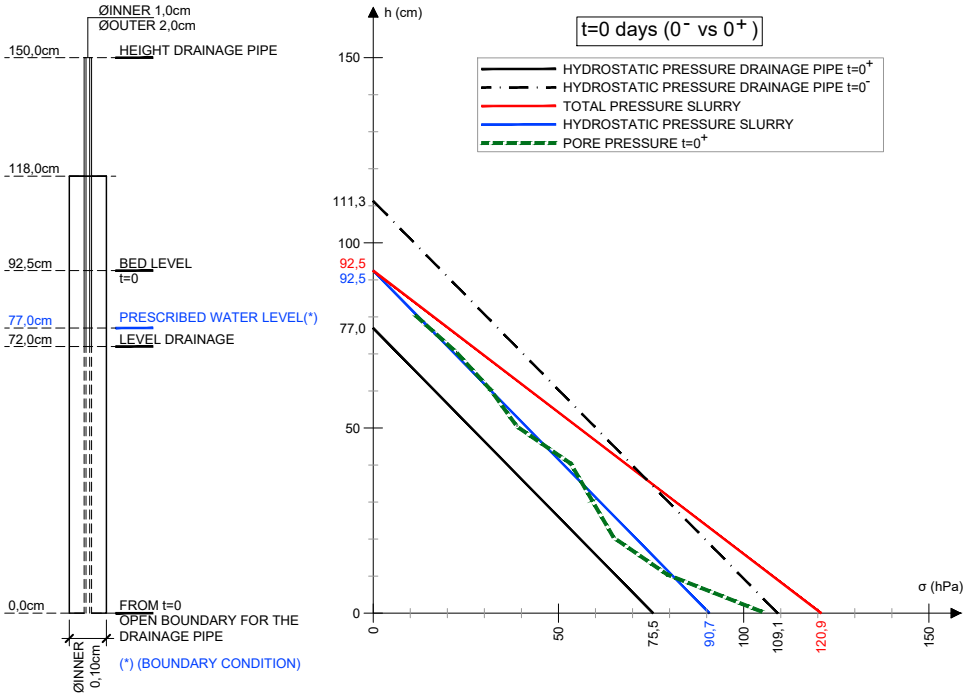

Figure 6.20: Pressure profiles at $t = 0$ days for the vegetated column during the performance of the consolidation and drying experiment. This figure includes the hydrostatic pressure in the drainage pipe at $t = 0^-$ (before connecting the pipe to the reference water table) and at $t = 0^+$ (after this connection by opening of the valve, see Figure 6.23).

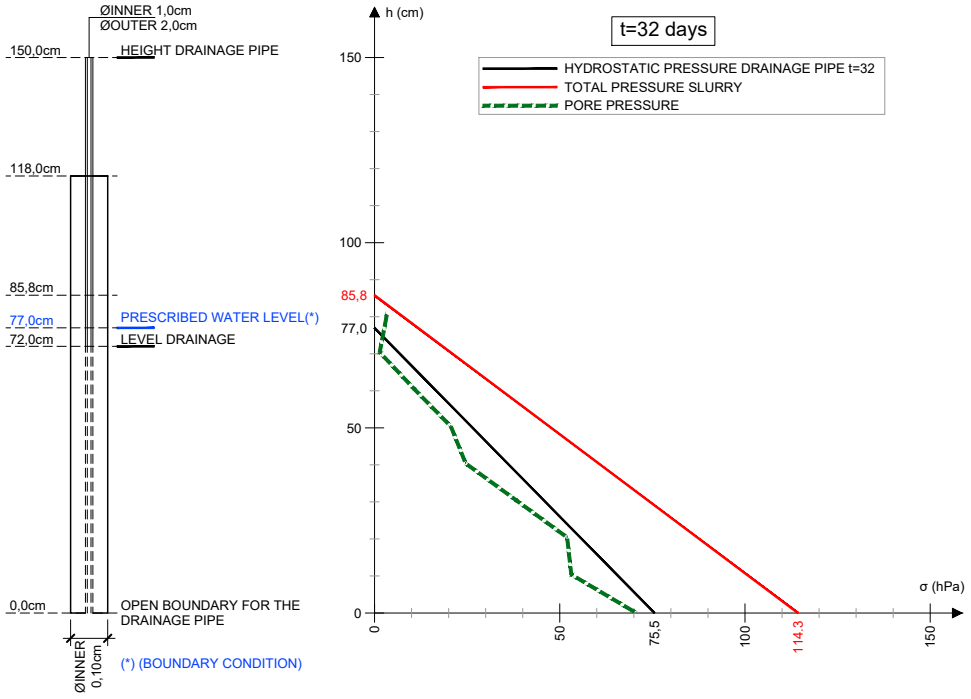

Figure 6.21: Pressure profiles at $t = 32$ days for the vegetated column during the performance of the consolidation and drying experiment.

The measured pore water pressures are smaller than $p_{h,dr}$ for the whole column. This implies that water flows from the drainage pipe into the slurry. The measured $p_{w,slurry}$ is zero at around 75 cm height, which suggests that the actual water table of the slurry is around this height. Thus, vegetation lowered the water table with respect to the control column. Therefore, this would imply that $p_{h,slurry}$= 73.5 hPa.

The positive pressures observed at t_∞ =129 days between 60 and 77 cm may indicate extra water flow to supply the roots above the porous part of the pipe (i.e. upwards water flow above 72 cm).

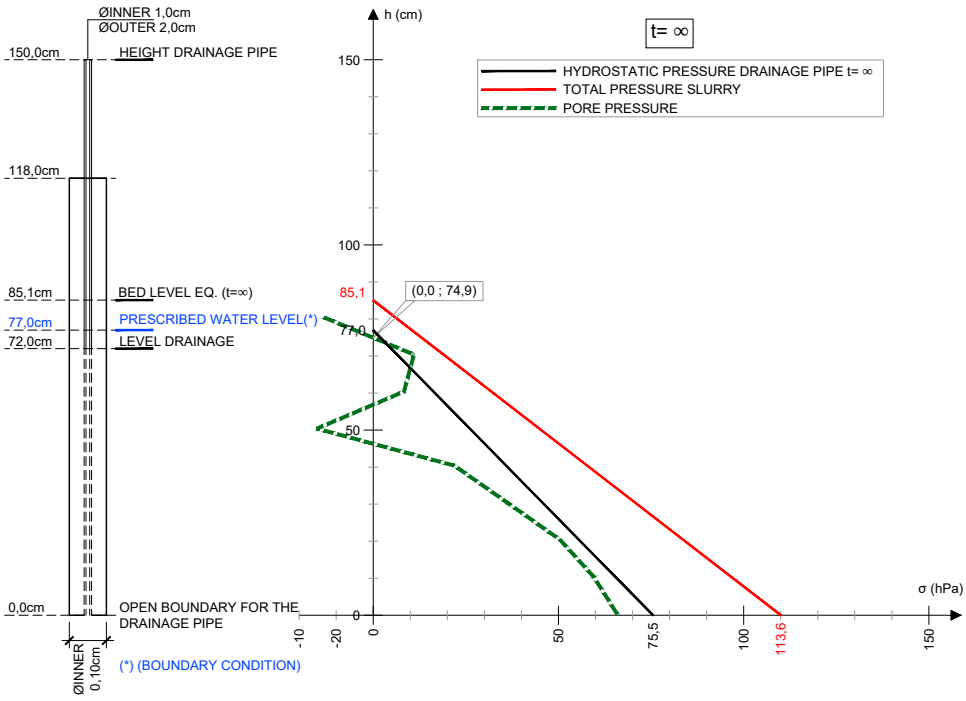

Figure 6.22: Pressure profiles at $t = \infty$ days for the vegetated column during the performance of the consolidation and drying experiment.

6.9. APPENDIX 6D: THE IMPACT OF THE DRAINAGE PIPE

The drainage towards the pipe is likely to affect the consolidation behaviour of the slurry, notably during the first stages of the tests. To check the impact of this drainage on the slurry consolidation, an extra column with a drainage pipe permeable between 70 and 72 cm was monitored. Through these permeable 2 cm, this column was connected with the reference water table of 77 cm, in the same way as the other columns. The consolidation behaviour in this column without drainage was compared with that in the control column and the vegetated column. Figure 6.23 shows the three columns discussed

in this appendix.

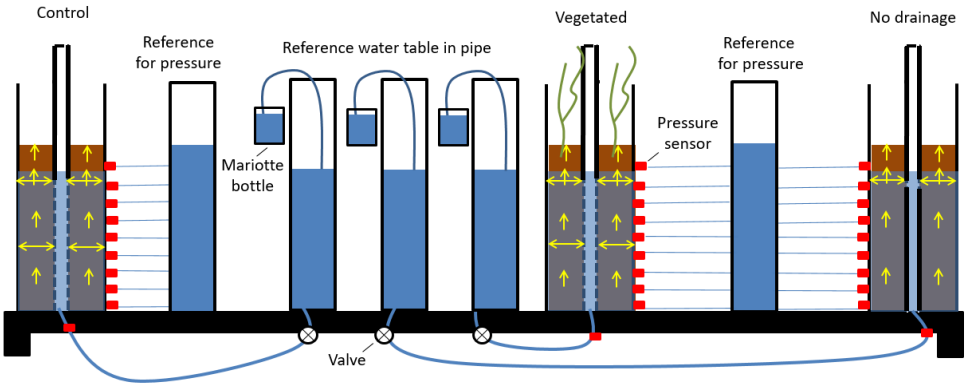

Figure 6.23: Sketch of the three columns. The columns are equipped with pressure sensors (red squares). The pressures measurements are taken relative to a constant water pressure to increase accuracy. The water table in all pipes is induced at 77 cm by connecting them to a reference basin with this constant water level. Each column is connected to its own reference water table (not shown) in order to measure the water flows. The water flows are measured with Mariotte bottles connected to the reference basins. For the control and the vegetated columns, the pipe is permeable over a length of 72 cm. For the column without drainage, horizontal flow is only allowed between 70 and 72 cm, to connect the column with the reference water table of 77 cm.

The water fluxes and the theoretical evaporation rate are shown in Figure 6.24. The maximum evaporation was calculated as the average flux for the control column (bare soil, drainage) after the equilibrium bed height was attained. The measured water fluxes then represent the maximum evaporation rate of the soil for the given room conditions. Chapter 5 showed that, when sediment dries and a crust is being formed, the soil structure collapses but remains largely saturated.

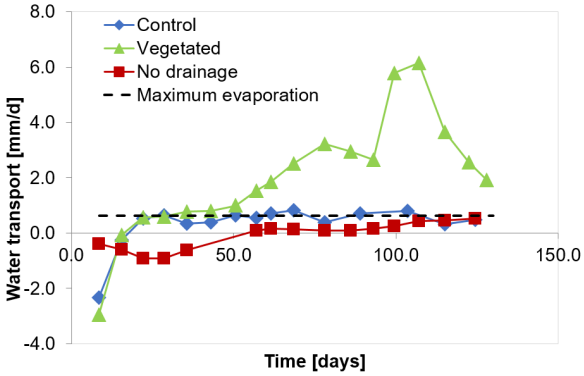

Figure 6.24: Water fluxes in all columns in comparison with the maximum evaporation. Negative values stand for fluxes out of the sediment column

The negative fluxes in Figure 6.24 mean that the water flows out of the sediment column towards the reference water table basin. This happens during the beginning of

the experiment because pore water is being expelled by consolidation. For the column with no drainage, the fluxes are smaller but last longer. At the end of the experiment, this column has reached the theoretical evaporation rate. The effect on the transpiration caused by plants it is the difference between the fluxes of the control and the vegetated columns. This effect of plants can be observed from day 30 (plants need a couple of weeks to enroot) and reaches the maximum values after day 100.

The settling curves for the different columns are shown in Figure 6.25. The presence of plants did not affect the evolution of the interface, presumably because of the continuous water input supplied from the reference water column and sediment armouring by roots. The equilibrium bed height was reached at t = 75 days for the control column and the vegetated column. However, for the column with no drainage, the settling pattern is different: slower settling rate at the beginning but a more compacted bed at equilibrium. Furthermore, this equilibrium is reached later (after 125 days).

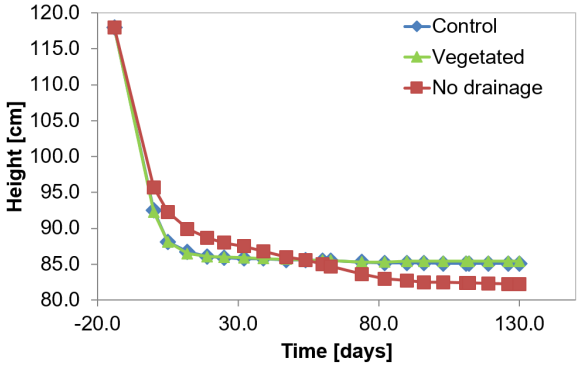

Figure 6.25: Evolution of the sediment interface of the the three columns.

The slower initial consolidation rate and the final lower bed height for the column with no drainage ay be explained by the different initial conditions. The difference is that water could not escape directly via the pipe and only vertical flow of water was possible from the bottom up to 70 cm high. It is hypothesized that the top part is over-consolidated because, at the upper part: 1) some flow of water towards the pipe was possible (between 70 and 72 cm) and 2) water could escape via evaporation. These results are therefore a physical prove of the results from the 1DV-slurry model presented in chapter 4.

The majority of the pore water sensors installed in the column with no drainage were defective and stopped working immediately. This happened with all the sensors of the same (defective) batch. Consequently, from this column there are the pore water pressure data available at two column heights. Figure 6.26 shows the absolute pore water pressure measured by these two sensors and the sensors at the same height of the control column. This figure shows that, 17 cm below the water table (i.e., at z = 60 cm from the bottom), the absolute pore water pressure decreased faster for the control column. This implies that excess pore water pressures are dissipated more rapidly and, therefore, the consolidation rate is larger. Furthermore, Figure 6.26 shows that the uppermost sensor (z = -3 cm) recorded negative pressures (suctions) for the column with no drainage. This suggests

that a crust is formed in this column. This is a different situation than in the control column, where a positive pressure of 0.49 kPa was measured. Furthermore, this value of pressure implies that the water table was at the sediment surface (85.1 cm for the control column).

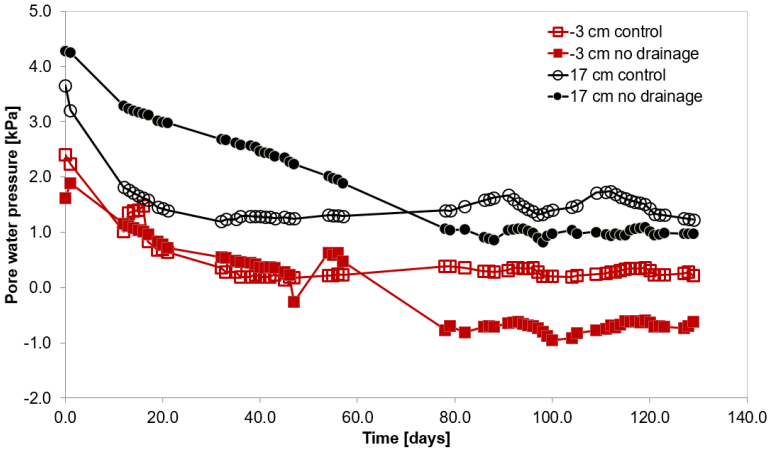

Figure 6.26: Absolute pore water sensor 3 cm above (labelled as -3 cm) and 17 cm below the water level of 77 cm. Such values correspond to an absolute height of 80 and 60 cm from the bottom of the column, respectively.

6.10. APPENDIX 6E: SYNTHESIS OF THE EFFECT OF THE EXPERIMENTAL BOUNDARY CONDITIONS

A detailed analysis of the measured pore water pressure profiles at different time steps showed that, for the control column (without vegetation), the pore pressure equaled to zero only at the surface of the sediment. Thus, the water table stayed around the surface and never lowered to the prescribed 77 cm because of the small values of the hydraulic conductivity. However, for the column with vegetation, after the time step at which the reed started to actively drain the sediment, the water table lowered to up 75 cm. Therefore, the set-up succeeded in keeping the hydraulic boundary conditions (water supply) at a constant level for all the columns but did not control the water table as expected beforehand for the control column. Only with the drainage effect of the vegetation the lowering of the water table beyond 77 cm was possible. Furthermore, the drainage pipe drastically affected the pressure equilibrium in the sediment column at two moments:

1) Prior to the start of the experiment, at the moment of filling the columns with the slurry, water immediately flowed from the sediment into the drainage pipe. This speeded up consolidation by drainage, mostly at the lower layers of the sediment. This is the reason why in a parallel experiment, where the drainage pipe was sealed with plastic to prevent drainage, showed a smaller initial consolidation rate. For the sealed column, water could not escape immediately through the drainage pipe and only self-weight consolidation was possible.

2) At the moment $t = 0$, the drainage pipe was connected to the reference water columns in order to set the constant water level herein at 77 cm from the bottom of the column. At the moment of connection, the level of water inside the drainage pipe lowered immediately from 111.3 to 77 cm. This change in the hydrostatic pressure in the drainage pipe inversed the flow of water. For the case of 107 cm, this flow was from the drainage pipe towards the slurry and it changed to from the slurry towards the drainage pipe for the case of 77 cm.

Furthermore, for the case where drainage was not allowed at the bottom of the column, this unconsolidated bottom layer of sediment experienced the weight of a denser uppermost layer. This upper layer was over-consolidated by drainage between the 70 and 72cm of the pipe and is denser and less permeable. As a consequence, larger final settlements occurred.

6.11. APPENDIX 6F: A MODEL FOR RADIAL DRAINAGE

In this appendix, a Darcy-type equation, which describes the boundary conditions of the vegetation experimental set-up, is derived. First, the Darcy Law and continuity equations are presented. Then, the physics of a flow towards a well is introduced. After this necessary background information, the model to calculate the hydraulic conductivity during the experiments is presented. This model is derived step by step by increasing the complexity. First, the radius of the experimental columns is assumed to be equal to infinity and the case is studied for the situation without internal sinks and with internal sinks. Then, the equation is adjusted for a column with finite radius. This situation, with finite radius and internal sinks, represents the conditions of the performed experiment.

6.11.1. BACKGROUND: DARCY LAW AND CONTINUITY EQUATION

In a general form, Darcy equation can be written as:

$$J_w = -\frac{K}{\mu}\nabla P \tag{6.5}$$

where J_w (m/s) is the water flux as measured in the laboratory, K (m^2) is the intrinsic permeability (*Fredlund et al.*, 2012), μ (kg/ms) is the viscosity of the suspending fluid (i.e., Markermeer water) and ∇P is the applied gradient pressure. In soil mechanics, it is common to use the hydraulic conductivity k in m/s (*Terzaghi and Peck*, 1967), which in the present thesis is defined as:

$$k = K\frac{\rho g}{\mu} \tag{6.6}$$

The gradient in pressure is a vector that is opposite to the vector of the water flow, as the flow of water goes from regions of high pressure P_{high} to regions of low pressure P_{low}. To ensure that we have $K > 0$ a minus sign in front of K is necessary. For unidirectional flows, as studied by Darcy, one gets:

$$J_w = \frac{K}{\mu}\frac{P_{high} - P_{low}}{L} \tag{6.7}$$

where the pressure gradient $(P_{high} - P_{low})/L$ is the applied (macroscopic) pressure gradient on the sample of length L.

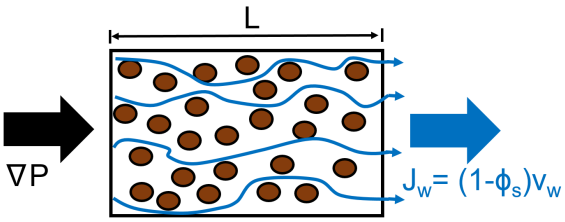

Figure 6.27: Water, under a pressure gradient ∇P, is forced into a porous medium. J_w (m/s) is the measured flux of water coming out of the porous medium, where v_w is the velocity of water inside the soil pores.

The flux J_w represents a macroscopic flux and is defined as the volume of water exiting the porous medium per unit of surface (see Figure 6.27). Its units are therefore $(m^3/s)/m^2 = m/s$. It can be linked to the microscopic flux of water v_w that flows inside the incompressible soil pores by realising that:

$$J_w = \frac{dV_w}{dV} v_w = \phi_w v_w = (1-\phi_s) v_w \tag{6.8}$$

where dV_w is the small element of volume of water at a height z, dV a little element of the total volume and ϕ_w and ϕ_s are the volumetric concentrations of water and soil respectively. By the definition of hydrostatic pressure, one can write:

$$P(z) = \rho_w g z + P_{atm} \tag{6.9}$$

where z is the distance between free water and the point where the pressure is measured. The pressure P_{atm} is the atmospheric pressure.

6.11.2. BACKGROUND: THE CONTINUITY EQUATION AND FLOW TOWARDS A WELL

The local form of the continuity equation (valid for a position (r,z) in cylindrical coordinates or (x,y,z) in Cartesian coordinates) is given by:

$$\frac{\partial \rho}{\partial t} + \nabla \cdot (\rho \cdot v) = \rho \cdot (q_{source} - q_{sink}) \tag{6.10}$$

where ρ is the density of the medium. The velocity of the fluid is given by $v = J$. Note that the dimensions of q_{source}; q_{sink} are in $(1/s)$ and that they represent microscopic flows as they are defined at a given position (r,z). One can therefore see these sinks and sources as flows per (microscopic) volume, i.e. $(m^3/s)/m^3 = 1/s$. It may be assumed that, inside the volume element considered, sources and sinks (q_{source}; q_{sink}) exist. In these sources and sinks, matter (and mass) can be appearing or disappearing: for instance, roots that can take up water, or a leaking pipe can release water. The first term of this continuity equation accounts for a compressible medium.

However, for the case vertical well is placed in the soil (Figure 6.28), having an uptake rate of Q_0 (m^3/s) over the height H, the general continuity equation cannot be used and adaptations are needed. The volume element is defined as the tube of height H and thickness $(R - r_0)$ where r_0 is the radius of the well.

The continuity equation in cylindrical coordinates gives:

$$\nabla \cdot v = -q_{sink} \tag{6.11}$$

and therefore:

$$\frac{J_r}{r} + \frac{\partial J_r}{\partial r} = -q_{sink} \tag{6.12}$$

Here, J_r is the flux of water in the radial direction. The general solution to Equation 6.12 is:

$$J_r = \frac{A(z)}{r} - q_{sink}\frac{r}{2} \tag{6.13}$$

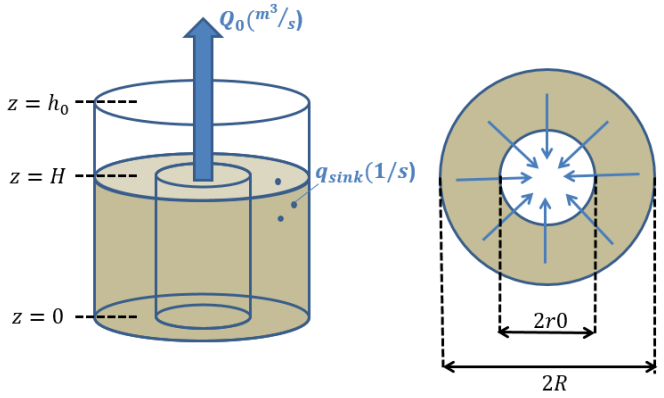

Figure 6.28: Schematic representation of the volume element (grey): it is a porous tube in which water flows radially towards the well that is placed in its centre. The tube is in contact with water at $z = H$, and the air/water interface is at $z = h_0$. This water level in the drainage pipe is kept constant.

where $A(z)$ is an integration constant that only depends on z and represents the initial boundary conditions. In the following, it assumed that A does not depend on z and the flows are identical at each height z in the column. This is a necessary hypothesis since in the experiment only the flow over the whole length of the column was measured. Therefore, there is no measured information about the flow at a given layer, only the flow integrated over H (the height of the column). Thus, it is not know how A varies over z in reality.

6.11.3. VERTICAL WELL, RADIUS R IS INFINITY AND WITHOUT INTERNAL SINKS IN THE SEDIMENT

In this section, an equation for the simplest case of a vertical well placed in the soil with and the radius R is infinity and no internal sinks (no roots or other uptakes) is derived. In this case, only the measured total Q_0 (m^3/s) in the drainage pipe over the height H (see Figure 6.28) is accounted and q_{sink}=0. Because there is no sink term within the sediment:

$$J_r = \frac{A(z)}{r} \tag{6.14}$$

By integration of J_r over z, one finds (note that Q_0 is defined in the opposite direction of the unit vector):

$$\int_0^H J_r(r) 2\pi r dz = -Q_0 \tag{6.15}$$

$$A 2\pi H = -Q_0 \tag{6.16}$$

which implies:

$$A = \frac{-Q_0}{2\pi H} \tag{6.17}$$

and

$$J_r = \frac{-Q_0}{2\pi H r} \tag{6.18}$$

From the Darcy equation,

$$J_r = \frac{-K}{\mu}\left(\frac{dP}{dr}\right) = \frac{-Q_0}{2\pi H r}; \frac{dP}{dr} = \frac{-\mu Q_0}{K 2\pi H r} \tag{6.19}$$

Integrating P in the r direction yields:

$$P(r,z) = \frac{-A\mu}{K}\ln\left(\frac{r}{r_0}\right) + B(z) \tag{6.20}$$

where B(z) is an integration constant that only depends on z. The last boundary condition is: $P(r = r_0, z) = P_0$, where P_0 is a given hydrostatic pressure, and therefore:

$$P(r) = P_0 + \frac{Q_0\mu}{2\pi K H}\ln\left(\frac{r}{r_0}\right) \tag{6.21}$$

Note that the logarithm is always positive when $r > r_0$ which indicates that the pressures becomes lower towards to centre of the circle – which is in agreement with the fact that water always flows from regions of high pressures to regions of low pressures. This yields:

$$\Delta P = P(r = R) - P(r = r_0) = \frac{\mu Q_0}{2\pi K H}\ln\left(\frac{R}{r_0}\right) \tag{6.22}$$

This last equation agrees with literature studying the flow towards wells (e.g *Todd and Mays*, 2005). Equation 6.22 is obtained with no restriction about the water flow at R. Indeed, the flow of water is then non-zero:

$$J_r = \frac{Q_0}{2\pi R} \tag{6.23}$$

However, for large R the flux goes to zero.

6.11.4. VERTICAL WELL, RADIUS R IS INFINITY AND UPTAKE OF WATER BY INTERNAL SINKS

In this section, Equation 6.22 is adapted for the case that there are both a well and internal sinks. Examples of an internal sink are the roots of plants, that are assumed to be homogeneously distributed in the soil. Evaporation is accounted for as an internal sink, which is a simplification. The total water that is taken up by evaporation (in the control column) and by the roots and evaporation (in the sediment column with plants) is Q_{sink} (m^3/s). Q_{sink} is linked to q_{sink} (1/s) by dividing by the volume V=$\pi(R^2$-$r_0^2)H$:

$$q_{sink} = \frac{Q_{sink}}{\pi(R^2 - r_0^2)H} \tag{6.24}$$

The sink term only works within the soil: the water taken by the plants will not flow in the inner column. Therefore at the inner column one has:

$$\int_0^H \frac{A}{r_0} 2\pi r_0 dz = -Q_0 \tag{6.25}$$

which, from the continuity Equation 6.13, yields:

$$J_r = \frac{-Q_0}{2\pi r H} - \frac{Q_{sink}}{\pi(R^2 - r_0{}^2)H}\frac{r}{2} \tag{6.26}$$

6.11.5. VERTICAL WELL, FINITE SIZE COLUMN AND UPTAKE OF WATER BY INTERNAL SINKS

This is the case of the experiment performed. In this case, the problem is similar to the one discussed above, except that the boundary condition at the exterior r=R is changed. For the column, the boundary becomes that there is no flow through the column wall, hence:

$$J_r(r = R) = 0 \tag{6.27}$$

Therefore, from Equation 6.26:

$$Q_0 = -\frac{R^2}{(R^2 - r_0^2)} Q_{sink} \tag{6.28}$$

which gives:

$$J_r = \frac{Q_{sink}}{2\pi r H}\frac{R^2}{\left(R^2 - r_0^2\right)} - \frac{Q_{sink}}{\pi\left(R^2 - r_0^2\right)H}\frac{r}{2} \tag{6.29}$$

$$J_r = \frac{Q_{sink} r}{2\pi\left(R^2 - r_0^2\right)H}\left(\frac{R^2}{r^2} - 1\right) \tag{6.30}$$

The associated pressure gradient can be found using Darcy:

$$J_r = \frac{-K}{\mu}\frac{\partial P}{\partial r} \tag{6.31}$$

which gives:

$$P(r) = \frac{\mu Q_{sink}}{2\pi K\left(R^2 - r_0^2\right)H}\left(R^2 \ln(r) - \frac{r^2}{2}\right) + C \tag{6.32}$$

where C is an integration constant. The water inside the inner well is kept at constant height h_0. This implies that

$$P(r = r_0) = P_{atm} + \rho_w g(h_0 - z) \tag{6.33}$$

Therefore the integration constant is found and:

$$P(r,z) = \frac{\mu Q_{sink}}{2\pi K\left(R^2 - r_0^2\right)H}\left(R^2 \ln\left(\frac{r}{r_0}\right) - \frac{r^2}{2} + \frac{r_0^2}{2}\right) + P_{atm} + \rho_w g(h_0 - z) \tag{6.34}$$

yielding

$$\Delta P = P(R,z) - P(r = r_0, z) \tag{6.35}$$

$$\Delta P = \frac{\mu Q_{sink}}{2\pi K\left(R^2 - r_0^2\right) H}\left(R^2 \ln\left(\frac{R}{r_0}\right) - \frac{R^2}{2} + \frac{r_0^2}{2}\right) \tag{6.36}$$

and

$$\Delta P = \frac{\mu Q_{sink} R^2}{2\pi K(R^2 - {r_0}^2) H}\left(\ln\left(\frac{R}{r_0}\right) - \frac{1}{2} + \frac{{r_0}^2}{2R^2}\right) \tag{6.37}$$

The term between brackets is always positive, and in the limit of large R one finds:

$$\Delta P = \frac{\mu Q_{sink}}{2\pi K H} \ln\left(\frac{R}{r_0}\right) \tag{6.38}$$

which corresponds to the general case (i.e. Equation 6.22) except that here the flow is generated by the Q_{sink}.

Finally, from Equation 6.37 and the correlation between the intrinsic permeability K (m^2) and hydraulic conductivity k (m/s) (see Equation 6.6), the equation needed to calculate the hydraulic conductivity in the present chapter is obtained:

$$k = \frac{\rho g Q_{sink} R^2}{2\pi \Delta P(R^2 - {r_0}^2) H}\left(\ln\left(\frac{R}{r_0}\right) - \frac{1}{2} + \frac{{r_0}^2}{2R^2}\right) \tag{6.39}$$

The results are presented in the main body of the chapter, see Figure 6.7. Note that, with the data measured (total flow in/out of the column), only the average hydraulic conductivity of the whole column can be calculated. In order to calculate vertical hydraulic conductivity profiles of Figure 6.7, the assumption that the flow is equally distributed over the whole length was made. This is a bigger assumption for the column with plants, since where the plants are more active the flows may be larger. In the same way, for the uppermost layers of the column without plants, the flows induced by evaporation are underestimated.

7

Conclusions

Things are not always what they seem;
the first appearance deceives many;
the intelligence of a few
perceives what has been carefully hidden.

Plato

7.1. CONCLUSIONS

IN Lake Markermeer (The Netherlands), an artificial wetland is being built using fine soft sediment from the lake. The major objective of this wetland is to improve the water quality and ecosystem of the lake. A second objective is to learn from the construction of this pilot project, improving techniques to build with soft sediment. During construction, fine sediment from the bed of the lake is dredged and pumped by mechanical means into the project area. This sediment is referred to as a slurry in this thesis. Two major practical questions that are relevant when it comes to building of islands with fine soft sediment are:

1. what is the fastest and cheapest way to build land from slurries with sufficient strength to serve as a nature reserve?
2. what is the role of sediment composition and vegetation on the consolidation and drying behavior of the slurries?

These practical questions led to the scientific questions addressed in this thesis:

1. what is the role of the initial conditions (concentration and stress state) of a slurry on the consolidation rates and ultimate strength of the deposits?
2. how are these rates and strength affected by the composition of the sediment, bearing in mind that such a slurry will experience variations in oxidation during construction and when emerging above water?
3. how are these rates and strength affected by vegetation?
4. how can the mechanical properties be measured with traditional techniques as input to models for predicting the consolidation behavior of slurries.

From a soil mechanical point of view, slurries should be regarded as (partly) over-consolidated sediment-water mixtures. The influence of over-consolidation on the consolidation behavior is therefore an important aspect in the present thesis. The questions above are addressed with a series of laboratory experiments and some numerical modeling on sediment samples from Lake Markermeer. First, consolidation experiments in a settling column at low initial concentrations below the gelling point (virgin consolidation) and at high initial concentration (slurry) were performed. Then, consolidation material parameters were obtained from the virgin consolidation settling tests. These parameters were compared with the parameters obtained from the Seepage Induced Consolidation test for the case of over-consolidated initial conditions. Numerical simulations were performed with a 1DV consolidation model to quantify the influence of the degree of over-consolidation and of the consolidation parameters on consolidation rates and ultimate strength of the deposits. Furthermore, the roles of sand and amount and type of organic matter on the consolidation parameters were assessed. This was done with Incremental Loading and Constant Rate of Strain tests. The effects of sand and amount and type of organic matter on the drying behavior were assessed with Hyprop tests. Finally the effect of the endemic species of vegetation *Phragmites australis* (i.e. common reed) on the consolidation and drying was assessed.

The conclusions of these studies are reported in the Chapters 2 – 6, and summarized in Sections 1.1 to 1.4 of the present chapter. In Section 2, the results are synthetized from a holistic point of view, whereas conclusions with respect to implications and recommendations for further research are given in Sections 3 and 4, respectively.

7.1.1. EFFECT OF THE COMPOSITION OF THE SOLID PHASE

SAND CONTENT

The effect of the natural variability of sand content of Markermeer sediment was studied. Furthermore, some samples were manipulated to simulate the effect of segregation occurring during the construction of the Marker Wadden.

Multiple samples with varying sand contents were tested upon loading with IL (Incremental Loading) and CRS (Constant Rate of Strain) tests. The IL tests showed that the σ-ϕ relations can overlap if sand is treated as a passive substance, accounted for through a correction of ϕ. The results also showed that the transition between cohesive and non-cohesive behavior, referred to as TFC (transition fines content) occurs at a sand content > 40%. At a sand content of 70%, the slurry exhibits a granular character. The undrained shear strength also showed an overlap in the c_u-ϕ_{corr} relations for these sand contents. The influence of particle size on the drying behavior of Markermeer sediment was large, as expected from literature. The SWRCs (Soil Water Retention Curves) were presented as a relation between measured suction pressures and water ratio WR, where WR is ratio of water and solids volume. Sandy sediments exhibit mainly capillary binding of water and, therefore, released most of the water at high suctions. This capillary binding is even more important for the clayey sediments studied, because of the smaller pores herein. However, the clayey samples also exhibited adhesive binding and water was thus released starting from lower suction values. Furthermore, this fine sediments had a larger WR than sandy sediments for a given value of suction because they bind more water.

ORGANIC MATTER CONTENT

The degree of oxidation or degradation of the organic matter (OM) influenced the plasticity of Markermeer sediment. Furthermore, the type of OM also influenced its behavior under shear, loading and drying. Thus, it was found to be a key parameter which largely affects the sediment behavior.

Some samples were treated by chemical oxidation and oven drying. These showed much smaller LL and PL than the original sediment. This lower plasticity implied also a lower ability of the treated samples to bind water. Consequently, deformation under loading of the treated samples was smaller because there was less water present to be expelled. For these treated samples, a small increase of ϕ_s caused a faster development of effective stress. This implied steeper ϕ_s - σ_{eff} curves. However, the effective stress was smaller with respect to the non-treated samples at the same ϕ_s. In the same line, the undrained shear strength of the treated samples was also smaller than for the non-treated samples. This may be explained by the loss of cementing organic matter due to the oxidation. Therefore, there was less organic matter present to bind the sediment particles. Another consequence of the loss of cementing OM was the increase of the TFC: the treated samples with 40% sand behaved as sand dominated.

The lower ability of the treated samples to bind water was also observed during the drying experiments. The SWRC curves of these samples were steeper. This means that, because less water is present, the WR reduces less upon a suction increase than for the case of non-treated samples. Contrary, the natural sample SW2B with most labile OM showed a less steep SWRC. Furthermore, using the Van Genuchten model showed that its parameters were strongly influenced by the type of OM. The OI/HI ratio was found to be

a good proxy for the degree of degradation of OM. The values of this proxy increase with the degree of degradation of the OM. The Van Genuchten parameters were found to be more clearly correlated to the OI/HI ratio than to the amount of OM.

The more labile OM of the natural sample SW2B not only influenced the drying behavior of this sample but also its plasticity. Despite of the lower amount of OM and clay, the high lability of OM made this sample as plastic as other samples with larger OM and much larger clay content. Finally, Nuclear Magnetic Resonance (NMR) spectroscopy tests were performed to quantify the different organic groups present in Markermeer sediment. These tests were inconclusive. However, they still provided a valuable information because they identified some of the functional groups present and showed how heterogeneous the OM of the sediments studied was. Furthermore, these tests represented the first NMR analyses performed on Dutch sediments.

MINERALOGY

The mineralogical composition was quantitatively measured with X-Ray Diffraction (XRD). However, the plasticity chart and the activity proved to be a cheap and efficient way to estimate the clay minerals present on a clayey sediment sample.

There is a large amount of clay minerals in the samples studied. Herein, 2:1 phyllosilicates (illite I, smectite S and I/S mixed layers), which have a large swelling/shrinkage potential, were the most abundant. Together, they reached up to 35.6% of the total sediment composition. The strong shrinkage potential of these minerals was observed at the last stages of the drying experiments, when the clayey samples shrunk considerably. Furthermore, the swelling potential of these minerals was observed during the CRS tests. The rebound during unloading measured with the CRS represents only the elastic properties of the sediments, i.e., the above mentioned swelling of the clay particles.

The clay mineralogy analysis was an important tool in the present research. It allowed to show that the minerals present in the different samples are similar. Thus, mineralogy was dismissed as a cause for the different behavior between the samples. Most importantly, it allowed to properly design the treatment, including oxidation, of the samples: the presence of carbonates was enough to buffer pH upon oxidation with H_2O_2. Furthermore, the quantification of the mineralogy showed that no mineralogical changes occurred by the treatment with H_2O_2.

7.1.2. LINKING FLUID AND SOIL MECHANICS

The present thesis dived into the interface between fluid and soil mechanics. In particular, the relationship between the soil mechanics consolidation coefficient c_v and the consolidation coefficient γ_c in the Gibson equation, using fractal theory was explained. A new equation was also presented for the coefficient of compressibility C_c. Furthermore, as explained above, the fractal approach was successfully applied on the analysis of soil mechanics tests such us IL, CRS, SIC and Fall Cone tests.

The values of C_c were found to be of the same order of magnitude as in traditional soil mechanics literature. However, the measured C_{sw} coefficients were found to be up to two orders of magnitude smaller than for clayey sediments described in soil mechanics literature. This is because the swelling coefficients measured in the present research only quantified the microscopic elastic swelling, as explained above.

Finally, the Hyprop test was used to analyse the drying behavior of slurries. A new sample preparation procedure for slurries was designed. The pressure measurements were analyzed and corrected for mass loss. A correction for the initial offset of the device was implemented. The occurrence of self-weight consolidation was analysed and found to be negligible. During the tests, the formation of an almost fully saturated crust was observed. The device was concluded to be a cheap and efficient way to study the drying of slurries.

7.1.3. EFFECT OF THE INITIAL CONDITIONS

The effect of the initial conditions (concentration and stress state) on the mechanical properties of slurries was analysed in chapters 3 and 4. It was shown that over-consolidated initial conditions could be induced by different processes such as mixing and drying of the slurries. Extra load is thus not per se necessary to achieve an over-consolidated state. Chapter 3 showed that atmospheric drying of the samples induced different degrees of over-consolidated behavior. Chapter 4 showed that samples also exhibited over-consolidated behavior when mixed during sample preparation. Because of this mixing, the samples tested with the SIC test exhibited an over-consolidated behavior. This resulted in a different set of material parameters than from the settling column tests, where sediments experienced virgin consolidation and did not exhibit over consolidated behavior. Thus, the initial stress state and concentration of the sediment has to be known to determine the material parameters.

The 1DV-slurry model was used to study the effect of over-consolidation and the consolidation parameters on the in situ properties of reclaimed soils. The results showed that, if a virgin consolidated bed is remixed after it had reached equilibrium, further consolidation can still occur. This results in larger bed densities and thinner layers than with virgin consolidation. Contrary, when a virgin consolidating bed was remixed during the first phase of consolidation, there were no changes on equilibrium height and density with respect to the virgin conditions.

7.1.4. DRAINAGE EFFECT BY *Phragmites australis*

A column set-up was designed to study the consolidation of soft sediment while controlling the hydraulic boundary conditions, and allowing drainage. The set-up includes pressure sensors on the column wall which measure the vertical pore water pressure distribution. A consolidation model accounting for the boundary conditions of the set-up was developed to calculate the hydraulic conductivity of the sediment.

The experiment performed with this set-up compared the consolidation and drying of Markermeer sediment with and without the presence of *Phragmites australis* (common reed) . The results showed that reed induced suctions in the pore water pressure profile, specially between 40 and 60 cm from the bottom of the column. Furthermore, the water loss by evapotranspiration with the presence of reed amounted to 3.9 mm /day, whereas the evaporation of bare sediment was 0.6 mm/ day. Consequently, the calculated depth-averaged hydraulic conductivity was 40% larger in the column with reed. Moreover, day-night cycles were observed in the pressures, which could be linked to the respiration of reed. It is also expected that vegetation reduced the pore size distribution, which would increase the air entry value, but this was not measured.

Finally, no differences in the thickness of the bed layer were found between the columns with and without vegetation. This may be due to armouring by roots preventing further settling by evapotranspiration in the vegetated column.

7.2. SYNTHESIS

The upper part of a slurry as obtained from mechanically mixing normally consolidated fine sediment, is over-consolidated, and forms a crust-like layer with reduced permeability. This crust affects consolidation rates, and may even alter the equilibrium density and strength profile of the consolidating slurry. When the slurry would emerge above water, evaporation further increases density and strength, reducing permeability further. The Hyprop experiments showed that the crust thus formed remains close to fully saturated under the conditions tested. Such an over-consolidated state can also be attained by drying samples to the air, as is common practice in laboratory experiments (e.g. as in the standard for the determination of Atterberg limits). In all cases the permeability and effective stress followed a power law behavior with a fractal dimension identical to that obtained from virgin consolidation tests. However, the coefficients of these relations can increase substantially. This implies that material properties should be measured at the actual conditions of the samples, and cannot be obtained from extrapolation of virgin consolidation experiments.

Removal of organic material by chemical oxidation including heating and rewetting reduces the cohesion of the sediments considerably: the sediment activity remains more or less constant, but the critical clay content above which sediment becomes cohesive increases largely. The treated samples exhibited more sand-like behavior.

The present thesis showed that traditional soil mechanical measurements give appropriate results in assessing the mechanical properties of slurries. Also in over-consolidated state, these slurries exhibit self-similar structures (i.e., a unique relationship exists between aggregate size and number of primary particles), and the mechanical properties may be described with power laws, using a fractal dimension.

The experiments with vegetation are not easy to interpret because of some unforeseen complications deriving from the experimental setup. However, the measurements showed daily variations in pore water pressures as a result of the cyclic vegetation activity. The results further suggest that the vegetation may have two opposing effects:

1. Next to water transport through the roots, there are strong indications that drainage paths are formed along the roots, dissipating pore water over- and under-pressures effectively. This effect would enhance consolidation rates,
2. The roots also armor the soil, enhancing its strength on a macroscale, thus decreasing consolidation rates.

The experimental data suggest that, in the experiments performed in this research, the second effect is more important. However, it is unknown how generic this conclusion is.

7.3. IMPLICATIONS FOR BUILDING WITH SOFT SEDIMENTS

The present research is connected to the Marker Wadden wetland construction for the restoration of Lake Markermeer. Ultimately, a successful Marker Wadden project gives significant national and international attention to the Building with Nature design philosophy and techniques. The Marker Wadden project has already proven to catch international attention, due to its multidisciplinary design. Thus, the Building with Nature techniques and the fundamental knowledge generated from the Marker Wadden are likely to be adopted by others. This creates a vast utilisation potential of the results of the present research. The results of the present research showed which aspects need to be addressed in a design phase of a project using fine sediments as construction material. The results are thus generally applicable to other projects using fine sediments as building material. Furthermore, it is expected that these fine sediments will be more often used for construction because sandy sediment is becoming scarce.

There is an increasing awareness about the benefits of accounting for ecology when building in natural systems. The present thesis contributed to this by showing the beneficial use of plants as an ecological engineer which increased drainage. Thus, plants could be used instead traditional means, such as geotextiles. Furthermore, plants can armor the sediment by their roots, protecting from erosion while enhancing the ecosystem value.

Awareness is also increasing over the last decades about the importance of space in coastal and riverine areas for natural morphological changes. Consequently, more flexible and dynamic structures and solutions are being implemented instead of hard walls to protect against flooding in such areas. The knowledge of fine sediments consolidation and strength development as presented in the present thesis is directly applicable to the use of such sediments, for example, as reinforcement of dikes or to the development of salt marshes for coastal protection. The results of this thesis also showed the importance of the composition of the solid phase on the mechanical behavior of fine sediments. The results showed, amongst others, that residual settlement in the Marker Wadden can be significantly different if segregation occurs. Furthermore, the fact that the organic matter type affected the mechanical properties more than the OM amount stresses the importance of the measurement of the reactivity of the OM when using mud as construction material. The Rock Eval test was shown to be an easy and efficient way to assess this lability and, therefore, its inclusion in sediment characterization protocols is recommended. Moreover, attention must be paid to the fact that when oxidation of OM occurs during the construction process, the mechanical behavior of the sediment will presumably change. Thus, it is recommended to quantify the impact that OM oxidation would have with some preliminary tests prior to construction.

The material parameters from settling column tests were found to be not directly applicable to over-consolidated slurries. Therefore, the determination of material parameters should be done with sediment samples experiencing the same actual stress state than during the construction process. For the case of the slurries used in the Marker Wadden construction, the SIC test seems a suitable device to determine the material properties provided an adequate sample preparation is performed that mimicks the stresses experienced during the dredging process. The effect of sample preparation and the initial stress state were found to affect the mechanical behavior of the sediment studied. Therefore, attention should be paid to the processes of sediment collection (with a dredger or

otherwise), mixing and disposal of the sediment. Regarding mixing, not only the mixing method but also the density were found to be important. Initial concentrations much larger than the gelling point were found to provide denser and stronger final beds but less thick. For the case of the Marker Wadden, the project requirements are to create habitat for birds and provide a certain surface of the wetland above water. Because birds are not very heavy, the use of not very large initial concentrations may help to achieve the project requirements.

The formation of an almost fully saturated crust was observed during drying. This crust is more impermeable than the underlying sediment and retards the expulsion of water. Therefore, unconsolidated mud may be present under such a crust. Thus, in general, it may be beneficial to allow consolidation under water as long as possible during construction of a wetland. Contrary, allowing the formation of a crust may be beneficial if a stronger upper layer is required, provided that a larger consolidation and lower bearing capacity are not a problem. A stronger upper layer protects again erosion as likely to occur, for instance, during storms.

7.4. RECOMMENDATIONS FOR FURTHER RESEARCH

The results of the present thesis yield interesting lines of future research. Regarding organic matter, further work on the identification of the different organic functional groups present and their effect in the physical behavior of cohesive sediments is recommended. Furthermore, the effects of drying and chemical oxidation of the treatment applied could be separated and more natural oxidation procedures without chemicals could be tested. Moreover, the effects of solid composition can easily be included in the model by adapting accordingly the values of the input material parameters.

With respect to the effect of the initial concentration and stress state, the design of a protocol for the determination of the material properties is necessary. A first step to gain the knowledge for such a protocol is the performance of settling column experiments at different c_0 by remixing the sediment for different time steps and rates of mixing. This can provide a more quantitative result of the effects of these factors on the final bed density and thickness. Furthermore, performing SIC tests with subsamples from such settling experiments, would give insight in the material parameters and the initial stress state.

Regarding the effect of vegetation, the study of different autochthonous species and the quantification of the effect of the roots in the soil structure is recommended. Finally, further work in the extension of the fractal modelling to the drying phase and the inclusion of the effects of drainage in the 1DV-slurry model is necessary.

Ultimately, the Marker Wadden is a huge living lab and valuable knowledge could be acquired by monitoring. Consolidation rates, density and pore pressure profiles development, drying and cracking of the uppermost crust and changes of composition caused by oxidation are some of the main physico-chemical parameters to monitor. Herein, the comparison of consolidation rates and density profiles evolution of areas below and above water is interesting. Furthermore, the in situ study of the effect of biota (e.g. birds) and bioturbation (e.g. by worms) in the consolidation, compositional changes and cohesion of the clayey sediment is recommended. If there is the opportunity to test diverse filling protocols in various experimental compartments, large scale study of the effect of different initial (stress) conditions is also advised. Finally, the Marker Wadden

gives the opportunity to study the effect of different plant species on consolidation, drying and ripening of the sediment.

REFERENCES

Abate, G., and J. C. Masini (2003), Influence of pH and ionic strength on removal processes of a sedimentary humic acid in a suspension of vermiculite, *Colloids and Surfaces A: Physicochemical and Engineering Aspects*, *226*, 25–34, doi:10.1016/S0927-7757(03)00418-7.

Abu-Hejleh, A. N., D. Znidarčić, and B. L. Barnes (1996), Consolidation characteristics of phosphatic clays, *Journal of Geotechnical Engineering*, *122*(4), 295–301, doi:10.1061/(asce)0733-9410(1996)122:4(295).

Al-Shayea, N. A. (2001), The combined effect of clay and moisture content on the behavior of remolded unsaturated soils, *Engineering Geology*, *62*(4), 319–342, doi:10.1016/S0013-7952(01)00032-1.

Angers, D. A., and J. Caron (1998), Plant-induced changes in soil structure: Processes and feedbacks, *Biogeochemistry*, *42*(1/2), 55–72, doi:10.1023/a:1005944025343.

Armour, D., and V. Drnevich (1986), Improved techniques for the constant-rate-of-strain consolidation test, in *Consolidation of Soils: Testing and Evaluation*, pp. 170–170–14, ASTM International, doi:10.1520/stp34614s.

Artifon, V., E. Zanardi-Lamardo, and G. Fillmann (2019), Aquatic organic matter: Classification and interaction with organic microcontaminants, *Science of The Total Environment*, *649*, 1620–1635, doi:10.1016/j.scitotenv.2018.08.385.

ASTM (2014), D4186M – 12E1. standard test method for one-dimensional consolidation properties of saturated cohesive soils using controlled-strain loading.

ASTM (2016), D6836– 16. standard test methods for determination of the soil water chararcteristic curve for desorption using a hanging column, pressure extractor, chilled mirror hygrometer , and /or centrifuge.

Bain, J. A. (1971), A Plasticity Chart as an Aid to the Identification and Assessment of Industrial Clays, *Clay Minerals*, *9*, 1–17, doi:10.1180/claymin.1971.009.1.01.

Baldock, J. a., J. M. Oades, a. G. Waters, X. Peng, a. M. Vassallo, and M. a. Wilson (1992), Aspects of the chemical structure of soil organic materials as revealed by solid-state 13 C NMR spectroscopy, *Biogeochemistry*, *16*, 1–42.

Barciela-Rial, M., J. C. Winterwerp, J. Griffioen, and T. van Kessel (2015), Consolidation and strength development by horizontal drainage of soft mud deposits in Lake Markermeer, in *Book of Abstracts NCR-Days*, pp. 62–64.

Barciela-Rial, M., B. A. van den Bosch, J. C. Winterwerp, L. A. van Paassen, J. Griffioen, and T. Kessel (2017), The effect of initial conditions on the consolidation of mud, in *Pedocchi, F. et al. (Ed.) INTERCOH 2017 - 14th International Conference on Cohesive Sediment Transport Processes, 13 to 17 November 2017, Montevideo, Uruguay: book of abstracts*.

Barciela-Rial, M., B. A. van den Bosch, T. van Kessel, J. Griffioen, and J. Winterwerp (submitted), Consolidation of slurries, *Canadian Geotechnical Journal*.

Barciela-Rial, M., L. van Paassen, J. Griffioen, T. van Kessel, and J. Winterwerp (under review), The effect of solid phase composition on the drying behaviour of Markermeer sediment, *Vadose Zone Journal*.

Barshad, I. (1955), Absorptive and Swelling Properties of Clay-Water System, *Proc. First Nat. Conf. on Clays and Clay Tech., Bulletin Division of Mines California*, *169*(70), 70–77, doi:10.1346/CCMN.1952.0010108.

Bartholomeeusen, G., G. C. Sills, D. Znidarčić, W. V. Kesteren, L. M. Merckelbach, R. Pyke, W. D. Carrier, H. Lin, D. Penumadu, H. Winterwerp, S. Masala, and D. Chan (2002), Sidere: numerical prediction of large-strain consolidation, *Géotechnique*, *52*(9), 639–648, doi:10.1680/geot.2002.52.9.639.

Barton, D. H. R., and M. Schnitzer (1963), A new experimental approach to the humic acid problem, *Nature*, *198*(4876), 217–218, doi:10.1038/198217a0.

Been, K., and G. C. Sills (1981), Self-weight consolidation of soft soils: an experimental and theoretical study, *Géotechnique*, *31*(4), 519–535, doi:10.1680/geot.1981.31.4.519.

Behar, F., V. Beaumont, and H. L. D. B. Penteado (2001), Rock-eval 6 technology: Performances and developments, *Oil & Gas Science and Technology*, *56*(2), 111–134, doi:10.2516/ogst:2001013.

Bergaya, F., and G. Lagaly (2013), General introduction, in *Developments in Clay Science*, pp. 1–19, Elsevier, doi:10.1016/b978-0-08-098258-8.00001-8.

Beven, K., and P. Germann (1982), Macropores and water flow in soils, *Water Resources Research*, *18*(5), 1311–1325, doi:10.1029/wr018i005p01311.

Blight, G. E. (2003), The vadose zone soil-water balance and transpiration rates of vegetation, *Géotechnique*, *53*(1), 55–64, doi:10.1680/geot.2003.53.1.55.

Breemen, N. V., and P. Buurman (2002), *Soil Formation*, Springer.

Breitmeyer, R. J., and L. Fissel (2017), Uncertainty of soil water characteristic curve measurements using an automated evaporation technique, *Vadose Zone Journal*, *16*(13), 0, doi:10.2136/vzj2017.07.0136.

Brigatti, M., E. Galán, and B. Theng (2013), Structure and mineralogy of clay minerals, in *Developments in Clay Science*, pp. 21–81, Elsevier, doi:10.1016/b978-0-08-098258-8.00002-x.

Brooks, R. H., and A. T. Corey (1964), Hydraulic properties of porous media and their relation to drainage design, *Transactions of the ASAE*, *7*(1), 0026–0028, doi:10.13031/2013.40684.

BS (1990a), 1377-1:1990. Methods of test for soils for civil engineering purposes. general requirements and sample preparation.

BS (1990b), 1377-2:1990. Methods of test for soils for civil engineering purposes. classification tests.

Burland, J. B. (1990), On the compressibility and shear strength of natural clays, *Géotechnique*, *40*(3), 329–378, doi:10.1680/geot.1990.40.3.329.

Burroughs, E. R., C. H. Luce, and F. Phillips (1992), Estimating Interrill Erodibility of Forest Soils, *Transactions of the ASAE*, *35*(5), 1489–1495, doi:10.13031/2013.28757.

Buurman, P., T. Pape, J. A. Reijneveld, F. de Jong, and E. van Gelder (2001), Laser-diffraction and pipette-method grain sizing of dutch sediments: correlations for fine fractions of marine, fluvial, and loess samples, *Netherlands Journal of Geosciences*.

Cabalar, A. F., and W. S. Mustafa (2015), Fall cone tests on clay-sand mixtures, *Engineering Geology*, *192*, 154–165, doi:10.1016/j.enggeo.2015.04.009.

Carrie, J., H. Sanei, and G. Stern (2012), Standardisation of Rock-Eval pyrolysis for the analysis of recent sediments and soils, *Organic Geochemistry*, *46*, 38–53, doi:10.1016/j.orggeochem.2012.01.011.

Catana, M. C. (2006), Compaction and water retention characteristics of champlain sea clay, Ph.D. thesis, University of Ottawa, doi:10.20381/ruor-18655.

Chen, Y., C. Thompson, and M. Collins (2012), Saltmarsh creek bank stability: Biostabilisation and consolidation with depth, *Continental Shelf Research*, *35*, 64–74, doi:10.1016/j.csr.2011.12.009.

Chenu, C. (1993), Clay- or sand-polysaccharide associations as models for the interface between micro-organisms and soil: water related properties and microstructure, *Geoderma*, *56*(1-4), 143–156, doi:10.1016/0016-7061(93)90106-u.

Clemente, J., E. Gregorich, A. Simpson, R. Kumar, D. Courtier-Murias, and M. Simpson (2012), Comparison of nuclear magnetic resonance methods for the analysis of organic matter composition from soil density and particle fractions, *Environmental Chemistry*, *9*(1), 97–107.

Clemente, J. S., A. J. Simpson, and M. J. Simpson (2011), Association of specific organic matter compounds in size fractions of soils under different environmental controls, *Organic Geochemistry*, *42*(10), 1169–1180, doi:10.1016/j.orggeochem.2011.08.010.

Cognon, J. M., I. Juran, and S. Thevanayagam (1994), Vacuum consolidation technology-principles and field experience, in *Proceedings Conference on Foundations and Embankments Deformations*, vol. 2, pp. 1237–1248.

Crawford, C. (1988), On the importance of rate of strain in the consolidation test, *Geotechnical Testing Journal*, *11*(1), 60–62, doi:10.1520/gtj10646j.

Dankers, P. (2006), On the hindered settling of suspensions of mud and mud-sand mixtures, Ph.D. thesis, Delft University of Technology.

Dankers, P., and J. Winterwerp (2007), Hindered settling of mud flocs: Theory and validation, *Continental Shelf Research*, *27*(14), 1893–1907, doi:10.1016/j.csr.2007.03.005.

Dankers, P., B. Wichman, and M. van K Kerkvoorde (2015), Eindrapportage pilot markermeer moeras (in dutch), *Tech. rep.*, RWS, Royal Haskoning, Deltares, Buro Bakker.

De Lucas Pardo, M. (2015), Effect of biota on fine sediment transport processes: A study of lake markermeer, Ph.D. thesis, Delft University of Technology.

De Vriend, H. J., M. van Koningsveld, S. G. Aarninkhof, M. B. de Vries, and M. J. Baptist (2015), Sustainable hydraulic engineering through building with nature, *Journal of Hydro-environment Research*, *9*(2), 159–171, doi:10.1016/j.jher.2014.06.004.

Deer, W., R. Howie, and J. Zussman (1992), *An introduction to the rock-forming minerals (2nd ed.)*., Longman Scientific & Technical.

Derrick, P., J. McKee, S. Johnson, and M. Mendelsohn (2007), Poplar island environmental restoration project: Project successes, lessons learned, and future plans, in *Proceedings of the world dredging congress*, vol. 1, pp. 487–500.

Disnar, J. R., B. Guillet, D. Keravis, C. Di-Giovanni, and D. Sebag (2003), Soil organic matter (SOM) characterization by Rock-Eval pyrolysis: Scope and limitations, *Organic Geochemistry*, *34*, 327–343, doi:10.1016/S0146-6380(02)00239-5.

Dorioz, J., M. Robert, and C. Chenu (1993), The role of roots, fungi and bacteria on clay particle organization. an experimental approach, *Geoderma*, *56*(1-4), 179–194, doi:10.1016/0016-7061(93)90109-x.

Dumbleton, M. J., G. West, and G. Dumbleton, M. J., & West (1966), Some factors affecting the relation between the clay minerals in soils and their plasticity, *Clay minerals*, *6*(3), 179–193, doi:10.1180/claymin.1966.006.3.05.

Durner, W., and D. Or (2005), *Encyclopedia of Hydrological Sciences*, chap. Chapter 73: Soil Water Potential Measurement, p. 1089–1102, John Wiley & Sons, Ltd.

Duursma, R. A. (2015), Plantecophys - an r package for analysing and modelling leaf gas exchange data, *PLOS ONE*, *10*(11), e0143,346, doi:10.1371/journal.pone.0143346.

Ehrenfeld, J. G., B. Ravit, and K. Elgersma (2005), Feedback in the plant-soil system, *Annual Review of Environment and Resources*, *30*(1), 75–115, doi:10.1146/annurev.energy.30.050504.144212.

EN (2012), 15935:2012. sludge, treated biowaste, soil and waste -determination of loss on ignition.

Erwin, R. M., J. Miller, and J. G. Reese (2007), Poplar Island environmental restoration project: Challenges in waterbird restoration on an island in Chesapeake Bay, *Ecological Restoration*, *25*(4), 256–262, doi:10.3368/er.25.4.256.

Fagherazzi, S., and D. J. Furbish (2001), On the shape and widening of salt marsh creeks, *Journal of Geophysical Research: Oceans*, *106*(C1), 991–1003, doi:10.1029/1999jc000115.

Fermor, P. M., P. D. Hedges, J. C. Gilbert, and D. J. G. Gowing (2001), Reedbed evapotranspiration rates in england, *Hydrological Processes*, *15*(4), 621–631, doi:10.1002/hyp.174.

Flemming, B. (2000), A revised textural classification of gravel-free muddy sediments on the basis of ternary diagrams, *Continental Shelf Research*, *20*(10-11), 1125–1137, doi:10.1016/s0278-4343(00)00015-7.

Fox, P. J., H.-F. Pu, and J. T. Christian (2014), Evaluation of data analysis methods for the CRS consolidation test, *Journal of Geotechnical and Geoenvironmental Engineering*, *140*(6), 04014,020, doi:10.1061/(asce)gt.1943-5606.0001103.

Fredlund, D. G., H. Rahardjo, and M. D. Fredlund (2012), *Unsaturated Soil Mechanics in Engineering Practice*, Wiley-Interscience.

Friend, P., P. Ciavola, S. Cappucci, and R. Santos (2003), Bio-dependent bed parameters as a proxy tool for sediment stability in mixed habitat intertidal areas, *Continental Shelf Research*, *23*(17-19), 1899–1917, doi:10.1016/j.csr.2002.12.001.

Ganesalingam, D., N. Sivakugan, and J. Ameratunga (2013), Influence of settling behavior of soil particles on the consolidation properties of dredged clay sediment, *Journal of Waterway, Port, Coastal, and Ocean Engineering*, *139*(4), 295–303, doi:10.1061/(ASCE)WW.1943-5460.0000183.

Garg, A., J. L. Coo, and C. W. W. Ng (2015), Field study on influence of root characteristics on soil suction distribution in slopes vegetated with cynodon dactylon and schefflera heptaphylla, *Earth Surface Processes and Landforms*, *40*(12), 1631–1643, doi:10.1002/esp.3743.

Gerke, H., and R. Kuchenbuch (2007), Root effects on soil water and hydraulic properties, *Biologia*, *62*(5), doi:10.2478/s11756-007-0110-8.

Gerretsen, P. (2014), Design research houtribdijk marker wadden., *Tech. rep.*, Vista Svasek Hydraulics, The Netherlands.

Ghabbour, E. a., G. Davies, M. E. Goodwillie, K. O'Donaughy, and T. L. Smith (2004), Thermodynamics of peat-, plant-, and soil-derived humic acid sorption on kaolinite, *Environmental Science and Technology*, *38*(12), 3338–3342, doi:10.1021/es0352101.

Ghestem, M., R. C. Sidle, and A. Stokes (2011), The influence of plant root systems on subsurface flow: Implications for slope stability, *BioScience*, *61*(11), 869–879, doi:10.1525/bio.2011.61.11.6.

Gibson, R. E., G. L. England, and M. J. L. Hussey (1967), The Theory of One-Dimensional Consolidation of Saturated Clays, *Géotechnique*, *17*(3), 261–273, doi:10.1680/geot.1967.17.3.261.

Grabowski, R. C., I. G. Droppo, and G. Wharton (2011), Erodibility of cohesive sediment: The importance of sediment properties, *Earth-Science Reviews*, *105*(3-4), 101–120, doi:10.1016/j.earscirev.2011.01.008.

Guggenheim, S., and R. T. Martin (1995), Definition of clay and clay mineral: Joint report of the AIPEA nomenclature and CMS nomenclature committees, *Clays and Clay Minerals*, *43*(2), 255–256, doi:10.1346/ccmn.1995.0430213.

Haliburton et al. (1978), Guidelines for dewatering/densifying confined dredged material., *Technical Rep. DS-78-11, U.S. Army Engineer. Waterways Experiment Station, Vicksburg, Mississipi.*

Hart, G. F. (1986), Origin and classification of organic matter in clastic systems, *Palynology*, *10*(1), 1–23, doi:10.1080/01916122.1986.9989300.

Haynes, R. J. (2005), Labile Organic Matter Fractions as Central Components of the Quality of Agricultural Soils: An Overview, *Advances in Agronomy*, *85*, 221–268, doi:10.1016/S0065-2113(04)85005-3.

Hendriks, H. (2016), The effect of ph and the solids composition on the settling and self-weight consolidation of mud, Master's thesis, Delft University of Technology.

Hillel, D. (1998), *Environmental Soil Physics: Fundamentals, Applications, and Environmental*, Academic Press, San Diego.

Holm, D. (2016), Influence of strain rate in crs tests: A laboratory study of three swedish clays, Master's thesis, KTH, School of Architecture and the Built Environment (ABE), Civil and Architectural Engineering, Soil and Rock Mechanics. Sweeden.

Holtz, R. (1987), Preloading with prefabricated vertical strip drains, *Geotextiles and Geomembranes*, *6*(1-3), 109–131, doi:10.1016/0266-1144(87)90061-6.

Holtz, R. D., and W. D. Kovacs (1981), *An Introduction to Geotechnical Engineering*, Prentice Hall.

Huang, B., and C. Bowers (1986), Development of greenhouse solar systems for bulk tobacco curing and plant production, *Energy in Agriculture*, *5*(4), 267–284, doi:10.1016/0167-5826(86)90026-4.

Huerta, A., G. A. Kriegsmann, and R. J. Krizek (1988), Permeability and compressibility of slurries from seepage-induced consolidation, *Journal of Geotechnical Engineering*, *114*(5), 614–627, doi:10.1061/(asce)0733-9410(1988)114:5(614).

Humphrey, D., and R. Holtz (1986), Reinforced embankments—a review of case histories, *Geotextiles and Geomembranes*, *4*(2), 129–144, doi:10.1016/0266-1144(86)90020-8.

Ibanez Sanz, M. (2018), Flocculation and consolidation of cohesive sediments under the influence of coagulant and flocculant, Ph.D. thesis, Delft University of Technology.

Imai, G. (1979), Development of a new consolidation test procedure using seepage force., *SOILS AND FOUNDATIONS*, *19*(3), 45–60, doi:10.3208/sandf1972.19.3_45.

ISO (2004), 11275:2004. Soil quality - determination of unsaturated hydraulic conductivity and water-retention characteristic - wind's evaporation method.

ISO (2016), 17892-12:2016. Geotechnical investigation and testing - laboratory testing of soil - part 12: Determination of atterberg limits.

ISO (2017), ISO 14688-1:2017. Geotechnical investigation and testing - identification and classification of soil - part 1: Identification and description.

ISO/TS (2004a), 17892-5:2004. Geotechnical investigation and testing - laboratory testing of soil - part 5: Incremental loading oedometer test.

ISO/TS (2004b), 17892-6:2004. Geotechnical investigation and testing - laboratory testing of soil - part 6: Fall cone test.

ISO/TS (2004c), 17892-3:2004. Geotechnical investigation and testing - laboratory testing of soil - part 3: Determination of particle density - pycnometer.

ISO/TS (2014), 17892-1:2014. Geotechnical investigation and testing - laboratory testing of soil- part 1: Determination of water content.

Jacobs, W. (2011), Sand-mud erosion from a soil mechanical perspective, Ph.D. thesis, Delft University of Technology.

Jones, C. G., J. H. Lawton, and M. Shachak (1994), Organisms as ecosystem engineers, *Oikos*, *69*(3), 373, doi:10.2307/3545850.

Jones, M. (1998), Colloidal properties of humic substances, *Advances in Colloid and Interface Science*, *78*, 1–48, doi:10.1016/S0001-8686(98)00058-X.

Jorstad, K., Salbu, B., and Roaldser, E. (1982), Vertical distribution of trace elements in fresh water saline water and sediments from lake Rorholtfjorden , Norway, *Chemical Geology*, *36*, 325–347.

Kaiser, K., and G. Guggenberger (2003), Mineral surfaces and soil organic matter, *European Journal of Soil Science*, *54*(June), 219–236, doi:10.1046/j.1365-2389.2003.00544.x.

Kassiff, G., and A. B. Shalom (1971), Experimental relationship between swell pressure and suction, *Géotechnique*, *21*(3), 245–255, doi:10.1680/geot.1971.21.3.245.

Keller, T., and A. R. Dexter (2012), Plastic limits of agricultural soils as functions of soil texture and organic matter content, *Soil Research*, *50*(1), 7–17, doi:10.1071/SR11174.

Kodešová, R., V. Kodeš, A. Žigová, and J. Šimůnek (2006), Impact of plant roots and soil organisms on soil micromorphology and hydraulic properties, *Biologia*, *61*(19), doi:10.2478/s11756-006-0185-7.

Kohut, C. K., and C. J. Warren (2002), *Soil Mineralogy with Environmental Applications*, chap. Chlorites, pp. 531–553., SSSA Book Ser. 7. SSSA, Madison, WI.

Kontert, M., and J. Vandenberghe (1997), Comparison of laser grain size analysis with pipette and sieve analysis: a solution for the underestimation of the clay fraction, *Sedimentology*, *44*(3), 523–535, doi:10.1046/j.1365-3091.1997.d01-38.x.

Kramer, P. J., and J. S. Boyer (1995), Roots and root systems, in *Water Relations of Plants and Soils*, pp. 115–166, Elsevier, doi:10.1016/b978-012425060-4/50005-x.

Kranenburg, C. (1994), The fractal structure of cohesive sediment aggregates, *Estuarine, Coastal and Shelf Science*, *39*(6), 451–460, doi:10.1016/S0272-7714(06)80002-8.

Kumar, G. V., and D. M. Wood (1999), Fall cone and compression tests on clay±gravel mixtures, *Géotechnique*, *49*(6), 727–739, doi:10.1680/geot.1999.49.6.727.

Lafargue, E., F. Marquis, and D. Pillot (1998), Rock-eval 6 applications in hydrocarbon exploration, production, and soil contamination studies, *Revue de l'Institut Français du Pétrole*, *53*(4), 421–437, doi:10.2516/ogst:1998036.

Laloui, L., M. Nuth, and B. François (2010), Mechanics of unsaturated soils 1, in *Mechanics of Unsaturated Geomaterials*, pp. 29–54, John Wiley & Sons, Inc., doi:10.1002/9781118616871.ch2.

Lambe, T. W., and R. V. Whitman (1969), *Soil Mechanics (Series in Soil Engineering)*, Wiley.

Lange, B., P. Lüescher, and P. F. Germann (2009), Significance of tree roots for preferential infiltration in stagnic soils, *Hydrology and Earth System Sciences*, *13*(10), 1809–1821, doi:10.5194/hess-13-1809-2009.

Leong, E. C., and H. Rahardjo (1997), Review of Soil-Water Characteristic Curve Equations, *Journal of Geotechnical and Geoenvironmental Engineering*, *123*(12), 2, doi:10.1061/(ASCE)1090-0241(1997)123:12(1106).

Leung, A. K. (2016), Grass evapotranspiration-induced suction in slope: case study, *Environmental Geotechnics*, *3*(3), 155–165, doi:10.1680/envgeo.14.00010.

Leung, A. K., A. Garg, and C. W. W. Ng (2015), Effects of plant roots on soil-water retention and induced suction in vegetated soil, *Engineering Geology*, *193*, 183–197, doi:10.1016/j.enggeo.2015.04.017.

Li, A. L., and R. K. Rowe (2001), Combined effects of reinforcement and prefabricated vertical drains on embankment performance, *Canadian Geotechnical Journal*, *38*(6), 1266–1282, doi:10.1139/t01-059.

Libes, S. (2009), *Introduction to Marine Biogeochemistry*, Academic Press.

Lim, T. T., H. Rahardjo, M. F. Chang, and D. G. Fredlund (1996), Effect of rainfall on matric suctions in a residual soil slope, *Canadian Geotechnical Journal*, *33*(4), 618–628, doi:10.1139/t96-087.

Liu, J. C., and D. Znidarčić (1991), Modeling one-dimensional compression characteristics of soils, *Journal of Geotechnical Engineering*, *117*(1), 162–169, doi:10.1061/(asce)0733-9410(1991)117:1(162).

Lobet, G., L. Pagès, and X. Draye (2011), A novel image-analysis toolbox enabling quantitative analysis of root system architecture, *Plant Physiology*, *157*(1), 29–39, doi:10.1104/pp.111.179895.

Lobet, G., V. Couvreur, F. Meunier, M. Javaux, and X. Draye (2014), Plant water uptake in drying soils, *Plant Physiology*, *164*(4), 1619–1627, doi:10.1104/pp.113.233486.

Lu, N., and M. Khorshidi (2015), Mechanisms for soil-water retention and hysteresis at high suction range, *Journal of Geotechnical and Geoenvironmental Engineering*, *141*(8), 04015,032, doi:10.1061/(asce)gt.1943-5606.0001325.

Lu, N., and W. J. Likos (2004), *Unsaturated Soil Mechanics*, Wiley.

Luque de Castro, M., and F. Priego-Capote (2010), Soxhlet extraction: Past and present panacea, *Journal of Chromatography A*, *1217*(16), 2383–2389, doi:10.1016/j.chroma.2009.11.027.

Mao, J.-D., W.-G. Hu, K. Schmidt-Rohr, G. Davies, E. Ghabbour, and B. Xing (2000), Quantitative characterization of humic substances by solid-state carbon-13 nuclear magnetic resonance, *Soil Science Society of America Journal*, *64*(3), 873, doi:10.2136/sssaj2000.643873x.

Marinho, F. A. M. (2006), A method of estimating the soil-water retention curve for plastic soils, in *Unsaturated Soils*.

Martins, F. B., L. A. Bressani, M. R. Coop, and A. V. D. Bica (2001), Some aspects of the compressibility behaviour of a clayey sand, *Canadian Geotechnical Journal*, *38*(6), 1177–1186, doi:10.1139/t01-048.

Merckelbach, L. M. (2000), Consolidation and strength evolution of soft mud layers, Ph.D. thesis, Delft University of Technology.

Merckelbach, L. M., and C. Kranenburg (2004a), Equations for effective stress and permeability of soft mud–sand mixtures, *Géotechnique*, *54*(4), 235–243, doi:10.1680/geot.2004.54.4.235.

Merckelbach, L. M., and C. Kranenburg (2004b), Determining effective stress and permeability equations for soft mud from simple laboratory experiments, *Géotechnique*, *54*(9), 581–591, doi:10.1680/geot.2004.54.9.581.

Mermut, A. R., S. H. Luk, M. J. M. Römkens, and J. W. A. Poesen (1997), Soil loss by splash and wash during rainfall from two loess soils, *Geoderma*, *75*(3-4), 203–214, doi:10.1016/S0016-7061(96)00091-2.

Mietta, F. (2010), Evolution of the floc size distribution of cohesive sediments, Ph.D. thesis, Delft University of Technology.

Mietta, F., C. Chassagne, and J. C. Winterwerp (2009), Shear-induced flocculation of a suspension of kaolinite as function of pH and salt concentration., *Journal of colloid and interface science*, *336*(1), 134–41, doi:10.1016/j.jcis.2009.03.044.

Mikutta, R., M. Kleber, K. Kaiser, and R. Jahn (2005), Review : Organic Matter Removal from Soils using Hydrogen Peroxide ,sodium hypochlorite, and disodium peroxodisulfate, *Soil Science Society of America Journal*, *69*, 120–135, doi:10.2136/sssaj2005.0120.

Mitchell, J. K. (1976), *Fundamentals of Soil Behaviour*, John Wiley & Sons Inc.

Mitchell, J. K., and K. Soga (2005), *Fundamentals of soil behavior, 3rd Edition*, vol. 40, xiii + 577 pp., John Wiley & Sons, doi:10.2136/sssaj1976.03615995004000040003x.

Mitsch, W. J., L. Zhang, K. C. Stefanik, A. M. Nahlik, C. J. Anderson, B. Bernal, M. Hernandez, and K. Song (2012), Creating wetlands: Primary succession, water quality changes, and self-design over 15 years, *BioScience*, *62*(3), 237–250, doi:10.1525/bio.2012.62.3.5.

Monkul, M. M., and G. Ozden (2007), Compressional behavior of clayey sand and transition fines content, *Engineering Geology*, *89*(3-4), 195–205, doi:10.1016/j.enggeo.2006.10.001.

Moore, G. E., D. M. Burdick, C. R. Peter, and D. R. Keirstead (2012), Belowground biomass ofPhragmites australisin coastal marshes, *Northeastern Naturalist*, *19*(4), 611–626, doi:10.1656/045.019.0406.

Moore, J. R. C., D. M. & Reynolds (1989), *X-ray Diffraction and the Identification of Clay Minerals*, Oxford University Press.

Mostofa, K. M., T. Yoshioka, A. Mottaleb, and D. Vione (Eds.) (2013), *Photobiogeochemistry of Organic Matter*, Springer Berlin Heidelberg, doi:10.1007/978-3-642-32223-5.

Murray, H. H. (2006), Chapter 2 structure and composition of the clay minerals and their physical and chemical properties, in *Developments in Clay Science*, pp. 7–31, Elsevier, doi:10.1016/s1572-4352(06)02002-2.

Nelson, D. W., and L. Sommers (1996), *"Total carbon, organic carbon, and organic matter." In:Methods of Soil Analysis, Part 2, 2nd Ed.*, pp. 9:961–1010., Agronomy.American Society of Agronomy, Inc. Madison, WI.

Nepf, H. M. (2012), Flow and transport in regions with aquatic vegetation, *Annual Review of Fluid Mechanics*, *44*(1), 123–142, doi:10.1146/annurev-fluid-120710-101048.

Newman, B. D., B. P. Wilcox, and R. C. Graham (2004), Snowmelt-driven macropore flow and soil saturation in a semiarid forest, *Hydrological Processes*, *18*(5), 1035–1042, doi:10.1002/hyp.5521.

Nguyen, B. T., J. Lehmann, W. C. Hockaday, S. Joseph, and C. A. Masiello (2010), Temperature sensitivity of black carbon decomposition and oxidation, *Environmental Science & Technology*, *44*(9), 3324–3331, doi:10.1021/es903016y.

Nimmo, J. (2004), *Encyclopedia of Soils in the Environment, vol. 3*, chap. Porosity and pore size distribution, p. 95–303, Elsevier.

Nocilla, A., M. R. Coop, and F. Colleselli (2006), The mechanics of an italian silt: an example of 'transitional' behaviour, *Géotechnique*, *56*(4), 261–271, doi:10.1680/geot.2006.56.4.261.

Noguchi, S., Y. Tsuboyama, R. C. Sidle, and I. Hosoda (1997), Spatially distributed morphological characteristics of macropores in forest soils of hitachi ohta experimental watershed, japan, *Journal of Forest Research*, *2*(4), 207–215, doi:10.1007/bf02348317.

Noordhuis, R., B. G. van Zuidam, E. T. H. M. Peeters, and G. J. van Geest (2016), Further improvements in water quality of the Dutch Borderlakes: two types of clear states at different nutrient levels, *Aquatic Ecology*, *50*(3), 521–539, doi:10.1007/s10452-015-9521-8.

Oades, J. M. (1984), Soil organic matter and structural stability: mechanisms and implications for management, *Plant and Soil*, *76*(1-3), 319–337, doi:10.1007/BF02205590.

Odum, H. T., and B. Odum (2003), Concepts and methods of ecological engineering, *Ecological Engineering*, *20*(5), 339–361, doi:10.1016/j.ecoleng.2003.08.008.

Orozco-López, E., R. Muñoz-Carpena, B. Gao, and G. A. Fox (2018), Riparian vadose zone preferential flow: Review of concepts, limitations, and perspectives, *Vadose Zone Journal*, *17*(1), 0, doi:10.2136/vzj2018.02.0031.

Pająk-Komorowska, A. (2003), Swelling, expansion and shrinkage properties of selected clays in the Mazowsze province, central Poland, *Geological Quarterly*, *47*(1), 55–62.

Perillo, C., S. Gupta, E. Nater, and J. Moncrief (1999), Prevalence and initiation of preferential flow paths in a sandy loam with argillic horizon, *Geoderma*, *89*(3-4), 307–331, doi:10.1016/s0016-7061(98)00087-1.

Peters, J. F., and E. S. B. Iv (2010), Percolation Threshold of Sand-Clay Binary Mixtures, *Journal of Geotechnical and Geoenvironmental Engineering*, *136*(2), 310–318, doi:10.1061/(ASCE)GT.1943-5606.0000211.

Piccolo, A., S. Nardi, and G. Concheri (1996), Micelle-1ike conformation of humic substances as revealed by size exclusion chromatography, *Chemosphere*, *33*(4), 595–602, doi:10.1016/0045-6535(96)00210-x.

Pons, L. J., and I. S. Zonneveld (1965), Soil ripening and soil classification: Initial soil formation in alluvial deposits and a classification of the resulting soils, *International Institute for Land Reclamation and Improvement*, (13), 1–128.

RAW124 (2005), *"Proef 124. Bepalen van het gehalte organisch materiaal en gehalte CaCO3, gloeiverlies; gravimetrie." Rationalization and Automatisering Grond, Water en Wegenbouw. Dutch specification system.In Dutch).*

Rawls, W. J., Y. A. Pachepsky, J. C. Ritchie, T. M. Sobecki, and H. Bloodworth (2003), Effect of soil organic carbon on soil water retention, *Geoderma*, *116*(1-2), 61–76, doi:10.1016/S0016-7061(03)00094-6.

Reid, D., and A. Fourie (2015), The influence of slurry density on in situ density, in *18th International Seminar on Paste and Thickened Tailings, 2015 5-7 April, Perth*, pp. 95–106.

Reubens, B., J. Poesen, F. Danjon, G. Geudens, and B. Muys (2007), The role of fine and coarse roots in shallow slope stability and soil erosion control with a focus on root system architecture: a review, *Trees*, *21*(4), 385–402, doi:10.1007/s00468-007-0132-4.

Rietveld, H. M. (1969), A profile refinement method for nuclear and magnetic structures, *Journal of Applied Crystallography*, *2*(2), 65–71, doi:10.1107/S0021889869006558.

Rijkswaterstaat (1995), Geologische en bodemkundige atlas van het markermeer, *Tech. rep.*, Rijkswaterstaat IJsselmeergebied, Lelystad.

Rijniersce, K. (1983), A simulation model for physical soil ripening in the ijsselmeerpolders., *Tech. rep.*, Ministerie van verkeer en waterstaat.

Rozari, P. D. (2009), Sediments and Nutrient Dynamics in the Lake Markermeer , The Netherlands, *Indonesian Journal of Chemistry*, *9*(1), 62–69.

Saaltink, R. (2018), Wetland eco-engineering with fine sediment, Ph.D. thesis, Utrecht University.

Saaltink, R., S. C. Dekker, J. Griffioen, and M. J. Wassen (2016), Wetland eco-engineering: Measuring and modeling feedbacks of oxidation processes between plants and clay-rich material, *Biogeosciences*, *13*(17), 4945–4957, doi:10.5194/bg-13-4945-2016.

Saaltink, R. M., S. C. Dekker, J. Griffioen, and M. J. Wassen (2018), Vegetation growth and sediment dynamics in a created freshwater wetland, *Ecological Engineering*, *111*(August 2017), 11–21, doi:10.1016/j.ecoleng.2017.11.020.

Sanderson, J. (1983), Water uptake by different regions of the barley root. pathways of radial flow in relation to development of the endodermis, *Journal of Experimental Botany*, *34*(3), 240–253, doi:10.1093/jxb/34.3.240.

Santagata, M., A. Bobet, C. T. Johnston, and J. Hwang (2008), One-dimensional compression behavior of a soil with high organic matter content, *Journal of Geotechnical and Geoenvironmental Engineering*, *134*(1), 1–13, doi:10.1061/(asce)1090-0241(2008)134:1(1).

Schelle, H., L. Heise, K. Jänicke, and W. Durner (2013), Water retention characteristics of soils over the whole moisture range: A comparison of laboratory methods, *European Journal of Soil Science*, *64*(6), 814–821, doi:10.1111/ejss.12108.

Schindler, U., and L. Müller (2006), Simplifying the evaporation method for quantifying soil hydraulic properties, *Journal of Plant Nutrition and Soil Science*, *169*(5), 623–629, doi:10.1002/jpln.200521895.

Schindler, U., W. Durner, G. von Unold, L. Mueller, and R. Wieland (2010), The evaporation method: Extending the measurement range of soil hydraulic properties using the air-entry pressure of the ceramic cup, *Journal of Plant Nutrition and Soil Science*, *173*(4), 563–572, doi:10.1002/jpln.200900201.

Schindler, U., J. Doerner, and L. Mueller (2015), Simplified method for quantifying the hydraulic properties of shrinking soils, *Journal of Plant Nutrition and Soil Science*, *178*(1), 136–145, doi:10.1002/jpln.201300556.

Schultze, E., and A. Moussa (1961), Factors affecting the compressibility of sand, *5th International Conference Soil Mechanics and Foundation Engineering*, *1*, 335–340.

Schumacher, B. A. (2002), "methods for the determination of total organic carbon (toc) in soils and sediments." technical report april., *Tech. rep.*, Ecological Risk Assessment Support Center, U.S. Environmental Protection Agency, Las Vegas.

Shaw, H. G. (1972), The preparation of orientated clay mineral specimens for x-ray diffraction analysis by a suction-onto-ceramic method., *Clay Minerals*, *9*, 349–350.

Sheahan, T. C., and P. J. Watters (1997), Experimental verification of CRS consolidation theory, *Journal of Geotechnical and Geoenvironmental Engineering*, *123*(5), 430–437, doi:10.1061/(asce)1090-0241(1997)123:5(430).

Shipton, B., and M. Coop (2012), On the compression behaviour of reconstituted soils, *Soils and Foundations*, *52*(4), 668–681, doi:10.1016/j.sandf.2012.07.008.

Siedlecki, M., W. Pawlak, K. Fortuniak, and M. Zieliński (2016), Wetland evapotranspiration: Eddy covariance measurement in the biebrza valley, poland, *Wetlands*, *36*(6), 1055–1067, doi:10.1007/s13157-016-0821-0.

Sills, B. G. (1998), Development of structure in sedimenting soils, *Philosophical Transactions of the Royal Society A: Mathematical, Physical and Engineering Sciences*, *356*(1980), 2515–2534, doi:10.1098/rsta.1998.0284.

Simpson, D. C., and T. M. Evans (2016), Behavioral Thresholds in Mixtures of Sand and Kaolinite Clay, *Journal of Geotechnical and Geoenvironmental Engineering*, *142*(2), 1–10, doi:10.1061/(ASCE)GT.1943-5606.0001391.

Simpson, M. J., A. Otto, and X. Feng (2008), Comparison of Solid-State Carbon-13 Nuclear Magnetic Resonance and Organic Matter Biomarkers for Assessing Soil Organic Matter Degradation, *Soil Science Society of America Journal*, *72*(1), 268, doi:10.2136/sssaj2007.0045.

Six, J., H. Bossuyt, S. Degryze, and K. Denef (2004), A history of research on the link between (micro)aggregates, soil biota, and soil organic matter dynamics, *Soil and Tillage Research*, *79*(1), 7–31, doi:10.1016/j.still.2004.03.008.

Skempton, A. W. (1953), The colloidal "activity" of clays, in *Proc. 3rd Int. Conf. Soil Mechanic Foundation Engineering*, vol. 1, pp. 57–61., Zurich : Organizing Committee, ICOSOMEF, [1953-1954].

Skempton, A. W. (1969), The consolidation of clays by gravitational compaction, *Quarterly Journal of the Geological Society*, *125*(1-4), 373–411, doi:10.1144/gsjgs.125.1.0373.

Skempton, A. W., and O. T. Jones (1944), Notes on the compressibility of clays, *Quarterly Journal of the Geological Society*, *100*(1-4), 119–135, doi:10.1144/gsl.jgs.1944.100.01-04.08.

Smethurst, J. A., D. Clarke, and W. Powrie (2006), Seasonal changes in pore water pressure in a grass-covered cut slope in London Clay, *Géotechnique*, *56*(8), 523–537, doi:10.1680/geot.2006.56.8.523.

Smith, R., and H. Wahls (1969), Consolidation under constant rates of strain, *Journal of the Soil Mechanics and Foundations Division*, *95*(2), 519–540.

Smoor, A. C. (2015), The impact of overburden pressure on unsaturated shrinkage behaviour of fine-grained soils, Master's thesis, Delft University of Technology.

Soukup, D. a., L. Vegas, B. J. Buck, and W. Harris (2008), Preparing Soils for Mineralogical Analyses, *Soil Science*, (5), 13–31, doi:10.2136/sssabookser5.5.

Sowers, G. F. (1979), *Introductory Soil Mechanics and Foundations: Geotechnical Engineering (4th Ed.)*, Macmillan, New York.

Standard, E. (2012), *Sludge, treated biowaste, soil and waste -Determination of loss on ignition. EN 15935:2012*.

Suku, S., T. Knipfer, and W. Fricke (2014), Do root hydraulic properties change during the early vegetative stage of plant development in barley (hordeum vulgare)?, *Annals of Botany*, *113*(3), 385–402, doi:10.1093/aob/mct270.

Taylor, R. K., and T. J. Smith (1986), The engineering geology of clay minerals: swelling, shrinking and mudrock breakdown, *Clay Minerals*, *21*(March 1985), 235–260, doi:10.1180/claymin.1986.021.3.01.

Terzaghi, K. (1923), Die berechnung der durchlassigkeitzifer des tones aus dem verlauf der hydrodynamischen spannungserscheinungen. mathematish-naturwissenschaftliche, klasse. Part IIa (in German), *Akademie der Wissenschaften, Vienna*, *132*(3/4), 125–138.

Terzaghi, K., and R. Peck (1967), Soil mechanics in engineering practice. 2nd edition,., *John Wiley, New York*.

Terzaghi, K., R. B. Peck, and G. Mesri (1996), Soil Mechanics in Engineering Practice, Third Edition, *Wiley-Interscience Publication, John Wiley and Sons, Inc.*, *48*(1-2), 664 pp., doi:10.1016/S0013-7952(97)81919-9.

Thevanayagam, S. (1998), Effect of Fines and Confining Stress on Undrained Shear, *Journal of Geotechnical and Geoenvironmental Engineering*, *124*(6), 479–491, doi:10.1061/(ASCE)1090-0241(1998)124:6(479).

Thevanayagam, S., T. Shenthan, S. Mohan, and J. Liang (2002), Undrained fragility of clean sands, silty sands, and sandy silts, *Journal of Geotechnical and Geoenvironmental Engineering*, *128*(10), 849–859, doi:10.1061/(asce)1090-0241(2002)128:10(849).

Tisdall, J. M., and J. M. Oades (1982), Organic matter and water-stable aggregates in soils, *Journal of Soil Science*, *33*(2), 141–163, doi:10.1111/j.1365-2389.1982.tb01755.x.

Todd, D. K., and L. Mays (2005), *Groundwater Hydrology 3rd Edition*, John Wiley & Sons.

Tollenaar, R. N. (2017), Experimental investigation on the desiccation and fracturing of clay., Ph.D. thesis, Delft University of Technology.

Tollenaar, R. N., L. A. van Paassen, and C. Jommi (2018), Small-scale evaporation tests on clay: influence of drying rate on clayey soil layer, *Canadian Geotechnical Journal*, *55*(3), 437–445, doi:10.1139/cgj-2017-0061.

Toorman, E. a. (1999), Sedimentation and self-weight consolidation: constitutive equations and numerical modelling, *Géotechnique*, *49*(6), 709–726, doi:10.1680/geot.1999.49.6.709.

Torfs, H., H. Mitchener, H. Huysentruyt, and E. Toorman (1996), Settling and consolidation of mud/sand mixtures, *Coastal Engineering*, *29*(1-2), 27–45, doi:10.1016/s0378-3839(96)00013-0.

Umehara, Y., and K. Zen (1980), Constant rate of strain consolidation for very soft clayey soils, *Soils and Foundations*, *20*(2), 79–95, doi:10.3208/sandf1972.20.2_79.

UMS (2015), *Manual HYPROP*, UMS GmbH, Gmunder Straße 37, Munich, Germany, version 2015-01, 96 pp ed.

Van den Bosch, B. A. P. (2016), The effect of initial concentration on the consolidation behaviour of mud: A study on lake markermeer sediment, Master's thesis, Delft University of Technology.

Van Duin, E. H. S. (1992), Sediment transport, light and algal growth in the Markermeer., Ph.D. thesis, Agricultural University, Wageningen.

Van Genuchten, M. T. (1980), A closed-form equation for predicting the hydraulic conductivity of unsaturated soils, *Soil Science Society of America Journal*, *44*(5), 892, doi:10.2136/sssaj1980.03615995004400050002x.

Van Kessel, T., and G. de Boer (2009), Calibration suspended sediment model Markermeer, *Deltares report 4612*.

Van Ledden, M., W. van Kesteren, and J. Winterwerp (2004), A conceptual framework for the erosion behaviour of sand–mud mixtures, *Continental Shelf Research*, *24*(1), 1–11, doi:10.1016/j.csr.2003.09.002.

Van Olphen, E. J. C. (2016), Consolidation behaviour of soft cohesive soils, the correlation between different scale model tests: Case study of the marker wadden, Master's thesis, Delft University of Technology.

Van Paassen, L., R. Tollenaar, and C. Jommi (2018), Investigating some irregularities observed during suction measurements using the hyprop device., in *7th International Conference on Unstaurated Soil Mechanics*.

Vergani, C., and F. Graf (2015), Soil permeability, aggregate stability and root growth: a pot experiment from a soil bioengineering perspective, *Ecohydrology*, *9*(5), 830–842, doi:10.1002/eco.1686.

Visser, E. J. W., T. D. Colmer, C. W. P. M. Blom, and L. A. C. J. Voesenek (2000), Changes in growth, porosity, and radial oxygen loss from adventitious roots of selected mono- and dicotyledonous wetland species with contrasting types of aerenchyma, *Plant, Cell and Environment*, *23*(11), 1237–1245, doi:10.1046/j.1365-3040.2000.00628.x.

Vörösmarty, C. J., M. Meybeck, B. Fekete, K. Sharma, P. Green, and J. P. Syvitski (2003), Anthropogenic sediment retention: Major global impact from registered river impoundments, *Global and Planetary Change*, *39*(1-2), 169–190, doi:10.1016/S0921-8181(03)00023-7.

Wagner, J.-F. (2013), Mechanical properties of clays and clay minerals, in *Developments in Clay Science*, pp. 347–381, Elsevier, doi:10.1016/b978-0-08-098258-8.00011-0.

Waldron, L. J., and S. Dakessian (1982), Effect of grass, legume, and tree roots on soil shearing resistance, *Soil Science Society of America Journal*, *46*(5), 894, doi:10.2136/sssaj1982.03615995004600050002x.

Watabe, Y., K. Yamada, and K. Saitoh (2011), Hydraulic conductivity and compressibility of mixtures of nagoya clay with sand or bentonite, *Géotechnique*, *61*(3), 211–219, doi:10.1680/geot.8.p.087.

Wershaw (1989), *NMR of Humic Substances and Coal. Techniques, Problems and Solutions*, CRC Press.

Wichman, B. (1999), Consolidation behaviour of gassy mud: Theory and experimental validation, Ph.D. thesis, Delft University of Technology.

Wind, G. (1966), Capillary conductivity data estimated by a simple method, *Tech. rep.*, Institute for land and water management research.

Winterwerp, J. (1999), On the dynamic of high-concentrated mud suspensions, Ph.D. thesis, Delft University of Technology.

Winterwerp, J. C., and W. G. van Kesteren (2004), *Introduction to the Physics of Cohesive Sediment Dynamics in the Marine Environment, Volume 56 (Developments in Sedimentology)*, Elsevier Science.

Wissa, A. E. Z., J. T. Christian, E. H. Davis, and S. Heiberg (1971), Consolidation at constant rate of strain, *Journal of the Soil Mechanics and Foundations Division*, *97*(10), 1393–1413.

Zeelmaekers, E. (2011), Computerized qualitative and quantitative clay mineralogy: Introduction and application to known geological cases, Ph.D. thesis, University of Leuven.

Zentar, R., N.-E. Abriak, and V. Dubois (2009), Fall cone test to characterize shear strength of organic sediments, *Journal of Geotechnical and Geoenvironmental Engineering*, *135*(1), 153–157, doi:10.1061/(asce)1090-0241(2009)135:1(153).

Zhuang, J., K. Nakayama, G.-R. Yu, and T. Urushisaki (2001), Estimation of root water uptake of maize: an ecophysiological perspective, *Field Crops Research*, *69*(3), 201–213, doi:10.1016/s0378-4290(00)00142-8.

Znidarčić, D., and J. C. Liu (1989), Consolidation characteristics determination for dredged materials, in *Proceedings 22nd Annual Dredging Seminar,Ctr. for Dredging Studies, Texas A&M Univ., College Station.*, pp. 45–65.

Zuur, A. (1958), Bodemkunde der Nederlandse bedijkingen en droogmakerijen. Deel C. Het watergehalte, de indroging en enkele daarmede samenhangende processen. Coll. dictaat, *Tech. rep.*, Directie van de Wieringermeer, Wageningen.

Zwieniecki, M. A., M. V. Thompson, and N. M. Holbrook (2002), Understanding the hydraulics of porous pipes: Tradeoffs between water uptake and root length utilization, *Journal of Plant Growth Regulation*, *21*(4), 315–323, doi:10.1007/s00344-003-0008-9.

ACKNOWLEDGEMENTS

I would like to start by thanking my promotors Han Winterwerp and Jasper Griffioen: thanks for giving me the opportunity to do my PhD in a project I really believe in and for sharing your knowledge with me. Furthermore, thanks Han for always making time to answer my questions and for teaching me, among many other evident and important things, that a short sentence is often more effective. I believe I learnt to be a bit less wordy from you (I know what you are thinking and I agree: still not enough). Thanks Jasper for being such a source wisdom and for inviting me to some hydrological excursions, which played an important role on my learning about this beautiful country. On the practical side, thanks for your very detailed explained and thus easily understandable comments. Together with my promotors, I would like to thank Thijs van Kessel for being always available to discuss and join all committee meetings. I also would like thank Thijs for his great sense of humour, often even noticeable during his presentations at conferences.

This PhD thesis is part of the "Smart Ecosystems: Regime shifts from mud systems to dynamic wetlands" consortium and I would like to thank all the parties herein, specially to everyone who gave me feedback during the meetings. I must highlight two people here. First, Martin Wassen, for being the leader of this consortium. I guess that, by getting the funding, you are the ultimate responsible person for the fact that now I live in The Netherlands. Secondly, Rémon Saaltink, for being present in some of the parts of my PhD I enjoyed the most. This may not be only related to my big interest in ecology but also to the fact that you are great person.

Thanks to the Hydraulic Engineering Department of TU Delft where I was appointed. Specially to Ad Reniers for always being emphatic, understanding and willing to help. Talking about empathy, I would like thanks Claire Chassagne for being such a generous person. You came close to me during the most challenging moment of my PhD, when I was not so productive, and helped me to regain confidence. I really enjoyed the scientific discussions we had. You always asked me why I was doing everything: answering to all your why's helped me to put all the pieces of the puzzle together.

The coordinators and technicians from the Fluid Mechanics and Water Management labs have been an important part of my research given the large amounts of experiments I performed: thanks to you all. Special thanks to Sander de Vree for being so easily reachable and being willing to think along for a solution. Also special thanks to Mohammed Jafar for being a supportive and caring person. Thanks to the DEMO workshop. You made all the column set-ups I dreamed become true, even tough I believe I have sometimes *challenged your future.*

Thanks to all the PhD peers in the "Lapp" and second floor: to the Labdies for all the fun moments and great conversations; to Victor, Lodewijk and Yorick for their Matlab and Latex tips, to *Los Tíos* for making me feel at home and being so wise (I miss you so much!), to Stuart for being the best buddy during our adventure as supervisors of the study trip to

India and Sri Lanka, to María and Gonzalo for opening their heart to me and always being available to listen and give advice.

Apart from PhD candidates and technicians, there are other people I met in the Lapp that became my friends: Nena and Bart. Thanks to Nena for volunteering to come with me to the field (and save the campaign!) and for the amazing outdoors activities you always organise, which help me to improve my English in the meanwhile. Thanks to Bart for showing me where to find *staff and stuff* when I just "landed" at TU Delft, for the nice museum advice and for your huge help with the Dutch lines of this thesis.

Despite of being appointed at the hydraulic department, I spent a significant amount of time at the Geo - Engineering laboratory performing experiments. Herein, I would like to thank the technicians but also some scientific staff, namely: Leon van Paassen for the very (chaotic) and inspiring brainstorming moments; Phil Vardon for being very approachable, reliable and always being willing to discuss and Cristina Jommi for making time in her full agenda to help me with some doubts.

Because I did not have enough with doing experiments in three different labs of TU Delft, I also went to Deltares to do so. Here, I would like to thank Saskia for showing me where everything was in the FCL lab and keeping an eye on my muddy samples. Regarding the experiments at FCL, Barend van der Bosch must be acknowledged for his good performance of the SIC tests for his MSc thesis, which I further analysed in the present dissertation. I also would like to thank the technicians of the Geo lab and the expert Maria Konstantinou for their big help performing the CRS tests.

Thanks to my friends from childhood and university: Cristina, Alba, Adrián and Javi for being so supportive and feeling so close despite of the distance. Apart from being an awesome friend, I also have to acknowledge Javi for helping me to improve the quality of a couple of figures of one chapter.

Above everything and everyone, I am thankful to my family. And with family I refer also to my cousins, aunts, uncles and grandmas. I had the luck to grow up in a very supportive family who loves to spend time together and knows how to make such a time really fun. Actually, foreign friends who visited me there, like my dear Nikhil, preferred to spend time with you rather than sightseeing. This means something: *sois geniales*.

During my PhD thesis I lost two of the people who influenced the most the *persona* I am nowadays: my father and my best friend from childhood. These were too big and too painful losses. It was at this moment when the Netherlands gave me a present: Tom. Thank you so much for your patience, generosity, love, the great discussions and for having liked me even when I was not so shiny.

This thesis is dedicated to the person I have ever admired the most: my father. He will always be a source of strength and inspiration to me.

List of Figures

List of Tables

CURRICULUM VITÆ

María Barciela Rial was born on 6th July 1989 in Vigo (Spain), where she lived until she completed a scientific pre-university education at the (public) IES Santa Irene high school in 2007. Expending her childhood by the coast and often accompanying her father to his work influenced her decision for an university degree. She moved to A Coruña to study at the Escuela Técnica Superior de Ingenieros de Caminos, Canales y Puertos. There she first obtained her Bsc in Civil Engineering (2007-2010) with a minor in hydraulics and, later, her beloved MSc in Water Engineering (2010-2012). She coursed the last year of this master in French at the $ENSE^3$ school of the *Institut National Polytechnique* de Grenoble. This was a very positive experience who made her dream with a career abroad surrounded by friends from different cultures and backgrounds. After completing her master's degree, María joined again the company where she had done an internship the first year of her master's: Aquática Ingeniería Civil. Between 2012 and 2014 she intercalated working in some projects of this company with other opportunities at the Sea for Society project and the Environmental Engineering Lab (Environmental Engineering Group, University of A Coruña). In July 2014, she moved to Delft, The Netherlands to do her PhD within the Marker Wadden Building with Nature project, which resulted in the present thesis. Since August 2019, she works as a researcher for the Sustainable River Management group at the HAN University of Applied Sciences.

List of Publications

Journal papers

- Saaltink*, R. M., M. **Barciela-Rial***, T. van Kessel, S.C. Dekker, H.J. de Boer, C. Chassange, J. Griffioen, M. J. Wassen, and J.C. Winterwerp (2019): Drainage of soft cohesive sediment with and without Phragmites australis as an ecological engineer, *Hydrology and Earth System Sciences Discussions*, https://doi.org/10.5194/hess-2019-194. *Shared first authorship.
- **Barciela-Rial**, M., L. van Paassen, J. Griffioen, T. van Kessel, and J.C. Winterwerp (under review), The effect of solid phase composition on the drying behaviour of Markermeer sediment, *Vadose Zone Journal*.
- **Barciela-Rial**, M., B. A. van den Bosch, T. van Kessel, J. Griffioen, and J.C. Winterwerp (submitted), Consolidation of slurries, *Canadian Geotechnical Journal*.
- **Barciela-Rial**, M., P.J. Vardon, J. C. Winterwerp, J. Griffioen, and T. van Kessel (submitted), The effect of composition and stress state on the consolidation of slurries, *Canadian Geotechnical Journal*.

National and International conferences

- **Barciela-Rial**, M., J. C. Winterwerp, J. Griffioen and T. van Kessel (2015), Consolidation and strength development of soft mud deposits by horizontal drainage, in Toorman, E.A. et al. (Ed.) INTERCOH 2015 - 13th International Conference on Cohesive Sediment Transport Processes, 7 to 11 September 2015, Leuven, Belgium: book of abstracts
- **Barciela-Rial**, M., J. C. Winterwerp, J. Griffioen, and T. van Kessel (2015), Consolidation and strength development by horizontal drainage of soft mud deposits in Lake Markermeer, in Book of Abstracts NCR-Days, pp. 62–64.
- **Barciela-Rial**, M., J. C. Winterwerp, L.A. van Paassen, J. Griffioen, and T. van Kessel (2016), The Markerwadden: the influence of the sand fraction on the ripening behaviour of Markermeer sediment, in Book of Abstracts NCK-Days 2016, pp 10.
- **Barciela-Rial**, M., J. C. Winterwerp, J. Griffioen, L. A. van Paassen and T. van Kessel (2016), The effect of organic matter oxidation and drying on the geomechanical behavior of anoxic mud, in: American Geophysical Union, Fall Meeting 2016, abstract EP33A-0963.
- **Barciela-Rial**, M., B. A. van den Bosch, J. C. Winterwerp, L. A. van Paassen, J. Griffioen, and T. Kessel (2017), The effect of initial conditions on the consolidation of mud, in Pedocchi, F. et al. (Ed.) INTERCOH 2017 - 14th International Conference on Cohesive Sediment Transport Processes, 13 to 17 November 2017, Montevideo, Uruguay: book of abstracts.
- **Barciela-Rial,** M. (2018), Consolidation of slurries below and above water. Kennis en Innovatieprogramma Marker Wadden (KIMA) Congres.

- Dekker, S., R. Saaltink, H. de Boer, M. **Barciela-Rial**, T van Kessel, J. Griffioen, J. C. Winterwerp, and M. Wassen (2018), Building with nature in wetlands: Plants accelerate soil forming processes of newly deposited fine sediments, in Geophysical Research Abstracts Vol. 20, EGU2018-4006, EGU General Assembly 2018.
- **Barciela-Rial**, M., J. C. Winterwerp, J. Griffioen, and T. van Kessel (2018), The Marker Wadden: Consolidation of slurries below and above water. EcoShape Building with Nature conference.
- **Barciela-Rial**, M., J. C. Winterwerp, J. Griffioen and T. van Kessel (2019), Consolidation and drying of slurries: an overview, in Book of Abstracts NCK-Days 2019, pp. 26.